Aspects of the tectonics of the Greater Caucasus and Western South Caspian Basin

Abduelmenam Alburki and UNSPECIFIED

Department of Earth Sciences, University of Durham

Aspects of the tectonics of the Greater Caucasus and Western South Caspian Basin

A thesis submitted to the University of Durham

for the degree of Doctor of Philosophy in the

Faculty of Science

By

Abduelmenam Abdusalam Alburki

2015

Abstract

The main objectives of this project are to (a) understand the relationship between climate, topography and the tectonics in the Greater Caucasus belt, (b) construct regional geological cross-sections showing major stratigraphic sequences and structures along the belt using the focal mechanisms of the earthquakes events, (c) evaluate the evolution and development of a single fold structure (Yasamal anticline) and (d) investigate strain accommodation mechanisms using 3D Move to unfold the Yasamal structure.

Topographic variations were investigated to understand the interplay between topography, climate and the tectonics of the Greater Caucasus range and compare the findings with other active and inactive belts (Pyrenees, Northern Tibetan Plateau and Himalayas). There is a correlation between elevation changes and climate along the Greater Caucasus belt, where the gradual reduction of the mean altitude, has a close relationship with a wetter climate, and the sharper altitude decrease with a drier climate. And the elevation changes are strongly correlated with the Moho depths underneath the region. The relief along the belt is extremely high, with a strong correlation between the high relief and the large thrusts in the region. And the relief of the eastern part is slightly low compared with the western part of the belt, even though the eastern part is more active than the western part.

The structural study undertaken at regional scale for the Caucasus belt and the western side of the South Caspian Basin gave insights on the style of deformation in the basin and the evolution of the Greater Caucasus belt and the preferred distribution, geometry and formation mechanism of the structural elements. The regional cross-sections along the Greater Caucasus were constructed and constrained by using focal mechanisms show that the belt is deformed by active thrust faults that dip inwards from the margins of the range where the northern thrusts are dipping south, and the southern thrusts are dipping to the north, these results have contrary to some previous models that emphasise only south-directed thrusting.

The spatial arrangement, geometry and temporal evolution of spectacular kilometre-amplitude fold structures actively forming in Cenozoic sediments on the uplifted western margin of the South Caspian Basin are described and strain accommodation mechanisms established using 3D Move to unfold the Yasamal structure enabled a reconstruction of pre-folding templates and predictively model the fold-

related deformation at small-scale. The 3D model of the Yasamal anticline shows that the anticline hinge has about 30° south-directed plunging. The area was characterized by a low rate of sedimentation and high rate of uplift in the Upper Pliocene. The minor structures (accommodating the overall strain in the anticline) are developed throughout the entire anticline. Compressional strain is present at the anticline hinge line, and the extensional strain dominates the anticline limbs. Suggesting potential extensional structures development in the anticline flanks, which correspond with the field observations in the Yasamal valley confirming that; the small normal faults are concentrated within the anticline flanks, and the contractional deformation bands along the hinge area of the anticline.

Table of Contents

List of Figures

List of Tables

List of Abbreviations

$\Delta \mathbf{l}$	Change of the length
$\Delta \mathbf{lR}$	Length change rate
2D	Two Dimensions
3D	Three Dimensions
$\mathbf{A} - \Delta \mathbf{lR}$	Length changes average
$\mathbf{A} - \Delta \mathbf{lR}$	Length change rate average
AB	Apsheron-Balkhan
AF	Akhtyr Fault
Al	Alazani
AP	Apsheron Peninsula
AT	Achara Trialet belt
AZ	Axial Zone
BB	Billion Barrels
BP	British Petroleum
CMT	Centroid Moment Tensor
CSCB	Central South Caspian Basin
DEM	Digital Elevation Model
DSS	Deep Seismic Sounding
$\mathbf{e}$	Longitudinal strain
e1	Extensional strain
e3	Compressional strains
EHB	Engdahl Hillst Buland
ETOPO	Topographic and bathymetric map
GB	Great Balkhan
GC	Greater Caucasus
GCB	Greater Caucasus Basin
GCT	Greater Caucasus Trough
GIS	Geographic information system
GMT	Generic Mapping Tools
GPS	Global Positioning System
Ikonos	High resolution satellite imagery
ISC	International Seismological Centre
KAS	Kalin Suite
KB	Kura Basin
KD	Kopet Dagh
KDMB	Kopet Dagh Mollass Basin
KS	Kirmaky Suite

l	Final bed length
L.d.p	Length of the deformation period
LC	Lesser Caucasus
LiDAR	Light Detection and Ranging
LKB	Lower Kura Basin
LKB	Lower Kura Basin
lo	Original bed length
MC	Middle Caspian
MCT	Main Caucasus Thrust
NKG	Post Kirmaky Clay Suite
NKP	Post Kirmaky Sand Suites
NPF	North Pyrenean Fault
NPFT	North Pyrenean Frontal Thrust
NPZ	North Pyrenean Zone
NSCB	Northern South Caspian Basin
PFT	Pshekish Tynauz Fault
PK	Pre-Kirmaky Sand Suite
PTF	Pshekish-Tyrnyauz Fault
RB	Rioni Basin
LMS	Laser Measurement system
RLF	Racha Lechkhumy Fault
RLFZ	Racha-Lechkhumy Fault Zone
S	shortening percentage
SA	Sevan Akera
SCB	South Caspian Basin
SLR	Single-lens reflex camera.
SP	Scythian Platform
SPOT	Satellite Pour l'Observation de la Terre in French which means (Satellite for observation of Earth) in English.
SPZ	South Pyrenean Zone
SRTM	Shuttle Radar Topography Mission
T	Talysh
TΔl	Total change of the length
TCF	Trillion Cubic Feet
TCMB	Terek–Caspian Molasse Basin
T-L.d.p	total length of the deformation period
TLS	Terrestrial Laser Scanning
TOF	Time of Light
TP	Turan Platform
TS	Total Shortening percentage

USGS-NEIC	U.S. Geological Survey–National Earthquake Information Centre
UTM	Universal Transverse Mercator
WC	West Caspian
WGS	World Geodetic System
WTB	West Turkmenian Basin

Declaration

No part of this thesis has previously been submitted for a degree at this or any other university. The work described in this thesis is entirely that of the author, except where reference is made to previously published or unpublished work.

Abduelmenam A. Alburki
Durham University
Department of Earth Science
2015

Acknowledgements

Praise is to **ALLAH** the lord of the worlds, for his generous blessings, guidance and aid to complete this work.

My utmost deep and sincere gratitude goes to my supervisors, Professor Ken McCaffrey and Professor Mark Allen for their enthusiasm, inspiration, encouragement, knowledge and support constructive comments throughout this work. Thank you very much Ken and Mark for one of a kind supervision.

My deepest gratitude and love to my dear beloved mother and father may ALLAH preserve and protect them, who are the first encourager and supporter to me in continuing my education.

I would like to give the special thanks to my family “my wife and my children” for giving me love, happiness and joy; and for their endless support, encouragement and patience.

I would also like to thank my brothers and sisters for their patience, constant encouragement and moral support. And I am very thankful for my (parents, brothers and sisters in law) for their continuous encouragement and support.

Thanks of course to all my friends and colleagues and all of the other people I have met in the department who really were the supporters that gave me patience to complete this thesis.

This work would not have been possible without the generous support and tolerance of the Libyan Cultural Attaché London, and their contribution to this research is greatly acknowledged.

Abduelmenam Alburki

Dedication

In the Name of Allah the most Beneficent, the most Merciful

To my dear beloved parents (Mr. Abdusalam Alburki and Mrs. Edhaiba Mohamed), my wife, my brothers, my sisters, my children “Absi, Omer and my sweet daughter Munya” and to anyone who are waiting for my success, I would like to dedicate this work.

Abduelmenam Alburki

Chapter I

Introduction

1. Introduction

1.1. General introduction to the area under investigation

Azerbaijan is a country in the Caucasus region of Eurasia, located at the intersection of Western Asia and Eastern Europe. It is bordered by the Caspian Sea to the east and surrounded by five countries; Russia, Georgia, Armenia, Turkey and Iran (Figure 1.1). It has an area of around 86600 km^2. Azerbaijan is one of the oldest petroleum-producing regions globally, with oil and gas being exploited in this region for more than a century and a half. Subsequently a large number of scientists have studied the occurrences of the oil and gas in this region.

The area under investigation comprises the Azerbaijani part of the South Caspian Basin (SCB), that formed mainly during the Pliocene-Quaternary and the Caucasus mountain belt, which is divided into the Greater Caucasus to the north, the Lesser Caucasus to the south and the Kura lowland between the two (Figure 1.1). The rocks that underlie Azerbaijan are part of the Cenozoic fold belt that includes the Middle Caspian Basin and South Caspian Basin to the east of the country (Buryakovsky et al., 2001; Khain et al., 1991).The Apsheron- Balkhan sill occupies the northern side of the South Caspian Basin and it is considered to be an important geological and bathymetric feature separating the South Caspian Basin from the Middle Caspian Basin.

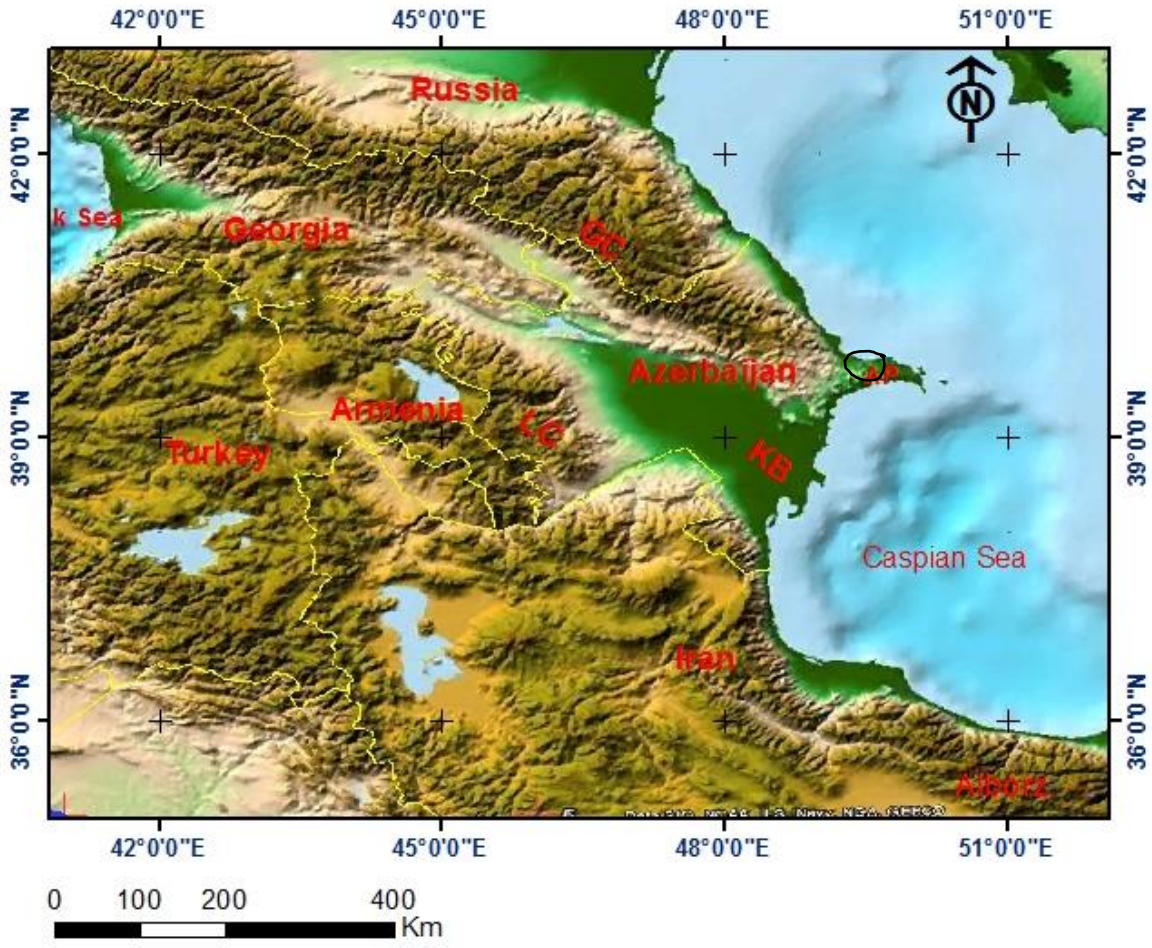

Figure 1.1.ETOPO map showing the location of the study area, GC= Greater Caucasus, LC = Lesser Caucasus KB = Kura Basin and the small black circle shows Yasamal Anticline location.

The basement to the SCB formed long before the Pliocene-Quaternary, but development of tectonic structures continues to the present (Gurevich and Chilingar, 1995). The late Cenozoic events have formed many folds in the SCB, for instance the Yasamal fold (Figure 1.2), also known as Shubani, which was the main anticlinal structure studied in this project and is located about 10 km to the west of Baku (capital of Azerbaijan). Other anticlines include Kirmaky to the north of Baku and Malyi Kharami to the south east of the Greater Caucasus. Individual folds axial traces in the Apsheron Peninsula are curved and the anticlines show significant strike differences compared with folds in the Greater Caucasus. The folds are also linked with mud volcanoes that occur on the fold hinge lines or at fold intersections (Allen et al., 2003).

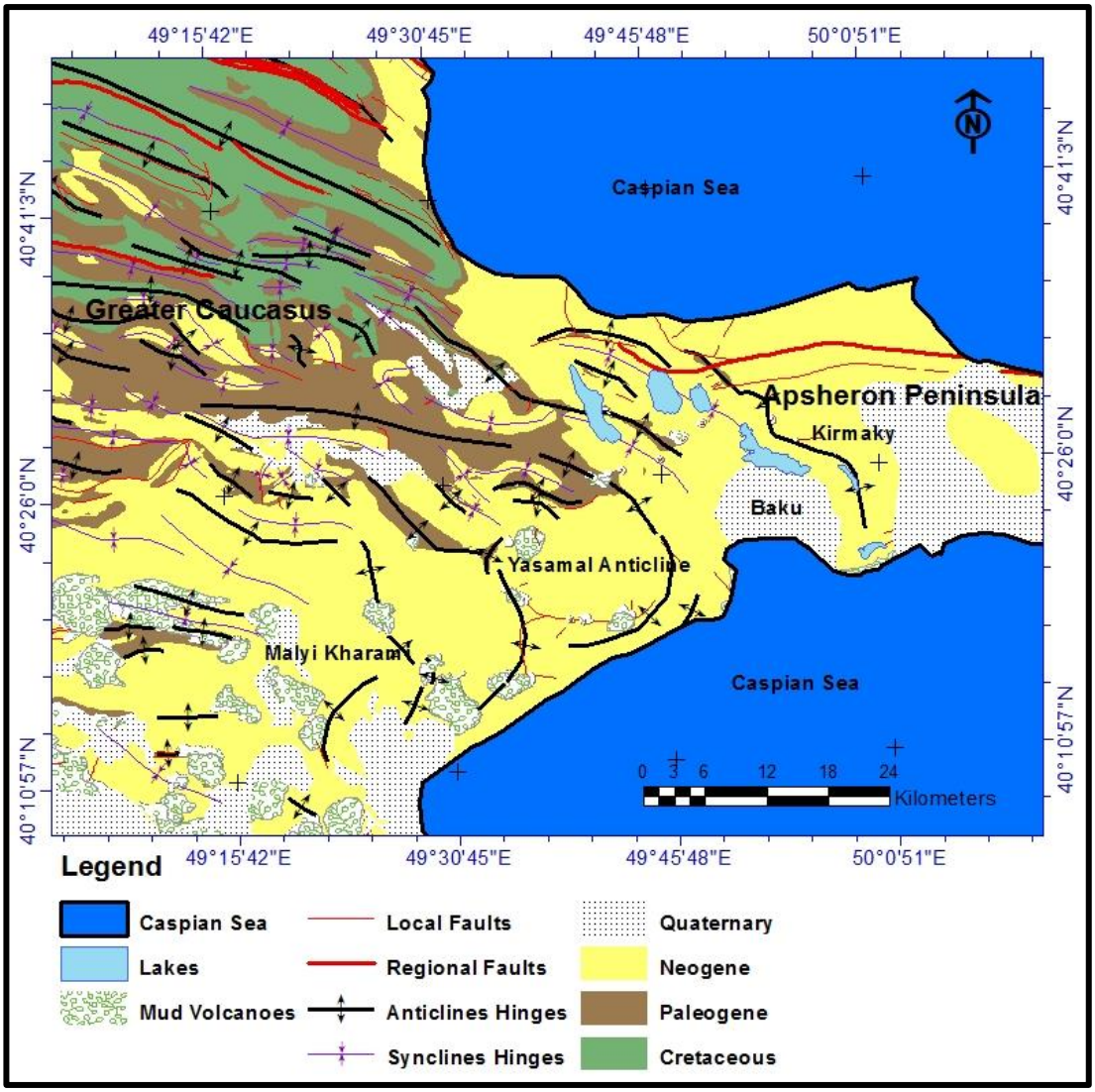

Figure 1.2. Eastern Greater Caucasus Geologic map showing the main anticlines in Eastern GC (Allen et al., 2003).

Tectonically the region surrounding the SCB has been divided into four tectonic units. Unit (1) consists of the Turan and Scythian platforms to the north-east and the north-west of the basin respectively. Unit (2)is a series of orogenic belts surround the SCB and comprise the Greater Caucasus to the west of the South Caspian Basin, the Alborz to the south, the Kopet-Dagh to the east, and the Great Balkhan to the north of the basin. Unit (3) is represented by foreland basins and includes the Terek–Caspian molasse basin in the north-eastern Greater Caucasus and the Kopet-Dagh molasse

basin in the northern Kopet-Dagh orogen. Finally, unit (4) surrounding the SCB are magmatic or volcanic belts and the associated basins, comprising the Karabakh magmatic belt, the Eastern Pontides, the Achara-Trialet zone and in the far west of the SCB, the Erevan-Ordubad Basin and the Talysh Basin to the west of the South Caspian Basin (Brunet et al., 2003).

1.2. Aims and scope of the present study

The aim for this study is to understand the development of structures and the tectonic evolution of the eastern part of the Caucasus Mountains and western onshore part of the SCB. The overall objective is to describe the structural styles in the fold and thrust belts of the Greater Caucasus Belt and Apsheron Peninsula along the northern margin of the Arabia-Eurasia collision zone.

The methodology included compilation and analysis of existing topographical, geological and structural databases (represented by digital elevation models, geological maps and detailed field datasets). Topographic variations were investigated to understand the interplay between tectonics and geomorphic processes and climate of the Greater Caucasus Mountain range. Exposed structures were mapped using these remote sensing datasets, and the relationships between exposed and subsurface structures was examined by constructing geological cross-sections along the Greater Caucasus, focusing on the eastern side of the mountain belt.

Using freely available satellite imagery, this work produced a detailed map and cross sections of the Yasamal fold using structural data, including laser scans, previously collected by (McCaffrey, K. J. W., and others 2007) and made available to the project by BP Azerbaijan.

1.3. Thesis outline and style

This thesis has been divided into seven chapters. This first chapter introduces the area under investigation, the aims and scope of the present study and structure of the thesis. The contents of chapters from two to seven are outlined separately below;

Chapter 2: Background and literature review of South Caspian Basin

This chapter illustrates the most significant features of the geographical, geological and tectonic setting of the study area, stratigraphy, and hydrocarbon occurrence and potential source rocks, including a general review of the previous work.

Chapter 3: Methodology and datasets

This chapter addresses the overview of methods and data used in this thesis, and describes the workflows that were used to interpret the data and to create and construct maps and cross sections.

Chapter 4: Topographical studies

This chapter summarises an investigation of the relationship between the tectonics, topography and climate in the Caucasus and compares the results with other active and inactive belts (Greater Caucasus, Pyrenees and Himalayas).

Chapter 5: The major structural elements of the Greater Caucasus belt and the western South Caspian Basin

This chapter reports the structural study undertaken at regional scale for the Greater Caucasus belt and the western side of the SCB. The style of deformation in the SCB and the evolution of the Caucasus belt are described and the preferred distribution, geometry and formation mechanism of the structural elements discussed.

Chapter 6: Structural interpretation and tectonic inferences from a detailed study of the Yasamal anticline

This chapter presents the results of an investigation of the structural elements at small scales for the Yasamal fold and its surroundings, to illustrate the accommodation of shortening at the scale of an individual fold structure.

Chapter 7: Conclusions and future work

The main conclusions arising from this research project and recommendations for future work are presented.

Chapter II

Geologic background and literature review of the South Caspian Basin and adjacent areas

2. Geologic background and literature review of the South Caspian Basin and adjacent areas

2.1. Introduction

The Caspian Sea was situated between only two countries, Iran and the Union of Soviet Socialist Republics (USSR) before the collapse of the USSR; however, at the present it is located between five countries: Azerbaijan, Russia, Kazakhstan, Turkmenistan and Iran. The SCB comprises the southern part of the Caspian Sea and its neighbouring onshore areas with almost 45% of the basin located in Azerbaijan. The basin is about 680 km in length from north-south and 547 km east-west with more than 60% of the basin area covered by Caspian Sea (lake) water, (Figure 2.1).

2.1.1. Geographic overview of the SCB

The SCB can be divided into three sub-basins from west to east;

- The**Kura sub-basin** in the western SCB, bounded by Greater Caucasus (GC) to the north west, Lesser Caucasus (LC) and Talysh to the southwest, and the Azerbaijani Caspian Sea coast to the east;
- The **West-Turkmenian sub-basin** is bounded by Kopet-Dag to the east, the Balkhans to the north and Turkmen and the Iranian Caspian Sea coast to the southwest and south respectively and;
- The **Central sub-basin** is bordered by West-Turkmenian sub-basin to the east, Kurian sub-basin to the west, the Apsheron-Balkhan sill to the north and Alborz mountains to the south (Nadirov et al., 1997) (Figure 2.1).

Further subdivisions for the main thickest part of the offshore basin, the central sub-basin are:

- **Northern South Caspian Basin**: up to 26 km in thickness close to Apsheron sill.
- **Pre-Alborz trough**: up to 20 km in thickness to the south-east of the South Caspian Basin (Brunet et al., 2003; Knapp, 2000).

According to this division which reflects the change in sediment thickness increasing from south to north, there is an indication that there is a northward subduction of the South Caspian crust underneath the Middle Caspian Crust (Knapp, 2000).

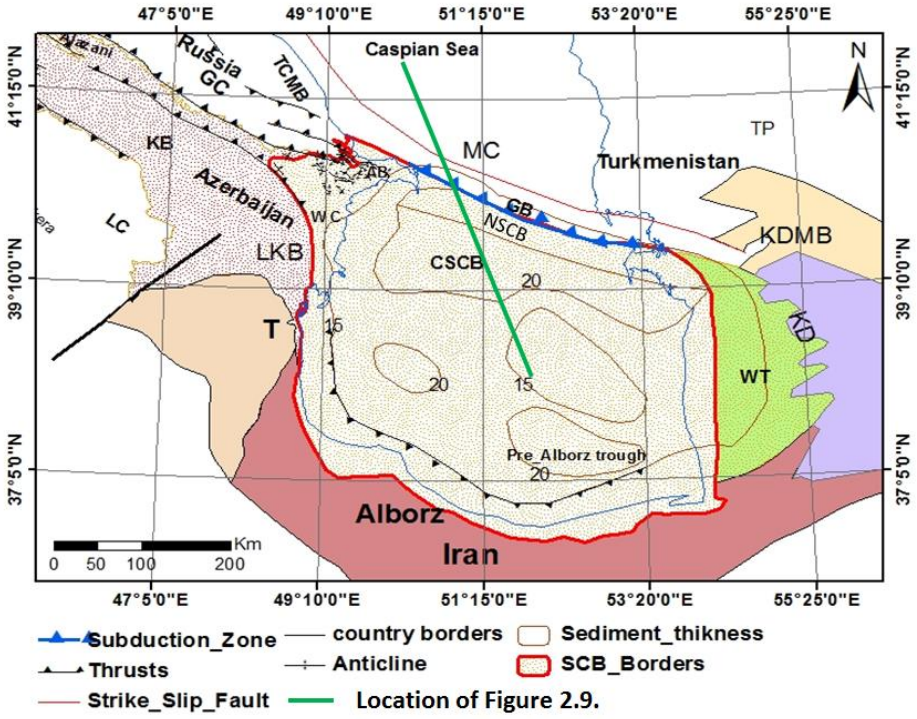

Figure 2.1. Map showing the major features of the SCB and its surroundings, GC = Greater Caucasus, LC=Lesser Caucasus, KD=Kopet Dagh, KB=Kura Basin, LKB=Lower Kura Basin, NSCB= Northern South Caspian Bas (Nadirov et al., 1997)in,CSCB=Central South Caspian Basin, NSCB=Northern South Caspian Basin, WT=West-Turkmenian, T=Talysh, MC=Middle Caspian, GB=Great Balkhan, AB=Apsheron-Balkhan, TCMB=Terek–Caspian Molasse Basin, KDMB=Kopet-Dagh Molasse Basin, WC=West Caspian, TP=Turan Platform. Modified after Brunet et al. (2003) and Nadirov et al. (1997).

2.2. Regional geological setting of the SCB.

The present form of the South Caspian Basin was created during the Pliocene (Gurevich and Chilingar, 1995), and the deformation comprises large anticlines and synclines which have been intruded by mud volcanoes (Devlin et al., 1999). The Caspian Sea basins are some of the principal places of hydrocarbon accumulation in the Earth (Devlin et al., 1999), and the SCB is considered as one of the areas of great economic importance, due to it is containing several huge oil fields. However, the geological knowledge of this region is still somewhat imperfect.

The age of the basement of the SCB is debated with some authors proposing that it is Jurassic, e.g. (Brunet et al., 2003; Granath, 1996; Zonenshain and Pichon, 1986) and others suggesting that it is Palaeocene (Abrams and Narimanov, 1997; Berberian, 1983a). The crust of the SCB is very different from that of the surrounding regions, as demonstrated by the Russian Deep Seismic Sounding (DSS) experiments in the 1950s and 1960s. There is general agreement that the basement has the geophysical characteristics of oceanic crust(Mangino and Priestley, 1998). This basement exists under > 20 km thickness of sediments, which increases approaching the basin centre (Jackson et al., 2002), Thus the SCB is one of the thickest sedimentary covers in the earth.

There are active earthquake belts bordering the SCB on all sides. In the Kopet Dagh region, which bounds the northeast side of the basin, the Alborz to the south and the Talysh to the west, the earthquakes are shallow and not deeper than thirty kilometres(Jackson et al., 2002). However along the Apsheron Balkhan sill (Apsheron-Pribalkhan Zone) to the north of the basin the earthquakes occur at depths deeper

than 80km (Figure 2.2). The depths of these earthquake events suggest that there is a subduction zone underneath the central Caspian. Furthermore, this subduction is in the early stages of formation as all earthquakes in this sill occur at depths less than 100km (Jackson et al., 2002; Priestley et al., 1994).

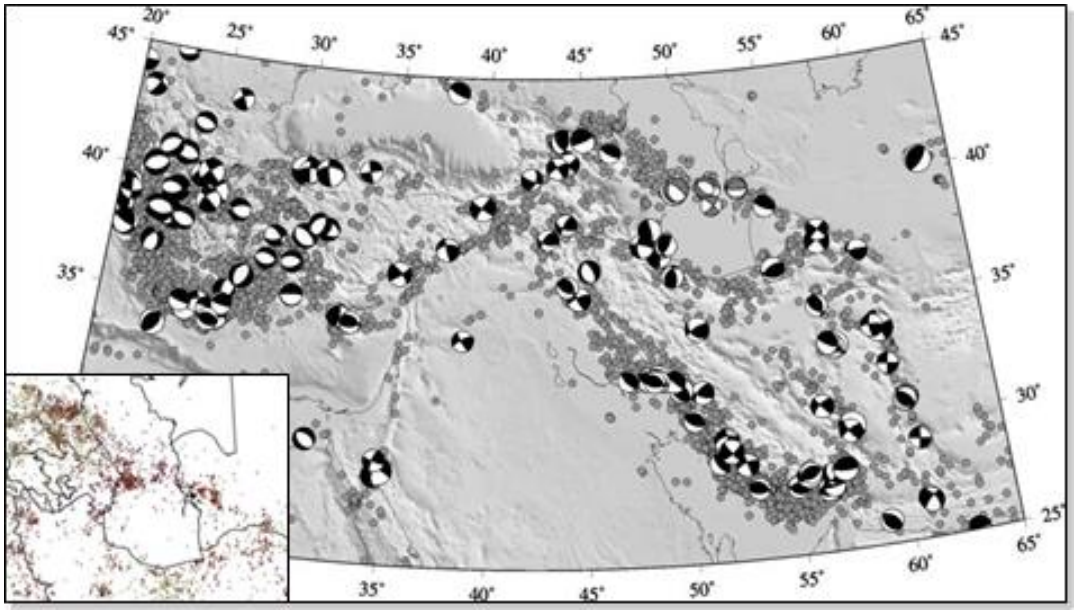

Figure 2.2. Arabia–Eurasia collision zone seismicity, where earthquakes as deeper than 30km are represented by grey focal mechanisms in Apsheron Balkhan region, from Allen et al. (2004).

The complex structural element represented by the SCB is a part of the Alpine fold belt area between the Mediterranean to the west and the Himalayas to the east (Shikalibeily and Grigoriants, 1980). The thick sedimentary cover has low seismic velocity values from about 4 to 5.5 km/s, and this thick sedimentary cover occurs above a high velocity layer with values between 6.5 to 7.8 km/sec indicative of basaltic crust. Thus there is a gap in velocity between 5.5 to 6.5 km/s (Rezanov and Chamo, 1969).

Normal continental crust is sedimentary cover with velocity up to about 5.5 km/s, above ‘granitic’ crust with velocity between 5.8 and 6.5 km/s and then ‘basaltic’ crust underneath the granitic crust with velocity about 6.5 to 7.8 km/s (Jackson et al., 2002). In the same context, by studying many profiles across the West-Turkmen depression with many deep wells and outcrops, Rezanov and Chamo (1969) have determined the SCB crust layers depending on the velocities of longitudinal waves as a Cenozoic layer with velocity of 3.9-4.2 km/s, a Paleocene - Late Cretaceous layer with velocity of 4.2 to 4.6 km/s, Early Cretaceous layers with velocity of 5.2 to 5.6 km/s, and then the basement with a velocity of 6.5 to 7.8 km/s.

Accordingly, there is no layer with velocity between 5.8 and 6.5 km/s in the South Caspian Basin, which can be related to the ‘granitic crust’ beneath the sediments and above the ‘basaltic’ crust. A number of authors suggest that the absence of a 'granitic' layer in the SCB is because the area was uplifted in the Mesozoic and the upper crust was eroded and consequently the lower crust was exposed and underwent subsidence and sedimentation (Mangino and Priestley, 1998; Rezanov and Chamo, 1969; Shikalibeily and Grigoriants, 1980). The alternative explanation is that there was a period of significant extension in the region, such that new oceanic crust was formed. However, the timing and the regional context of this extension are not agreed.

The Moho beneath the basin has a broad arch-like structure (Figure 2.3) with the sedimentary cover is much thicker within basin and reduced in thickness towards the borders to the east and west, where its gradient is about 1km/5km to the west whereas it is 1km/20km to the east, however the overall thickness of the crust increases towards the margins (Jackson et al., 2002).

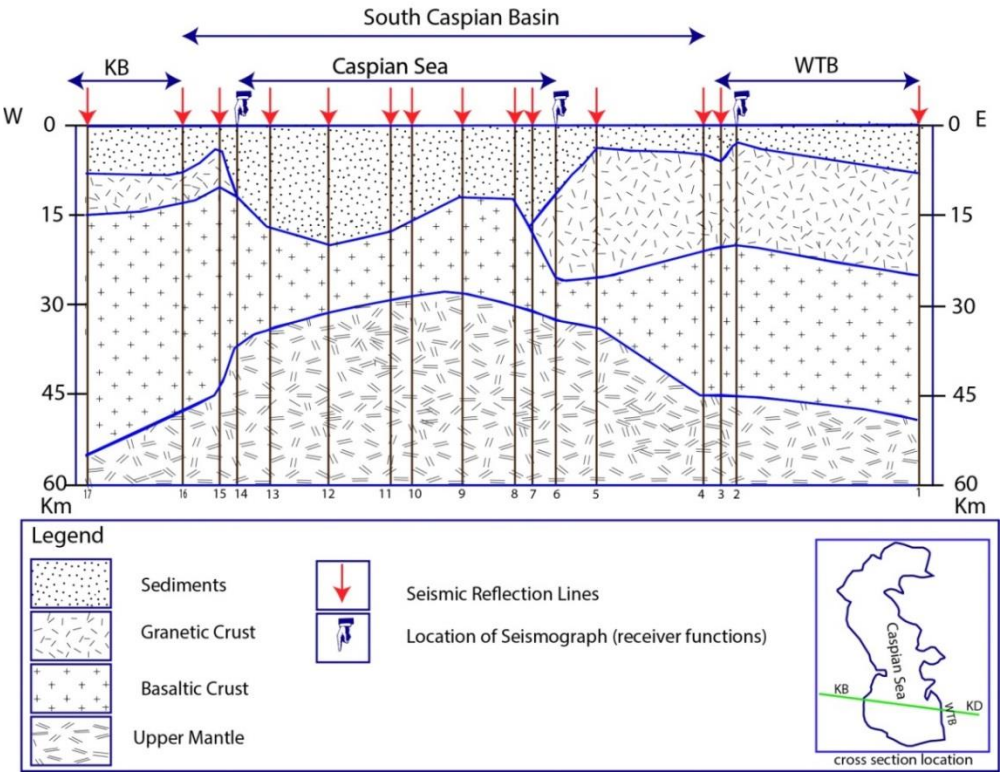

Figure 2.3. Crust and upper mantle cross-section of the south Caspian Basin region extending from the Kopet Dagh to the east and Kura Basin to the west of the basin, showing the main crustal layers recognized by their wave velocities which are from upper to lower; (sediments with velocity under 4.8km/s, 'granitic' between 4.8-6.4km/s, 'basaltic' between 6.4-7.4km/s upper mantle≥8.0) after (Artyushkov, 2007; Jackson et al., 2002; Mangino and Priestley, 1998). KB = Kura Basin, KD = Kopet Dagh, WTB = West Turkmenian Basin.

The basement of the South Caspian Basin itself is aseismic and rigid, witnessed by the lack of earthquake focal mechanisms within it. However, it is bordered by active tectonic units. Northward movement of Arabia is accommodated by the major seismically active tectonic units surrounding the South Caspian Basin (Jackson et al., 2002) (Figure 2.4). The present movement of the basin has a westward component relative to both Iran to the south and the rest of Eurasia to the north (Allen et al., 2002a; Hollingsworth et al., 2009; Jackson et al., 2002; Masson et al., 2006; Priestley,

1994). This component is represented by left-lateral strike-slip faulting in the Alborz and right-lateral slip in the Kopet-Dagh.

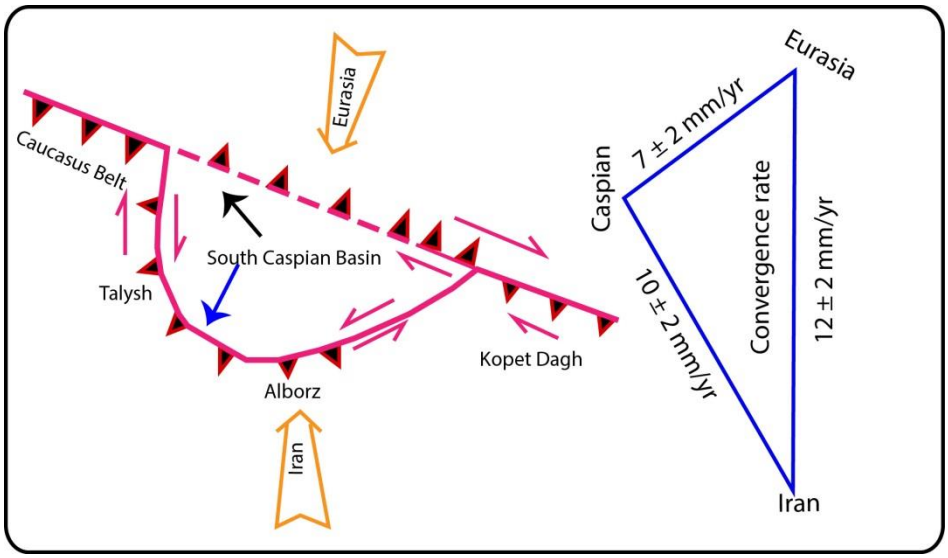

Figure 2.4. Sketch of the potential active tectonics of the SCB, the left hand sketch showing south to southwest under-thrusting in the west, south-west, south and east of the basin and north under-thrusting in the central Caspian, as well as showing the right and left lateral strike slip in Kopet Dagh and Alborz respectively, estimated SCB directions relative to Eurasia and Iran are illustrated in black and blue arrow in order. And the right hand sketch is a velocity triangle illustrating the relative motion between Eurasia, Iran and the SCB, after Jackson et al. (2002) and Allen et al. (2004)

2.3. Tectonic surroundings of the South Caspian Basin

2.3.1. Platforms

There are two platforms to the north of the SCB, which were formed throughout the Late Triassic and Early Jurassic and these platforms are represented by;

1. **Scythian Platform:** located in the north-western part of the South Caspian Basin, and to the north of the Greater Caucasus Platform (Figure 2.5) (Brunet et al., 2003).
2. **Turan Platform:** in the north-eastern part of the basin, converted southward to the foreland of the Kopet-Dagh (Figure 2.5) (Brunet et al., 2003; Thomas et al., 1999).

2.3.2. Foreland basins

The surrounding foreland basins record important information on the development of the SCB.

2.3.2.1. Terek–Caspian molasse basin

This basin is located in the north-eastern Greater Caucasus, to the south of the Scythian Platform (Figure 2.5), and is considered to be the foreland basin to the Greater Caucasus (Brunet et al., 2003; Saintot et al., 2006b). Subsidence started in the upper part of the Middle Jurassic 'Callovian' and continued until the Eocene.

2.3.2.2. Fore Kopet-Dagh molasse basin

This basin is about 45km wide, situated between Kopet-Dagh orogen and Turan Platform on the north-western part of the SCB. It is about 2.5 km thick (Upper Oligocene – Quaternary) overlying about 7km of Jurassic–Palaeogene strata deposited on its southern margin (Khain, 1994).

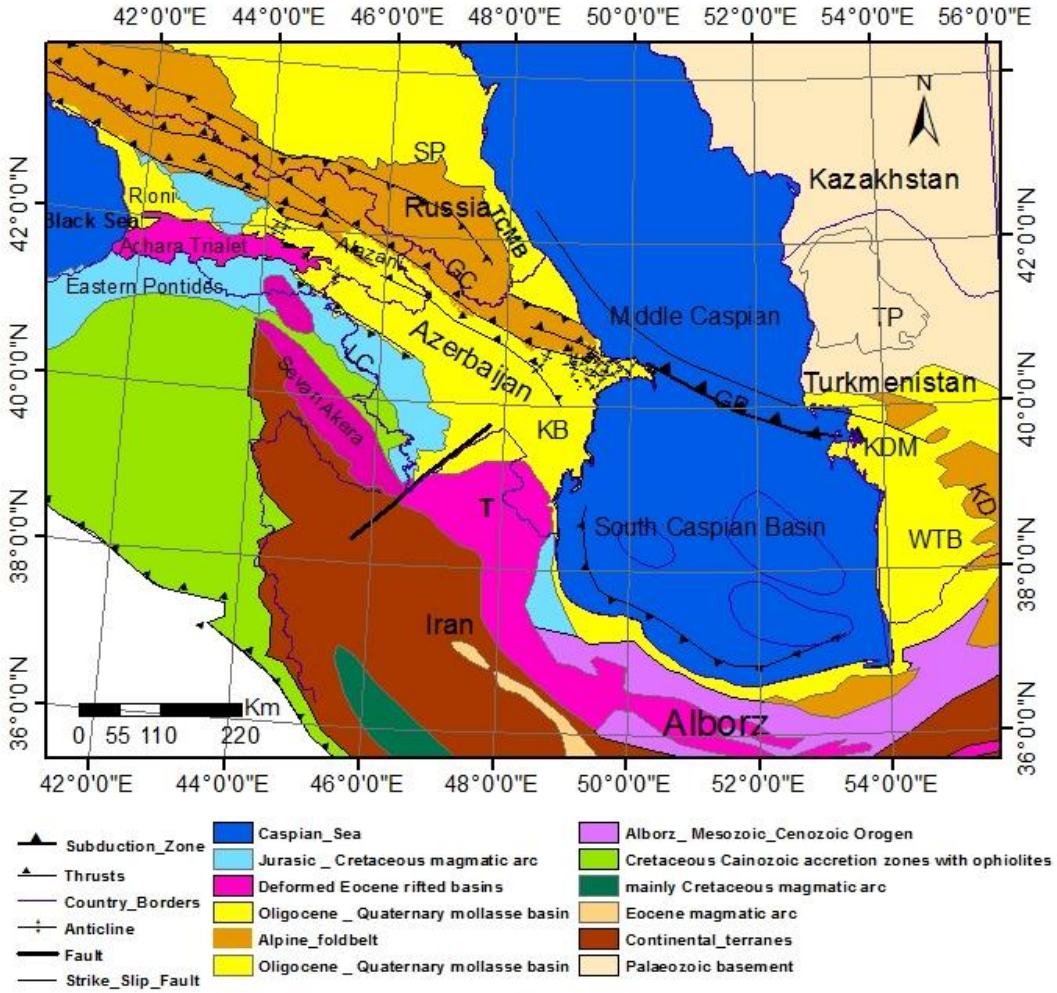

Figure 2.5. Simplified geologic map showing the main tectonic units of the South-Caspian area, GC = Greater Caucasus, LC=Lesser Caucasus, KD=Kopet Dagh, KB=Kura Basin, T=Talysh, GB=Great Balkhan, AB=Apsheron-Balkhan, TCMB=Terek–Caspian Molasse Basin, KDM=Kopet Dagh Molasse basin, TP=Turan Platform, SP= Scythian Platform. Modified after (Brunet et al., 2003).

2.3.3. Orogenic belts

Many orogenic belts surround the SCB, and it is important to understand these belts to investigate the Azerbaijan and SCB structures. These belts comprise the Apsheron-Balkhan sill to the north of the SCB and the east of Azerbaijan which extend to the northwest of Turkmenistan, the Greater Caucasus and Lesser Caucasus to the west of the SCB, the Talysh region south-west of the SCB, and the Alborz and Kopet-Dagh to the south and south-west of the basin respectively.

2.3.3.1. The Apsheron-Balkhan sill

The Apsheron-Balkhan sill occupies the northern side of the South Caspian Basin and it is considered to be a most important bathymetric feature which separates the SCB from the Middle Caspian Sea (Figure 2.5). The Apsheron Peninsula is the onshore continuation of this feature, and the sill and peninsula areas are formed from a series of anticlines mainly directed parallel to the topographic feature (Nadirov et al., 1997) that have been cut by faults (Gurevich and Chilingar, 1995). The sill is linked to the Greater Caucasus to the north west of the basin and the Kopet Dagh to the east, and is regarded as a vital location for petroleum production (Kroonenberg et al., 2000). The Apsheron Balkhan sill also corresponds with the most seismically active region in the SCB (Figure 2.2).

2.3.3.2. The Caucasus Mountains

Philip et al. (1989) suggested that the Caucasus is deforming at a rate of about 0.13 cm/yr. The range is accommodating a minimum N-S shortening rate of about 10 mm/year calculated from Global Positioning System surveys of the Greater and Lesser Caucasus (Allen et al., 2003; Reilinger et al., 1997). The accumulated seismic moment tensor of earthquakes, shows a rate of the deformation in the Caucasus is 1.3 mm/yr.,

which is less than expected, and it has been proposed that much of the deformation is aseismic (Philip et al., 1989). Some authors (e.g. Philip et al., 1989) have proposed that the Greater Caucasus is cut by a major NE-SW strike-slip fault, based on apparent offsets in the Moho contours and large scale morphology of the range.

The Caucasus Mountains can be subdivided into three parts; the first is the Greater Caucasus orogen which is the northern part of the Caucasus belts and it is an isolated range trending WNW-ESE and the second is the Lesser Caucasus to the south, it is a less distinct region, on the northern side of the Turkish-Iranian plateau and the two parts are separated by the Transcaucasus (Koçyigit et al., 2000).

i. Greater Caucasus

The Greater Caucasus (GC) range is located to the north west of the SCB and to the east of the Black Sea. The orogen is a northwest trending linear belt, exceeding 1100km in length, Even though, the Greater Caucasus region is not broad, its elevation reaches more than 4000 m above sea level close to its core. This decreases eastwards towards the coast of the Caspian Sea and the Apsheron peninsula (Jackson et al., 2002).

The Greater Caucasus is a fold-and-thrust belt that was created as a consequence of Cenozoic shortening and collisional structural inversion of a former Jurassic–Palaeogene back-arc basin (Adamia et al., 2011a; Adamia et al., 2011b; Adamia et al., 1981; Adamia et al., 1977; Brunet et al., 2003; Ershov et al., 2003; Mitchell and Westaway, 1999; Ruban et al., 2007; Shevchenko, 1972). Shevchenko (1972) reported that the basement of the Greater Caucasus consists mainly of crystalline basement, which comprises late Palaeozoic granites. However, this Palaeozoic basement (granite)

which is exposed in the central part is poorly known (Mitchell and Westaway, 1999; Shevchenko, 1972).

The crust in the GC exceeds 60km thick continental crust, the oldest layer which is granitic exposure in the centre of the belt, and its sedimentary cover of Palaeozoic - Early Cenozoic hemipelagic deposits across the centre and the southern part of the belt(Adamia et al., 2011a).

The Greater Caucasus trough opened during the Early Jurassic time above a thinned continental crust or oceanic crust (Brunet et al., 2003; Zonenshain and Pichon, 1986). Another trough along the southern branch of the former deep-water basin, opened during the Callovian – Tithonian. The closure of the Greater Caucasus Trough took place gradually from 'Bartonian' times, with the most important stage of collision in the 'Serravallian and Langhian' times and the main uplift happening during the period of the Late Zanclean – Holocene times (Brunet et al., 2003; Ershov et al., 1999; Ershov et al., 2003).

ii. Lesser Caucasus

The Lesser Caucasus (LC) volcanic belt lies in the southern part of the Caucasus Mountain belts to the south of the Transcaucasus and the Greater Caucasus region, is located in portions of three countries; Azerbaijan, Georgia and Armenia. It is considered tectonically as an active zone created in the Neogene as a result of the Arabian-Eurasian collision (Allen et al., 2003; Joannin et al., 2010; Mitchell and Westaway, 1999).Philip et al. (1989) has suggested that the Jurassic to Miocene deposits of the western Lesser Caucasus are folded and thrusted over the southern edge of the Rioni Basin. The region of the Lesser Caucasus consists of late Albanian-early Campanian ophiolitic mélange (Koçyigit et al., 2000), and also Middle Jurassic

rocks (Sosson et al., 2010b). Koçyigit et al. (2000) suggested that the volcano-sedimentary sequences vary in facies and age and are predominant in the Lesser Caucasus. They recognised that there are three sequences of volcano-sedimentary rocks in this region, separated by angular unconformities. The first sequence is Late Eocene to Early Miocene volcano-sedimentary rocks, which reach a thickness of around 5500 m. The second sequence contains Late-Miocene to Early-Pliocene volcanic rocks that exceed 500m in thickness. The third sequence is Lower Pliocene to Quaternary volcano-sedimentary rocks, that reach about 1000 m in thickness (Koçyigit et al., 2000). However on the other hand Dileka et al. (2010), Sosson et al. (2010b) and Golonka (2004) reported that there are numerous of the Mesozoic ophiolites in the Lesser Caucasus mountain belt that belonged to the Tethyan ophiolitic suture zone. This has led to Mesozoic geodynamic interpretation that the belt is related to the Northern Neotethys ocean closure.

iii. Transcaucasus

The Transcaucasus basins are located between the Greater and Lesser Caucasus and include the eastern Kura and western Rioni Basins which open toward the Caspian and the Black Seas respectively (Ershov et al., 1999). The Kura Basin is situated to the west of the SCB, and is bounded to the north by the eastern sides of the Greater Caucasus, and by the Lesser Caucasus to the south (Figure 2.5). The thickness of the Kura basin sediments in the southeast exceeds 20km but it is 10-15km in most parts of the basin. There is ambiguity about the relationship between the Kura Basin and the Arabia-Eurasia collision zone (Forte et al., 2010). In their study Nadirov et al. (1997) proposed that the Kura Basin has largely covered a Jurassic to Cretaceous island arc.

2.3.3.3. The Alborz

On the southern boundary of the SCB there is a province of active deformation called the Alborz range (Allen et al., 2002a) which was created initially in the Ordovician - Silurian by separation from Gondwanaland (Stampfli et al., 1991), however the present Alborz range is the consequence of late Cenozoic crustal shortening (Figure 2.6). With geomorphic similarities to the Greater Caucasus region, the Alborz Mountains is a narrow belt about 100km in width from north-south and up to 600 km long. The Alborz reaches above 4km in elevation with some peaks up to about 5.67 km in the Quaternary volcano (Damavand) in the core of the region (Allen et al., 2003; Jackson et al., 2002). North-westward movement of the SCB and the northward convergence of the middle of Iran toward Eurasia, created the tectonic framework which occurs in the Alborz range (Ritz et al., 2006).

Stocklin (1974)showed that the northern and southern thrusts of the Alborz belts have transport directions to the north and south respectively(Stocklin, 1974). The most important folds and thrusts which occur in the area from the east to west in the Alborz range change trend from ENE to WNW strike in the east and west respectively (Allen et al., 2002a).

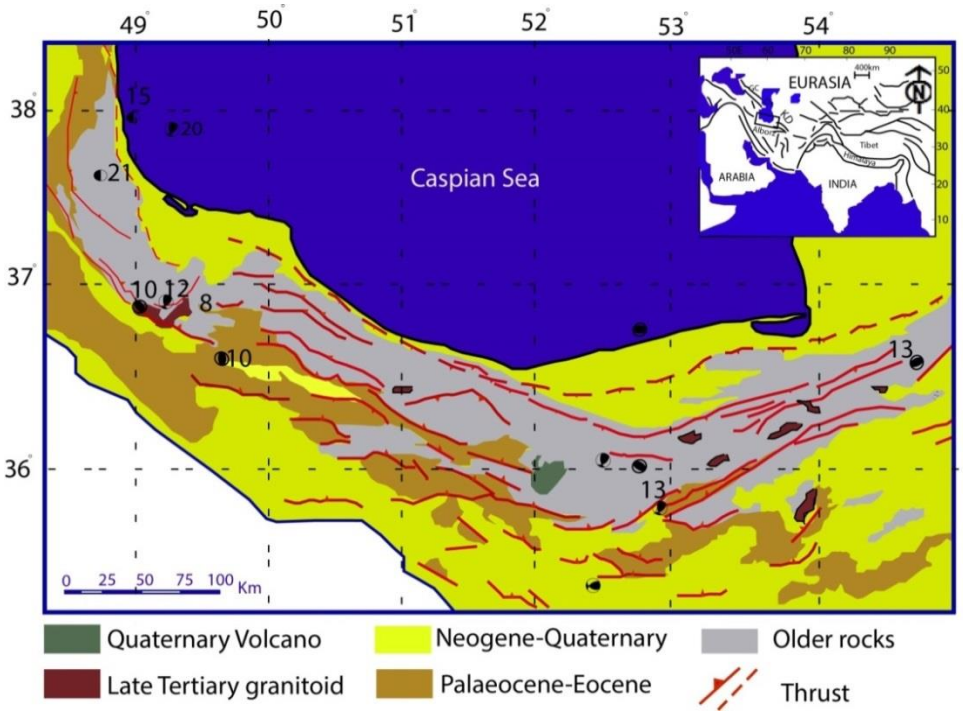

Figure 2.6. The Alborz region's geologic map from Allen et al. (2002a). Earthquake depths are shown by the numbers in (km).

2.4. South Caspian Basin Evolution and Stratigraphy

Estimates for the age of the oldest sedimentary strata in the SCB vary from Early Jurassic to Tertiary (Smith-Rouch, 2006). However, the Oligo-Miocene deposits of the Maykop Suite are the oldest proven strata that can be clearly identified across the basin. These mud-prone sediments occur at depths between 10–12 km in the centre of the basin, and are remobilised and extruded at the surface as mud volcanoes (Allen et al., 2003; Yakubov, 1971).

Additionally, the SCB has a huge amount of mud volcanism that is distributed all over the basin especially in the Azerbaijani sector (Nadirov et al., 1997). About one-third of the mud volcanoes that are known worldwide, are concentrated in this basin

(Yusifov and Rabinowitz, 2004)and located along the axes of anticlinal structures (Melik-Pashaev et al., 1983) (Figure 2.7).

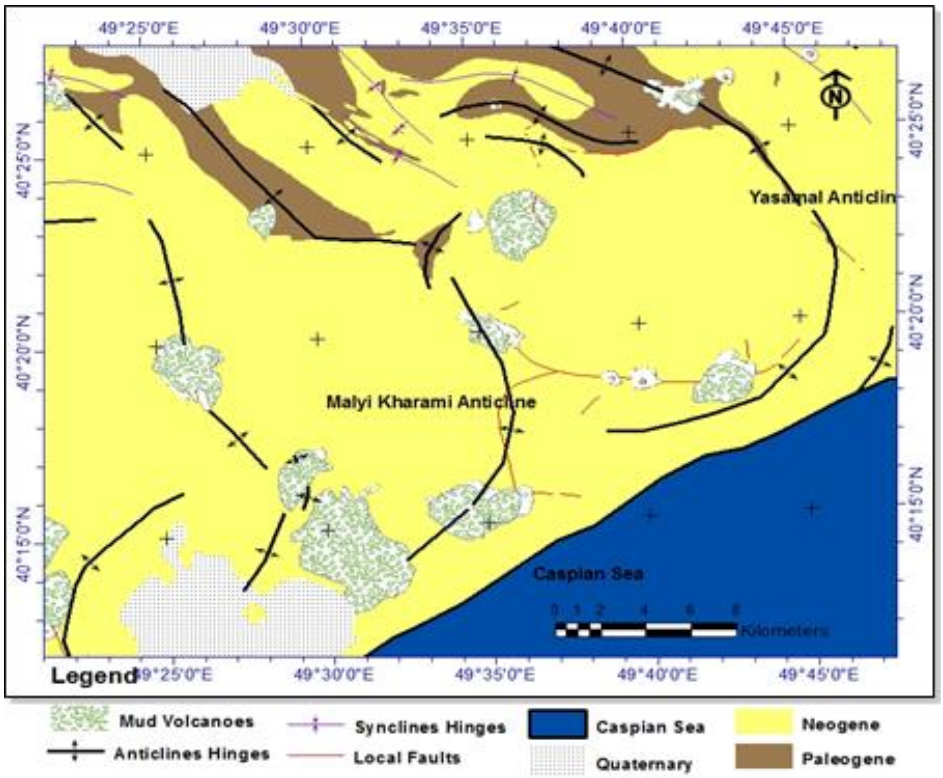

Figure 2.7. Geologic map shows the relationship between the Anticlines axis and mud volcanoes in part of the Azerbaijani sector of the SCB modified after Allen et al. (2003).

The most important regional source rock for hydrocarbons in the SCB is the Maykop Series. Hudson et al. (2008) divided the stratigraphic sections of east Azerbaijan (western part of the SCB) into three phases of Maykop Series strata, Early and late Oligocene (Rupelian and Chattian respectively) and Miocene. The Maykop passes conformably up-section into other, coarser units, such as the Diatom and Pontian suites (Figure 2.8). These sedimentary rocks are covered by late Miocene to early Pliocene fluvial–deltaic sands that are about 5km thick and were deposited in about 2Myr, and are known as the 'Productive Series'. The sediment came to the basin via many rivers, for example the Amu Darya River to the east, Kura River to the west and Volga Rivers to the north of the Caspian Sea. The Productive Series forms the main

hydrocarbon reservoir rocks in the basin (Jackson et al., 2002; Reynolds et al., 1998). This rapid deposition of sand above the mud sequence caused the over-pressure of the muds, and many of the hydrocarbon traps have been produced by post-depositional folding of the Productive Series (Jackson et al., 2002).

The basin is displaying a lack of stratigraphic continuity in some areas and it is also has a number of most important unconformities at the base of lower Miocene, and between the basement and the sedimentary strata (Figure 2.8).

2.4.1. Lower Permian strata

Lower Permian strata in the western part of the SCB (Apsheron and Kura) overlie pre-Permian basement, and are mainly marls, carbonaceous siltstones and limestones, signifying that the depositional environment was marine before the basin developed (Smith-Rouch, 2006).

2.4.2. Jurassic and Cretaceous sediments

In the Caucasus belt to the west of the SCB, Jurassic shales are exposed, and there are 3500m of Cenozoic and Cretaceous strata in the Lower Kura Depression deposited on 3000m of Jurassic volcanic rocks (Zonenshain and Pichon, 1986). The correlation between these rocks and equivalents in the deeper parts of the South Caspian Basin is still unclear.

2.4.2.1. Lower Jurassic rocks

Lower Jurassic rocks are present all over the Greater Caucasus belt, and reach up to 2km in thickness. Volcanoclastics comprise the vast majority of these sequences but

there are also some claystones, calcareous sandstones, and limestones (Smith-Rouch, 2006). During this time, sea covered most of the Caspian region from GC to the west to the Alborz and Kopet Dag regions to the south and south-west of the present Caspian Sea, and only small areas were emergent along these ranges (Lebedev et al., 1987). A huge emergent area to the north of the sea is thought to be the sediment supply region at that time.

2.4.2.2. Middle Jurassic rocks

Middle Jurassic rocks are approximately 1.5 – 3.5km thick and are in general tuff breccias, argillaceous shale and sandstones (Smith-Rouch, 2006). The basin became deeper during the Middle Jurassic where the shallow shelves were flooded bya transgressive phase in the southeast (Kopet Dag and Elburz).

2.4.2.3. Upper Jurassic to Lower Cretaceous

Egan et al. (2009) suggested that fossiliferous limestones of the Upper Jurassic to Lower Cretaceous were deposited in carbonate platforms in the Caucasus belts. In the Apsheron Peninsula region, the Upper Jurassic is between 0.6 – 2 km thick, and the lower and upper Cretaceous approximately 3km with about 1.5km of each. There is also approximately 10km thickness of Jurassic-Tertiary rocks in the eastern SCB (in the Kopet Dagh) (Green et al., 2009), based on seismic mapping and correlation with onshore successions.

2.4.2.4. Early Cretaceous strata

Rocks of this age range between 0.5 – 2km thick in the GC, and consist of calcareous flysch, mainly represented by clastic, tuffaceous, and calcareous rocks. There is about

0.9km thickness of Early Cretaceous shale with inter beds of marl and sandstone in the east and west of the Caspian Sea (Smith-Rouch, 2006). Interpretation of a number of wells in area to the northwest of the SCB in east Azerbaijan and the eastern side of the basin indicate that there is a relative tectonic constancy and stability in Early Cretaceous times (Smith-Rouch, 2006).

2.4.2.5. Late Cretaceous (Cenomanian)

By this time, the SCB was part of a back-arc basin that lay behind a series of island arcs between the Talysh and the Black Sea that was then covered by chalky deposits. The sequence of shallow marine Triassic to Cretaceous carbonates are present in the areas of the northern Kopet Dagh to the south-west of SCB and also in the Greater Caucasus mountains to the west of the basin on the Turan and Scythian platforms, covering Precambrian to Palaeozoic basement rocks (Green et al., 2009).

2.4.3. Cenozoic strata

2.4.3.1. Paleocene - Miocene

Smith-Rouch (2006) proposed that claystones, limestones and marls are the rock types which are most representative of the Palaeocene and Eocene strata. Furthermore, the sandstone, claystone, and organic-rich shales are representative of the Oligocene and Miocene strata “Maykop and Diatom groups”.

Based on a Geological Institute of Azerbaijan 2003 well report, Green et al. (2009) stated that the subsurface Paleocene and Eocene strata vary in thickness from 200-400m and 500-2000m respectively. Offshore, they propose a difference in thickness of Oligocene and Miocene strata in the range from approximately 1000m in the middle

area of the basin to around 2500m along the northern border of the SCB (Green et al., 2009).

i. Paleocene strata

These rocks have a thickness variation from one area to another around the basin. They reach about 1.7 km thick in the basin centre and more than 2.8 km thick in the north of the basin (Smith-Rouch, 2006).

ii. Eocene strata

During the Eocene, the Caspian Sea was separated from the Black Sea, and the sediment sources in Eocene were in the Alborz and Kopet Dag areas to the south and the Greater Caucasus region to the northwest of the basin. The strata are divided into Lower Eocene strata, which contain shale along with inter-bedded sandstone, limestone and marl and its thickness reaches about 0.8 to 1.2 km. these beds were followed by Middle Eocene strata with a thickness ranging from 0.1 to 0.4 km and an Upper Eocene sequence consisting of clay sediments with thickness of about 0.5 km (Smith-Rouch, 2006).

iii. Oligocene-Miocene sediments

The Oligocene sediments where deposited in a marine environment in the Caspian Sea from Kopet Dag to the east of the basin, with thickness of about 3km in the basin centre (Eyer et al., 1995). Organic-rich sediments accumulated in a marine environment in the early Miocene, creating the Maykop Suite. Strata consisting of shale, marl, sandstone and limestone were deposited in the Middle Miocene forming the Diatom Suite above the Maykop Suite (Berberian, 1983b).

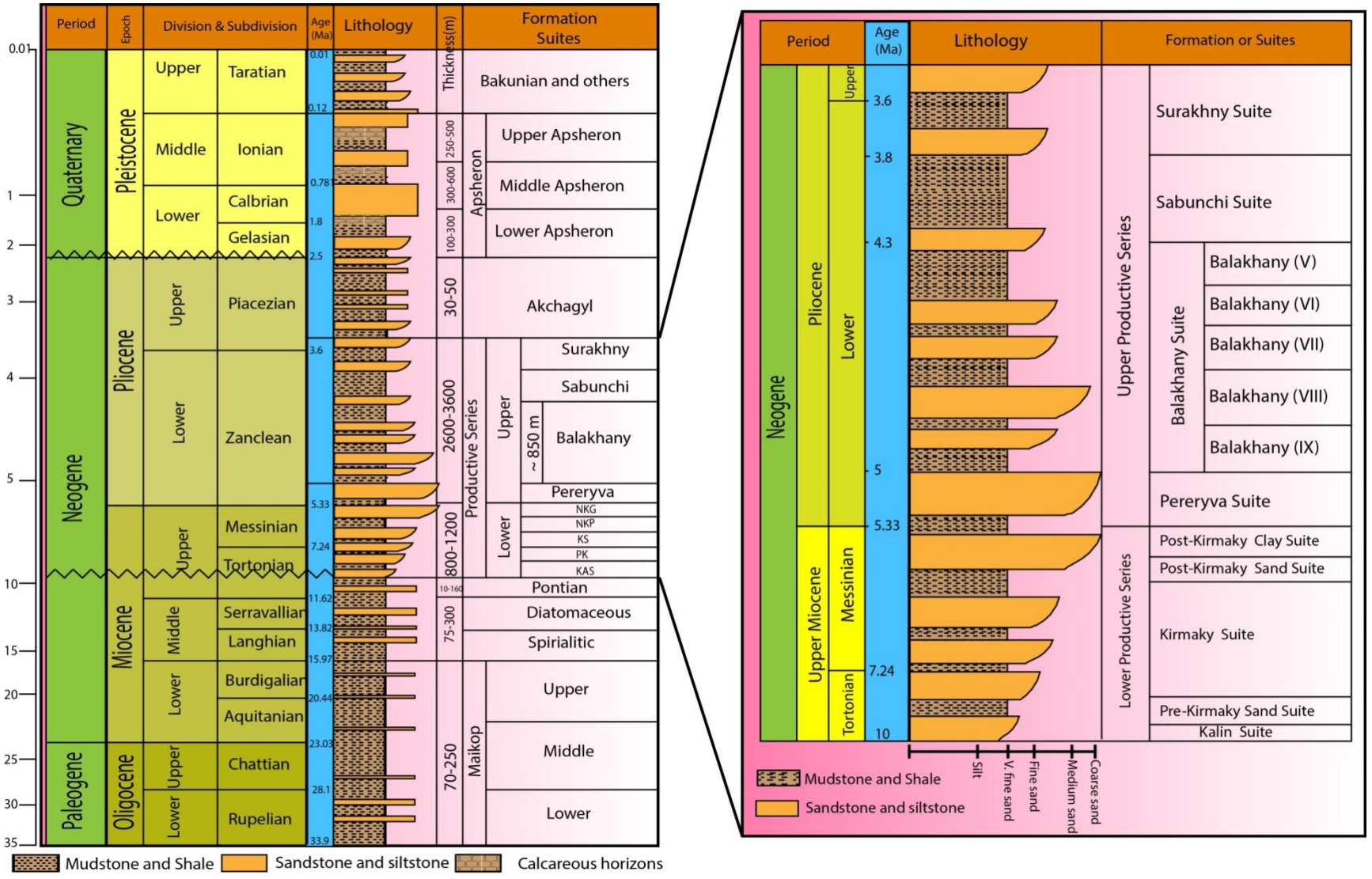

Figure 2.8. Stratigraphic column for the central South Caspian Basin (left hand side) modified after Devlin et al. (1999) and generalized stratigraphic column shows the lithology vertical changes of the Productive Series (right hand side) modified after Hinds et al. (2004).

2.4.3.2. Pliocene and Quaternary

An important change in sedimentation took place in the period just before Pliocene times. The area of the Caspian Sea today is about half of what it was before Pliocene times and was separated from the global ocean in the early Pliocene (about 5.3 Ma) in a large lake that included the Black Sea (Green et al., 2009; Jones and Simmons, 1996; Reynolds et al., 1998).

In the Kura Depression the thickness of early Pliocene deposits reaches more than 0.5 km of argillaceous sediments; however they increase in thickness and grain size towards the east via the Apsheron peninsula into the main South Caspian Basin. There is also an increase in thickness of the Pliocene sandstone strata close to the Apsheron Pribalkhan region at that time. There is evidence that there has been erosional processes operating in this region before the Pliocene era, where the upper Miocene is not present in several structures of the Apsheron Pribalkhan region (Frydl et al., 1995; Smith-Rouch, 2006).

The Productive Series of the upper Miocene/lower Pliocene ages is divided into two parts (Figure 2.8); The Early and Late Productive Series comprises the lower unit with a thickness in the range of 0.8 to 1.2 km, and the upper unit fluctuates between 2.6 and 3.6km in thickness. These Productive Series rocks are composed of shales and sandstones (Green et al., 2009; Smith-Rouch, 2006).

In the Upper Pliocene and overlaying the Productive Series, the Akchagyl Formation existed, which marks a return to open marine environments where this time records marine flooding and regional transgression. The period of the Plio-Pleistocene which considered as a compressional period that initiated by the end of the Productive Series

deposition, has witnessed the creation of the main offshore folds that known in the SCB (Green et al., 2009)

Figure 2.9a shows a structural cross-section from the central offshore part of the SCB to the north of the Apsheron Balkhan (Green et al., 2009), The section was drawn from a series of 2D deep seismic reflection lines and published information on the deep crustal structure of the area. The section shows the main tectono-stratigraphic units in the basin, which are included in Figure 2.8.

A relatively thin Cenozoic stratum exists in the northern part of the section (Figure 2.9 b), and they onlap over the Mesozoic sedimentary sequences which appear to have been subjected to rifting events represented by normal faults. The southern part of the cross section (Figure 2.9 c) shows Cenozoic sequences which are thicker than that in the northern part of the section, overlying Late Jurassic–Cretaceous sediment. Faulted and folded strata exist in the central part of the cross section and relate to the Apsheron Balkhan Ridge in the northern offshore part of the SCB.

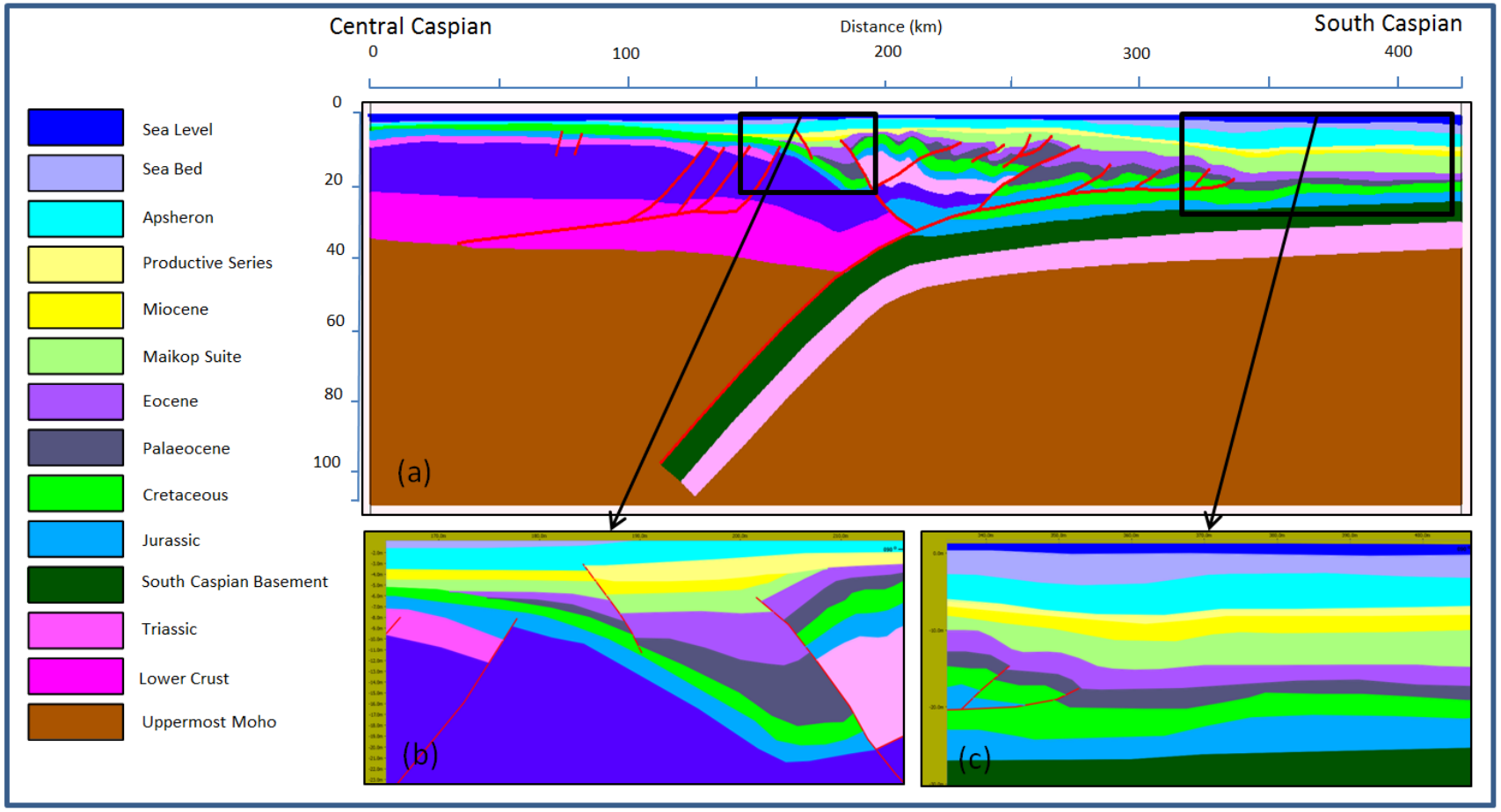

Figure 2.9. (a) Tectonic cross-section from Central Caspian to the South Caspian after Green et al. (2009), location shown in (Figure 2.1); (b) shows the northward onlap over the Mesozoic sedimentary sequences, (c) shows the thick Cenozoic sequences to the south.

2.5. Hydrocarbon Occurrence & Potential Source Rocks

2.5.1. Introduction and Exploration History

The Caspian Sea region is one of the world's most important oil-producing areas, with production that is nearly identical to the United States of America, and in addition, the Caspian Sea contains vast amounts of gas. Most of these oil and gas reserves in the Caspian Sea region have not been developed, and many areas of the Caspian region remain under exploration (Djevanshir and Mansoori, 2000). Approximately three hundred structures occur in the Azerbaijani section of the South Caspian Basin which might be oil-fields (Bagirov and Lerche, 1998; Mekhtiyev and Bagir-Zadeh, 1984). About 8km of sediments have been deposited just in 6-10 million years, with about 3km in the last 1-2 million years (Stephan J. D et al., 2008). Consequently, the basin is considered a young petroleum system, and the speed of sedimentation has caused disequilibrium in the basin (Stephan J. D et al., 2008).

Shallow digging by hand was the main approach for extracting oil until the early decades of the nineteenth century. Thereafter the importance of oil increased, which made it necessary to develop new extraction methods and led to the emergence of hand drilled wells that reached 20m in depth (Guliyev et al., 2003). *Semyenov*, an engineer from Russia, drilled the first oil well in history on the Bibi-heybat anticline of the Apsheron Peninsula in 1848 (Abrams and Narimanov, 1997; Narimanov, 1995). At the beginning of the 1900s or shortly before, work began on drilling in the offshore, and the Caspian Sea was the location for the first offshore well worldwide. An important improvement in offshore production initiated occurred in 1924, when a

wooden platform was built near Baku for well drilling, which was also a world first(Narimanov, 1995).

A great offshore oil field was discovered in 1949 in the eastern Apsheron Peninsula called 'Neft Dashlari'. To explore in deeper waters, portable exploration rigs were used in 1960's, and had reached up to 200m of water depth by 1979 (Guliyev et al., 2003).

(Klett et al., 1997) ranked the SCB Province as the 23rd largest petroleum Province worldwide, with known petroleum volumes of 17.4 (BB) billion barrels of oil and 36.0 (TCF) Trillion Cubic Feet of gas. Despite the fact that the stratigraphic interval for the hydrocarbon accumulations is from Paleocene to Pliocene or from Upper Cretaceous to Pliocene, the important hydrocarbon reserves (about 70%) are found in the Pliocene, where about forty productive horizons have been identified (Guliyev et al., 2003).

2.5.2. Oligocene–Miocene Maykop/Diatom Source Rock

It is widely believed that the Oligocene–Miocene Maykop/Diatom Shales (Figure 2.8)are the main petroleum source rock in the SCB (Inan et al., 1997) and it is present throughout the whole basin. Katz et al. (2000) confirmed that the oil source is the Maykop Suite. However, they were not able to show that the Diatom Suite was a source rock. In their investigation (Tawadros E. D et al., 2006) proposed that the hydrocarbons of the Azerbaijan district of the SCB were created by the Maykopian Group in the Oligocene and Early Miocene and they considered this group to be the potential source rocks for the basin's hydrocarbons, the oil then migrated and was trapped in the overlying Pliocene Productive Series.

Oligocene–Miocene Maykop Group has been divided into Lower, Middle and Upper Maikop (Abrams and Narimanov, 1997) (Figure 2.8), and they noted that oils that came from Upper Miocene reservoirs were almost certainly derived from the Lower Maikop Formation whereas oils produced from reservoirs of the early Piacenzian (Upper Pliocene) Productive Series and younger were most Probably derived from Middle, Upper Maikop and Diatom suite (Abrams and Narimanov, 1997).

2.6. Chapter Summary

Although there are many studies have described the tectonics and structures of the SCB and Caucasus regions which have very complex geology and the SCB is one of the most important economic areas worldwide, the geological knowledge of this region still somewhat imperfect.

This part of the project is illustrating the background of the SCB and the Caucasus region, to make a solid basis for the next chapters which i) use digital topography to relate the tectonics, landscape and climate of the Greater Caucasus, ii) describe the major structural elements of the Greater Caucasus belt, and the western SCB, iii) study and interpret the structures of the Yasamal anticline.

The complex structural element of the SCB is a part of the Alpine fold belt area between the Himalayas and Mediterranean. The Basin basement age is disputed between Jurassic and Palaeocene. There are active earthquake belts bordering the basin which are shallow <30km, except along the Apsheron Balkhan sill to the north of the basin which is the eastern continuation of the Greater Caucasus, where the depths exceed 80km, suggesting early stages of subduction zone beneath the central Caspian.

The Caucasus range is a part of the Alpine–Himalayan orogenic belt, created as a result of Arabia-Eurasia continental collision. The Greater Caucasus is largely a fold-and-thrust belt that was created as a consequence of Cenozoic shortening and collisional structural inversion of a former Jurassic–Paleogene back-arc basin. The crust in the belt exceeds 60km thickness, the oldest layer of which is granitic in nature and exposed in the centre of the belt. A sedimentary cover of Palaeozoic - Early Cenozoic deposits occurs across the centre and the southern part of the belt.

Chapter III

Methodology overview and Datasets

3. Methodology overview and Datasets

3.1. Geologic and Topographic Maps

All the available data were integrated using Move software version 2010.1 (subsequently updated to versions 2012.1, and 2013.1.2 as the project progressed), ArcGIS, Global Mapper, GoCAD and Google Earth and the work flow can be summarized as follows:

- The first task was to register available scanned maps. Scanning makes the analogue data available in a digital form. Main map data are a geological map at 1:500,000 for all of the Caucasus belt, six geologic maps at 1:200,000 scale covering the eastern part of the Greater Caucasus from theMinistry of Geology and Mineral Resources USSR (1960), and a map at 1:50,000 scale on the Yasamal Anticline from theMinistry of Geology and Mineral Resources USSR (1963).
- The processing software Move and Arc-Map (version 9.2) were applied to create automatically Arc Coverage files from the digitized data and this was used as a base to interpret the structures in the study area.
- A Digital Elevation Model (DEM) representing the topography as an image file was created automatically from contour lines (Figure 3.1a). This DEM was used to create the profile lines for cross sections that were constructed in 2D Move.
    - Cross sections were constructed from satellite imagery interpretations, the digital geological maps and previous published structural maps for the study area.

More detail on each of the specific workflows involved in each part of the study, is provided in the relevant chapter (chapters 4-6).

3.2. Satellite images

A remote sensing interpretation was conducted to map structures and morphometric features such as folds hinges and limbs, faults, mud volcanoes and the main rock types and stratigraphic boundaries in the study area. The sources that were used for remote sensing interpretation are:

ETOPO (Topographic and bathymetric map) and **SRTM** (*Shuttle Radar Topography Mission)* is a digital elevation model derived from radar interferometry data obtained during a space shuttle mission. This has resolution of 90m pixels from http://srtm.csi.cgiar.org(Jarvis et al., 2008), which give a sufficient resolution especially when conducting the investigation over large areas. SRTM data for Eurasia have a circular absolute geo-location error of about 9m with linear vertical absolute height error of 6.2m and linear vertical relative height error of 8.7m which met and exceeded the SRTM performance requirements, (≤20m, ≤16m and ≤10m respectively)(Rodriguez et al., 2005). In addition, such data can be analysed without the necessity for high-specification computers, however, it is difficult to recognise and categorise the geological features of the area being investigated using SRTM data alone. SRTM data was used for the topographic studies to map the geological and topographical features of the area under investigation and to verify the validity of existing and previously published maps (Figure 3.1b,c).

SPOT satellite imagery was used to identify the structures that were not observable by using other images because this imagery has high resolution (2.5m) (Figure 3.1d).

The geological and topographical features were interpreted digitally by using a number of software packages such as ArcMap-10, Global Mapper, Paradigm Go-Cad 2009.2, and Midland Valley's Move application. The latter offers a useful standalone

tool for data incorporation and for constructing cross-sections by using 2D-Move (where the data in this application is limited to the co-ordinates of (x & y) or (x & z)). In addition, the Midland Valley package was used to build 3D models by 3D-Move (where the data in this application has x, y and z coordinates). All of these structural and topographic interpretations were used to produce a new geologic map of the area, to enable cross sections to study the evolution of the structures in the region to be constructed. The database also provided a basis for morphometric studies of the Caucasus belt and the relationship between the tectonics and the morphometric processes and climate.

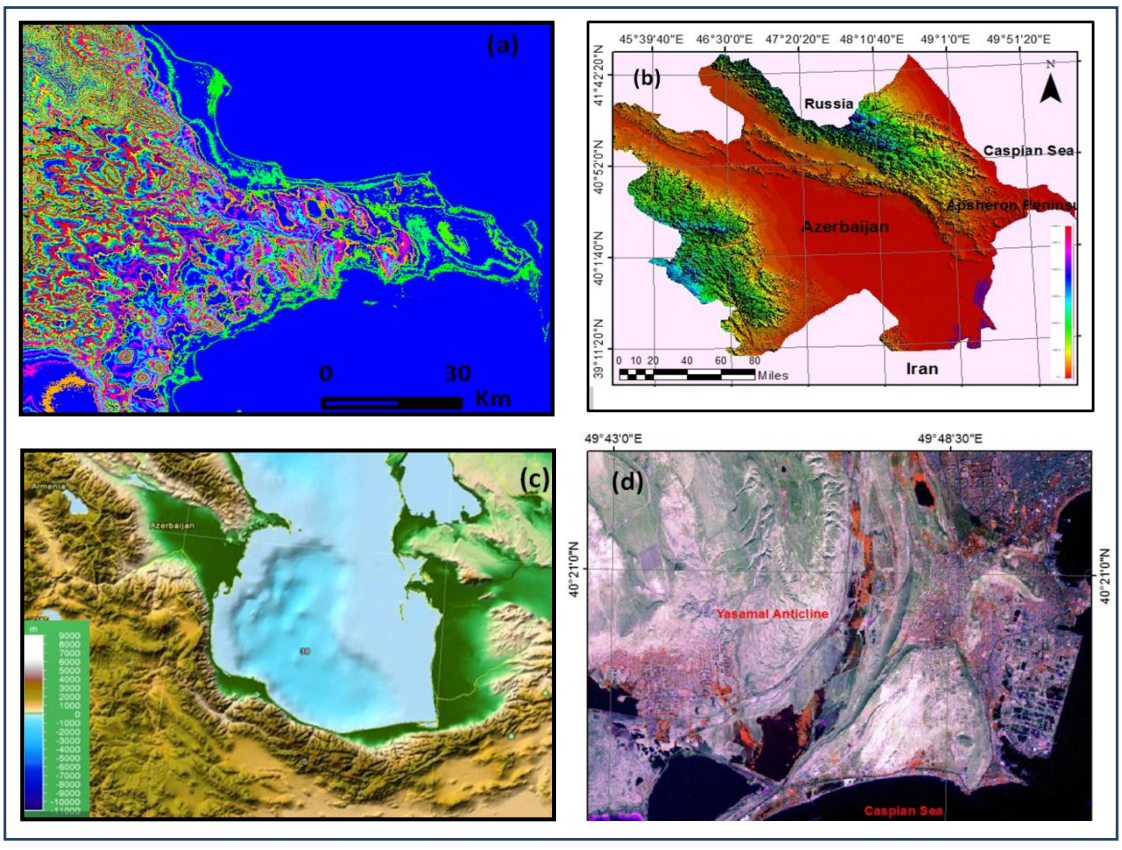

Figure 3.1. Showing some of data types used in this project: (a) is a contour map of Azerbaijani sector of the SCB, (b); is a SRTM DEM Map, of the Azerbaijan and GC, (c); ETOPO map of the SCB, (b and c) are used for the correlation between the tectonics and topography of the area under investigation, and (D) is a SPOT satellite imagery of the Yasamal Anticline.

3.3. Terrestrial laser scan data

A digital 3D field dataset for the Yasamal Anticline (Figure 3.2) to the west of Baku (Capital of Azerbaijan) was previously collected for BP Azerbaijan by McCaffrey, K.J.W & Jones R.R. in (2007) and made available to this study. These data enabled a very detailed interpretation of the Yasamal Anticline (reverse and strike-slip faults, small folds and layer boundaries). The aim here is to evaluate the evolution and development of Yasamal fold and then make a correlation between the geometry of this fold and the surrounding folds that are distributed in the South Caspian Basin. Furthermore the laser scan data used to create cross sections to enable comparison with those from geological maps of Yasamal Anticline and to investigate strain accommodation mechanisms using 3D Move to unfold the Yasamal structures.

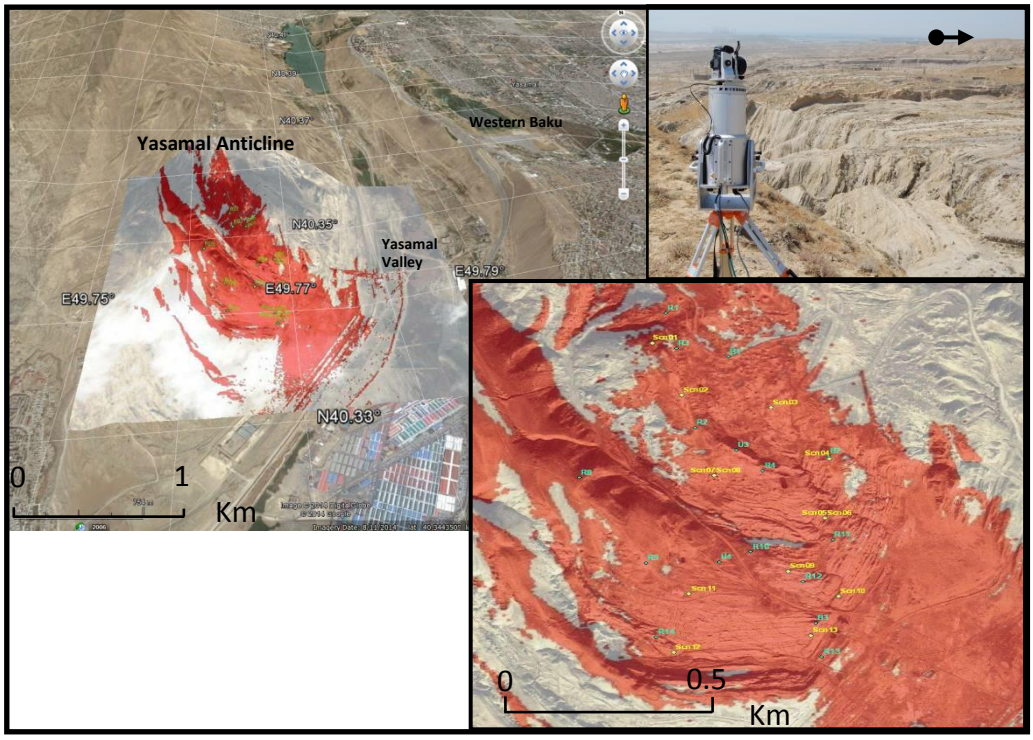

Figure 3.2. Shows an overview of the area (on Yasamal Anticline), that has been covered by the Terrestrial Laser Scanning (ground-based LiDAR). Yellow points refer to scan stations and light blue points refer to GPS survey points.

3.4. Workflows and Computer Software

This research makes extensive use of a variety of software packages to analyse and interpret the available data.

3.4.1. Structural Modelling (Small and large scale)

a. RiScan PRO Software is the software package for Riegl Terrestrial 3D Laser Scanner Systems. A large number of tasks associated with laser scanning including sensor configuration and acquisition, visualization, manipulation and archiving of the data (data include scans, digital images, GPS data, and coordinates of control points and tie points). RiScan PRO software has been used in this project to interpret faults, fractures, small folds and layer horizons in the laser scan that were collected previously for the Yasamal Anticline(Figure 3.3c).

b. **Paradigm GOCAD Software** is a software package for 3D modelling in geology (constructing horizon and fault surfaces and modelling) and in this study version 2009.2 was used. The structural and horizon interpretations from the laser scan data were joined into a single surface (Figure 3.3d).

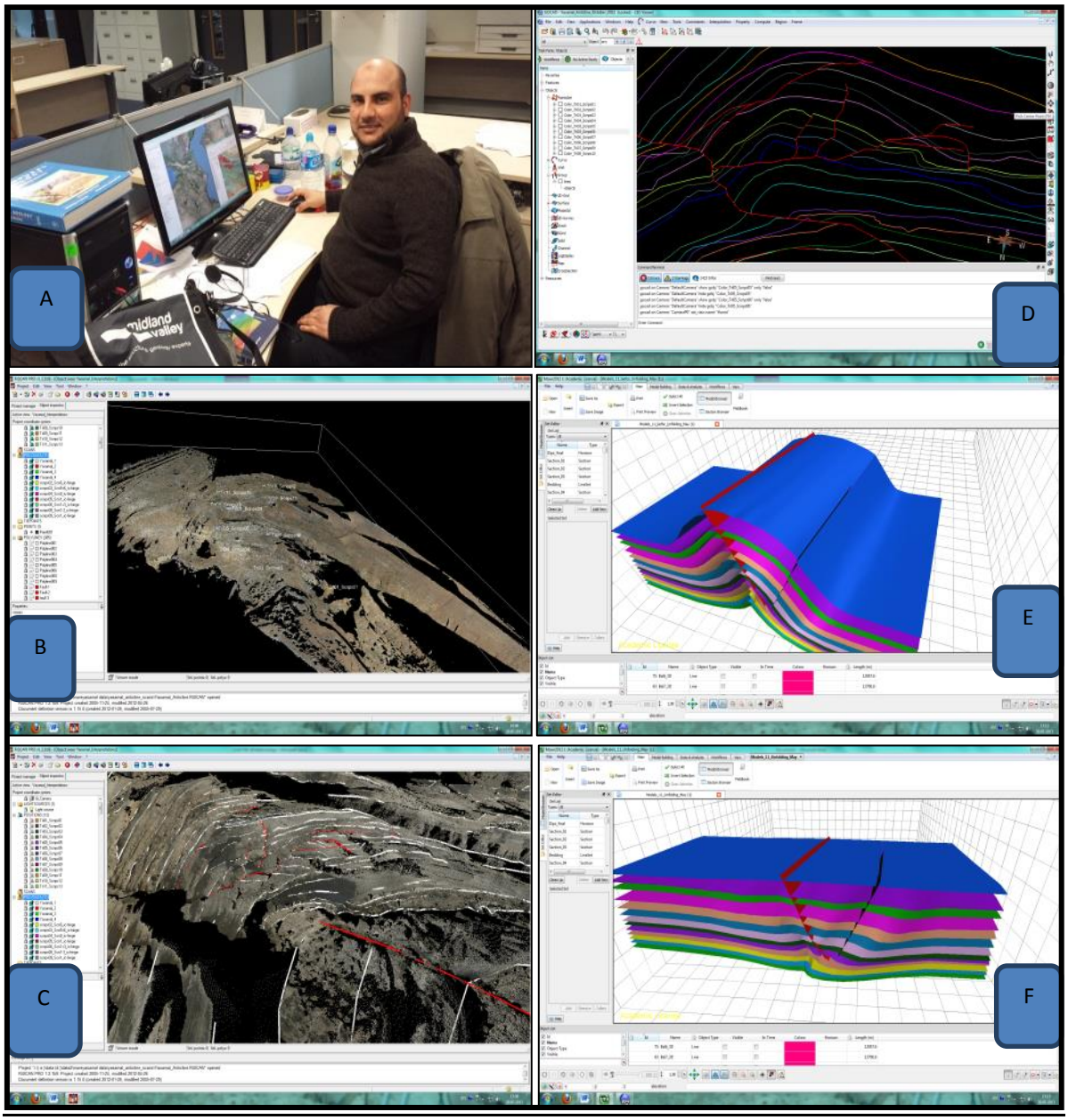

Figure 3.3. Examples of the data, their interpretations and results using variety of software that have been used in this project; (A) shows the author at his workstation, utilising analytical softwares, (B&C) show Terrestrial Laser Scanning data for Yasamal Anticline and their interpretation by using RiScan PRO Software, (D) is the same interpretation but after enhancement in Go-CAD and (E&F) show the models of the Yasamal Anticline before and after unfolding respectively.

a. Move Software; is structural modelling and analysis software package from (Midland Valley Exploration Ltd), used to build geometrically valid geological interpretations, to improve models and to test and understand geological concepts. This software includes 2D/3D model building and editing on surface or sub-surface models, and is considered an advanced structural modelling platform because it has Fracture, Geomechanical and Kinematic modelling modules (2D Move, 3D move) (Figure 3.3e-f)..

3.4.2. Geological and Morphological Studies (regional scale)

At the regional scale, the geological and morphological studies of the area under investigation many types of software have been used in the existing project;

a. Geographic Information System; ArcGIS (Arc-Map);

Geospatial database systems (Arc-Map Software) provide the platform for handling the large amount of data required to investigate the geological and topographical maps and remote sensing data.

The GIS data used in the existing project are of two types, the first type is spatial data, that represent the geographic location of features (normal and reverse, strike-slip faults, topographic contour lines), and the second is non-spatial (attribute) data; that provide descriptive information such as the geologic unit's name, abbreviation, description of those units, colour code of any element.

To provide a regional surface a geologic map of the whole area, 10 geological maps with different scales covering the area under investigation have been geographically registered and used together with the remote sensing data for detailed interpretation of the investigated region (Figure 3.4) is an example.

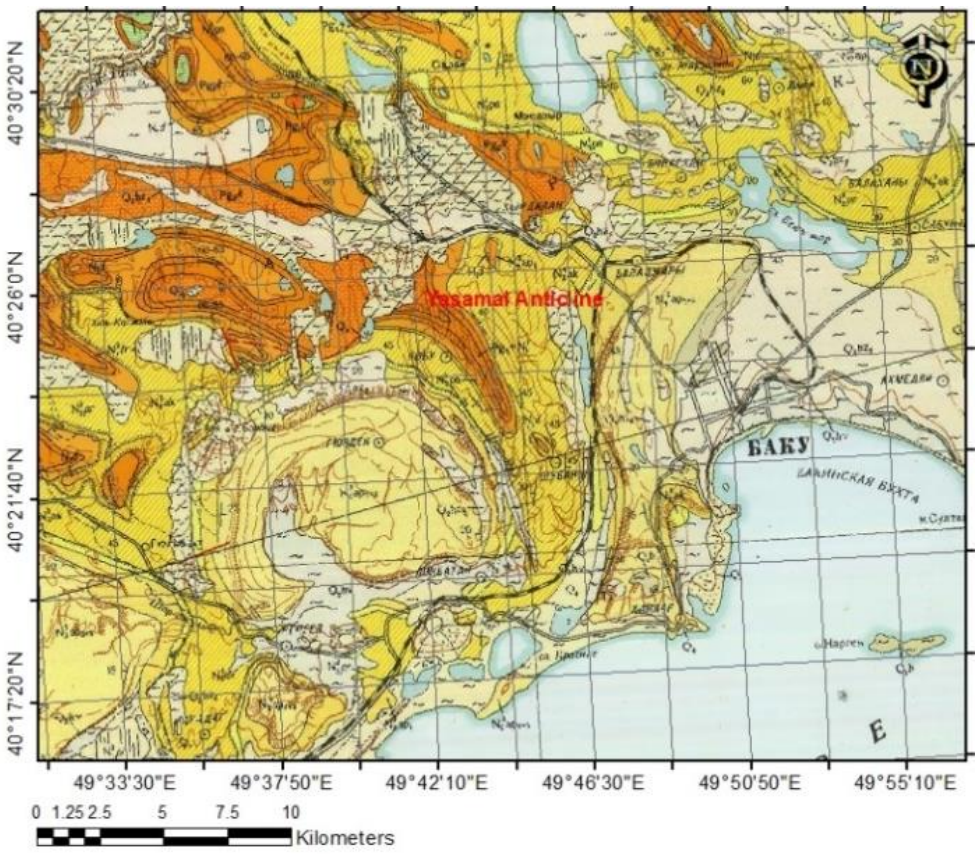

Figure 3.4. A geologic map of the Yasamal area, as an example of the geologic maps that were used in this project from the Ministry of Geology and Mineral Resources USSR (1963).

b. Global Mapper (Version 9.01);

Global Mapper is a (GIS) software package which is powerful tool especially useful for dealing with topographic data in vector or raster format. In the existing project this software was set to study the relationship or the correlation between the tectonics and the topography of the study area (Figure 3.1b, c).

3.5. Chapter summary

This study has been carried out using a diverse range of research methods, and the principal datasets, methods, workflows and software packages are reviewed in this chapter.

A large database containing information on structural features in the study region including folds, faults and fractures for the area under investigation were obtained from several sources, comprising geologic and topographic maps at 1:50,000 and 1:200,000 scales, field data (dip data, laser scan data and photographs), remote sensing data including freely available satellite imagery data (Ikonos, Spot, Mr-Sid images, SRTM and ETOPO) and published reports.

Chapter IV

Thecorrelation between tectonics, topography and the climate of the Greater Caucasus and comparator orogens

4. The correlation between tectonics, topography and the climate of the Greater Caucasus and comparator orogens

4.1. Introduction

Plate margin type and spatial setting are the main factors that determine the presence of mountain ranges and tectonic processes are the main control on their formation and evolution. Climate can be another important factor in mountain range development. Faster rates of erosion can cause faster exhumation, which therefore affects the structural style of a mountain range (Bishop et al., 2002; Gilchrist et al., 1994; Montgomery, 1994). Understanding how tectonics and climate impact on the topography is complicated and unclear because of the various processes that may affect erosion rate. Erosion affects the isostatic balance of the crustal block, where the vertical stress changes by material exhumation, and in turn this changes the distribution of structures and the rates at which they operate (Dahlen and Suppe, 1988). The surface processes resulting from climate are able to configure extreme relief and rugged topography by accelerating the tectonic processes as a result of reducing the lithospheric mass (Bishop et al., 2002) which means that reducing overburden allows further thrusting to take place.

The critical wedge taper theory that forms under horizontal compression is recognized as a worthy way to understand the morphology and the internal mechanics of the ancient and active orogens at large scale(Dahlen and Suppe, 1988).The first-order mechanics is illustrated by the similarity of a bulldozer pushing sand whereby a wedge grows self similarly as soon as the critical taper is reached (Dahlen and Suppe, 1988). The critical taper angle is that angle in between the detachment surface and the

surface slope of the wedge, which is controlled by strength stability and balance of the deforming wedge material and detachment surface (Figure 4.1). Critical taper deviations can occur as a result of instabilities in a wedge which occur in subcritical wedges (taper angles < critical value) and supercritical wedges (taper angles > critical value) where the wedge is considered unstable mechanically in both states and starts internally to deform to achieve the stable taper value(Dahlen, 1984). Insights from the critical taper wedge mechanics suggests that upper-crustal shortening plays an important role in developing the topography of the Greater Caucasus belt.

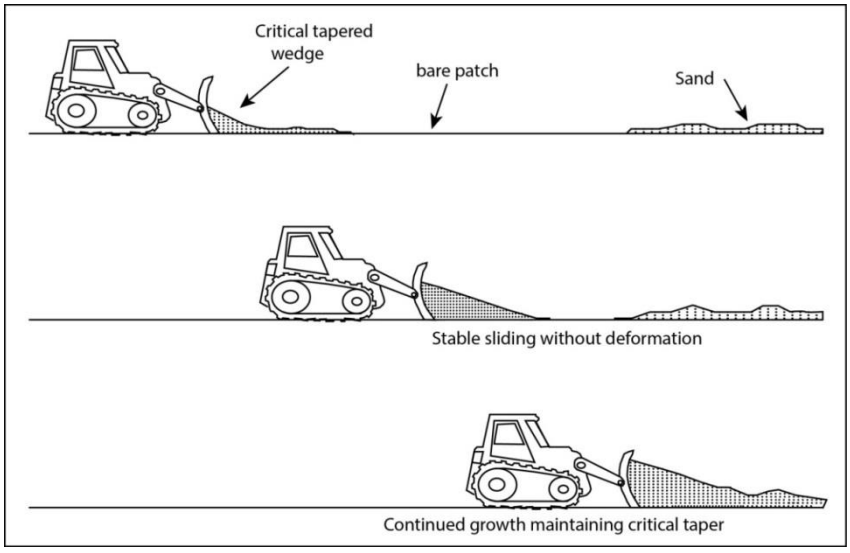

Figure 4.1. Illustrating the critical wedge theory as a wedge of sand in front of a moving bulldozer, the critical taper is the shape that is just strong enough to be slid over a bare patch without steepening or deforming, from Dahlen and Suppe (1988).

The mechanisms and processes involved in continental deformation, as well as those of mountain belt production and its development, are important questions in geological and topographical studies (Clark, 2012; Hatzfeld and Molnar, 2010). Therefore, this part of the research addresses the relationship between tectonics, climate, terrain and topography of the Greater Caucasus Mountains at the largest scale, and compares these features with selected other mountain ranges of the world.

These include active and inactive mountain belts, as well as volcanic and non-volcanic belts, and they vary in climate zones and location on the Earth. The comparator belts are the Pyrenees of Western Europe at the boundary between Spain and France which is a relatively inactive belt and the Tibetan Plateau between China and India which is an active belt. In particular, the Himalayas to the south of the plateau is considered to be an ideal place to study the relationship between tectonics, climate and surface processes because climate variability and geological processes are the cause of the western Himalayas drastic relief (Bishop et al., 2002; Shroder et al., 2000; Zeitler et al., 2001). The aim of the present study is to determine or better understand the role of climate in topographic development.

4.2. Topographical and Geographical setting of the Greater Caucasus.

4.2.1. Greater Caucasus Topography

The Greater Caucasus range is an elevated strip separating Europe and Asia that contains the highest peak in Europe, Mount Elbrus (which is a Quaternary volcano). This peak is located in the west of the belt and has an elevation of 5642m a.s.l., and mainly contains Quaternary volcanic rocks (from the geological map of the Elbrus stratovolcano. Scale 1:50,000 edited by Gurbanov et al. (2004)). The range is a 1200km long northwest-southeast trending linear belt, extending between the north-eastern Black Sea to the west and the Apsheron Peninsula and the Caspian Sea to the east. Its elevation decreases eastwards towards the coast of the Caspian Sea and the Apsheron peninsula. Overall the western part of the belt has a number of peaks that exceed 5,000m high surrounding the Mount Elbrus, such as Dykh-Tau at 5,205m in elevation, Shakhara at 5,201m and Koshtan-Tau at 5,151m high, whereas the highest peak in the eastern part does not exceed 4,500m high.

The Greater Caucasus is described as a fold-and-thrust mountain belt that was created as a consequence of the Cenozoic shortening and syn-collisional structural inversion of a former Jurassic to Palaeogene back-arc basin (Adamia et al., 2011a; Adamia et al., 2011b; Adamia et al., 1981; Adamia et al., 1977; Brunet et al., 2003; Ershov et al., 2003; Mitchell and Westaway, 1999; Ruban et al., 2007; Shevchenko, 1972). Shevchenko (1972) reported that the core of the western part of the belt consists mainly of crystalline basement, which comprises late Palaeozoic granites, however the bulk of the exposures are mainly Mesozoic sedimentary rocks.

4.2.2. Climatic setting and Annual precipitation

Climate is considered one of the chief factors that affect and contribute to development of landscape due to its control on the hydrologic system and consequently erosion. Climate conditions include temperature, precipitation, groundwater, glacial activity and wind. In the continents, the climate is affected not only by latitude but also by altitude, where temperatures in the highlands are lower than in low-lying areas.

The Greater Caucasus belt forms a boundary between the subtropical climatic zone and the temperate mid-latitude climate zone, obstructing the movement of cold and warm air masses from north to south and vice versa. Temperatures in the Caucasus belt depend on the location (north, south, east or west of the belt), elevation and the season. On average they range in winter from (-5°C) in the north, up to (6°C) in the southwest part of the belt and about (3°C) in the southeast. In summer, temperatures are similar in the north and south of the belt, whereas they have a discernible divergence between the east and west where in the eastern side the temperatures are higher than the western side of the belt (Bochud, 2011; Kurtubadze, 2008).

To the west of the belt and up to 2km in elevation, the winter is defined as lasting from December to February, with freezing temperatures from -5 to -15°C; however above 2km the winter lasts for about six months from October to April with temperatures from -7 to -20°C, with about 3m snow cover. The summer lasts from May to September with temperatures of 16-23°C, up to 2km, whereas the summer season lasts not more than two months in the crests above 4km high.

The climatic characteristics show differences moving from west to east across the belt. To the west, it is a maritime climate with increasing continental-type climate towards the East. Semi-arid climate is dominant in the north-western GC, and drier

climate (annual rainfall about 300 mm) in the northeast of the belt, whereas humid subtropical climate is prevalent in the southwest with precipitations exceed 1,500mm (Figure 4.2). The northern Lesser Caucasus has a climate similar to the southern Greater Caucasus at the same heights.

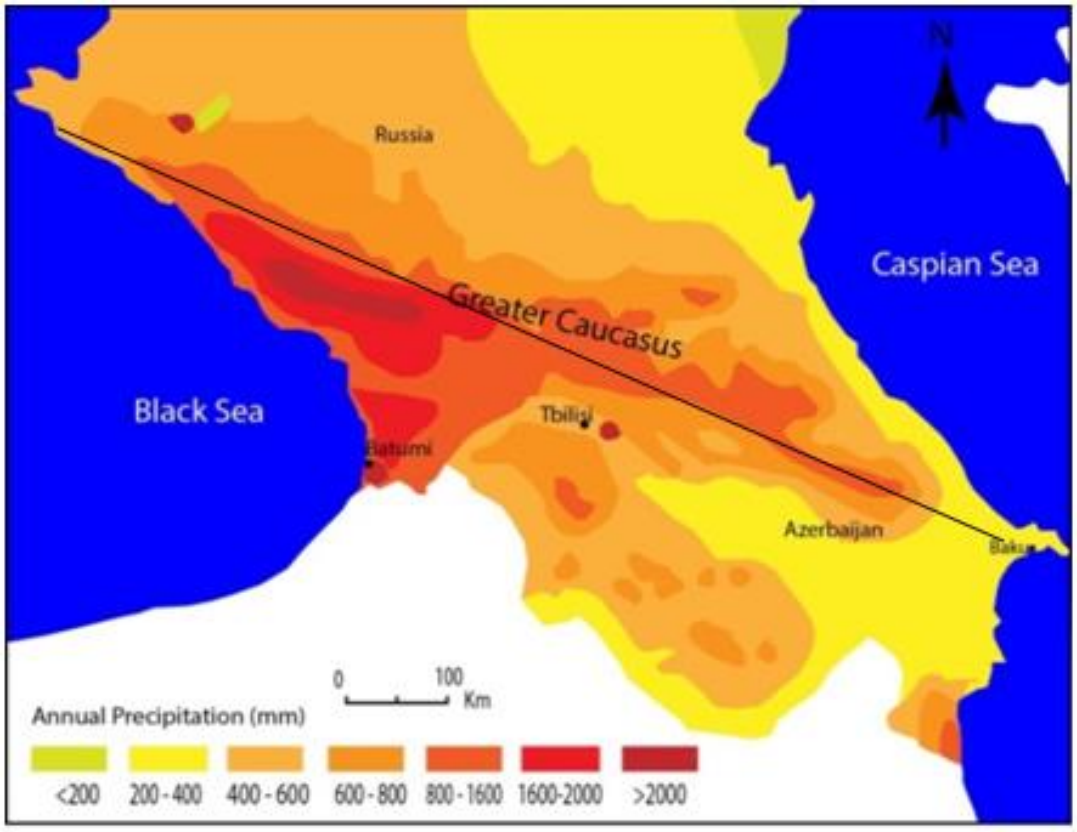

Figure 4.2. Annual precipitations map of the Greater Caucasus modified after Kotlyakov and Krenke (1980), the black line is location and orientation of the profile in Figure 4.10.

Precipitation varies from place to place and from one height to another, from the precipitation map of the Caucasus region modified after Kotlyakov and Krenke (1980)(Figure 4.2) it can be seen that the annual precipitations were greater in the western region of the belt than in the eastern part with about from 1– 4 m/yr. to the west and from 0.6 – 1.8 m/yr. to the east. The driest place over the entire belt is the north-eastern region, and the northern side of the belt has less precipitation than in the southern side. The average annual precipitations in specific areas are 2,704 mm in

Batumi, 497 mm in Tbilisi and 240 mm in Baku (Figure 4.2).The belt is known for dramatic accumulations of snow reaching 5m – 7m in some places, particularly in the south-western areas of the belt (Stokes et al., 2006).Also, the snowfall is low to the east and high to the west with existence of avalanches in the western area, where an area of about 1500 km^2 in the Greater Caucasus has covered by glaciers (Bedford and Barry, 1994), existed in the western and central parts of the belt, although the largest valley glaciers are mostly in the areas of over 4000m height which represent the central Greater Caucasus (Kotliakov and Krenkea, 1981).

4.2.3. Hydrographical setting

The hydrography of the Greater Caucasus is associated with major water bodies surrounding the belt represented by Caspian Sea, Black Sea and Azov Sea to the east, west and to the northwest of the belt respectively (Figure 4.3). The Caspian Sea represents the biggest closed sea worldwide, contains three parts (Froehlich et al., 1999). The northern Caspian is very shallow with an average depth of not more than 10 metres; the middle Caspian has a depth of about 190m in average; the southern Caspian has about 1,000m average depth (Firoozfar et al., 2012; Peeters et al., 2000). The Caspian Sea is fed by many rivers; however the Volga River to the north is the most important river that feeds the Caspian Sea, bringing about 80% of water into it. The Ural River to the north, Kura River and Terek River to the west, as well as the Iranian rivers to the south and the Atrek River to the south east of the sea supply the remainder (Figure 4.3). The water level today is about -28 m .a.s.l (Hoogendoorn et al., 2005).

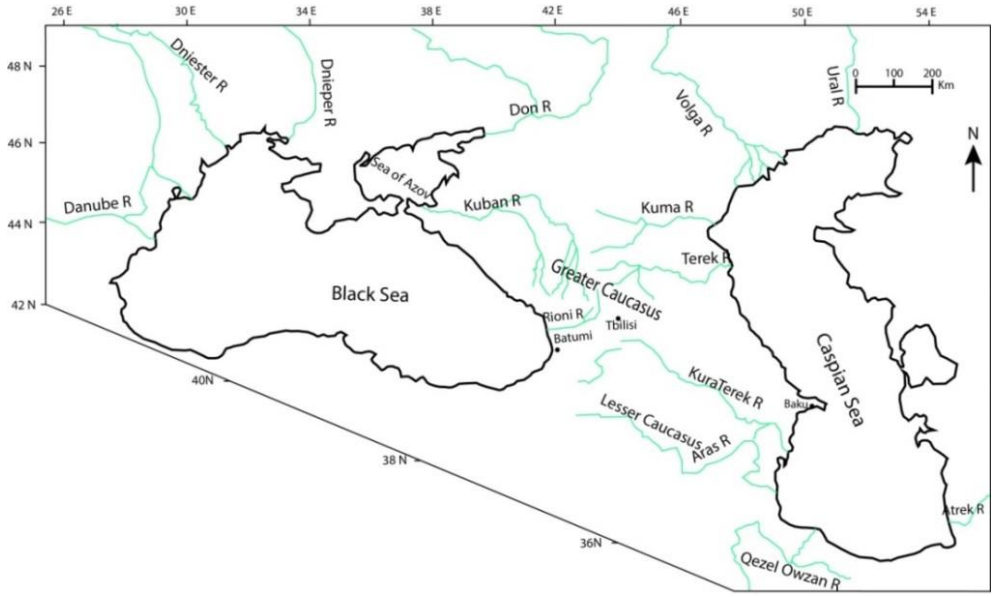

Figure 4.3. A map of the Caucasus area shows the rivers cutting the Greater Caucasus and feeding the Caspian, Black and Azov Seas.

The Black Sea is fed by numerous rivers, for example the Dnieper to the north, Dniester and Danube to the North West and the Rioni which comes from the Caucasus in the east. The Azov Sea is a shallow basin located at the northwest end of the Greater Caucasus belt; it is linked to the Black Sea by the Kerch Strait, and the main rivers feeding the sea are the Don to the north and the Kuban river to the east (Caspers, 1957).

The Greater Caucasus belt is the source for many river systems that affect the belt and its topography, represented by four main river systems;

- The Terek River runs from the north-eastern GC belt, and flows for about 623 km into the Caspian Sea.
- The Kuban River on the northern slope of the western part of the belt flows from the Mount Elbrus area into the Sea of Azov for about 870 km. In its high area, it flows in a deep and narrow gorge, and it is fed by glaciers and

high-mountain snow, and all its tributaries are initiated from the Greater Caucasus.

- The Kura river to the south of the Greater Caucasus flows into the Caspian Sea for about 1515 km through the Kura Basin between the Greater and Lesser Caucasus where it combines with the Aras river tributary (Hoogendoorn et al., 2005).

- The Rioni River flows from the southern of the central GC belt from areas of about 3000m a.s.l in the Racha region into the Black Sea for about 327km long and about 13,400 km² of drainage area.

4.3. Methods

To achieve the desired outcome and objectives, many techniques have been used in the analysis presented in this chapter, by involving many of the software packages described in the previous chapter.

4.3.1. Data collection

Remotely sensed data represents the main data that have been used to investigate the studied belt's topography, including digital elevation models (DEMs) and freely available satellite images, as well as climatic data such as precipitation, glacial activity and hydrographic information contained in previous publications.

The topographic dataset used in this chapter are digital elevation models (DEMs) from Shuttle Radar Topography Mission (SRTM) with resolution of 90m pixels from http://srtm.csi.cgiar.org(Jarvis et al., 2008), which give a sufficient resolution especially when conducting the investigation over large areas.

4.3.2. Topographic profile generation

An important element of this study is creation of multiple topographic profiles analysis across the Greater Caucasus, Pyrenees and Himalayas. Whereas it is routine to produce a single profile section line from SRTM data using Arc-Map or other GIS software, the present work uses many hundreds to thousands of parallel profiles generated by a newly-developed, automated routine. Such a large number of the topographic profiles provide detailed and accurate topographic analysis of the entire investigated range.

The motivation of using such technique and producing such a large number of profiles (which take much time and effort) is to acquire highly accurate results for the topographic interpretations, where digitally each profile has many points (in some profiles exceed 1,000 points) depending on the profile's length. These points show the location (latitude and longitude of the point) as well as its elevation.

By putting all these into one Excel file, the maximum, mean and minimum elevation of the profile is calculated. Afterward by applying this process to all profiles along the range, the accurate mean elevation of each profile is produced and then summarised in a plot perpendicular to the multiline profiles. For example in the Greater Caucasus belt the multiline summary profiles have been made from west to east along the belt summarising the 1040 individual profiles that have a NE-SW strike. The advantage of using such a technique is to obtain an accurate mean elevation for each of the NW-SE profiles of the Greater Caucasus.

To generate a digital topographic profile, a series of steps were followed; the appropriate SRTM data are re-projecting into the Universal Transverse Mercator coordinate system UTM WGS84 zone 38 Northern Hemisphere for Caucasus, zone 30 Northern Hemisphere for Pyrenees and zones 43-45 Northern Hemisphere for Himalayas and Tibetan Plateau. The data were then opened in ArcMap where a slope map was calculated.

To create the topographic profiles of these areas we used the RiScan package, but because of the size of the studied areas it is difficult for the software to create such a large number of profiles, consequently the area is divided into a set of rectangular sub-areas. These rectangles have the same orientation as the sections or profiles that were created, for example, in the Caucasus Mountains the rectangles are aligned

perpendicular to the belt in a southwest - northeast direction, with overlap between the neighbouring rectangles to avoid gaps when creating the sections. Sub-area creation was carried out using Global Mapper software in order to facilitate the cross section analysis in the RiScan software (Figure 4.4a).

All the rectangles were imported as an (xyz) grid into a RiScan project, and then a vertical plane was created in RiScan and rotated and translated to intersect the topographic surface in the chosen location and trend to create the first cross section perpendicular to the belt elongation (Figure 4.4a-d). A set of hundreds of cross sections are automatically created to cover the whole belt under investigation with a specific distance between neighbouring sections set in the section tool in the software. Then, the elevation and slope profiles were created and exported to text files to be opened as files in Excel, to enable calculation of the minimum, maximum, the mean elevation and slope of each section, all results are combined in one file to produce a summary chart for the whole area. The usefulness of this new technique is that it provides more accurate results than if using the conventional technique which just can draw all profiles without calculating the average elevation, relief or slope of each profile.

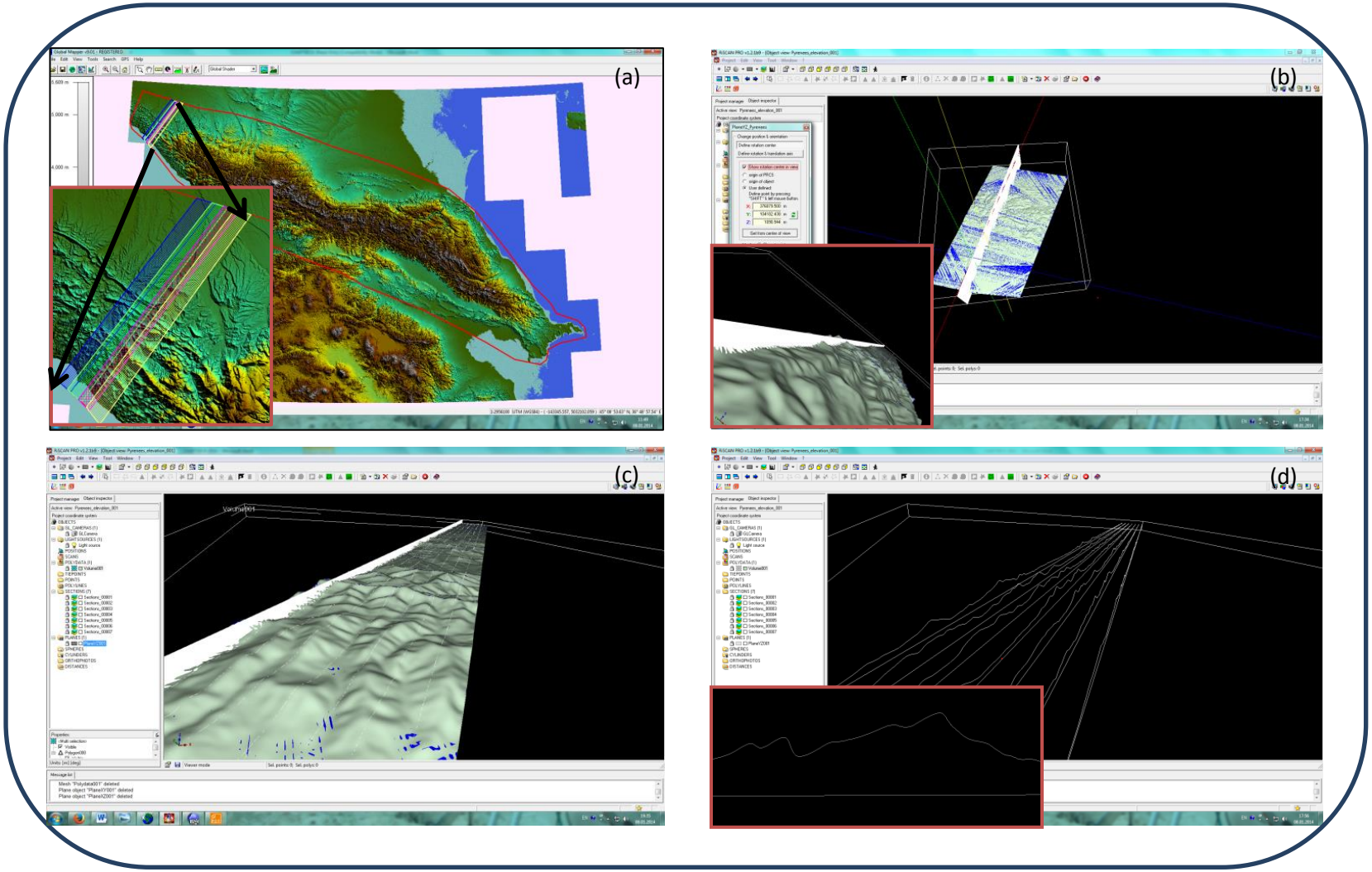

Figure 4.4.The steps to create slope and elevation profiles, where; (a) is SRTM data showing the division of the belt under study into small rectangles, (b) shows the profile plane in order to edit its direction and position (using RiScan software), (c) the data after creating the profiles, and (d) showing the sections or profiles with a fixed distance between every two neighbouring sections (and an example inset).

4.3.3. Local Relief map generation

The local relief is the amount of roughness of the terrain in a specific area and is the difference between the highest and lowest elevation in a selected square. Local relief of the areas under analysis can be calculated from the SRTM data (Figure 4.5a), each area was divided into 10 km^2 using Arc-Map (Figure 4.5b) as this area size was considered large enough to include the mean depressions and elevations of the given area. Selecting this box size was based on some published studies such as Clark et al. (2006), Liu-Zeng et al. (2008) and Montgomery and Brandon (2002). However, other studies have chosen 5 and 20 km box sizes (Ahnert, 1970; Sobel et al., 2003). The value of relief for each box is naturally changeable depending on its size, to overcome this obstacle, a ~10% overlap between each two adjacent windows in all sides has been taken in order to reduces the error rate of the local relief value (Figure 4.5c1). Taking this size of the boxes was depending on the whole area size and the roughness of the terrain, if the area was smaller than the existing area, the boxes should be 5km^2 or less and if it is bigger and the terrain is not very hard, the boxes should be 20km^2 or so, where the local relief is the difference between the highest and lowest elevation in a selected square. However there are some disadvantages in this way to choose the boxes sizes, where if the area was large and not very hard, and has one elevated point as well as low elevated point, the relief will be high but in fact it is not, where this high relief represent small area in the box and the rest of the box is very low relief.

Following this step, the boxes are projected onto the SRTM data and used for clipping the raster, to calculate the local relief value in each particular window,

(Figure 4.5c2). Once the local relief for each window in the area has been calculated, the boxes are grouped based on their relief values and are identified by a specific colour, (Figure 4.5d). By viewing all these groups in ArcMap the local relief map can be seen for the whole region (Figure 4.5e).

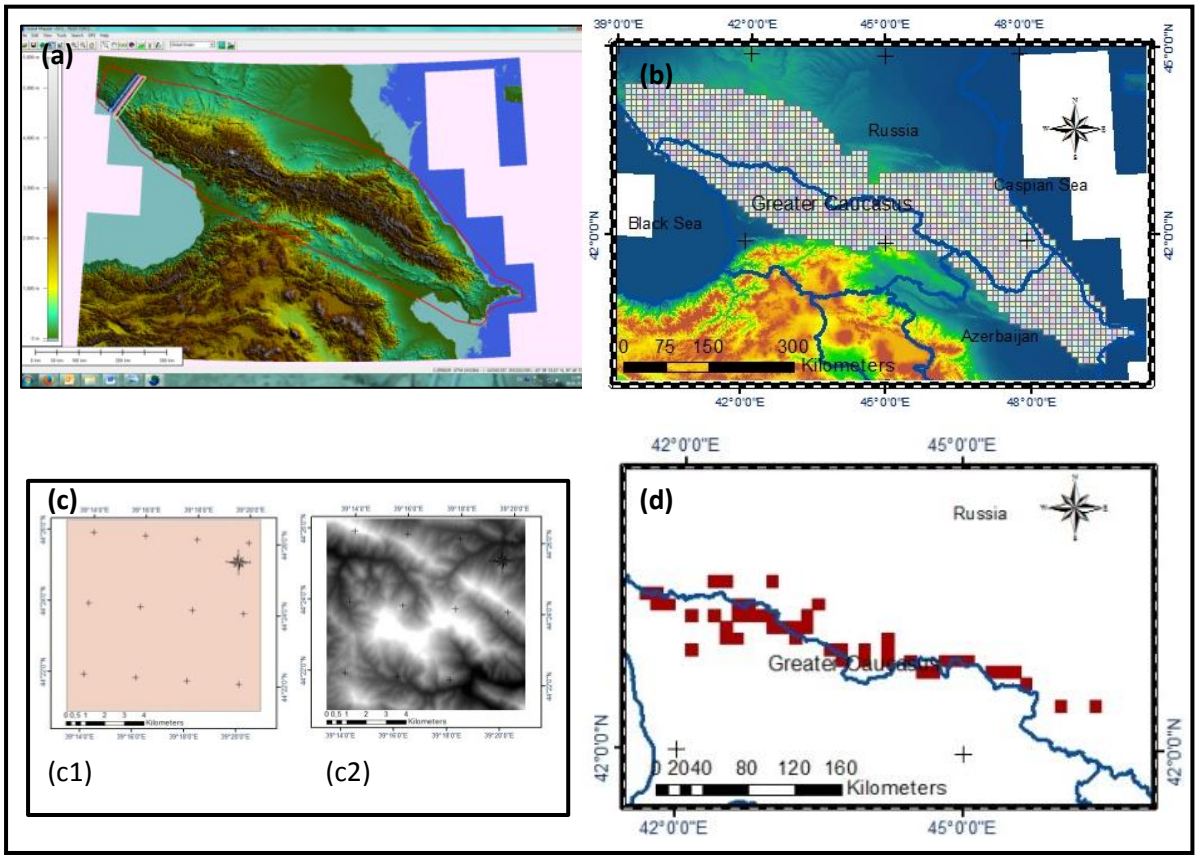

Figure 4.5. The process of local relief generation (a) is SRTM data showing the division of the belt under study is divided into small boxes, (b) Showing all squares that cover the entire area, (c) Showing the squares (with an area of 10 km^2) in small scale before and after relief calculation, (d) an example of one of relief groups (high relief group).

4.4. The correlation between the tectonics, topography and the climate of the Greater Caucasus belt

4.4.1. The correlation between local relief and elevation changes

Using the SRTM data, the local relief of the Greater Caucasus has been mapped over 1450 squares with an area of 10 km^2 each. The relief of each square has been derived to form a mosaic map that shows the relief of the entire belt (Figure 4.6).

Elevated areas in the Greater Caucasus have a much higher likelihood to be high relief areas than the low elevation regions, the relief is low in some squares that have high mean elevation, and vice versa (see Figure 4.6). Some squares have local relief less than 1850m with a mean elevation of about 3300m while there are others with a relief of more than 3000 at the same elevation. From Figure 4.6 it may be observed that the relief in the western part of the Greater Caucasus is slightly higher than the eastern part, although there are some areas in the eastern part with high relief. The area to the north of the Black Sea has high relief with low mean elevations, and the Apsheron peninsula region in the east has low relief and low elevations.

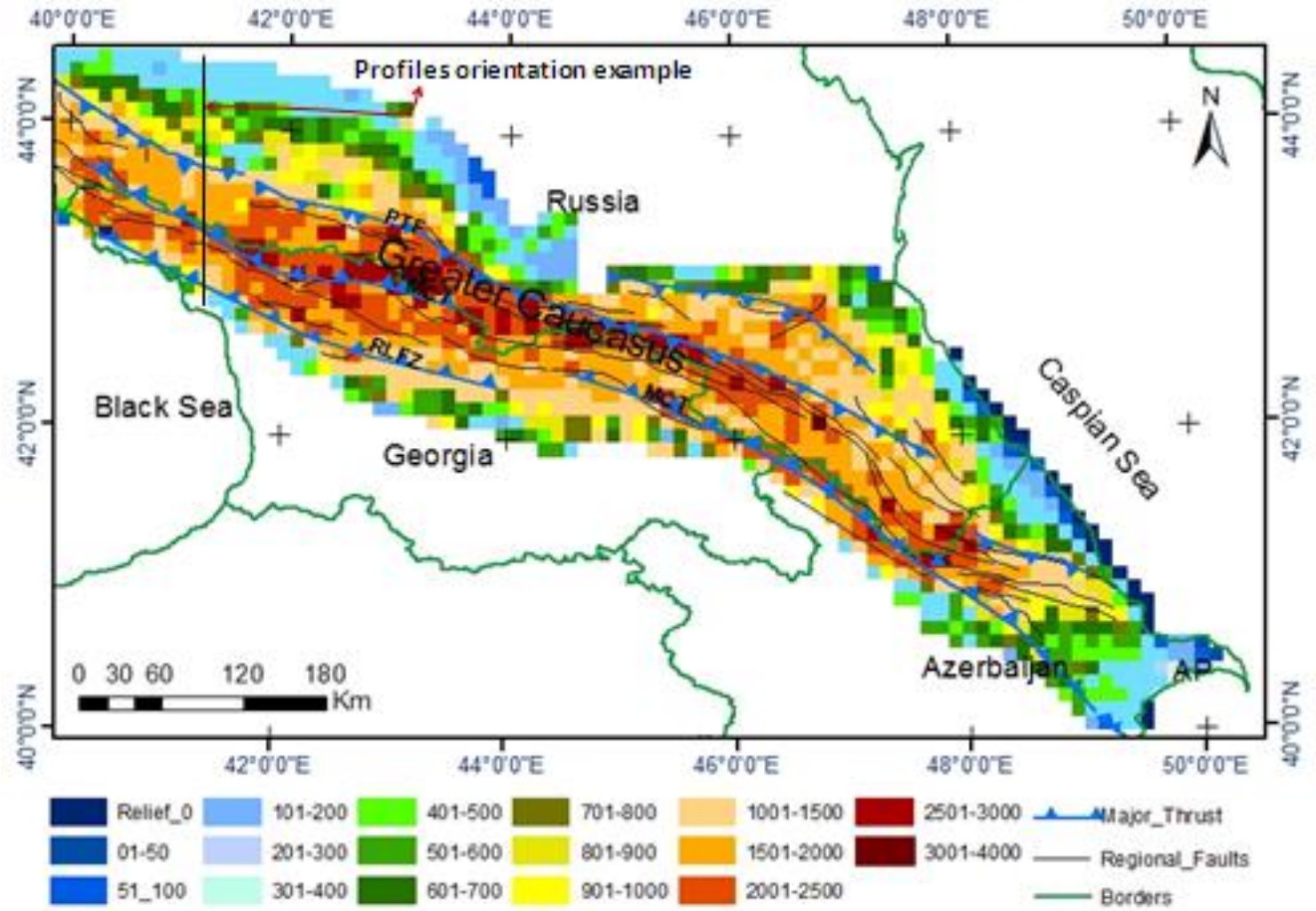

Figure 4.6. The local relief map of the Greater Caucasus belt, showing the relationship between the main faults and high relief areas in the belt. Regional faults were adapted from the Caucasus geologic map scale 1:500000. The line on the north western end of the map is showing the profiles orientations as an example. Different bin ranges were chosen just to elucidate the high relief in the belt, as if the same range was taken, it will be difficult to recognize the relationship between the high relief and the main structures in the belt.

Plots of local relief along the belt were created from the relief map by dividing it into 104 N-S sections based on the squares that have been already created for the relief map, the orientations of the sections were N-S and the maximum, minimum and the mean relief have been calculated for each section in order to plot a NW-SE profile (Figure 4.8), where the minimum relief profile in Figure (4.7b) come from the smallest value along the NE-SW profile of all squares that the profile go along them Figure (4.7a). The most advantage in averaging across the belt is that; the relief in this case represents the local relief of the whole belt, rather than taking simple profile which will just represents the relief for that profile location.

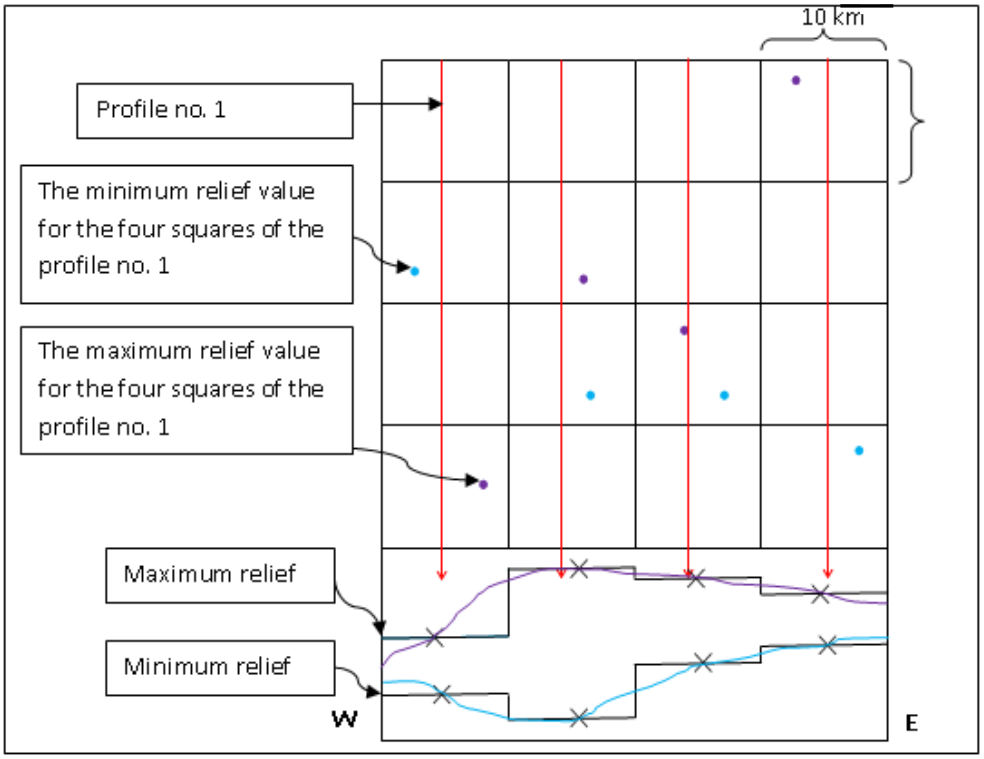

Figure 4.7. (a). An example showing how to create the maximum and minimum relief profiles (NW-SE) along the belt.

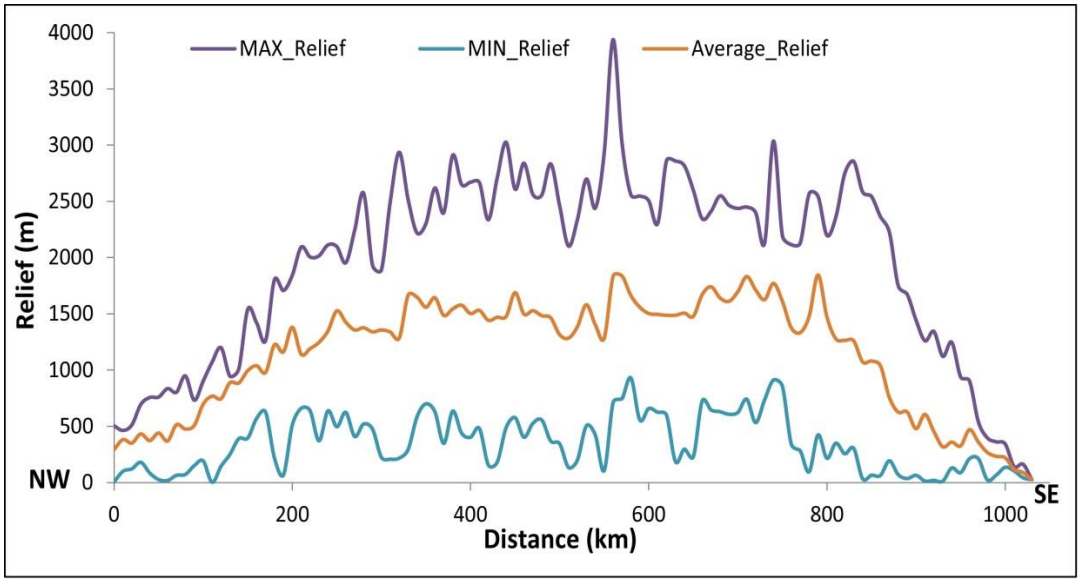

Figure 4.8. (b). NW-SE local relief profile along the Greater Caucasus belt which created from the relief map of the belt where it is divided into 104 NE-SW section and then maximum, minimum and the mean relief have been calculated of each section in order to plot this NW-SE profile.

Figure 4.9a, b show the plots of maximum, minimum and the mean elevation changes and slope for 1040 northeast-southwest sections that have been created in a NW-SE trend along the Greater Caucasus belt (from the Black Sea to the Caspian Sea). All these plots were produced to elucidate the relationship between local relief, elevation changes and slope along the belt. They show that there is a strong positive relationship between slope and elevation so that whenever the mean elevation increases the mean slope increases as well (Figure 4.9).

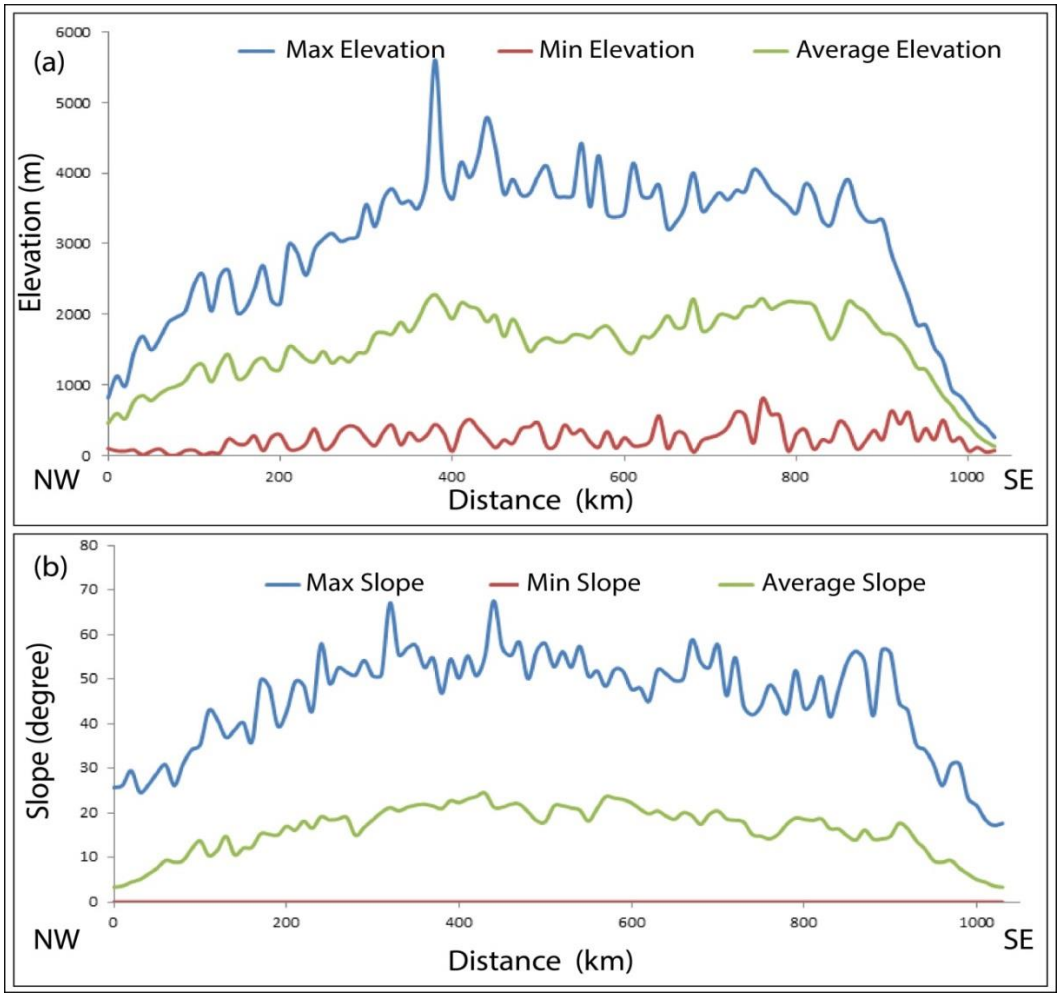

Figure 4.9. (a, b): Show plots of NW-SE maximum, minimum and the mean profiles of (a); the elevation changes and (b); the slope, of 1040 sections along the Greater Caucasus belt.

The relationship between the elevation changes and the local relief is more variable as discussed above. A positive relationship is still expected because whenever the elevation is very low the relief cannot be high, due to the reduction in the probability of deep valleys forming in such areas. From these plots of elevation changes, slope and local relief, the Greater Caucasus belt can be subdivided into three parts (western, central and eastern), and the elevation plot (Figure 4.9) shows that the elevations in the eastern part decrease sharply towards the east of the belt whereby the gradient of the mean elevation exceeds 10m/km (1%). In the western part, they decrease gradually towards the west of the belt where the gradient of the average elevation in this part does not reach 5m/km (0.5%).

4.4.2. The correlation between local relief and the tectonics of the belt

The Caucasian structural and geological evolution are strongly affected by the spatial setting of the belt, which is located in the Arabia-Eurasia collision zone, in turn part of the Alpine–Himalayan orogenic belt (Ershov et al., 2003). According to GPS surveys of the range appears that it is accommodating a minimum and maximum North-South shortening rate of approximately 5 and 13 mm/year respectively (Reilinger et al., 2006).

There is significant seismicity in the eastern Greater Caucasus belt, since the beginning of the 19th century there have been no earthquakes with magnitude >7.0 recorded in the belt as suggested by the Caucasus Region Earthquake Historical Records with the exception of the M 7.2 1991 Racha earthquake event which occurred on the southern slope of the Greater Caucasus west of Tbilisi (Georgia) (Triep et al., 1995). Seismicity of the Eastern Greater Caucasus has greater intensity compared with the western part of the belt. Seismicity has been recorded on both the northern and southern sides of the range in the eastern Greater Caucasus, whereas in the western side the earthquakes occur just in the southern side (Figure 4.11b).

An important feature to note from (Figure 4.6) is that the local relief of the belt is extremely high and complex, as more than 30% of the belt has relief (>2000m) which can be considered as high relief. There is also a strong association between the main Caucasus thrusts and the high relief regions, where almost all of large thrusts in the region are spatially distributed within the areas of high relief at the large scale.

The maximum local relief decreases towards both ends of the belt (Figure 4.10), however, the rate of decrease is greater towards the eastern end, compared to the western end of the belt. The gradient of the average relief towards the east is 7.25

m/km (0.725%), whereas towards the west is 3.8m/km (0.38%).The relief is apparently somewhat low in the Eastern Greater Caucasus (EGC) compared to the western part, even though the EGC is more active seismically than the western part (Figure 4.11b). The lower precipitation in the EGC, and therefore naturally the density of valleys is also less, resulting in a drop of local relief along this area (Figure 4.10).

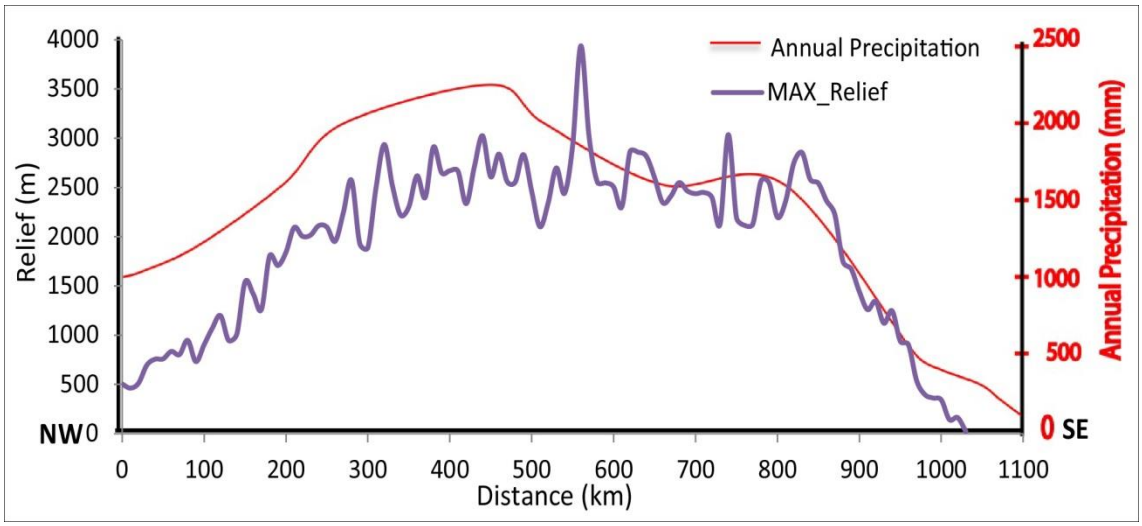

Figure 4.10. Showing the relationship between the local relief and precipitation, where the purple line is NW-SE local relief profile along the Greater Caucasus and the red line is the annual precipitation profile along the belt, the precipitation drawn along the black line in Figure (4.2) which is from Kotlyakov and Krenke (1980).

On the other hand, there is a positive correlation between relief changes and Moho depths underneath the Caucasus region which can be seen in (Figure 4.11a,c), and where the deepest Moho levels occur beneath the high local relief areas along the belt. However, the Moho depths reduce sharply to both the east and west, whereas the local relief changes sharply to the east and gradually to the west of the belt.

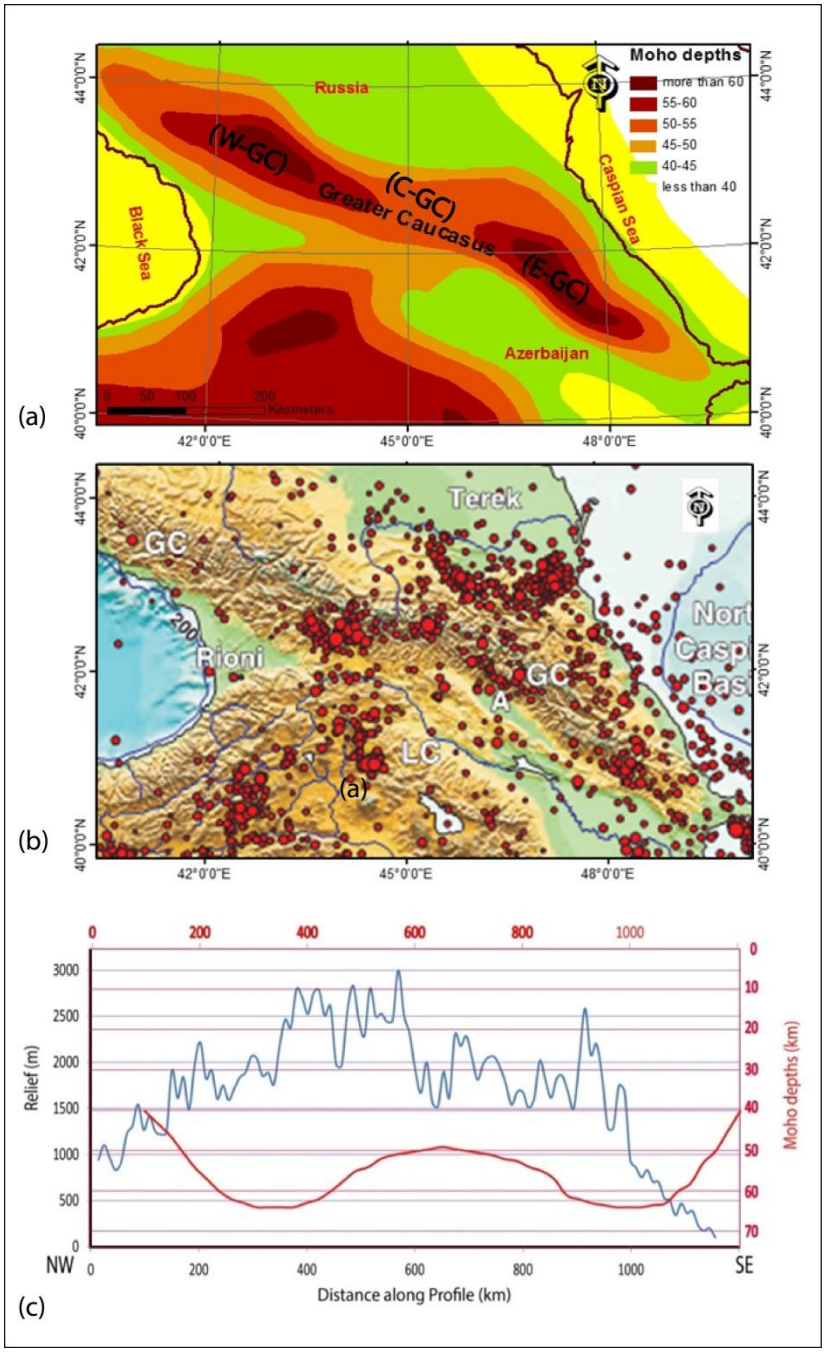

Figure 4.11. (a) showing the Moho depth map underneath the Greater Caucasus belt modified after Philip et al. (1989)& Shengalaya (1978), (b) Caucasian region seismicity shows the western part of the GC is almost quiet, and all earthquakes are distributed in the eastern part of the belt, after; Tan and Taymaz (2006) and (c) showing the correlation between Moho depths in red and local relief in blue along the Greater Caucasus from west to east. The Moho pattern is symmetrical whereas the relief pattern is asymmetrical. (W_GC, C_GC and E_GC are the Western, Central and Eastern Greater Caucasus). The relief profile is a direct profile from the relief map in Figure (4.6), which means it is not the averaging relief that calculated from the profile across the belt such as Figure 4.7.

4.4.3. The correlation between Topography and Climate of the Greater Caucasus belt

Climatic features show differences from east to west in the Greater Caucasus belt. A maritime climate is present in the west, a continental climate in the east and a drier climate in the northeast of the belt. From the precipitation map of the Caucasus region modified after Kotlyakov and Krenke (1980) (Figure 4.12a) it can be seen that the western part of the region is wetter than the eastern part. The relationship between the climate (represented by annual precipitation) and elevation changes across the Greater Caucasus can be examined in Figure 4.12, where the gradual reduction of the mean altitude which characterise the western region of the belt, has a close relationship with the region of wetter climate, whereas the elevations in the eastern part changed rapidly, and the precipitation rate is low in this part.

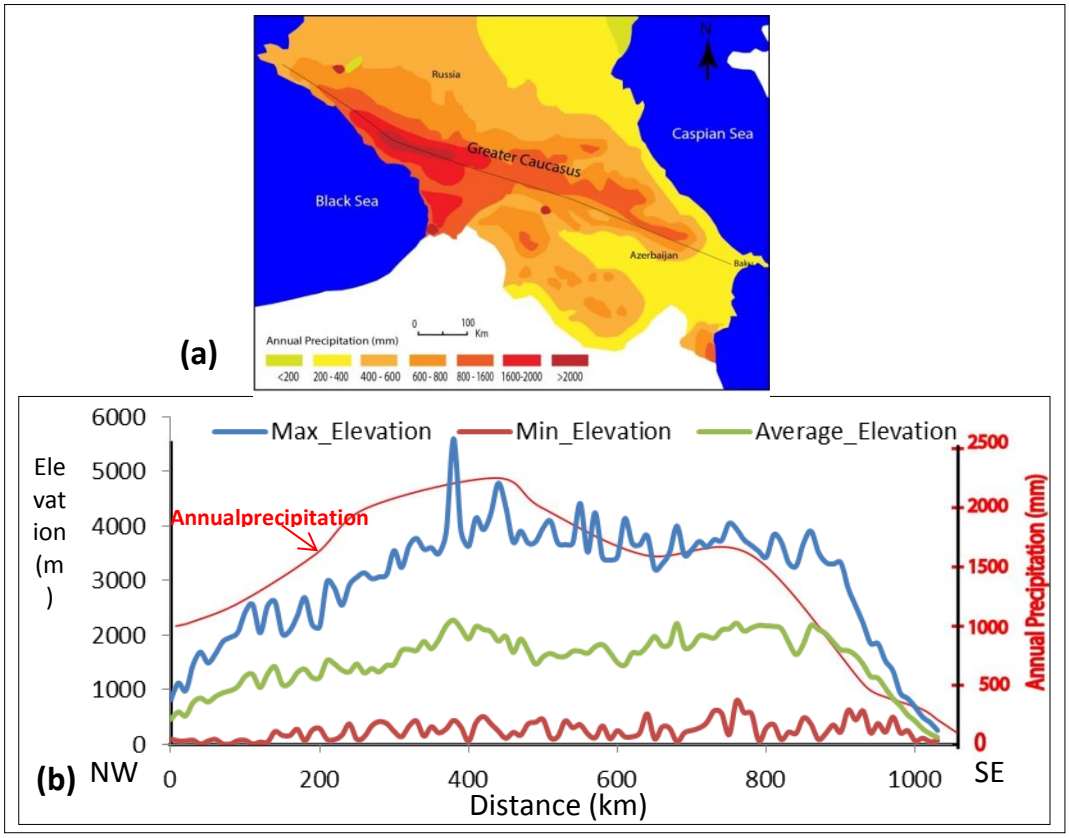

Figure 4.12. (a) Annual precipitation map of the Greater Caucasus modified after Kotlyakov and Krenke (1980), the black line along the Greater Caucasus in (a) is the location of (b) which is a plot represents the relationship between the elevation and the annual precipitation of the belt.

In contrast, the steep altitude decrease in the eastern part is in the area characterised by a dry climate. The cause of this gradient of elevation changes might be the climate, nevertheless it could be due to an alternative reason such as the tectonic activity. The eastern part is very active compared with the western part (Figure 4.11b).

The (south-north) elevation changes in the western part of the belt are shown in (Figure 4.9 a), where it can be observed that the elevation reduction is gradual to the north and sharp to the south, even though the climate is wetter to the south than to the north. On the other hand, north-south profiles along the central Greater Caucasus e.g.(Figure 4.13 c) show that the altitude changes are steep in both directions north and south, where the climate is similar on both sides, which is dryer than the western part of the belt. For the eastern part of the belt, the N-S profiles show that the elevation changes were gradual northward whereas somewhat steep southward despite a climate that is similar in both directions (Figure 4.13 b, d).

These results are contrary to what has been found from the study of the east - west elevation changes of the belt; however this discrepancy is expected, where the east-west profiles are along the tectonic strike and across most of the drainage whereas the north south profiles are across the tectonic strike and along the drainage.

The results can be compared with other active ranges where relationships between climate, geomorphology and tectonics have been explored, but to date most of these have focussed on changes parallel to the tectonic transport direction, rather than along strike as in this study (e.g. Montgomery et al., 2001; Godard et al., 2014). Climate

has been proposed variously as having a dominant role on the morphology and/or denudation of mountain ranges, e.g. in the Andes (Montogmery et al., 2001) or being very subordinate to tectonics, e.g. in the Himalayas (Godard et al., 2014). Where climatic control is suggested, high precipitation is regarded as enhancing denudation and steepening topographic profiles. Therefore it would seem odd if the gentler topographic profile along the western Greater Caucasus related to the climatic influence. An issue here is that it is difficult to deconvolve the effects of climate and tectonic shortening, which relates to far-field stresses acting upon a region. The next section addresses this issue by looking at the Pyrenees, which has not had significant tectonic shortening for millions of years, and probably as far back as the Miocene.

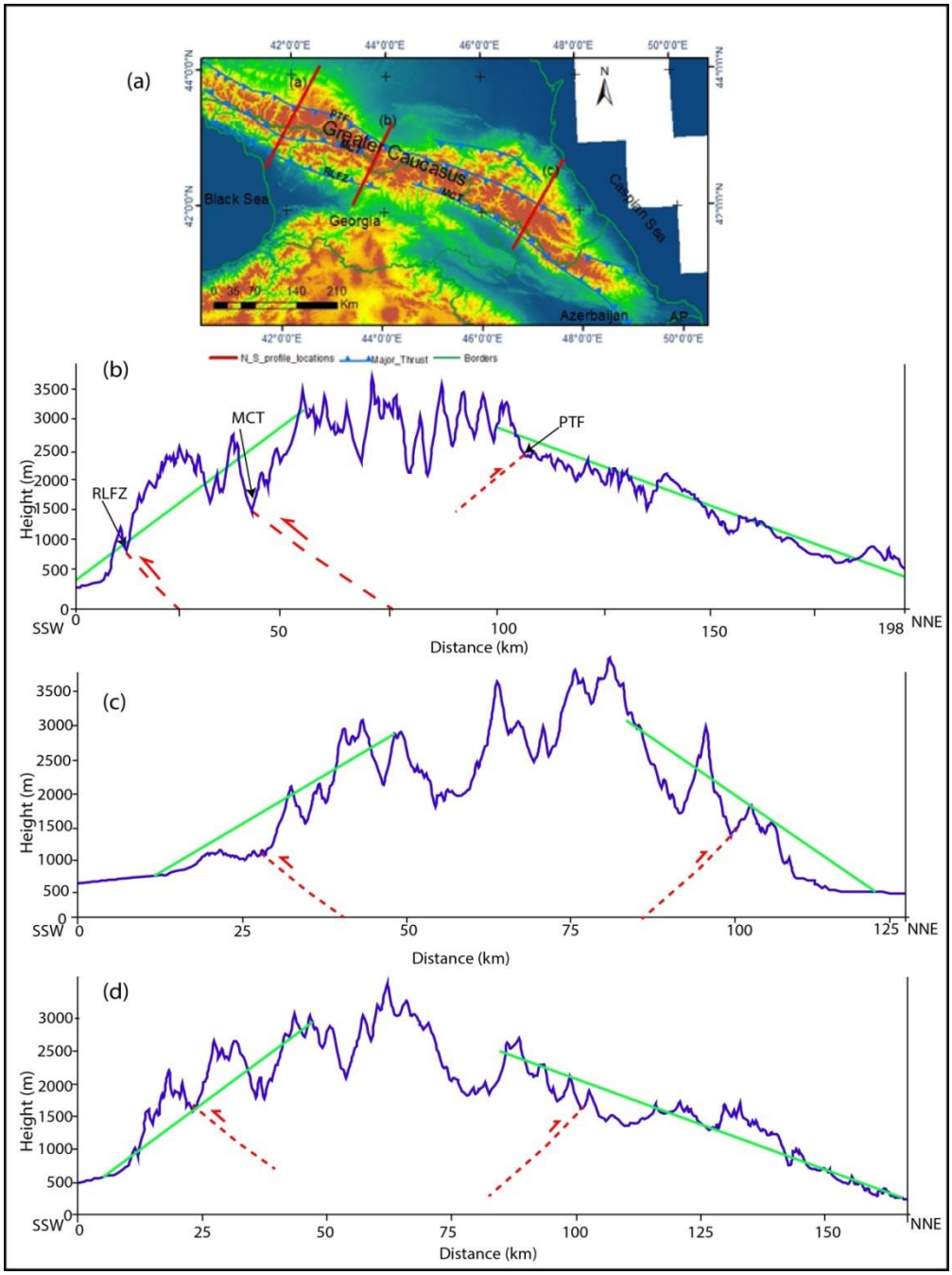

Figure 4.13. NE-SW profiles are showing the elevation changes along the Greater Caucasus, the profiles are almost perpendicular on the main structures along the belt; (a) is the location for the profiles in Figures; (b) western, (c) central, and (d) is the eastern Greater Caucasus belt. The major structures that represented by the red line which are perpendicular to them, are come from the geologic map of the Caucasus region that modified after (Adamia et al., 2011a; Brunet et al., 2003; Gamkrelidze, 1986).

4.5. Topographic comparisons between GC belt and other mountain belts of the world

The positive correlation between the elevation changes and local relief and their relationship with the climate of the Greater Caucasus, suggest that it may be useful to look at other mountain belts using a similar methodology. The selected mountain belts are: the Pyrenees Mountains located at the border between France and Spain, chosen because it is a long narrow belt with similar dimensions to the Greater Caucasus but is an inactive belt, the Northern Tibetan Plateau and the Himalayas were also studied, where the Himalayas is generally considered to be one of the most important places to study the relationship between climate, tectonics and topography due to its location where it occupies the southern rim of the Tibetan Plateau, also the climate is different from one region to another along the mountain belt and it is characterized by extreme relief in some areas.

4.5.1. Pyrenees Mountains

The Pyrenees range is primarily assumed to be the separating strip between Europe and Iberia. It is a linear belt trending WNW-ESE between the Bay of Biscay to the west, and the northeast corner of the Gulf of Lion, Mediterranean Sea to the east, and is about 400 km long and 160 km in width. Convergence took place predominantly in the early Tertiary (e.g. Fitzgerald et al., 1999). The belt is divided into four structural zones extending longitudinally parallel to the belt, represented by the South Pyrenean zone (SPZ) to the south, the Axial Zone, the North Pyrenean zone (NPZ), and the sub-Pyrenean zone (sPZ) to the north of the belt (Figure 4.14).

A major fault such as the north Pyrenean fault (NPF) between the axial zone and the north Pyrenean zone separates each of the two neighbouring zones. The north Pyrenean frontal thrust (NPFT) lies between the north Pyrenean zone and sub-Pyrenean zones. The highest summits in the belt exist in the central part in the Spanish Pyrenees and are Pico d'Aneto 3,404 m, Posets peak 3,375 m and Monte Perdido 3,355m a.s.l. (Alasset and Meghraoui, 2005; Babault et al., 2005; Labourdette and Jones, 2007).

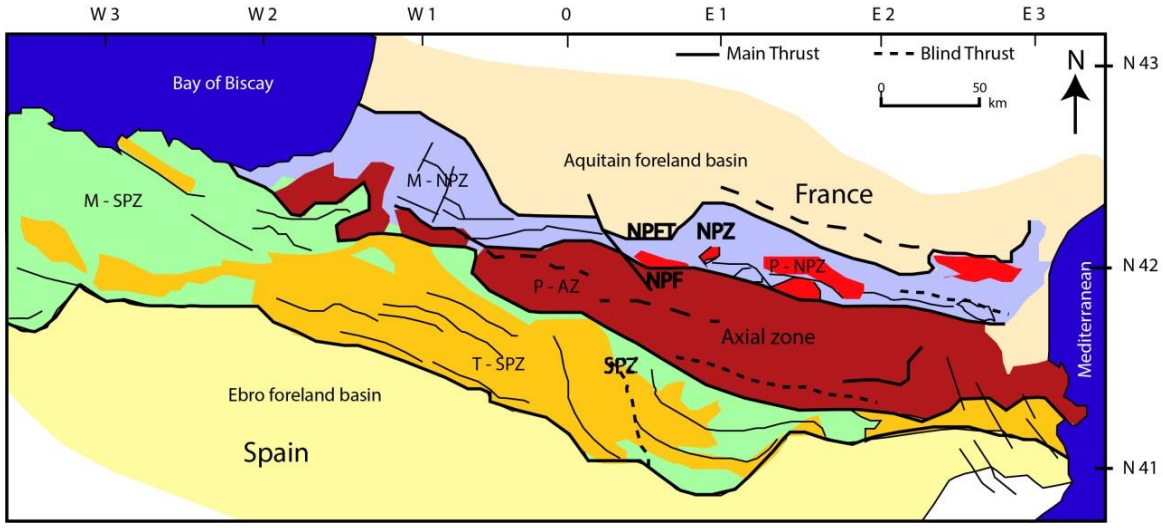

Figure 4.14. Location map of the Pyrenees, showing their structures and main tectonic units, where, (SPZ) is the South Pyrenean Zone, (NPZ) North Pyrenean Zone, (AZ) Axial Zone, (NPF) North Pyrenean Fault, (NPFT) North Pyrenean Frontal Thrust, (M) Mesozoic, (T) Tertiary, and (P) is the Palaeozoic outcrops modified after Labourdette and Jones (2007).

4.5.1.1. Pyrenees Climate

Climatically, the Pyrenees chain differs from one part to other, where it is wet to the west and dry to the east of the belt, and the northern part is colder than the southern part. The Pyrenees receive a high amount of precipitation in the western part due to its location close to Atlantic Ocean, from which moist air is blown via the Bay of

Biscay to the west of the belt (Figure 4.15). Glaciers are not present in the eastern part of the belt, due the lack of snowfall in this part, whereas in the western part there are some glaciers mainly on the snowy northern slopes of the central Pyrenees.

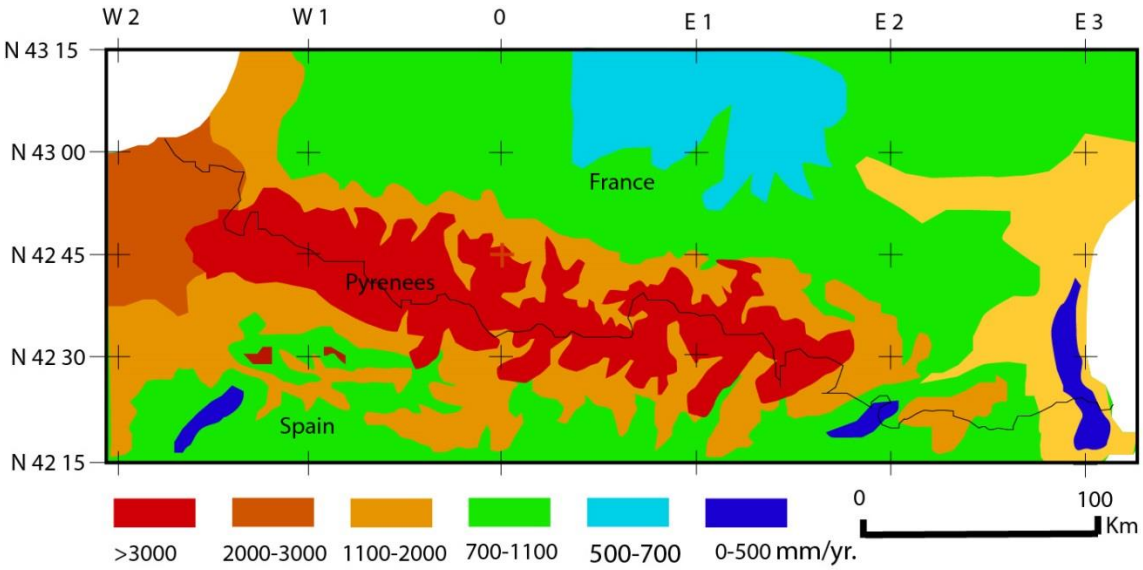

Figure 4.15. Annual precipitation map of the Pyrenees for the period of (1957-1973), modified after Frederic et al. (2008).

4.5.1.2. Elevation changes in Pyrenees Mountains

Figure 4.16 illustrates the maximum, minimum and average elevation of Pyrenees Mountains from west to east through creating 440 NNE-SSW cross sections along the belt by RiScan software, and then the axial profiles of the maximum minimum and the mean elevation have been created to illustrate the topographic gradient along the entire belt from east to west.

The results show that the average elevation climbs gently from west-to east in the western part of the Pyrenees, and declines more rapidly from west to east in the eastern part of the belt, where the gradient of the average elevation towards the west is 4m/km (0.4%), whereas towards the east it is 10.5m/km (1.05%), which shows a high degree of similarity with the Greater Caucasus topographic changes. The climate is

quite analogous to that in the Greater Caucasus where it is wet in the west and drier to the east. Consequently, this result can be used as an evidence to support the idea that the cause of the steep or gradual gradient of the elevation in a mountain belt could be the climate.

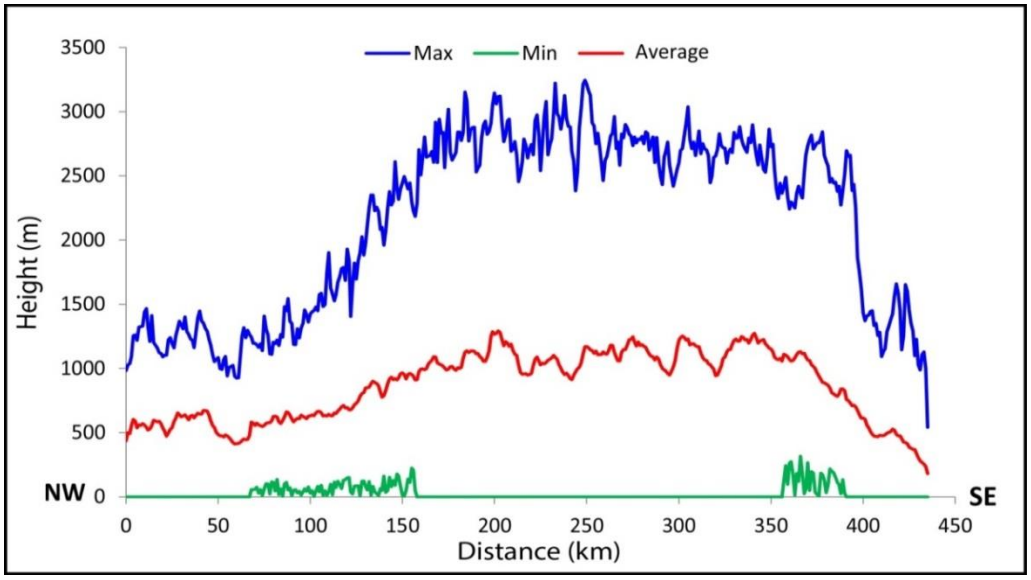

Figure 4.16. Showing plots of the maximum, average and minimum elevation of 440 sections along the Pyrenees Mountains.

4.5.1.3. Local relief, elevation changes and annual precipitations of Pyrenees

The local relief of the Pyrenees has been mapped by dividing the region into about 700 squares with an area of 10 km^2each (Figure 4.16).Obviously, there is a relationship between the elevation changes and local relief changes along the Pyrenees from west to east, the elevations have gradual reduction to the west and a sharp reduction to the east of the belt. In addition the local relief shows the same pattern where it changes from gradual in the west to rapid in the east (Figure 6.16). The area of highest local relief has the highest annual precipitation, which represents the Axial Zone (AZ) of the belt.

The implication of these results is that the along-strike morphology of a tectonically-quiescent mountain range shows a positive correlation with precipitation, but with two caveats. The first is that it is unclear how much of the gross morphology is inherited from the situation at the end of the active tectonic phase. The second is that, like the Greater Caucasus, the gentler slopes of the western Pyrenees are the opposite of what would be expected if higher precipitation produced greater erosion and denudation rates.

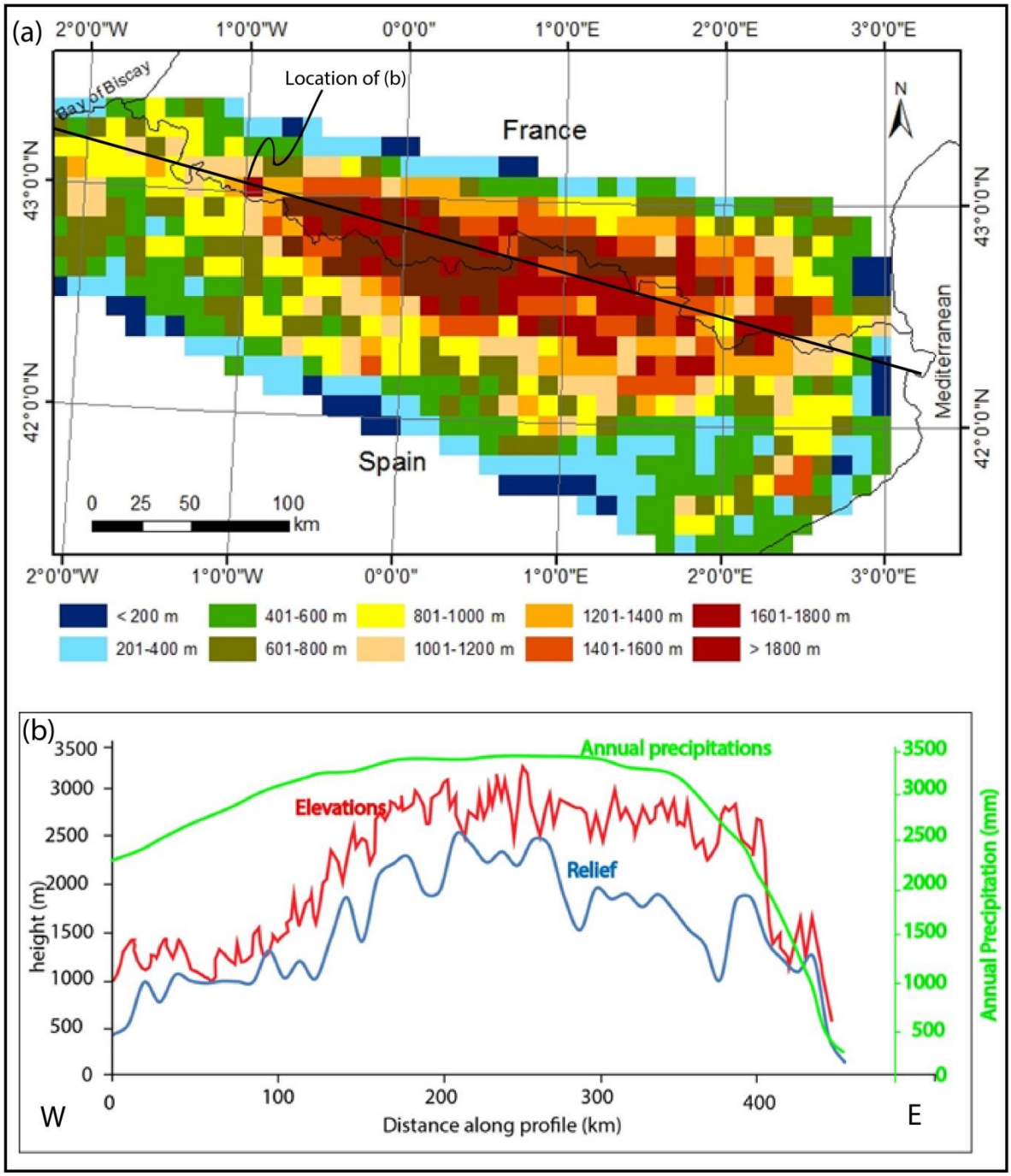

Figure 4.17. (a) Local relief map of the Pyrenees Mountains and (b) is a profile showing the relationship between the relief, elevation changes and the precipitations along the Pyrenees from west to east (the location of the profile is the black line on (a)).

4.5.2. Tibetan Plateau

The Tibetan Plateau (TP) is located in south-western China bordered by Bhutan and Nepal to the south, and India and Pakistan to the south-west (Figure 4.18). It represents the highest and largest plateau on the Earth with an area of about 2.3 million km^2 above 5km high bordered by steep sides to the south, north and west. The Earth's highest peak (Mt. Everest) exists on its southern side in the Nepalese Himalaya standing at 8,848m above sea level. The TP was formed as a result of Indian-Eurasian collisional convergence, causing shortening and thickening of the crust to ~80 km creating the Himalayas, Karakorum, and Tien Shan ranges (Fielding et al., 1994; Fielding, 1996; Hatzfeld and Molnar, 2010; Royden et al., 2008).

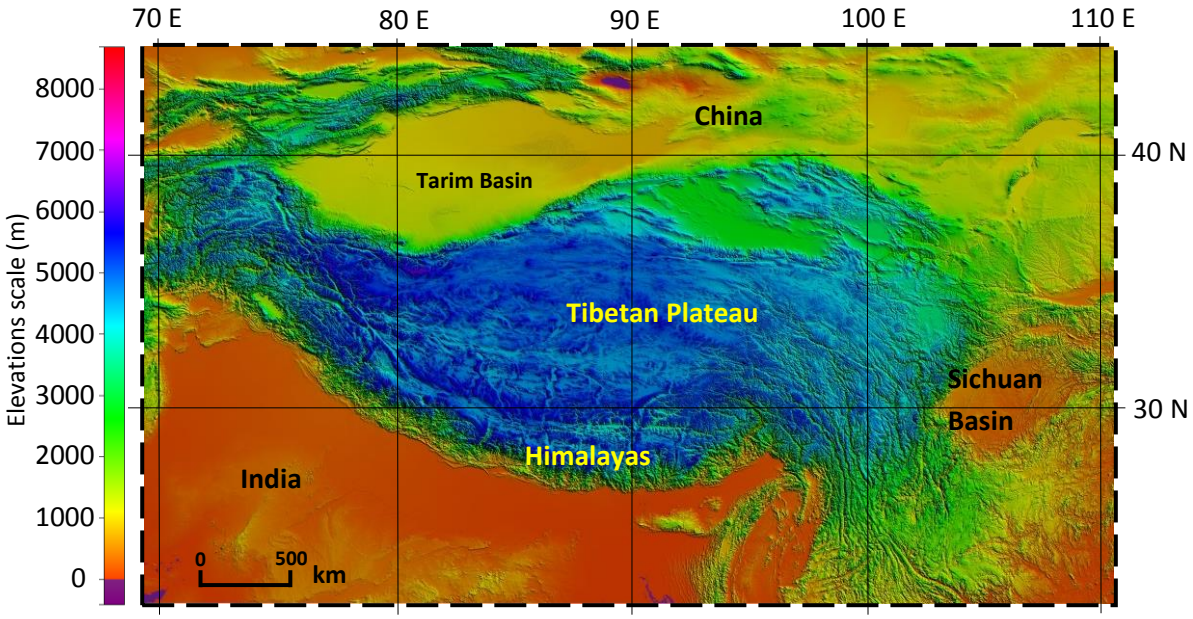

Figure 4.18. A Topographic map of the Tibetan Plateau, from SRTM data with 90m resolution.

Owing to its distinctive height and its large area, the Tibetan Plateau has a high impact on the monsoon for the whole of Asia (Tong et al., 2013; Webster et al., 1998; Yanai et al., 1992). Glaciers, which have begun to melt as a result of warming in recent centuries causing a reduction of the permafrost areas in the plateau, have led to a radical change of the hydrological cycle on the whole plateau (Tong et al., 2013). The region is known as the "Asian water tower", as it is considered to be the main source of many valleys and rivers that spread throughout Asia such as the Yellow River to the northeast of the plateau, the Indus river to the south west, the Koshi river to the south and Brahmaputra river to the southeast of the plateau which passes through India and Bangladesh before flowing into the Indian Ocean (Frauenfeld et al., 2005; Immerzeel et al., 2010; Tong et al., 2013).

4.5.2.1. The Tibetan Plateau climate

The rainfall or precipitation represents the most important factor affecting the hydrological regime, which in turn affects the landscape of the area (Gourley and Vieux, 2005). The Tibetan Plateau lacks extensive meteorological stations and rain gauge stations, particularly in areas with high elevation because of the terrain and weather difficulties, which results in a scarcity of information in such regions. Thus, the precipitation rate in the Tibetan plateau has not been determined precisely however there are estimated precipitations for the Tibetan Plateau and Himalayas, such as the estimated TP precipitation map by Liu Xiaodong et al. (2009) (Figure 4.19a) and the Himalayan precipitation map by Finlayson et al. (2002)(Figure 4.19b). All of these maps show that the precipitation of the eastern part of the plateau is greater than in the

western part. The Himalayan Alpine climate latitude range is between 28N to 33N, which varies with altitude due to temperature decreases in the highlands.

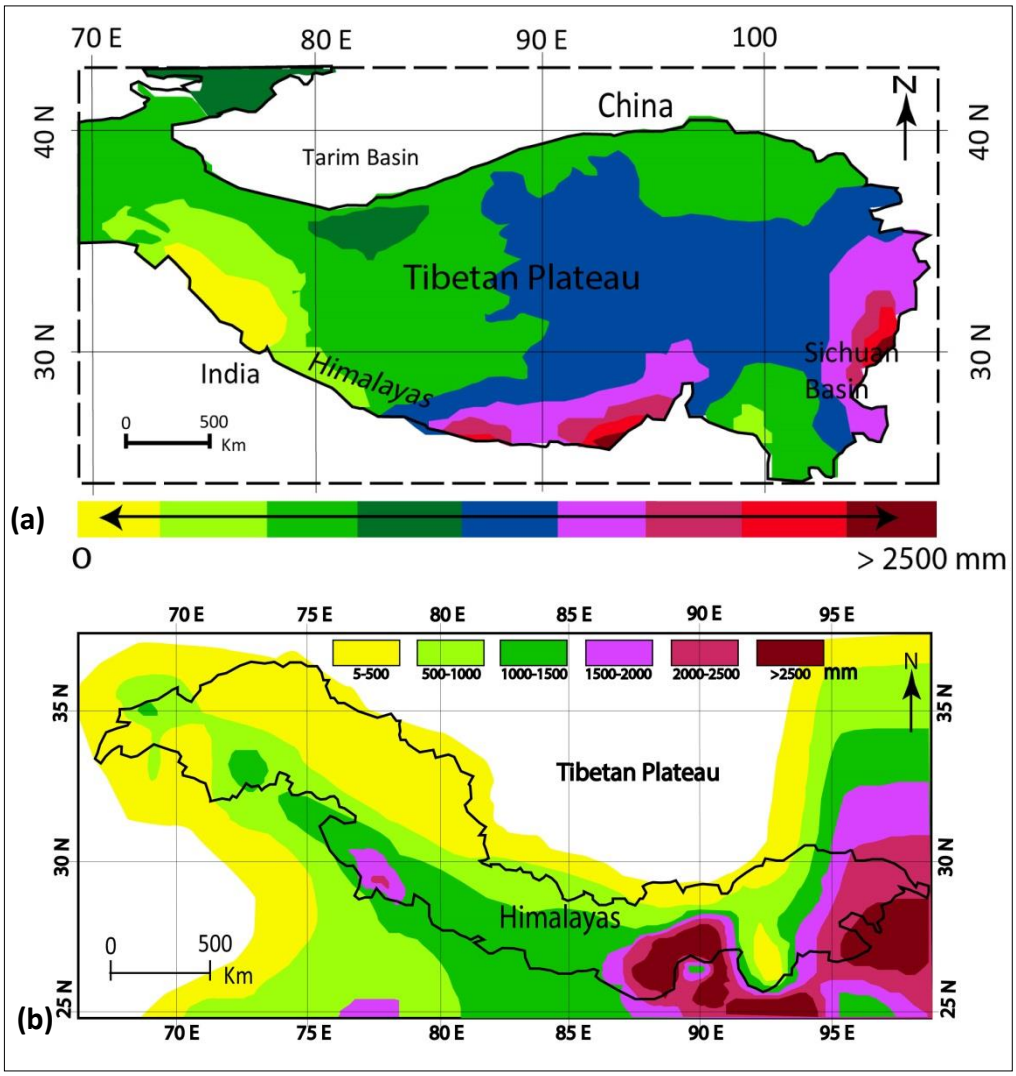

Figure 4.19. (a) showing annual precipitation map of the Tibetan Plateau modified after Liu Xiaodong et al. (2009), and (b) Annual precipitation map of the Himalayas modified after Finlayson et al. (2002).

4.5.2.2. Elevation changes along the TP edges

Topographic studies were applied on the northern side of the plateau, and Himalayas, where 588 NE-SW cross sections along the northern side of the plateau, and 660 (NE-SW) sections along the Himalayas on the southern plateau have been created in the same way as for the Greater Caucasus and Pyrenees, to see the elevation changes from west to east across the plateau rims.

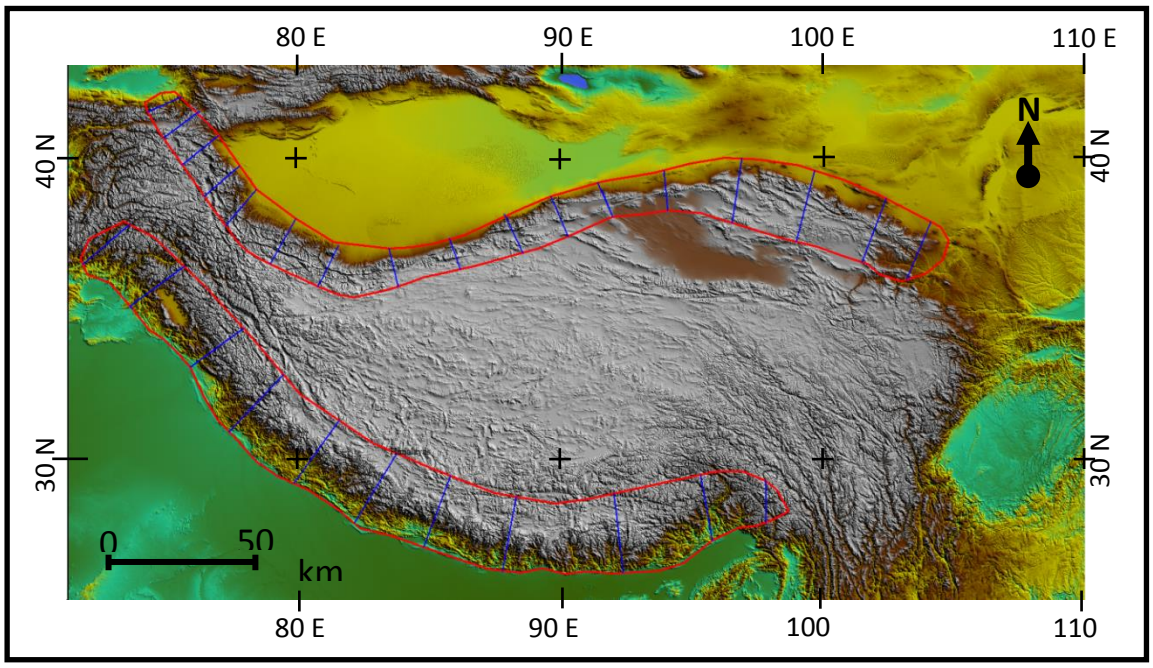

Figure 4.20. SRTM image of the Tibetan Plateau showing the location of the N-S cross sections of the northern and southern rims of the Plateau, red polygons are the areas covering by cross sections and the blue lines are some of the profile locations as examples to illustrate the orientation of the profiles.

i. Northern rim of the Tibetan Plateau

Figure 4.21 shows the plots of maximum, minimum and the mean elevation for the 588 N-S sections created 5km apart from west to east along the northern Tibetan Plateau, as they appear in Figure 4.20, which is containing a map of the Tibetan Plateau showing the locations and the orientations of some of those sections as an example. From the elevation chart, it can be noted that the elevations decreasing

sharply on both sides to the east and west of the plateau rim, where the gradient reach 10m/km (1%) towards the east and 12.8m/km (1.28%) towards the western side of the northern rim of the plateau, and the central region is inclined to the east.

By correlating the west - east elevation changes of the northern edge of the plateau with its climate (Figure 4.19a), it could be observed that there is a relationship between the elevation gradient and the climate of this edge of the Plateau where the climate is dry in both sides and the gradient of the elevation is steep in both sides Figures 4.18a and 4.20.

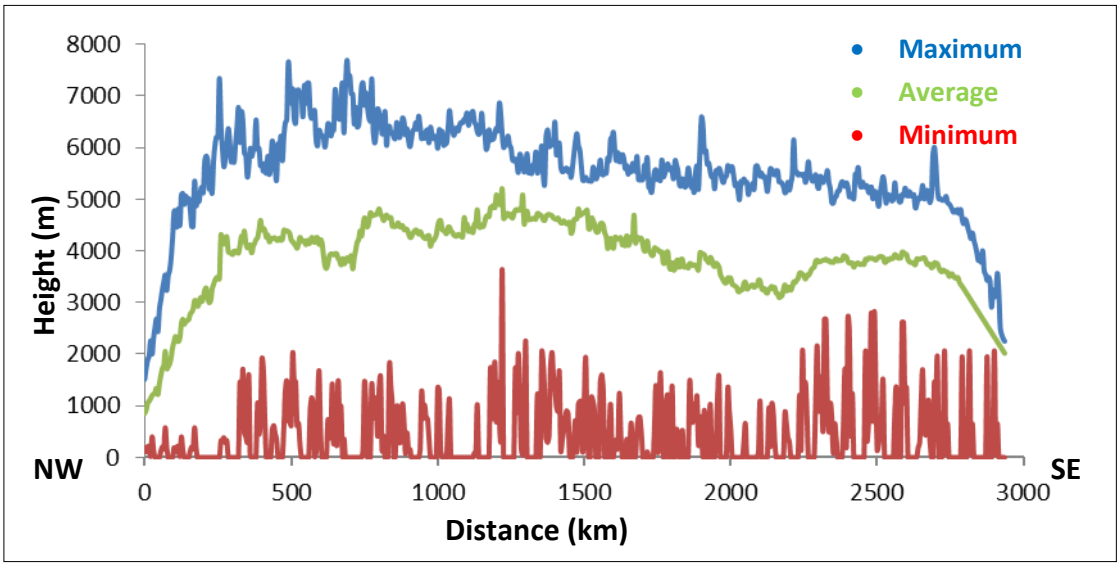

Figure 4.21. Plots of maximum, minimum and the average elevation of the northern rim of Tibetan Plateau.

ii. Southern Tibetan Plateau (Himalayas)

The Himalayas represents the southern edge of the TP, which includes the highest peaks of the world. Figure 4.22shows the plots of maximum, minimum and the mean elevation of 660 (N-W) sections that have been created with 5km spacing from west to east along the Himalayas, their locations and orientations are shown in (Figure 4.20).

From the elevation plots in Figure 4.22, it is noticeable and clear that the elevation in the western part of the mountains decreases sharply where the average elevation gradient reaches 7.5m/km (0.75%), whereas it decreases gradually in the eastern part of the region with elevation gradient of 3.25m/km (0.325%). And by correlating the elevation changes and the climate of the range, a relationship between the lower gradient side and wetter climate is apparent, and between the lower precipitation side with the higher gradient. Thus the Himalayas can be used as further evidence to support a hypothesis which says that the cause of a steep or gradual reduction of the elevation could be the climate.

It is also worth noting that the eastern side of the Himalayas is characterised by high local relief due to the high rate of precipitation which leads to an increase in the erosion and further deepening the rivers and valleys streams in this area.

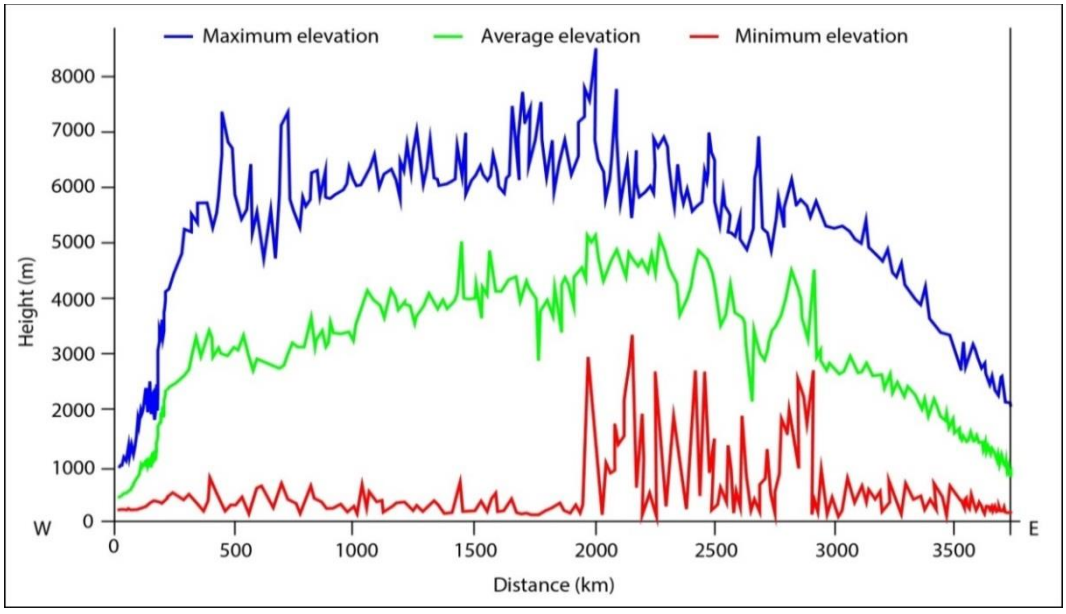

Figure 4.22. Showing the plots of the maximum, average and the minimum of the Himalayas elevation.

4.6. Chapter summary

In this chapter, the along axis topographic variation of mountain belts have been investigated. Elevations are decreases gradually in the western part of the Caucasus but in the eastern part, they reduce sharply. There is a high correlation between elevation changes and Moho depths underneath the Caucasus region. Earthquakes frequently occur in the eastern part of the Caucasus belt especially in the region of the Apsheron peninsula, whereas the western part of the belt is somewhat quiet.

The Greater Caucasus relief is extremely high, with a large correlation between the high relief and the large thrusts in the region. However, the relief of the eastern part of the belt is apparently somewhat low compared with the western part, even though the eastern part is more active than the western part. Although the high areas in the belt have a much higher probability to be high relief areas than of the low elevation regions, the relief is low in some places that have high elevation, and vice versa.

There is a correlation between elevation changes and climate, where the gradual reduction of the mean altitude which characterises the western area of the belt, has a close relationship with a wetter climate in this part, and the sharper altitude decrease characterises the eastern part with a drier climate. On the other hand, the elevation changes on the north-western side of the belt are gradual, whereas on the south-western side they are sharp and steep. This is despite the climate in the south-western area of the belt that is wetter than the north-western part, thus the elevation change/climate relationship across the Caucasus opposes the east-west along the mountain range. For the eastern side of the belt, the elevation changes were gradual

northward whereas somewhat steep southward despite the climate is similar in the both directions, with slightly drier to the north. This dissimilarity in results is because of the tectonic processes that have happened and are happening in the belt.

In the Pyrenees Mountains, the elevation changes gradually to the west and steeply to the east, in a similar way to the Greater Caucasus topographic changes, the climate pattern is quite similar to that in the Greater Caucasus being wetter to the west than to the east. In the Northern Tibetan Plateau rim, the elevation chart shows that the elevations decreases sharply in both sides east and west of the plateau and the central region is inclined to the east. Correlating the elevation changes of the northern rim of the plateau with its climate, the precipitation rates of this rim of the plateau are roughly equal on both sides with a very small increase in the east side causing the steep elevation changes in both sides. In Himalayas, the elevations in the western part change sharply, whereas they decline gradually in the eastern part of the belt.

The opographic changes have arisen over time by the various processes that may affect erosion rate. The erosion affects the isostatic balance of the crustal block, where the vertical stress changes by material exhumation, and in turn this changes the distribution of structures and the rates at which they operate. The surface processes resulting from climate are able to configure extreme relief and rugged topography by accelerating the tectonic processes as a result of reducing the lithospheric mass which means that reducing overburden allows further thrusting to take place.

In summary, the results support the suggestion that the climate is the main cause of the steep or gradual changes of the elevation, so that whenever the area is wet, the erosion rate will increase which lead to formation of a gradual elevation decrease and vice versa (in large scale).

Chapter V

The major structural elements of the Greater Caucasus belt and the western South Caspian Basin

5. The major structural elements of the Greater Caucasus belt and the western South Caspian Basin

5.1. Introduction and Geological setting

This chapter focuses on the spatial distribution, geometry and large-scale mechanisms of the regional-scale structural elements which have developed in the evolution of the Greater Caucasus (GC) belt and the western South Caspian Basin (SCB).

The Greater Caucasus belt is a fold-and-thrust mountain belt that has formed as a consequence of Cenozoic shortening and collisional structural inversion of a former Jurassic to Palaeogene back-arc basin (Adamia et al., 2011a; Adamia et al., 2011b; Adamia et al., 1981; Adamia et al., 1977; Brunet et al., 2003; Ershov et al., 2003; Mitchell and Westaway, 1999; Ruban et al., 2007; Shevchenko, 1972).

The structural and geological evolution of the Caucasus Mountains is strongly affected by their location at the Arabian and Eurasian convergent margin, from the north-eastern edge of the Black Sea Basin to the western edge of the South Caspian Basin (Figure 5.1). The range is a part of the Alpine–Himalayan orogenic belt (Ershov et al., 2003) created as a result of Arabia-Eurasia collision (Allen et al., 2003; Joannin et al., 2010; Mitchell and Westaway, 1999).

The oldest rocks exposed in the central part of the Greater Caucasus belt are Palaeozoic granites (Shevchenko, 1972), and the sedimentary cover is exposed across the range around the Palaeozoic core(Adamia et al., 2011a). Even though the eastern part has a lower relief and exhumation level than the western part of the belt, the active convergence across the range increases towards the east.

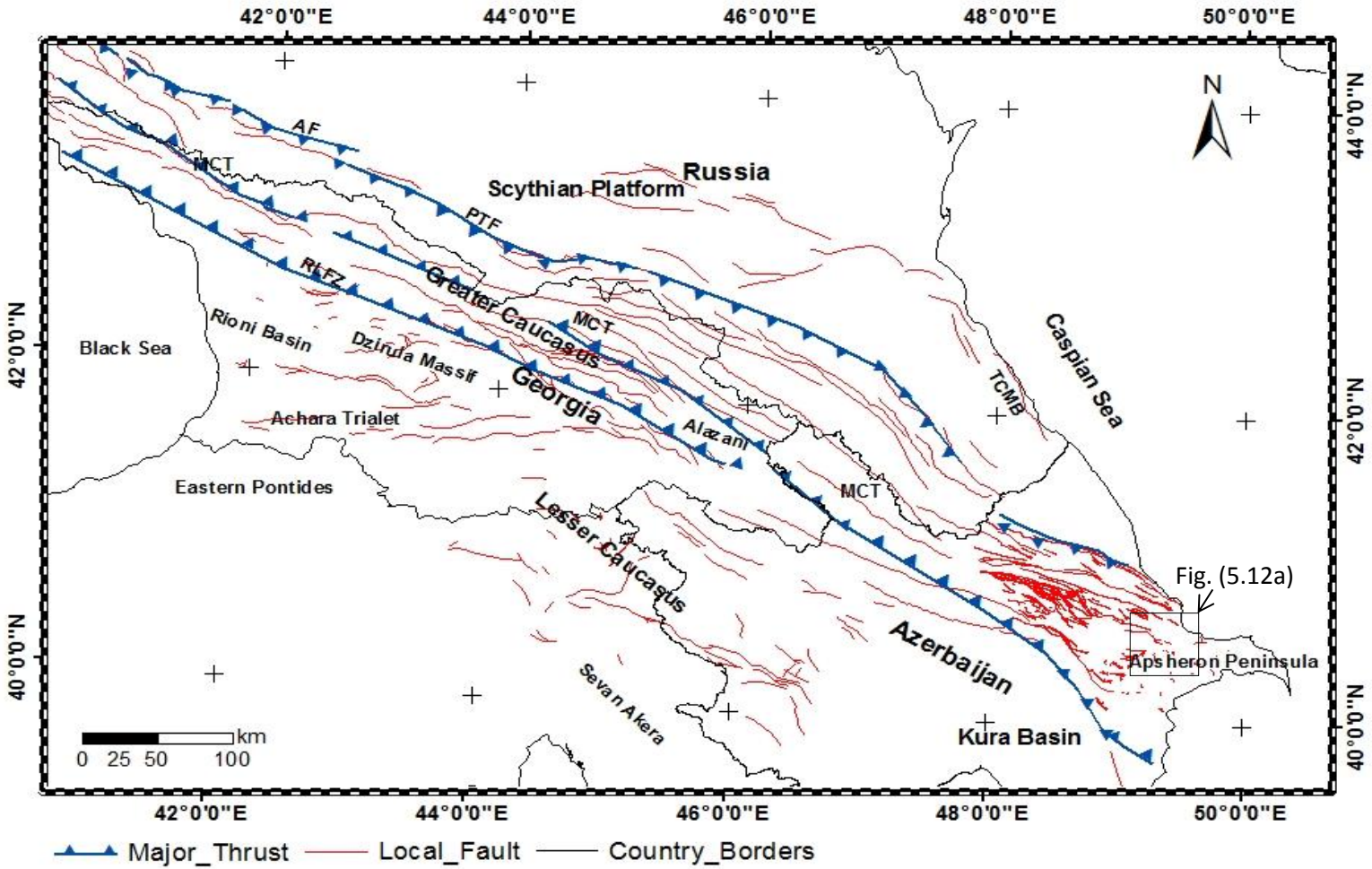

Figure 5.1. Location map of the Greater Caucasus showing the major structures in the belt, where; **MCT**=Main Caucasus Thrust, **AF**=Akhtyr Fault, **PTF**=Pshekish-Tyrnyauz Fault, **RLFZ**=Racha-Lechkhumy Fault Zone, **LC**=Lesser Caucasus, **SP**=Scythian Platform, **KB**=Kura Basin, **AP**=Apsheron Peninsula, **TCMB**=Terek–Caspian Molasse Basin, **RB**=Rioni Basin, **AT**=Achara Trialet belt, **SA**= Sevan Akera, **Al**=Alazani, the faults were interpreted by six geologic maps covering the Eastern Greater Caucasus with one covers the whole belt (scale 1:500,000), Google Earth™ and many published geologic maps of the area such as; (Adamia et al., 2011a; Avdeev and Niemi, 2011; Banks et al., 1997; Kekelia et al., 2008; Khain, 1975; Koçyigit et al., 2000; Martin-Gonzalez and Heredia, 2011; Mosar et al., 2010; Philip et al., 1989; Saintot et al., 2006b; Sosson et al., 2010b).

5.2. Regional tectonics and geodynamic setting

The region of the Caucasus can be divided into four main structural domains that formed before the Late Cretaceous-Paleogene volcanic belt and they are from south to north; Lesser Caucasus Arc, Achara-Trialet Belt, Dzirula Massif and Greater Caucasus (Adamia et al., 1977; Gamkrelidze, 1986; Zonenshain and Pichon, 1986) (Figure 5.2).

5.2.1. Lesser Caucasus Arc

The Lesser Caucasus Arc is composed of upper Jurassic to Cretaceous volcanic rocks (Robinson et al., 1995; Yilmaz et al., 2000), involving calc-alkaline series (basalt – andesite – dacite - rhyolite) rocks that formed as a result of Jurassic-Cretaceous island arc activity (north directed subduction to its southern edge). The belt continues toward the west (Eastern Pontides) and appears to lie unconformably above the Transcaucasian massif metamorphic series (Dzirula Massif) (Adamia et al., 1977; Gamkrelidze, 1986; Zonenshain and Pichon, 1986). The arc is bounded on the south by the Sevan Akera suture, which represents the region between the Lesser Caucasus and Anatolide-Tauride-Armenian block (Adamia et al., 2011a; Sosson et al., 2010b).

5.2.2. Achara-Trialet Belt

The Achara-Trialet Belt is located between western Lesser and Greater Caucasus, with north-vergent thrusts and folds deforming mafic to intermediate volcanic rocks of Cretaceous-Eocene times; it is considered as a narrow extensional back-arc basin that opened during the Late Cretaceous and accumulated sediments and volcanic rocks throughout the Eocene and Oligocene (Banks et al., 1997; Kazmin et al., 1986; Robinson et al., 1997; Yilmaz et al., 2000) (Figure 5.2).

5.2.3. Dzirula Massif

This region is a tectonic block between the Lesser and Greater Caucasus to the west, which contains metamorphic and igneous rocks (Proterozoic-Carboniferous) with granitoid intrusive rocks (Adamia et al., 2011b; Mayringer et al., 2011) (Figure 5.2).

5.2.4. Greater Caucasus

The Greater Caucasus range is subdivided into three parts; Jurassic and Cretaceous flysch deposits to the south, Palaeozoic basement and Jurassic flysch deposits in the axial part, and Jurassic-Cretaceous carbonates to the north of the range (Adamia et al., 2011a; Saintot et al., 2006a).

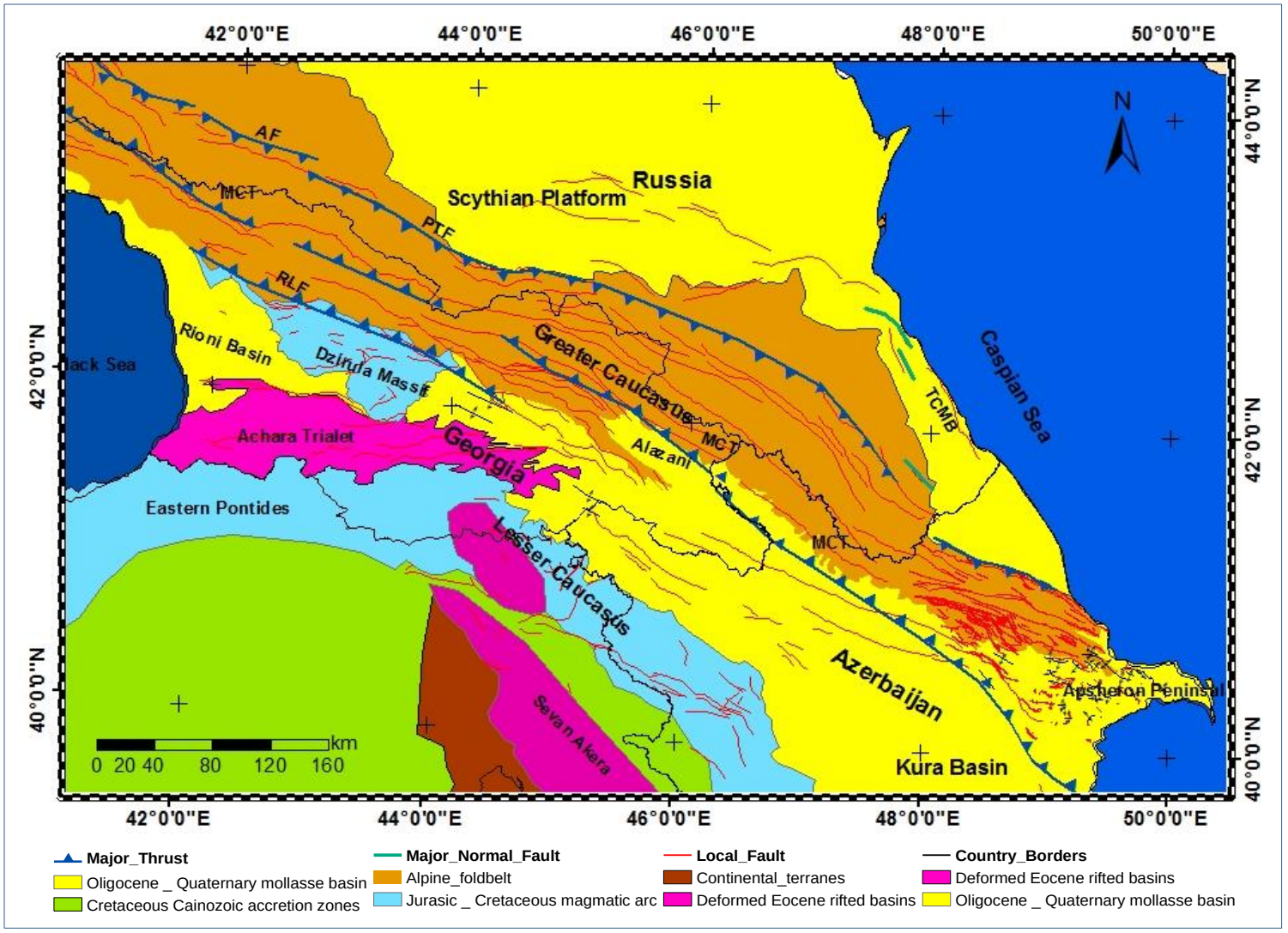

Figure 5.2. Simplified geologic map of the Caucasus region, showing the main tectonic units of the region modified after (Adamia et al., 2011a; Brunet et al., 2003; Gamkrelidze, 1986).

There is no active subduction regime underneath the main Greater Caucasus orogen however; it is bounded by deep Mesozoic sedimentary basins to the east and west of the belt which are filled with Cenozoic-Quaternary sediments. There are earthquake events at depths > 30 km in the area between the eastern Kura Basin and western South Caspian Basin, and Moho depth in this area is about 35km (Shengalaya, 1978), which might be due to under thrusting of the South Caspian crust underneath the Kura Basin crust (Allen et al., 2002b).A detached slab under the Lesser Caucasus has been detected to the west of the belt (Hafkenscheid et al., 2006).However to the east, the process of subduction has started because the crust underlying the SCB has been forced under the middle Caspian Sea along the Apsheron Sill from the Pliocene (Knapp et al., 2004; Priestley et al., 1994).

5.3. Caucasus Earthquakes activity

The Caucasus region earthquake record shows that it is an active zone, that is part of the Arabia-Eurasia collision zone (Allen et al., 2004; Allen et al., 2006; Jackson, 1992; Jackson et al., 2002; Philip et al., 1989; Priestley et al., 1994). Even though since the beginning of the 19th century there have been no earthquake with magnitude >7.0 recorded in the Greater Caucasus belt, as suggested by the Caucasus region earthquake historical records with the exception of the M 7.2 1991 Racha earthquake, significant seismicity (with magnitude less than 6.5) occurs in the belt. Seismicity of the Eastern Greater Caucasus has greater intensity compared with the western part of the belt (Tan and Taymaz, 2006). Seismicity has been recorded on both the north and south sides of the range in the eastern Greater Caucasus, whereas in the western side the earthquakes occur just in the southern side (Figure 5.3 and Figure 5.5).

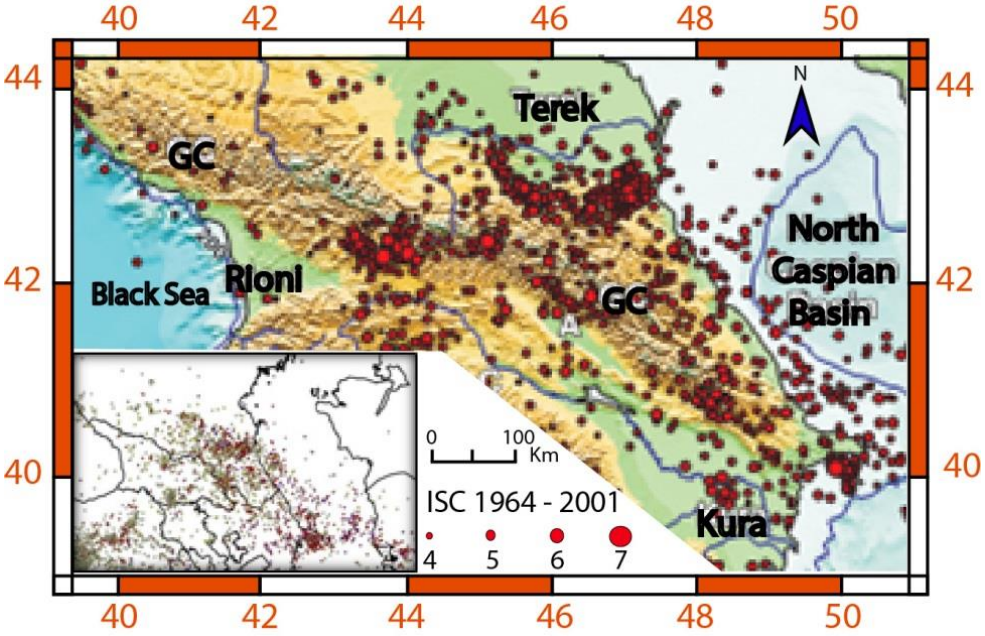

Figure 5.3. Seismicity of the Caucasus region with ISC (International Seismological Centre) epicentres for M>4 earthquakes that occurred during the period 1964-2001 from; Tan and Taymaz (2006).

There are some differences between the data resulting from the frequently used catalogues of earthquakes (such as the International Seismological Centre event catalogue (ISC), the U.S. Geological Survey–National Earthquake Information Centre catalogue (USGS-NEIC), Engdahl-Hillst-Buland (EHB), and Global (formerly Harvard) Centroid Moment Tensor (CMT) database, especially of the shallow depths earthquakes.

In shallow depth events it is difficult to identify the phases of the surface reflection waves (pP and sP) due to the complex rupture process, and in this case the depth may be stated deeper than the true depth. This can be seen in Table. 5.1 where in many events the focal depth is different from one catalogue to another; for instance; the focal depth of the 29/04/1991 Western Caucasus earthquake is reported as 22.3 km by CMT, 34.5 km by ISC and 7 km by USGS, however the waveform analysis byTan and Taymaz (2006) indicates that the centroid depth was 6 ±2 km, which has been used in this study.

Another example can be seen in one of the eastern Caucasus earthquakes in 16/12/1990, where Tan and Taymaz (2006) found that the centroid depth was 11±4 km, despite it being quoted as 17.6, 17.2, 15 and 33 km by CMT, ISC, EHB and USGS-NEIC respectively. Jackson and Mckenzie (1984) report that the centroid depth of the Western Caucasus event in 02/01/1978 was 10 km whereas other catalogue show different focal depths; it was 15 km by CMT, 12.7 km by ISC, 7km by EHB and 10 km by the USGS-NEIC catalogue.

In these catalogues, shallow events in the continental regions are commonly fixed at 10, 15, 20 and 33 km, which can be seen in the depth histograms of the

Caucasus region earthquakes in Figure 5.4a-d where, it can be observed that the USGS-NEIC CMT, ISC and EHB catalogues have many events with fixed depths at 10, 20 and 33 km.

The accurate centroid depths of the earthquakes have been taken from previous studies (Jackson and Mckenzie, 1984; Jackson et al., 2002; Mellors et al., 2012; Tan and Taymaz, 2006); all these data are shown in Table 5.1.In some cases, the catalogue data have been used due to the absence of the studied depths. From the hypo-central depth histograms of the earthquakes data that have been used in this study (Figure 5.4e) can be observed that most events occur in depths between 6km and 20 km, which indicate the absence of deep earthquakes.

Table 5.1. Source parameters of the earthquakes that have occurred in the Greater Caucasus belt between January 1978 and December 2012. The information has been used in GMT software to create a focal mechanisms map of the belt and construct cross sections.

No	Date	Long.	Lat.	Plane 1			Plane 2			Magnitude	Depth							
				S	D	R	S	D	R		CMT	ISC	EHB	USGS	TT06	JM84	Used	Ref.
1	02/01/1978	44.24	41.54	140	80	-178	50	88	-10	5.6	15	12.7	7	10	-	10	10	JM84
2	26/05/1978	46.55	41.96	280	17	71	120	74	96	5.2	23.5	36	24	38	-	38	24	EHB
3	23/02/1981	45.98	41.79	333	35	145	93	71	60	5.6	33	35	14.7	33	-	-	14.7	EHB
4	18/10/1981	45.31	43.26	124	34	126	263	63	68	5.2	33	34	26.9	33	-	-	26.9	EHB
5	19/11/1981	49.19	40.73	34	68	162	131	73	23	6.6	33	42	50	33	-	-	33	CMT
6	30/10/1983	42.17	40.29	211	73	-17	306	74	-162	5.5	11.6	16.1	15	15	9±2	-	9	T06
7	30/10/1983	42.18	40.39	221	82	-2	312	88	-172	5.5	33	10	7.6	17	-	-	7.6	EHB
8	18/09/1984	42.21	40.92	17	57	-13	114	79	-146	5.4	10	10	10	10	-	-	10	CMT
9	18/10/1984	42.48	40.59	123	42	119	266	55	66	5.4	10	19.1	35	60	-	-	10	CMT
10	4/7 1985	45.94	42.29	192	15	15	88	86	104	5.2	15	34.9	15	33	-	-	15	EHB
11	7 11 1985	42.41	40.36	233	58	22	131	72	146	5.8	10	31.4	35	33	-	-	10	CMT
12	13/05/1986	43.64	41.36	237	80	-1	328	89	-170	5.3	15	28.9	10	10	13±2	-	13	TT06
13	03/05/1988	47.54	42.4	126	16	89	308	74	90	6.8	15	10	20	22		-	15	CMT
14	07/12/1988	44.2	41	288	33	135	59	67	66	5.2	15	25.1	5	6	5±2	-	5±2	TT06
15	03/08/1989	45.36	43.59	278	42	81	110	49	98	5.5	17	28.3	35	18	-	-	17	CMT
16	16/12/1990	43.74	41.32	239	81	-1	329	89	-171	6.9	17.6	17.2	15	33	11±4	-	11±4	TT06
17	29/04/1991	43.65	42.49	288	39	106	87	53	77	6.1	22.3	34.5	17	7	6±2	-	6±2	TT06
18	29/04/1991	43.88	42.45	261	41	104	62	50	78	5.6	15	1.3	14	13	6±1	-	6±1	TT06
19	03/05/1991	43.2	42.59	315	47	127	87	55	57	6.2	15	34.4	3.7	10	8±2	-	8±2	TT06
20	15/06/1991	43.99	42.44	138	49	44	16	58	130	5.1	15	8.8	9	7	7±4	-	7±4	TT06
21	04/07/1991	44.12	42.33	154	37	65	4	57	108	6.2	19.7	11.6	15	20	8±2	-	8±2	TT06

Continued

No	Date	Long.	Lat.	Plane 1			Plane 2			Magnitude	Depth							
				S	D	R	S	D	R		CMT	ISC	EHB	USGS	TT06	JM84	Used	Ref.
22	06/10/1991	43.43	40.9	32	70	-3	123	87	-160	5.1	16.5	1.7	15	18	-	-	15	EHB
23	23/10/1992	45.07	42.5	302	13	144	67	83	80	5.2	15	16.4	16	16	18±2	-	18±2	TT06
24	31/08/1993	49.37	41.71	219	39	35	101	68	124	5.4	81.6	84.9	89.3	84	73±2	-	73	TT06
25	29/01/1995	40.72	40.16	211	70	1	121	89	160	5.6	33	29.5	-	-	-	-	29.5	ISC
26	27/11/1997	45.33	41.85	103	39	122	244	58	66	5.6	41.8	35.5	23.9	37	9±2	-	9±2	TT06
27	31/01/1999	46.84	43.16	111	33	66	319	60	105	5.6	30.1	51.2	13	13	9±1	-	9±1	TT06
28	21/02/1999	46.83	43.21	103	33	61	317	62	108	5.4	32.7	51.2	42	65	8±2	-	8±2	TT06
29	04/06/1999	47.45	40.8	193	40	68	40	53	107	5.3	32.7	13.1	14	33	16±2	-	16±2	TT06
30	03/12/1999	42.35	40.36	221	69	8	129	83	159	6	19.3	51	6.1	19	6±2	-	6±2	TT06
31	06/02/2006	43.53	42.65	324	31	118	112	63	74	5.3	14	23.5	17.7	17	-	-	14	CMT
32	11/10/2008	46.25	43.37	78	42	69	285	51	108	5.8	13	11.6	16	16	-	-	13	CMT
33	11/10/2008	46.19	43.34	103	43	101	268	48	80	5.3	18.8	15.2	17.5	9	-	-	17	EHB
34	07/09/2009	43.44	42.66	314	28	106	116	63	81	6	13.4	14.6	-	15	-	-	15	USGS
35	19/01/2011	42.66	41.96	58	42	44	292	62	123	5.3	19.3	10.4	-	10	-	-	10.4	CMT
36	18/08/2011	42.95	42.61	278	38	79	112	53	98	5	13.8	10.2	-	-	-	-	10.2	ISC
37	07/05/2012	46.79	41.55	300	8	102	108	82	88	5.9	11	11	-	11	-	-	11	CMT
38	07/07/2012	46.73	41.56	261	41	104	62	50	78	5.6	6	1.3	14	13	-	-	6	CMT
39	07/07/2012	48.44	40.75	315	47	127	87	55	57	6.2	15	34.4	3.7	8	-	-	8	USGS
40	14/10/2012	46.41	41.83	310	9	120	100	83	86	5.6	12	10	-	10	-	-	10	ISC
41	23/12/2012	41.07	42.43	214	76	178	305	88	14	5.8	16.1	10	-	10	-	-	16.1	CMT
42	25/12/2012	40.97	42.44	302	85	4	212	86	175	5.4	12	10	-	10	-	-	10	ISC

Note: **S** = Strike, **D** = Dip, **R** = Rake, **CMT** = Centroid Moment Tensor, **ISC**= International Seismological Centre, **EHB**= Engdahl Hillst **B**uland, **USGS**= U.S. Geological Survey–National Earthquake Information Centre, **TT06**= Tan and Taymaz (2006) and **JM84**= Jackson and Mckenzie (1984), the column "used" means the type of the data of each event that have been used in this study .

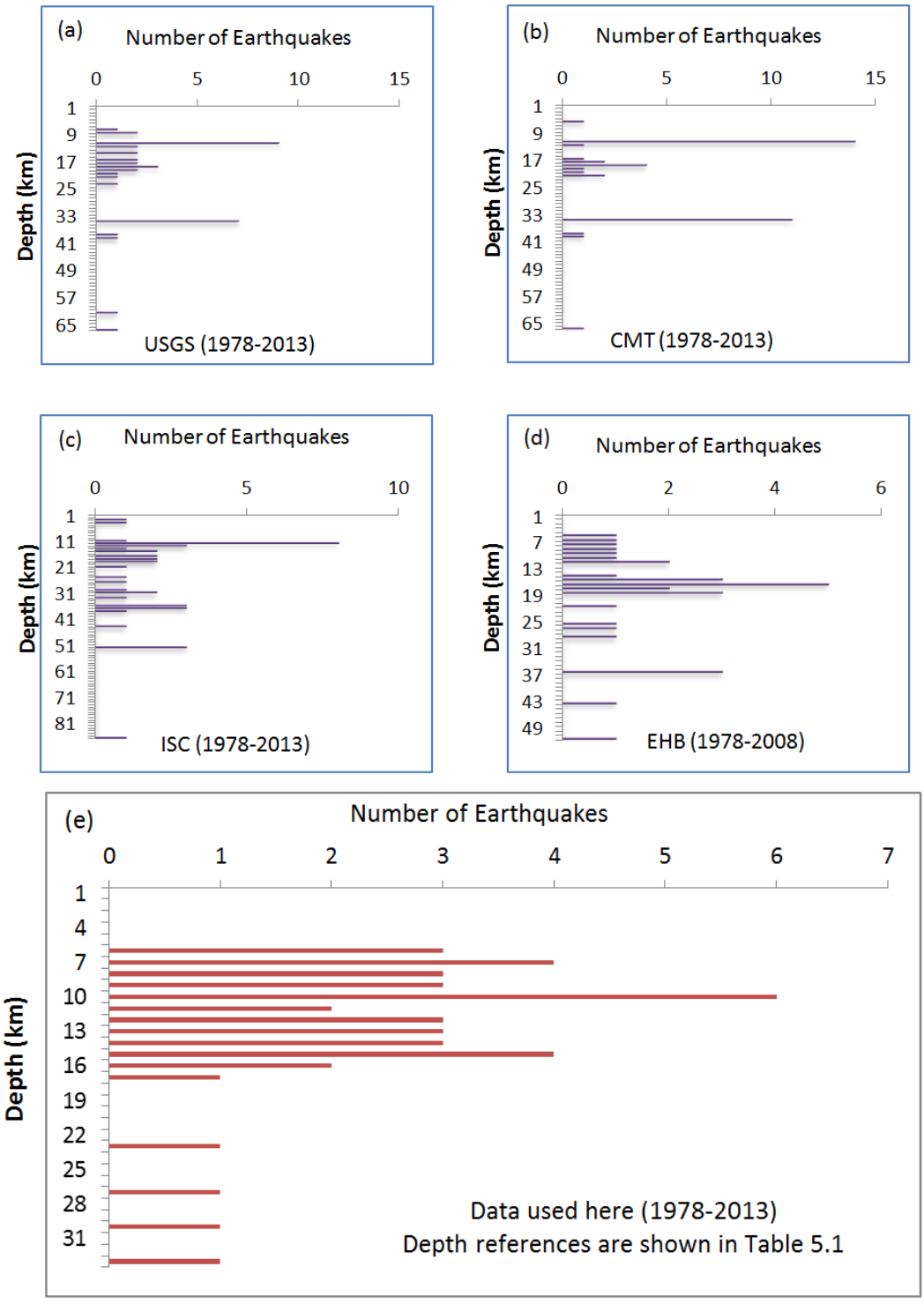

Figure 5.4. Depth histogram of the Caucasus region earthquakes, where (a-d) showing the fixed depths at 10, 20 and 33 km by USGS-NEIC, CMT, ISC and EHB catalogues, and (e) is a Depth histogram of the data that have been used in this project (events between (1978-2013) and depths references are shown in Table 5.1).

5.3.1. Focal mechanisms map and cross section creation

The earthquake data for the region were analysed and plotted by using the Generic Mapping Tools (GMT) software (Wessel and Smith, 1998).

5.3.1.1. Focal mechanisms map

By using the following command line (as an example) in the GMT software, a map of the focal mechanisms (locations, depths and magnitudes) can be created (Figure 5.6a,c);

psmeca input.file.txt –JM(scale) -Rw/e/s/n -Sa0.x –B10g10/10g10> bb.ps

Where:

- psmeca do read the data values from the given file and then produces Post Script code that will plot focal mechanisms on a map.
- The input file reads e.g.:

Long	Lat	Depth	Strike	Dip	Rake	Magnitude	Event
44.240	41.540	10.0	140	80	-178	5.6	1
46.550	41.960	38.0	280	17	71	5.2	2
38.050	44.400	33.0	301	12	93	5.7	3

- Sa: the scale of the beach balls.
- B<grid_x>g<annotation_x>/<grid_y>g<annotation_y>

From the data in the published catalogues, the higher seismic activity region is located in the southern flank of the western central part of the Greater Caucasus in Georgia (Figure 5.5), but many of these events are aftershocks of the M 7.2 Racha event.

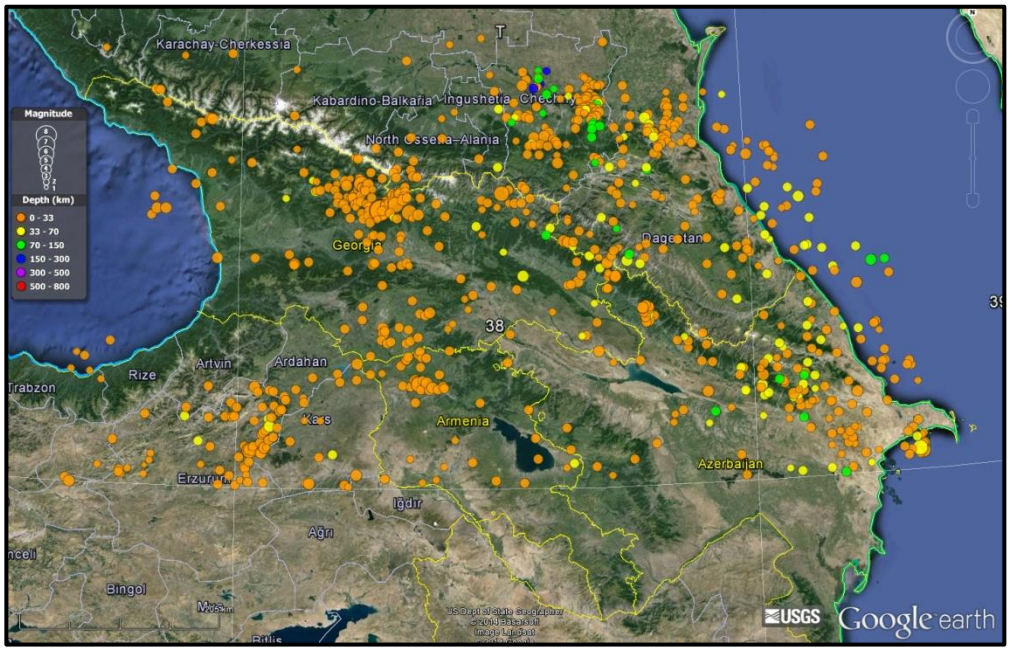

Figure 5.5. Map of the Caucasus area showing the distribution of the earthquake events that have been taken from the published catalogue (CMT).

5.3.1.2. Focal mechanisms cross section creation

To create a cross section of the focal mechanisms, another command has to be used (pscoupe) e.g. Figure 5.6b,c);

[pscoupe input.file.txt -Jx0.025/-0.1 –Aa46/48/41/43/90/400/0/30f -Sa0.5 -B100g100/5g5 >section.ps]

Where:

- The input file is the same file for the psmeca.
- -Jx0.025/-0.1: this plots the focal mechanisms in the right projection at the right scale on the page.

- -Aa: is followed by the start and finish points of the section line, in degrees, then the dip of section line (make it 90, usually), then the width at either side of the central line (so 400 km in the section), then the top of the section (0 is at the surface) and base (40 km in the example).
- -Sa0.3: sets the size of the focal mechanism.
- -B100g100/5g5: draws the box and gives the number of divisions, and how it is numbered.

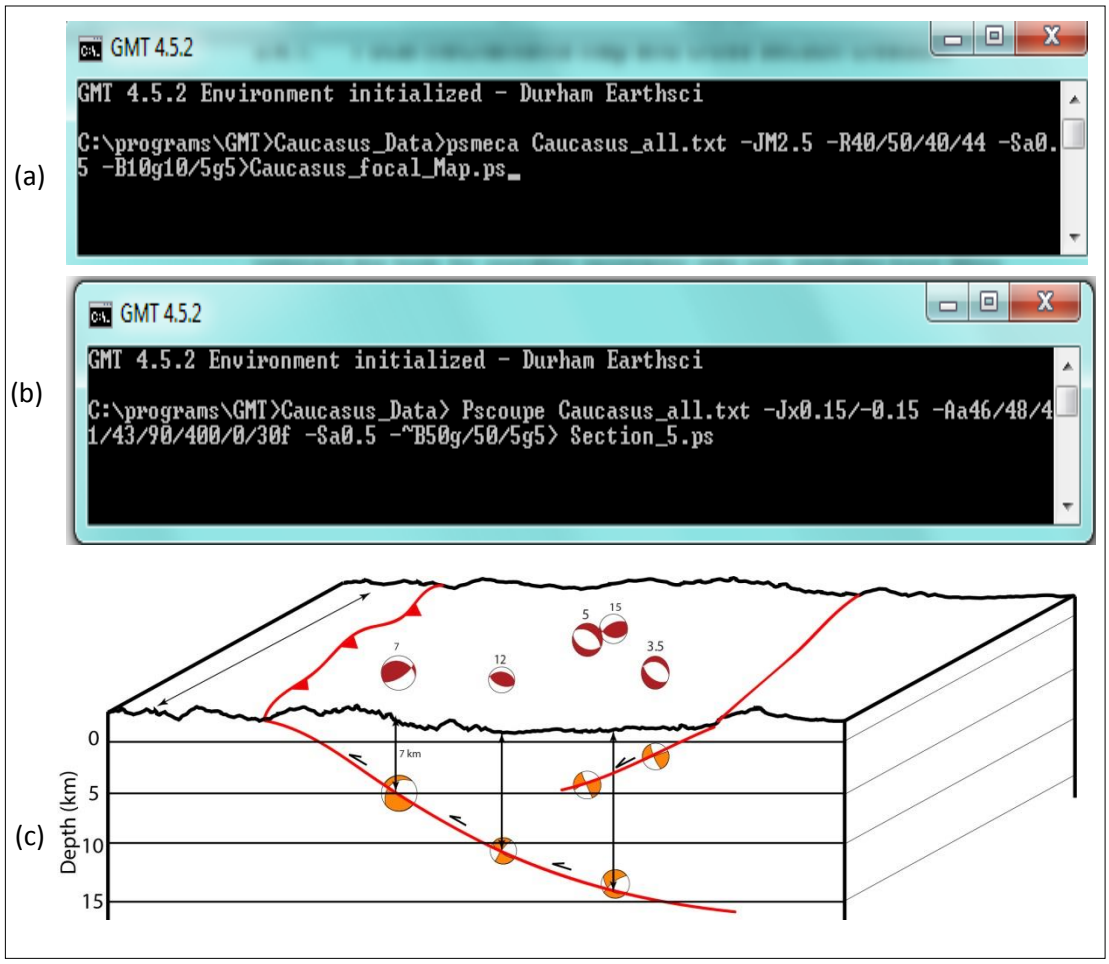

Figure 5.6. (a), (b) showing the command lines (as an example) in GMT software to create focal mechanisms map and cross section respectively, and (c) is a schematic map and cross section showing how to convert the focal mechanisms from map to cross section, (number above the focal mechanism refers to the event depth in km) (all depths here are relative to ground level and not to the sea level).

The map in (Figure 5.7) confirms that the strike-slip focal mechanisms are the predominant type in the Lesser Caucasus and the Anatolian Plateau to the south of the Greater Caucasus belt, and are linked with almost vertical fault systems; however in the Greater Caucasus the reverse focal mechanisms represent the main type, which are linked with the thrusting and NE-SW compression. Note that there is no seismicity evidence for the regional NE-SW strike-slip fault across the range, proposed by Philip et al. (1989).

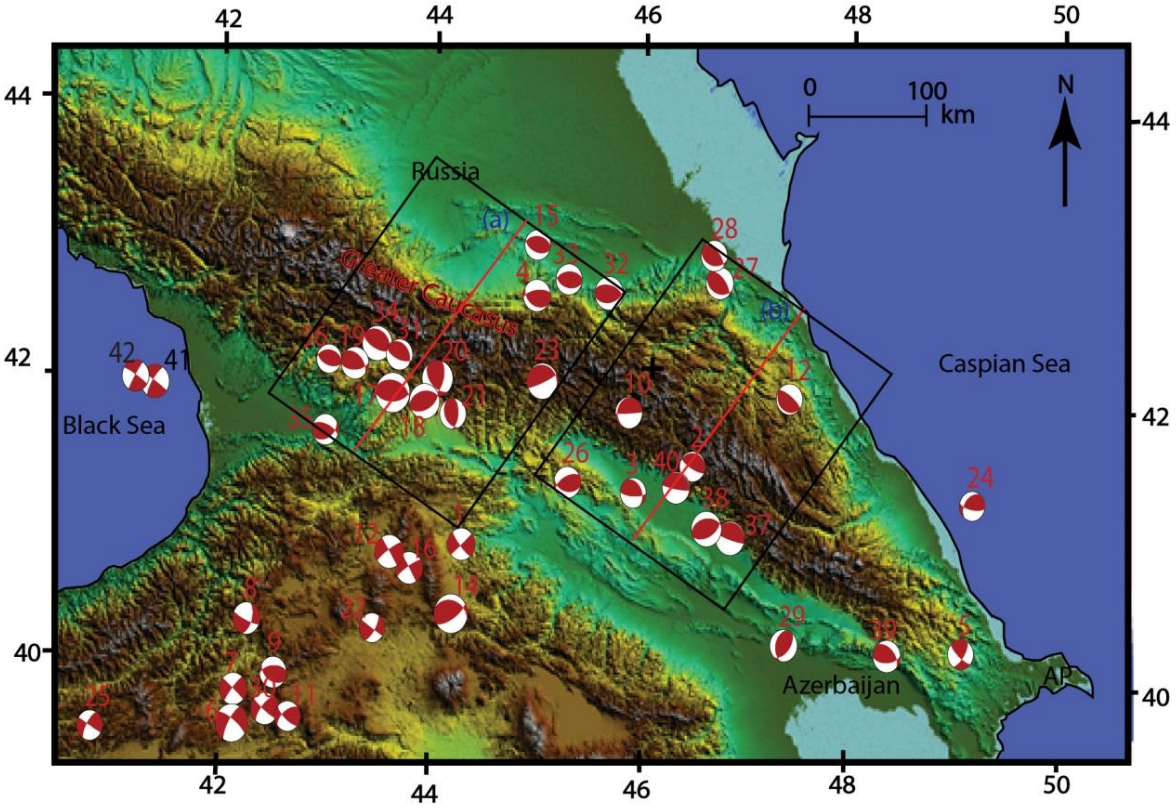

Figure 5.7. SRTM data on the Caucasus region with the distribution of the earthquake events that occurred during the period from 1977 to 2013. The focal mechanisms were created using the Generic Mapping Tools (GMT) software, (the red lines show the location of the sections in Figure 5.8 and

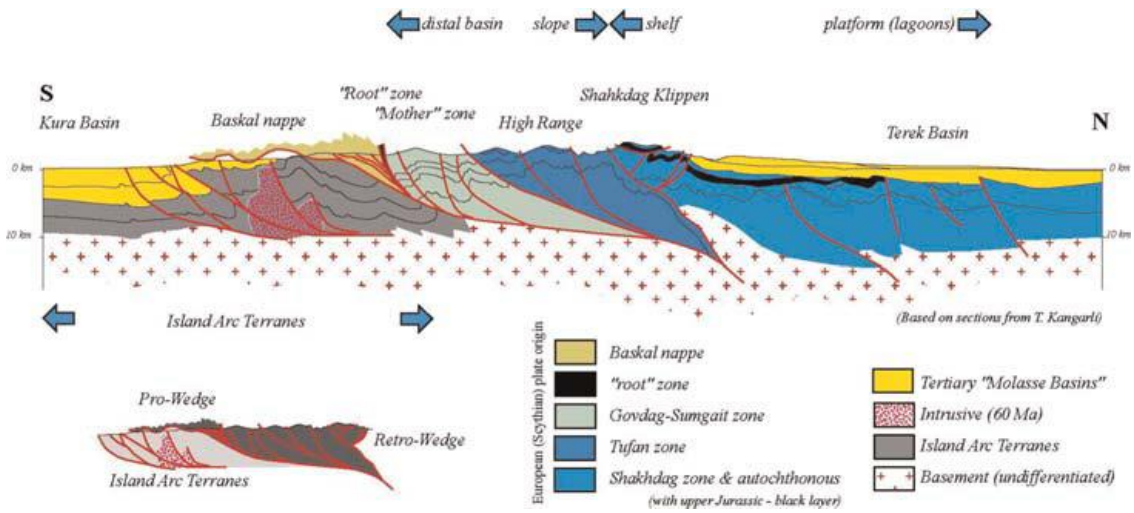

Figure 5.9 and the boxes are the area covered by the events that have been used in the sections). Note this map shows just the events with reliable depth and have magnitude more than 4.8.

After creating the creating the focal mechanisms cross sections by using the Generic Mapping Tools (GMT) software which takes the sea level as the top, the focal mechanisms depths moved and projected in a new section taking in account the ground level of each event (Figures 5.8 and 5.9).

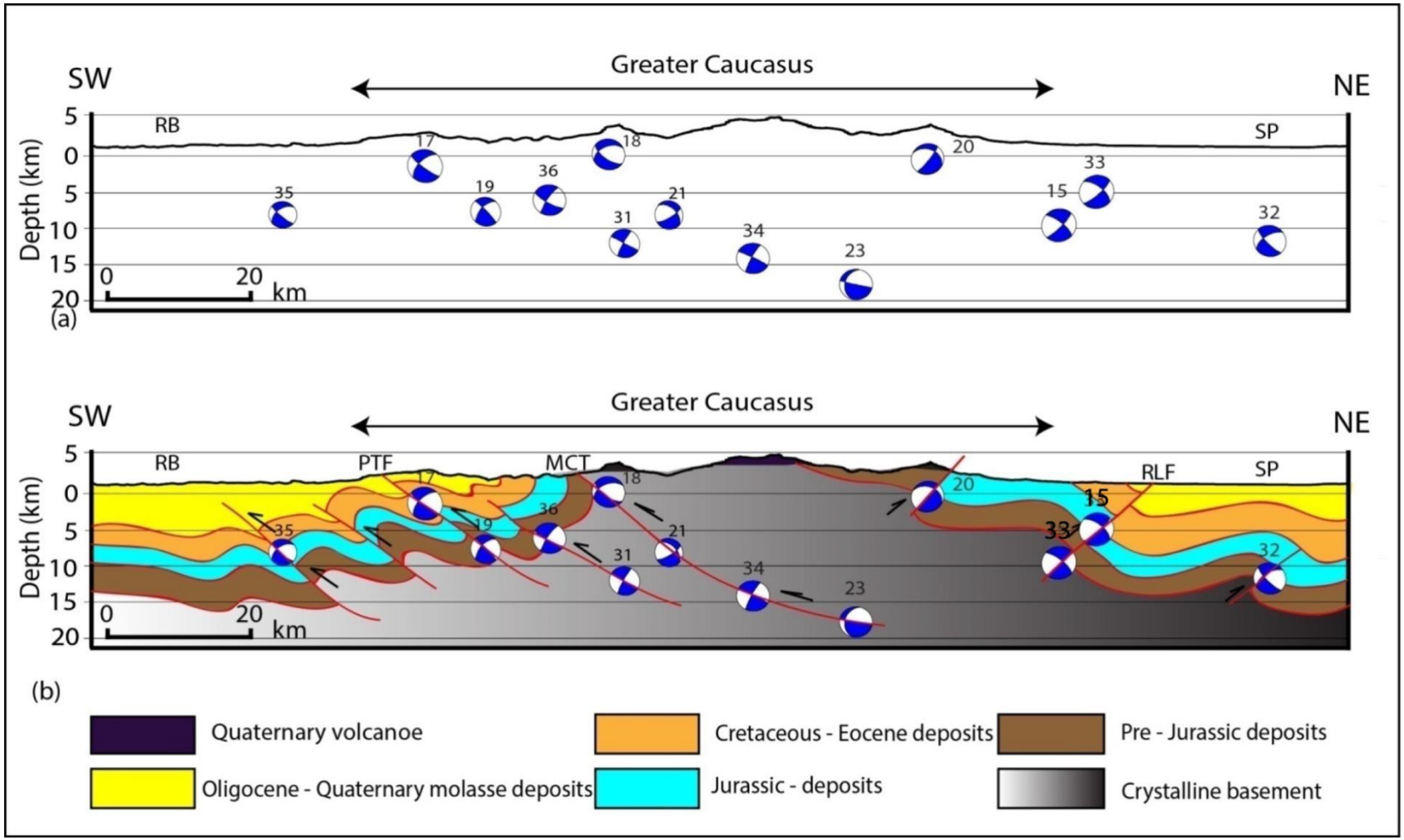

Figure 5.8. Cross section across the Greater Caucasus created by using the earthquake data that occurred in the belt in the period of 1977-2013, the focal mechanisms created by the Generic Mapping Tools (GMT) software, (a) showing the cross section of the focal mechanisms before interpretation, and (b) after interpretation; showing the faults and main thrusts of the belt; MCT= Main Caucasus Thrust, RLF= Racha Lechkhumy Fault, PFT= Pshekish Tynauz Fault, RB = Rioni Basin, SP = Scythian Platform and TCMB=Terek–Caspian Molasse Basin (numbers shown above the focal mechanisms are indicating the event numbers shown in Table 5.1), (location of the section is the box (a) shown in Figure 5.7). In cases where single event used to constrain structure, the fault plane was selected over Axial Plane from focal mechanism by comparing with the published and studied structures (e.g. events number 20, 32 on here, and number 12 on Figure 5.9) (Thrusts and stratigraphic subdivisions are shown in figure 5.2).

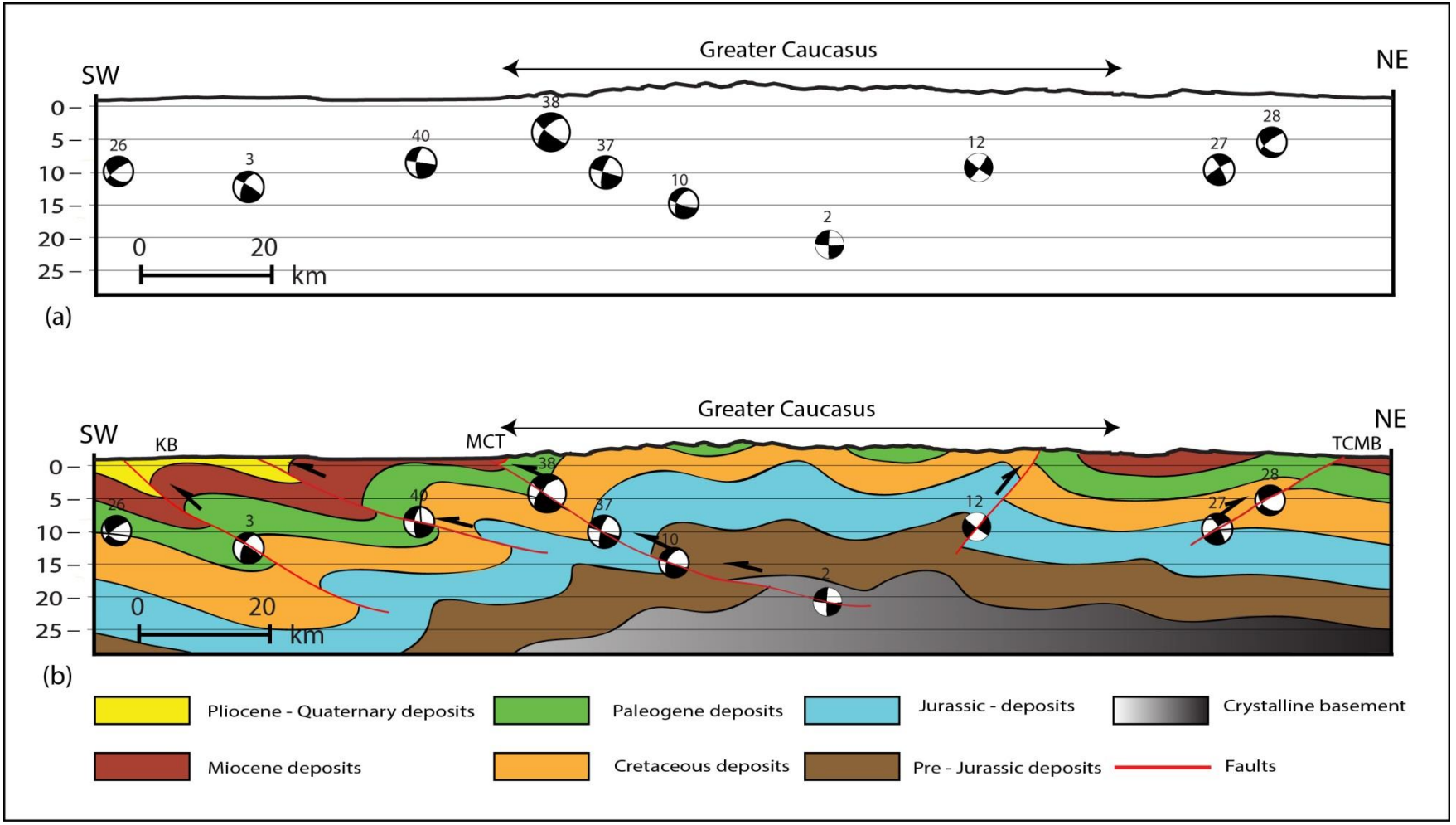
Greater Caucasus
SW
NE
0
5
10
15
20
25
26
3
40
38
37
10
2
12
27
28
0
20
km
(a)
Greater Caucasus
SW
KB
MCT
TCMB
NE
0
5
10
15
20
25
26
3
40
38
37
10
2
12
27
28
0
20
km
(b)
Pliocene - Quaternary deposits
Paleogene deposits
Jurassic - deposits
Crystalline basement
Miocene deposits
Cretaceous deposits
Pre - Jurassic deposits
Faults

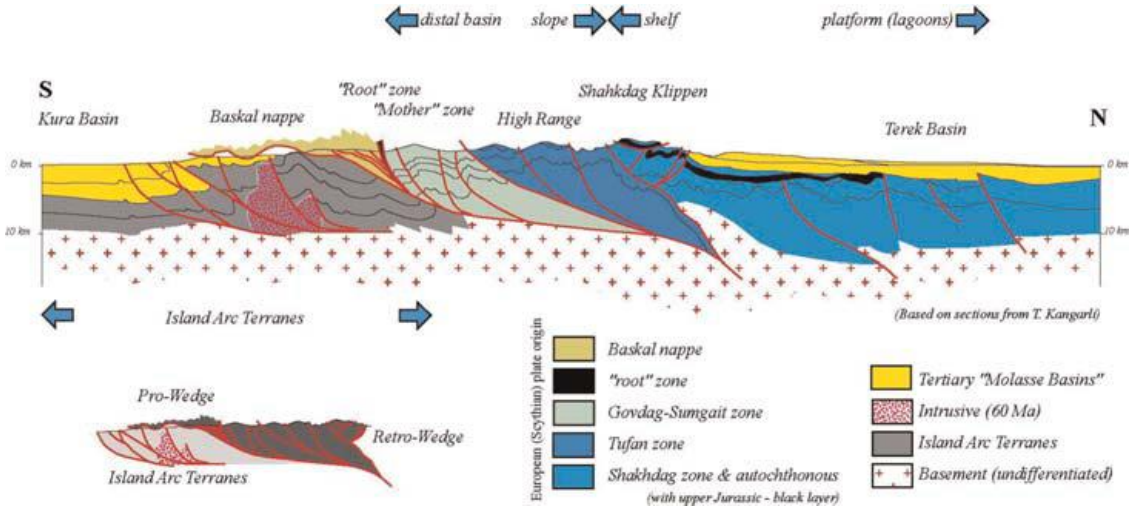

Figure 5.9. Cross section across the eastern Greater Caucasus, (a) is the cross section of the focal mechanisms before interpretation, and (b) after interpretation; showing the faults and main thrusts of the belt; MCT= Main Caucasus Thrust, KB = Kura Basin and TCMB=Terek–Caspian Molasse Basin (numbers above the focal mechanisms indicate to the event numbers shown in Table 5.1), (location of the section is the box (b) in Figure 5.7). (c) is a cross-section for the eastern Greater Caucasus from Egan et al. (2009), for a similar line to 5.9a and b. See text for discussion.

Despite the similarity of the earthquakes magnitudes on both sides of the Greater Caucasus (north and south), the depths varies, so that they are deeper in the southern than in the northern part of the belt. The sections in Figures 5.8 and 5.9, show that the southern flank of the belt is characterized by thrusts that have lower angle than those in the northern side.

By studying the focal mechanisms that distributed along the belt (depths, magnitudes etc.) and the structures of the belt, we can observe that the seismicity and the major faults are associated with each other. The map and the cross sections (Figures 5.7, 5.8 and 5.9) show the relationship between the high magnitude events (e.g. events in 29/04/1991, 04/07/1991, 07/09/2009, 07/05/2012 and 07/07/2012, up to *M* 6.2; Table 5.1) and the main thrusts on the belt especially in the southern flank, such as the Pshekish Tynauz Fault and the Main Caucasus Thrust, where a significant displacement is accommodated. And the lower magnitude earthquake events (e.g. events in 29/04/1991, 04/07/1991, 07/09/2009, 07/05/2012 and 07/07/2012, up to *M* 5.5; Table 5.1) are associated with the smaller thrusts in the belt such as RLF= Racha Lechkhumy fault, and many of the low magnitude events are linked with small faults that are distributed along the belt.

Comparing the published cross section through the central part of the eastern Greater Caucasus in Azerbaijan by Egan et al. (2009) (Figure 5.9c) with the new cross section of the same area which is drawn by using the focal mechanisms on the belt (Figure 5.9b), it can be noted that earthquake data suggest that thrusts dip are inwards, towards the core of the range. This is consistent with the conclusion of Jackson et al. (2002), although these authors did not attempt a cross-section

through the range to utilise the focal mechanisms in interpreting the deep structure. In the Egan et al. section the structural vergence is predominantly towards the south. Note that the Egan section covers the Terek basin to the north east of the belt, showing south-directed thrusts, whereas in the new cross section that area is not drawn.

An important aspect of the seismicity record is the scarcity of low angle planes for the earthquakes (≤ 10^{o}), which would be expected if there is a low-angle, seismically active detachment at the base of the fold-and-thrust belt. (A caveat here is that the instrumental record only covers a few decades: it could be argued that such an earthquake could yet occur on such a structure).

5.4. Caucasus Structures

5.4.1. The Greater Caucasus Folds

The most prevalent and spectacular tectonic features that exist in the Caucasus belt especially on the eastern side are the folds (Figures 5.10 and 5.12). These are the most important natural structure and reflect the manner in which the geometry of constituent rock layers has changed during the deformation under conditions of elastic to plastic strain. The Greater Caucasus Mountain Belt is a good example of a young orogenic belt that shows a variety of fold styles.

5.4.1.1. Spatial distribution of the Greater Caucasus folds

Folds in the Greater Caucasus are cross-cut by mud volcano structures, especially in the east of the belt (Figure 5.11a-b).

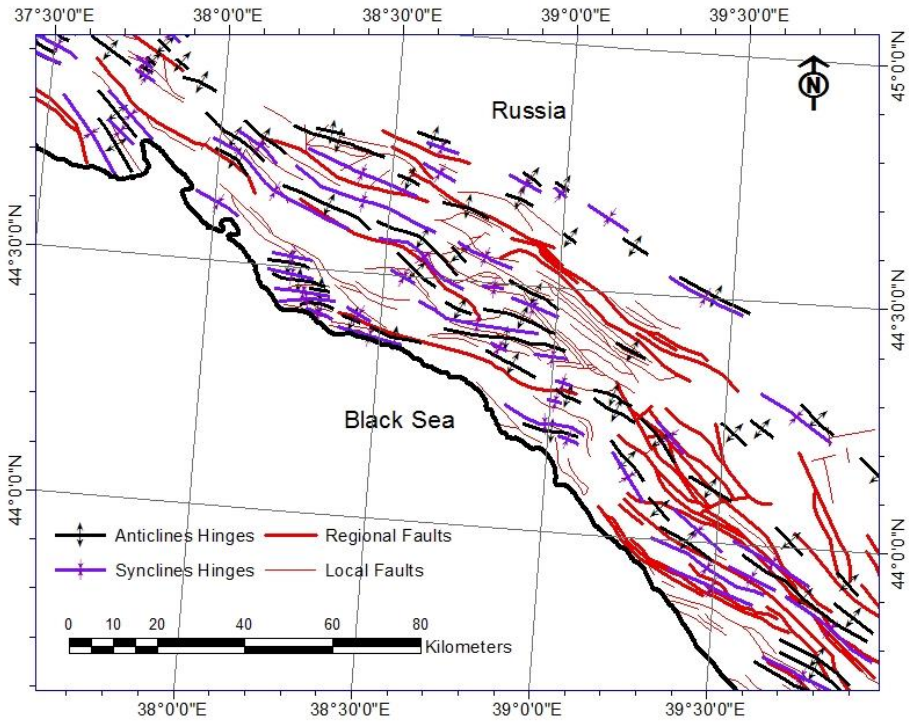

Figure 5.10. Structural map of the north west of the Greater Caucasus belt showing the regional and local faults and the folds distributions, new compilation interpreted by two geologic maps covering the western Greater Caucasus with one covers the whole belt (scale 1:500,000), Google Earth™ and many published geologic maps of the area such as; (Avdeev and Niemi, 2011; Banks et al., 1997; Saintot and Angelier, 2002).

The geographical and spatial distribution of folds and their intensity are varied along the Greater Caucasus belt, which also has different topographic aspects. Folds are linear and parallel to each other in the west of the Greater Caucasus belt (Figure 5.10c), whereas they are mostly curved and cut by mud volcanoes in the east of the belt and western part of the South Caspian Basin in Apsheron Peninsula (Figure 5.11a-b). These curved axial traces could indicate to thrusts displacement variations along the strikes of the folds (Allen et al., 2003; Alsop and Holdsworth, 2002). On the other hand from

Figure 5.12 can be observed that most folds have the regional WNW-ESE trend of the main Greater Caucasus belt, but a few folds have a more east-west orientation.

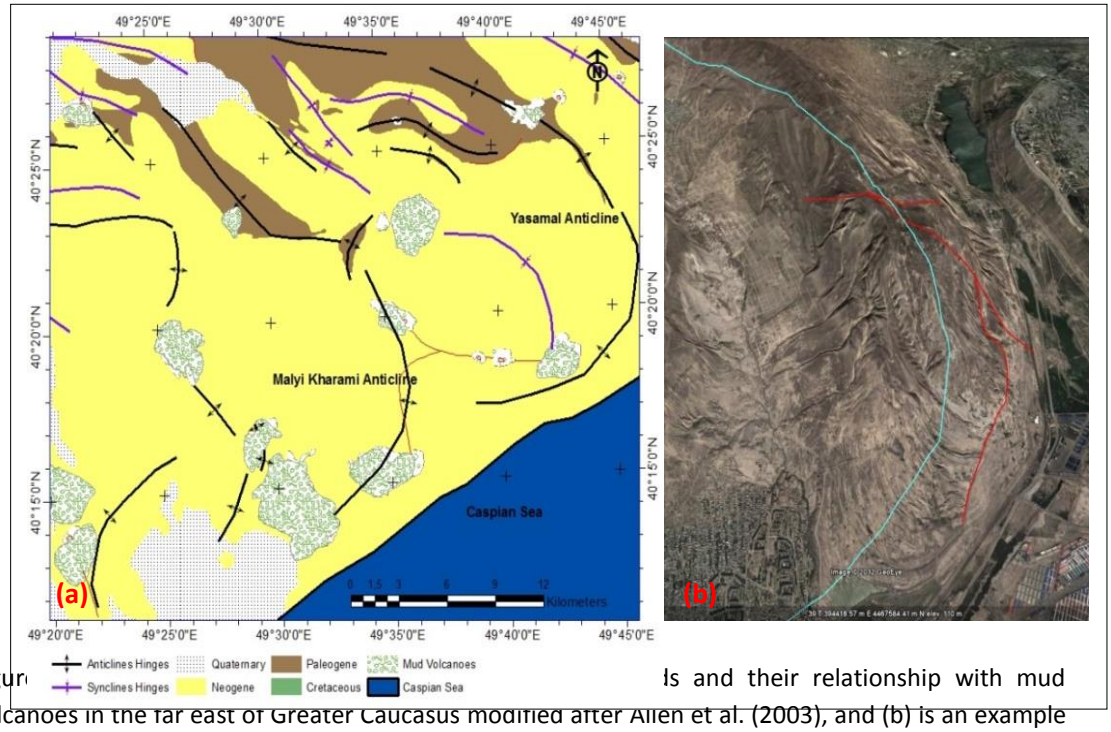

Figur ls and their relationship with mud volcanoes in the far east of Greater Caucasus modified after Allen et al. (2003), and (b) is an example of the faults (red lines) cutting folds of the Greater Caucasus (light blue line is the hinge of Yasamal anticline).

Fold axial traces in the Greater Caucasus belt are generally sub-parallel to each other; however, they do show differences in how they are arranged. The traces are offset from each other in en echelon patterns (

Figure 5.12) that are either random or with systematically stepped offset, associated with strike-slip faults. However the random pattern represents the more important pattern that is distributed in the eastern Greater Caucasus belt (Figures 5.12 and 5.13).

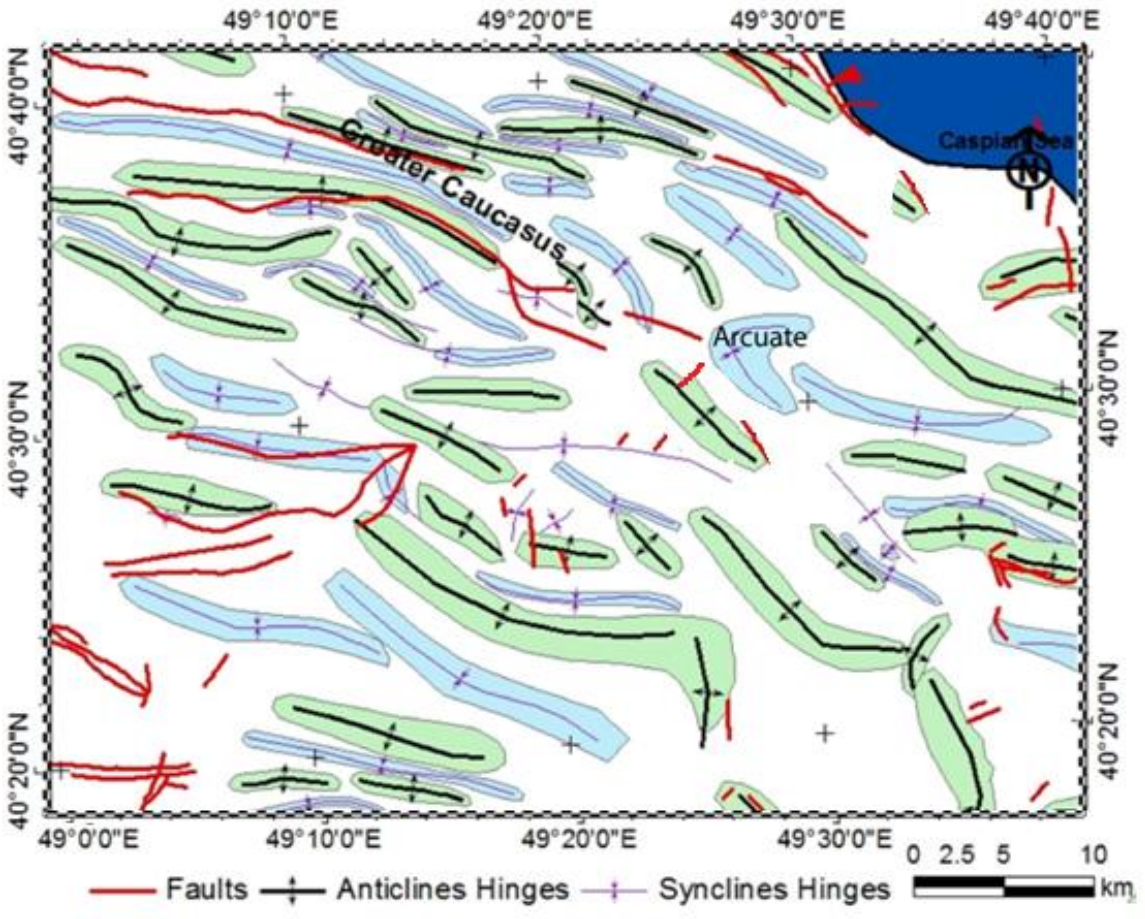

Figure 5.12. An example of the en echelon patterns of the eastern Greater Caucasus belt folds, using Azerbaijan geologic map scale 1:100.000 and satellite imagery (the polygons show the folds plan shapes), and location shown in Figure 5.1.

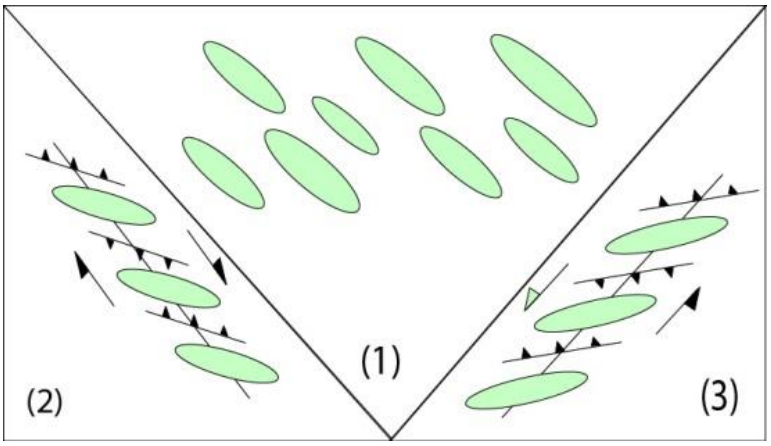

Figure 5.13.Illustrating the folds echelon offset; (1) shows the random echelon offset, (2) shows consistent en echelon offset associated with dextral strike slip faults and; (3) is showing the consistent offset associated with sinistral strike slip faults.

5.4.1.2. Geometry of the Greater Caucasus folds

Many types of satellite images as well as the published geologic and structural maps have been used to identify major structures of the Greater Caucasus belt. ArcMap, GoCad and Global Mapper packages were used with the purpose of validating and checking the structural analysis.

At the regional scale, the oldest rocks in the belt appear in the central and north-western part of the Greater Caucasus belt, composed of many zones of structural units, with the crystalline Palaeozoic and Jurassic rocks exposed in the core of the region near and to the north west of Elbrus Mountain. The younger rocks are exposed on the limbs and form the Black Sea coastal zone to the south of the core of the Greater Caucasus. It is easy to distinguish between the coastal zone and belt's core which matches with the major thrust of the belt (Saintot and Angelier, 2002) where the Main Caucasus Thrust is parallel to the a Greater Caucasus belt (Figures 5.1 and 5.2).

The Greater Caucasus folds vary in length from a few meters to tens of kilometres (

Figure 5.12). Furthermore the plan shapes of these folds are different from one to another and on opposite side along the belt. Folds that distributed along the central and western parts of the belt have linear plan shapes (Figure 5.10), whereas the folds in the eastern part of the belt are differ in their plan shapes from linear to oval plan shapes, in addition a number of them have more curved or arcuate shapes

such as Yasamal and Malyi Kharami to the far east of the belt (Apsheron Peninsula) (Figures 5.11, 5.12 and 5.14).

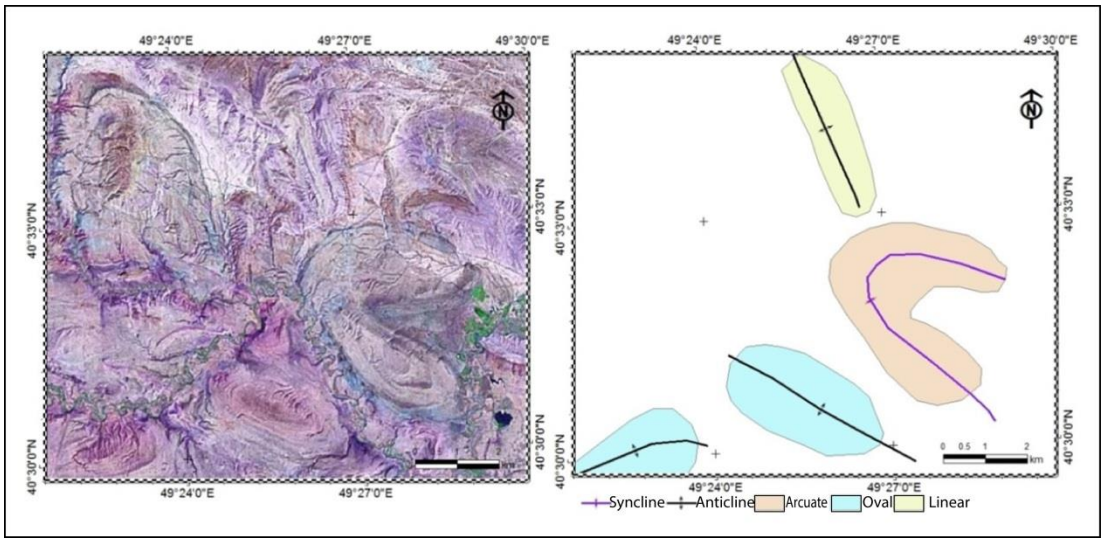

Figure 5.14.Part of eastern Greater Caucasus belt as appears on satellite imagery (MrSid) showing the fold plan shapes in the belt.

The Greater Caucasus folds are asymmetric folds where their limbs have unequal lengths as they appear in the cross section (Figure 5.15). Younger strata which are exposed along the north and south sides of the belt are folded into linear folds and have north vergence on the northern side and south vergence on the southern side. The aspect ratio of the eastern Greater Caucasus folds is somewhat low comparing with thewestern side.

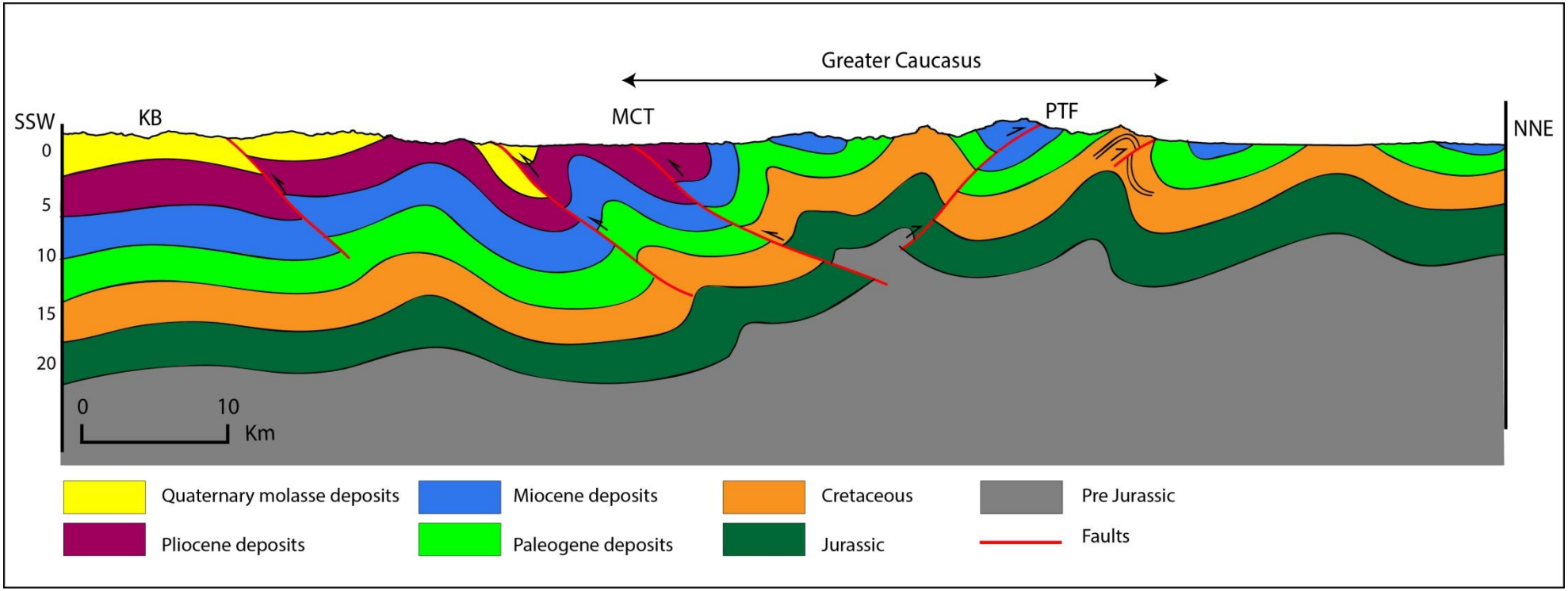

Figure 5.15.Cross section across the eastern Greater Caucasus belt showing the vergence directions of the folds along the area, KB= Kura Basin, MCT = Main Caucasus Thrust and PTF = Pshekish-Tyrnyauz Fault. This section has been made by 2D Move software with using the Azerbaijan geologic map.

5.4.1.3. Folding mechanisms in the Greater Caucasus belt

As a general rule, there are two main folding mechanisms for rocks. Whenever the mechanical influence of layering is strong, flexural folding mechanism occur (buckling and bending), otherwise, when it is weak, the passive folding mechanism take place (Davies and Reynolds, 1996; Groshong, 2006; Twiss and Moores, 1992).

Buckling is considered to be the most wide spread and common fold mechanism types in layered rocks, and occurs as a consequence of compression parallel or sub-parallel to the layers. Two types of strain states are related to the buckling mechanism, flexural flow strain and tangential longitudinal strain (Davies and Reynolds, 1996; Price and Cosgrove, 1990) (Figure 5.16).

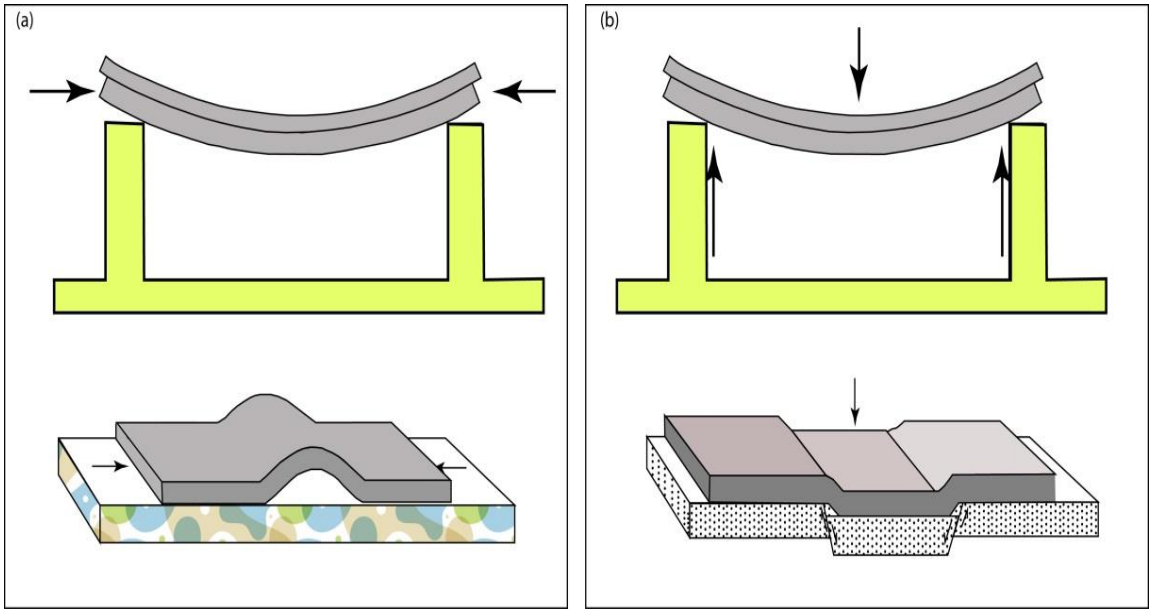

Figure 5.16. Sketches showing the compressions orientations and the main difference between buckling and bending mechanisms, after Price and Cosgrove (1990).

Folds with the buckling type of mechanism which are characterised by their periclinal geometry (whale-backs and saddle shapes), are well represented in the Greater Caucasus belt especially in its eastern part, with between 1:5 and 1:10 of half-wavelength/hinge length ratio.

Although the aspect ratios of buckle folds range between about 1:5 to 1:10, it is possible to generate larger folds by the linking of two originally separate buckles depending on the separation between the two. If the distance between each other is larger than their half-wavelengths, the folds will individually extended, whereas they further growth or linked if separation is around half-wavelength or less, which characterised by hinge deflection (Figure 5.17 a, b) respectively(Price and Cosgrove, 1990). Good examples of such folds in the Greater Caucasus belt can be observed, especially in the eastern part of the belt (Figure 5.17 c).

Bending occurs when the layer undergoing flexural folding has been made by a high angle compression to the layering trend. Folds that have been created by a bending mechanism are termed forced folds, which are required to form geometrically as the result of another processor formed when the sediments are bent by the movement along faults (generally dip-slip or oblique-slip faults) (Price and Cosgrove, 1990; Ramsay., 1967) (Figure 5.16).

One of the most characteristic features of forced folds formed in association with faults is their long hinge length relative to their half-wavelength (Price and Cosgrove, 1990). Such folds can be found in the Greater Caucasus belt and their hinges trend parallel to the belt (

Figure 5.12).

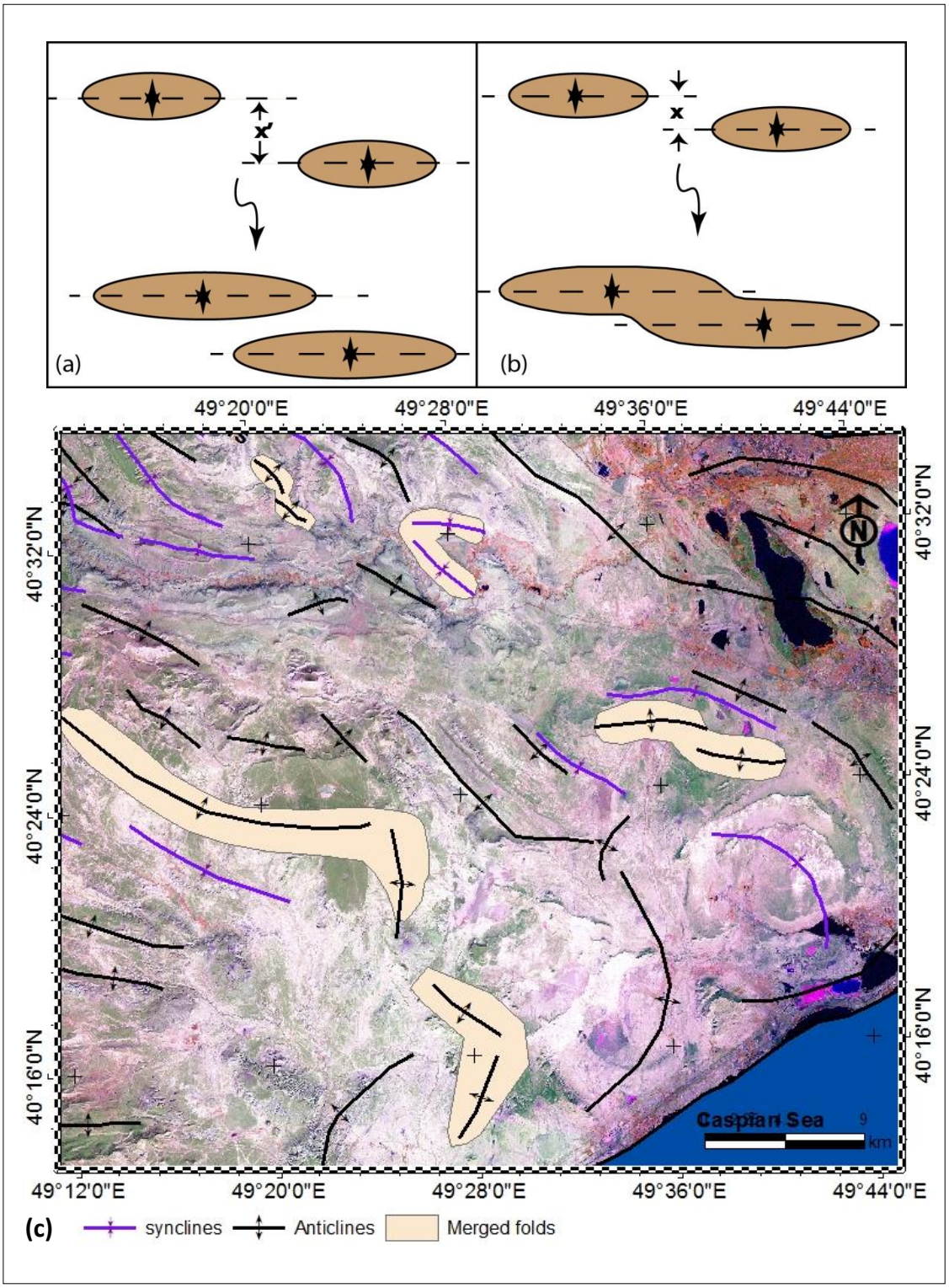

Figure 5.17. Diagram showing two neighbouring periclines separated by a distance (a) exceeding and (b) equal or less than the structure's half wavelength modified after Price and Cosgrove (1990), and (c) is an example of some linked buckle folds in the eastern part of the Greater Caucasus belt (in the polygons).

5.4.2. The Greater Caucasus Faults

5.4.2.1. Spatial distribution of the Greater Caucasus faults

The most important and predominant faults that are distributed in the Greater Caucasus Belt are thrust faults that mostly trend parallel to the NW-SE Greater Caucasus topographic trend. Examples include; a) the Main Caucasus Thrust (MCT), which is the main thrust along the belt, dipping to the north and cutting the entire sedimentary cover, b) the Racha Lechkhumy Fault (RLF) (dipping to the north) and located between the MCT and the Dzirula massif, and c) the Pshekish Tyrnyauz Fault (PTF) to the north of the belt as a back thrust of the belt with south dipping.

5.4.2.2. Greater Caucasus fault geometry

The thrusts in the Greater Caucasus fold and thrust belt have a NW-SE trend in the western part of the belt, and WNW-ESE in the eastern part. The major faults are the most important features in the structural and morphological framework of the Greater Caucasus and obviously mark contrasting morpho-tectonic boundaries in the Greater Caucasus (Figures 5.8, 5.9 and 5.15). The Main Caucasus Thrust crosses the Greater Caucasus from NW to SE. In the eastern Greater Caucasus the MCT splits into many faults, and bounds the highest topography of the Greater Caucasus. To the north of the Greater Caucasus and southern the Scythian Platform there is another major thrust characterising the belt called Pshekish-Tyrnyauz Fault (PTF), with strike of NW-SE, i.e. parallel to the belt. And to the south of the Greater Caucasus core there is an important fault zone termed the Racha-Lechkhumy Fault Zone (RLFZ), present elongated from the north east of the Black Sea, to the southern central Greater Caucasus belt, separating the belt and Rioni Basin (Figures 5.8, 5.9 and 5.15). Minor

faults are distributed in different parts of the structural zones along the belt and most of them have high angles of dip.

5.5. Chapter Summary

The main objective of conducting a remote sensing interpretation and studying the earthquake data in this chapter, were to identify the spatial distribution, geometry and the mechanisms of the dominant regional scale structural elements, which have developed in the course of the structural evolution of the Greater Caucasus belt and the western South Caspian Basin.

The study area is highly faulted, with a complex geological pattern; the faulting style in the region is reverse faulting, with a general NW-SE trend. According to GPS surveys by (Reilinger et al., 2006), it appears that the belt is accommodating about 5-13mm/year N-S shortening rate, and although the eastern part has lower relief than in the western part of the belt, the convergence across the range increases towards the east.

The Eastern Greater Caucasus Seismicity has greater intensity than in the western part, and it has been recorded on both the north and south sides of the range, whereas in the western side the earthquakes occur mainly on the southern side. Most events in the region occur in depths between 6km and 20km, which indicate to the absence of sub-crustal earthquakes. The highest seismic activity region is located in the southern flank of the western central part of the belt. It is confirmed that the reverse focal mechanisms represent the main type in the belt, which are linked with the thrusting and NE-SW compression. There is a relationship between high magnitudes and the main thrusts in the belt such as; the Main Caucasus Thrust with a significant

displacement is accommodated. The regional cross-sections along the Greater Caucasus that constrained by using focal mechanisms show that the belt is deformed by active thrust faults that dip inwards from the margins of the range. These results have contrary to some previous models that emphasise only south-directed thrusting. As well as the sections indicate that there is no detachment underneath the belt as some previous study have referred, e.g. (Dotduyev, 1987; Saintot et al., 2006a)

The frequency and spatial distribution of the folds are varied along the belt, and have different topographic aspects. Folding is more intense in the west than in the east of the belt, and is linear and parallel to each other in the west, whereas they are mostly curved and cut by mud volcanoes in the east of the belt. Most folds have the regional WNW-ESE trend of the main Greater Caucasus belt, but a few folds have a more E-W orientation. Fold axial traces are generally sub-parallel to each other, however, they do show differences in how they arranged. The traces are offset from each other in en echelon patterns that are either; random or systematically stepped offset associated with the strike-slip faults, however the random pattern represent the important pattern that distributed in the eastern side of the belt.

The length and the plan shapes of the GC fold are different, where they have linear plan shapes distributed towards the central and western parts of the belt, and others have oval plan shapes, in addition a number of them have more curved or arcuate shapes. The reverse faults represent the most important and predominant faults that are distributed in the belt mainly trending NW-SE, such as the (MCT) dipping to the north.

Chapter VI

Structural interpretation and tectonic inferences from a detailed study of the Yasamal anticline

6. Structural interpretation and tectonic inferences from a detailed study of the Yasamal anticline

6.1. Introduction

This chapter presents the results of an investigation of the detailed structural elements of the Yasamal Anticline and its surroundings, The study illustrates, using laser scan data and other field data, how small scale accommodation of upper crustal shortening has occurred in this part of the Caspian region.

Digital 3D field (TLS) and dip data collected at Yasamal have been used to create cross sections that were compared to those created from the published geological maps of the anticline, as well as a geologic map of Yasamal area with scale of 1:50,000, to interpret bedding and stratigraphic surfaces that define the major anticlinal structure, minor faults and other strain accommodation structures that have been observed. Using Move, these 3D surfaces have been projected into the shallow subsurface. This model has then enabled an evaluation of the evolution and development of the anticline and to investigate strain accommodation mechanisms using 3D Move to unfold and restore the structures to their pre-deformational state.

6.1.1. Yasamal Anticline Location

The Yasamal anticline (also known as Shubani) is located in the Apsheron Peninsula to the north-west of the SCB and at the southeast end of the Greater Caucasus belt, about 10km to the west of Baku (capital of Azerbaijan) (Figure 6.1).

6.1.2. Why choose Yasamal anticline specifically?

The upper Miocene, lower Pliocene Productive Series, which is divided into two parts, the Early and Late Productive Series, form the most important SCB reservoir strata and are well exposed in the Yasamal anticline (Reynolds et al., 1998). The

younger parts of the series (Balakhany to Surakhany Suites) are exposed at Yasamal Valley, specifically in the area of the south-southeast plunging anticlinal hinge (Figure 6.1). The E-W or the ENE-WSW orientation of the outcrops in the anticline's hinge zone gives excellent strike-oriented exposure of the depositional units (Hinds et al., 2004). And these exposed outcrops on the anticline's area are highly valuable as analogues for sub-surface hydrocarbon accumulations in offshore structures in the South Caspian.

The Productive Series rocks at Yasamal are mainly comprised of shales and sandstones. The fold hinge at Yasamal has exposed most of the Balakhany Suite subunits, which represent one of the most important producing units in the basin and form the main reservoirs in the Apsheron Peninsula in particular (Souque et al., 2010).

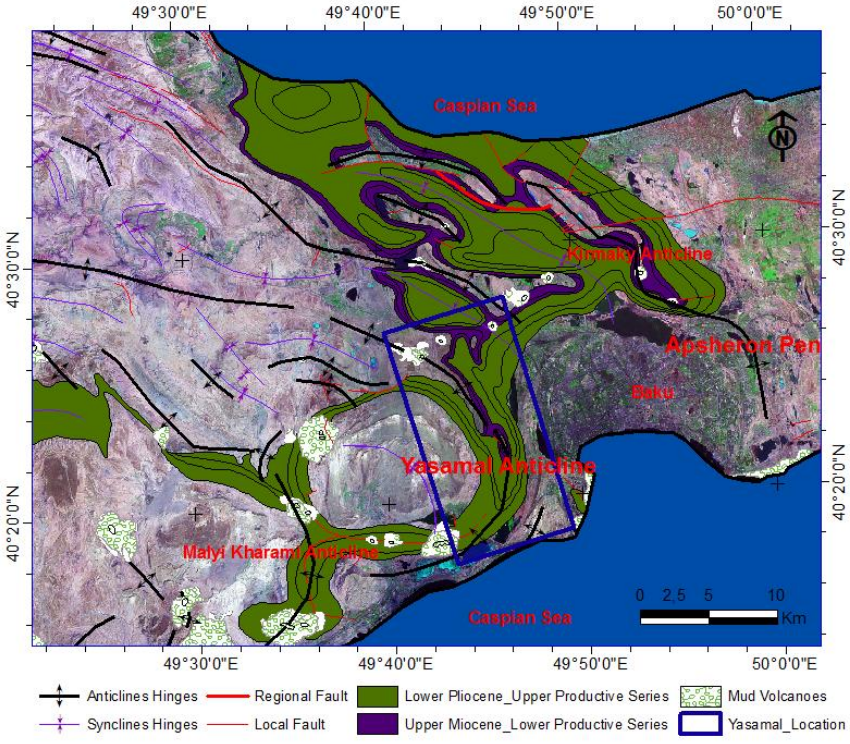

Figure 6.1. A location map of the Yasamal anticline and its adjacent anticlines in the Apsheron Peninsula, illustrating the outcrop patterns of the Productive Series.

6.2. Regional tectonic setting of the Apsheron Peninsula

A detailed geological background has been presented in chapter two. To summarise here; the Apsheron Peninsula (AP) is considered part of the SCB (western South Caspian Basin) (Figure 6.2).

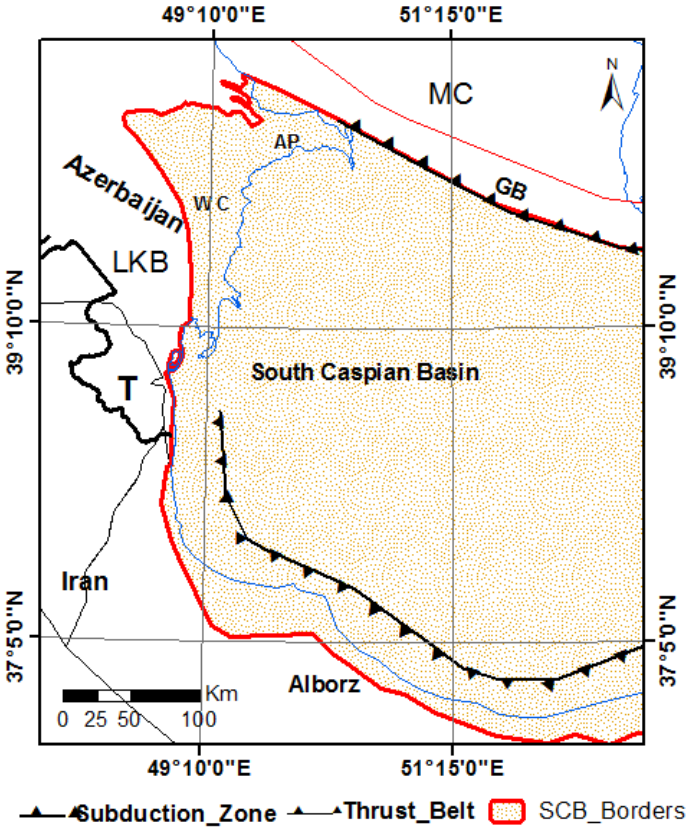

Figure 6.2. A map illustrates the extent of the South Caspian Basin along the Apsheron Peninsula. LKB=Lower Kura Basin, T=Talysh, GB=Great Balkhan, AP=Apsheron Peninsula, WC=West Caspian and MC=Middle Caspian. Modified after (Brunet et al., 2003; Nadirov et al., 1997).

The important regional source rocks for hydrocarbons in the basin is the Maikop (or Maykop) series which is a mud-prone sequence of Oligo-Miocene sedimentary rocks (Jones and Simmons, 1997). These are covered by about 5km of late Miocene to early Pliocene fluvial–deltaic sandstones. The 'Productive Series' was deposited in about 2Myrforming the main hydrocarbon reservoir rocks in the basin (Jackson et al., 2002; Reynolds et al., 1998). This speedy deposition of sand above the mud sequence

produces over-pressured muds. Many of the hydrocarbon traps have been produced by the syn- to post-depositional folding (Jackson et al., 2002).

Three Maikop series strata sequences characterise the stratigraphic sections of the Apsheron Peninsula. These span the lower and upper Oligocene into the lower Miocene (Hudson et al., 2008) (Figure 6.3).

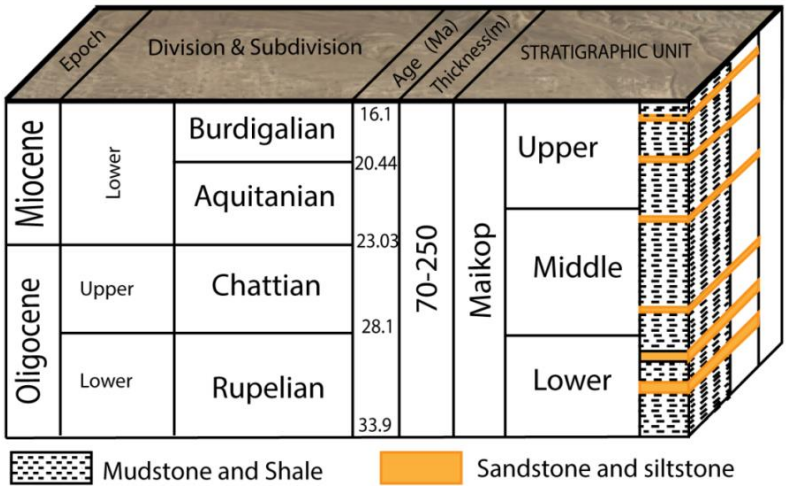

Figure 6.3. A stratigraphic column of the Maikop series in the Apsheron Peninsula, modified after Devlin et al. (1999) and Hudson et al. (2008).

6.2.1. An overview of the Apsheron Peninsula folds

During the Pliocene the regional contractional deformation led to the development of regional and local tectonic structures that has continued into the Holocene (Gurevich and Chilingar, 1995). These 'Alpine' events formed many folds in the basin such as the Yasamal fold, the main structure examined in this part of the project, but also other anticlines such as Kirmaky to the north of Baku, and Malyi Kharami to the south west of the Yasamal Anticline (Figure 6.4).

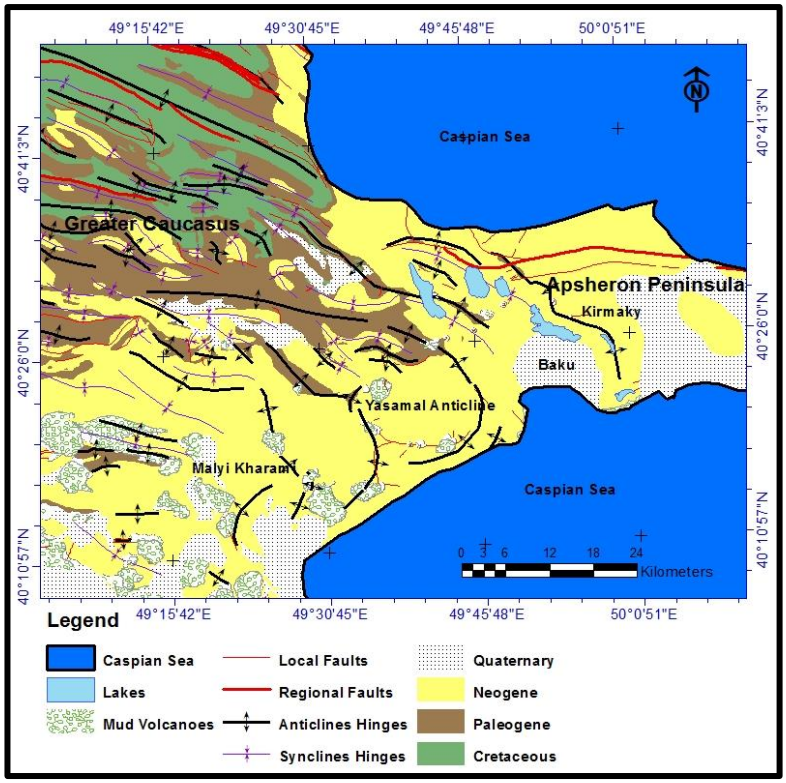

Figure 6.4. A simplified geologic map illustrating the Yasamal anticline and the adjacent anticlines in the Peninsula and the relationship between their curved hinges with the mud volcanoes, modified after (Allen et al., 2003).

Although the Apsheron Peninsula folds are located along strike from the Greater Caucasus belt, their style and stratigraphy are more related to the SCB. Firstly, there is an obvious strike variation displayed by individual anticlines on the Peninsula, with curved axial traces distinguishing most of these folds. This variation might reflect underlying thrust displacement variations along their strike, compared with the linear folds to the west in the Greater Caucasus. The folds are also linked with mud volcanoes that occur on the fold hinge lines (Allen et al., 2003; Alsop and Holdsworth, 2002).

Folds represent the most common structures in the peninsula and formed above a regional ductile detachment zone that is presumed to lie within Maikop shale at a depth of almost 11km. One model for the fault patterns manifest in the folds along the peninsula are; reverse faults in the lower part of the fold with a few that cut the entire

stratigraphy defining the folds), and normal faults in the upper part of the fold, with presence of a neutral zone in the area between the compressional and extensional areas (Devlin et al., 1999), Together with the layer bending, these faults accommodate the tectonic strain during the folding process (Figure 6.5).

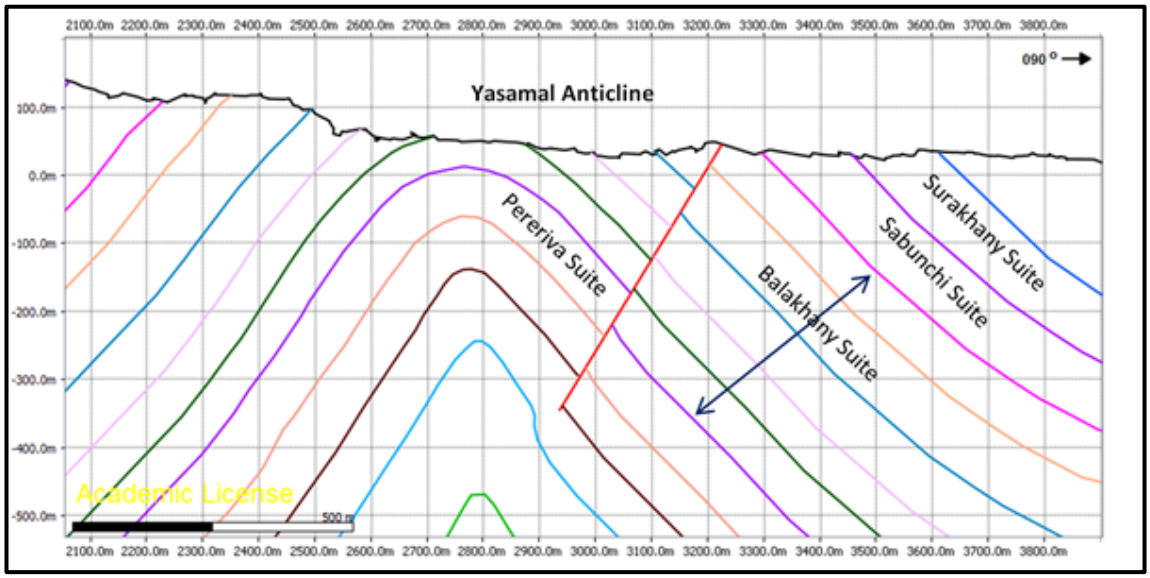

Figure 6.5. Interpreted cross section through the Yasamal anticline including a reverse fault cutting most of the productive series, and small normal faults in the upper parts of the fold, the section's location is shown as line (8) in Figure 6.16. (The section was constructed by the author from the Laser scan data).

6.3. Materials and methods

Terrestrial laser scanning (TLS) datasets collected from the southern part of the Yasamal anticline (collected for 'BP' Azerbaijan by McCaffrey, K.J.W & Jones R.R. in 2007) were made available to this study, and represent the main data that was interpreted in this part of the project. A GIS database of other structural data with information on structural features including folds, faults and fractures data was used as well.

6.3.1. Datasets

The database assembled for this study was obtained from a number of sources, comprising maps of the geology and topography of the area at different scales (1:50,000, 1:200,000, 1:500,000), field data (dip data, laser scan data and photographs), remote sensing data including freely available satellite imagery data (Ikonos, Spot, SRTM and ETOPO) and published reports e.g. (Allen et al., 2003; Jackson et al., 2002; Reynolds et al., 1998).

The available geologic and topographic data were integrated using Move software version (2012.1) from Midland Valley, ArcGIS, Global Mapper, and GoCad (2009.2). The processing softwares were applied to automatically create ArcGIS coverage files from the electronic geologic maps and field data. A digital elevation model (DEM) was created using a 20 metre contour map of the eastern Greater Caucasus, to produce the topographic profile lines for cross sections construction. These were constructed using laser scan data, digital geological maps and previous published structural maps, all of which were integrated within the 2DMove software.

6.3.2. Satellite images

A remote sensing interpretation was conducted to distinguish the structures and morphometric features such as fold hinges and limbs, faults, mud volcanoes and the main rock types and stratigraphic boundaries in the Apsheron Peninsula. Many sources were used for this stage e.g. SPOT satellite imagery, ETOPO (Topographic and bathymetric map) and SRTM (Figure 6.6). All those structural and topographic interpretations have been used to produce a new geologic map of the area with cross sections constructed to constrain the subsurface geometry of the folds.

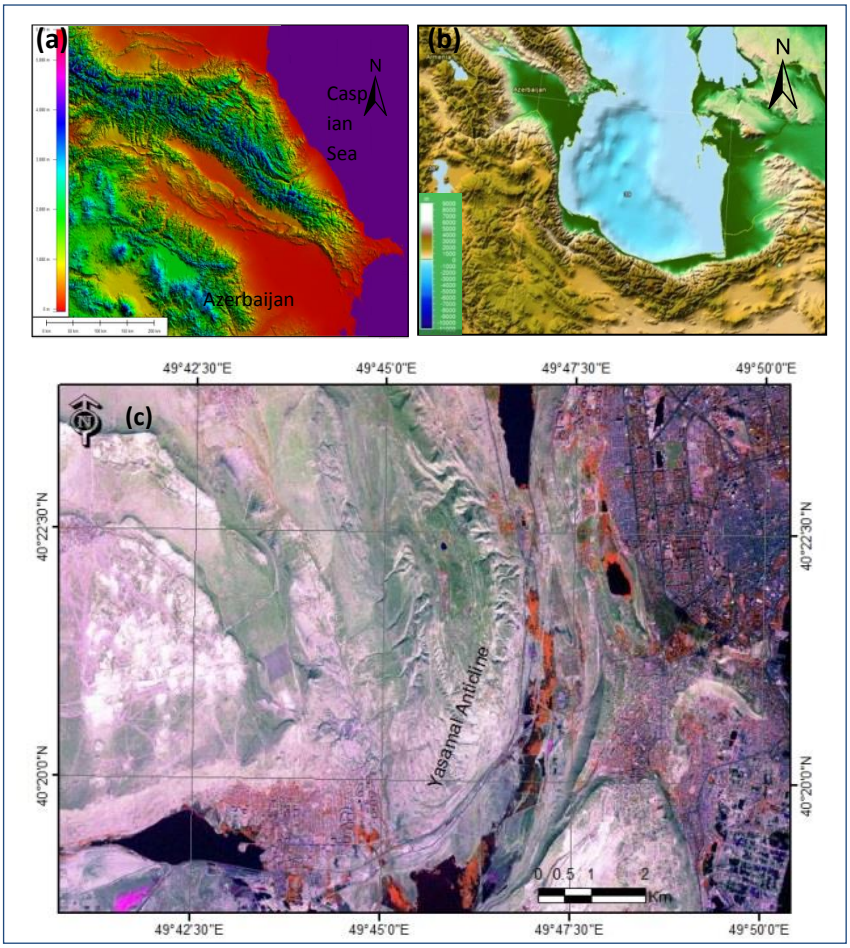

Figure 6.6. An illustration of some of the data types used in this part of the project: (a) is an SRTM DEM image of the Apsheron Peninsula and the eastern part of the Greater Caucasus, (b) ETOPO map of the SCB, and (c) is a SPOT satellite imagery of the Yasamal anticline.

6.3.3. Terrestrial laser scan data

Terrestrial Laser Scanning (TLS) method is a relatively new technique use for capturing high resolution digital topographic data. The technology has been used to record the detailed 3D forms of geological surfaces, including the layer boundaries, faults and fold hinges and limbs (McCaffrey et al., 2005). 3D point clouds acquired by terrestrial laser scanning can be analysed to provide quantitative structural or geological data in work station away from the situation of the field (Jones et al., 2008).

6.3.3.1. Principles and equipment details

Terrestrial laser scanner TLS that was used in this project is the Riegl LMS-z420i (Figure 6.7). This system is optimised for fast data collection and a long range (<800m) and may be used in different environmental conditions. Data resolution depends on the distance of the laser scanner relative to the target. The range is affected by laser beam angle (the range decreases with obliquity to an object target), the outcrop reflectivity (the range increases when the outcrop is lighter coloured) and the weather conditions (the range increase in clear weather).

6.3.3.2. Sensor components and types

There are two methods for distance calculation to produce the point cloud: phase and pulse or time of flight (TOF). The z420i scanner uses the second method because it gives respectable accuracy for an extensive range; hence it is often applied for observations of the earth surface in TLS.

At the present time the terrestrial laser scanning (TLS) is widely used in geological survey of structures such as studying the growth and development of the folds and faults more accurately than ever before. It is used in many disciplines such as elaborate study of geometric properties of a specific area or surface on the earth with scales from centimetres to hundreds of meters on targets with high reflectivity. Other examples of use in Earth Sciences include Rosser et al. (2005) whose used the terrestrial laser scanning for monitoring the process of hard rock coastal cliff erosion and Abellan et al. (2014)used TLS for rock slope characterization and monitoring. The same technology is used to capture rivers, vegetation and dune fields(Brodu and Lague, 2012).

The essential characteristic of the TLS RIEGL LMS z420i model is that it scans in a swath vertically (between -60° and +60° relative to a horizontal axis and rotates on a vertical axis (0°-360°) to scan horizontally. The laser fires at high frequency and a mirror system collects the return from the target surface. The time of light of the laser beam and its return allows the distance to the target to be calculated. Collected over a dense grid that encloses the target, these data may be used to image an outcrop in three dimensions. On the basis of this time-of-flight measurement technique of the laser, the terrestrial laser scanning allows a 3D point cloud (of x,y,z coordinates) to be acquired that can be used to analyse the areas of complex topography (Kasperski. J. et al., 2010).

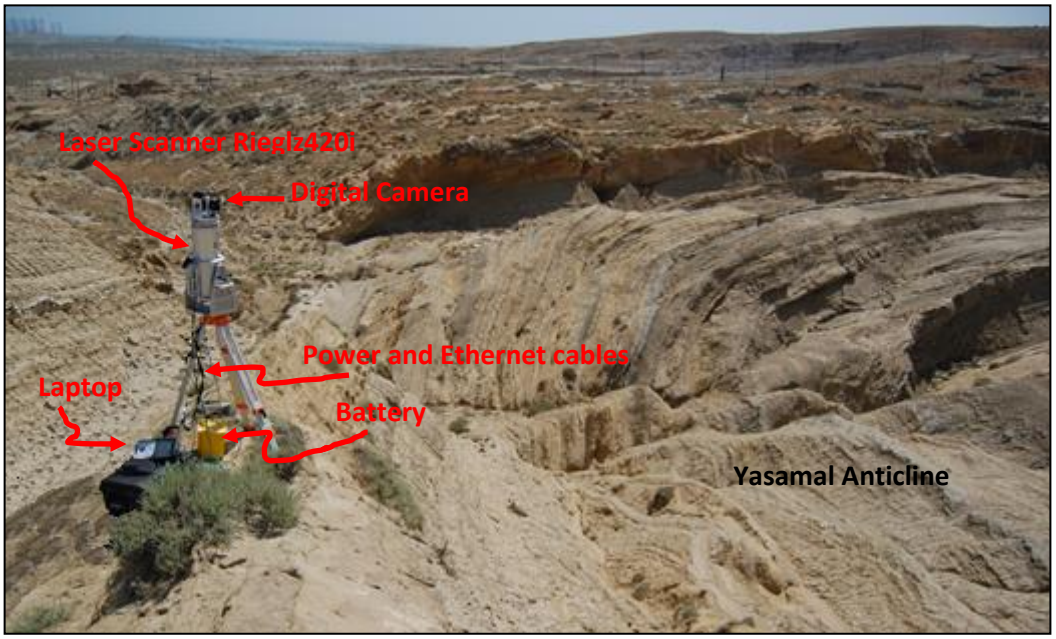

Figure 6.7. A typical terrestrial laser scanning setup components with the essential components for acquiring a point cloud dataset, (the photo is in the southern part of the Yasamal anticline).

Trees, vegetation cover or any solid object that lies in the path of the laser will cause are flection in front of the intended target. This represents one of the drawbacks of TLS technique as it is results in partial imaging of the target and the formation of 'shadow' zones in the data. This can mean that the target surfaces appears slightly camouflaged or cannot be easily recognizable because of these shadows on such surfaces since the laser cannot get through to them. The way to minimise this problem is to survey from several places and several directions (multiple tripod positions) and then overlap and merge the data to give more continuous coverage (Figure 6.8).

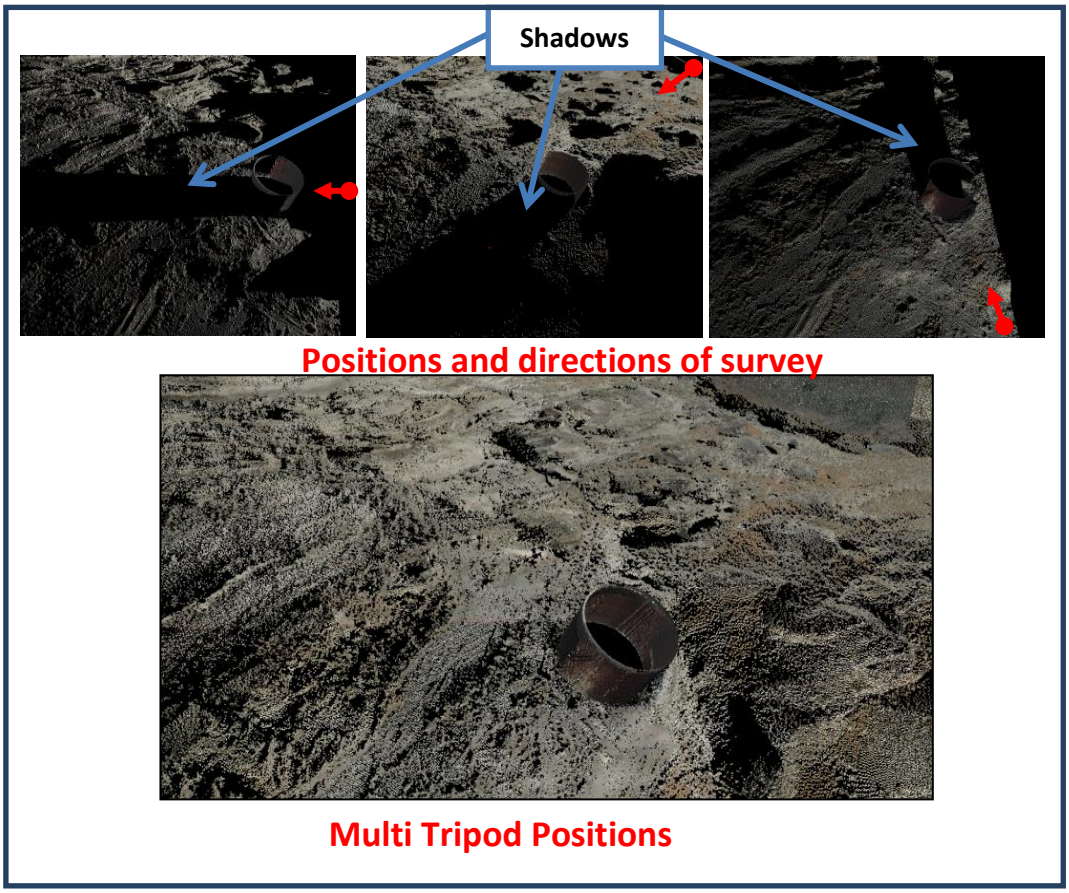

Figure 6.8. 3D view of terrestrial laser scans on Yasamal Anticline - Multiple scan positions combined to maximise data coverage (Red arrows are the scan positions).

6.3.4. Data processing

Most of the processing operations were conducted in the office and away from the field using dedicated laser scan software (RiScan Pro by Riegl) for the initial data reduction, this software enables the digital photographs taken with a SLR camera mounted on top of the scanner to be linked with the point cloud (Figure 6.9). In addition to Move package from (Midland valley) that was used to creating the cross sections, surfaces and 3D models of the Yasamal anticline, and GoCAD software was used for some additional interpretation enhancements.

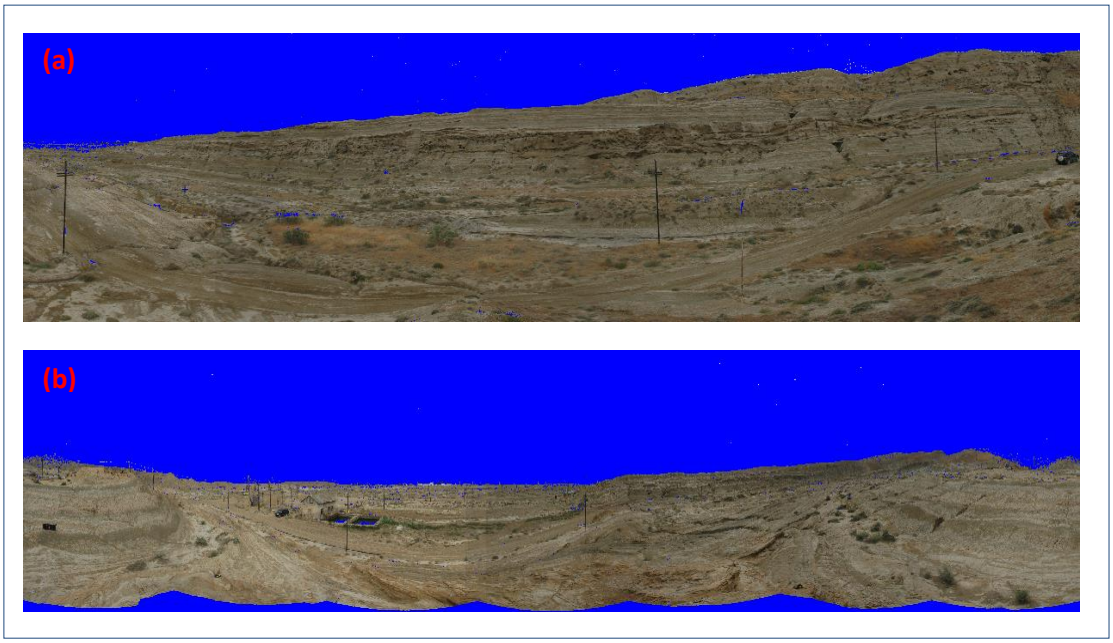

Figure 6.9. Showing the linked photographs by using (RiScan Pro), (a) is photograph for 180° and (b) is for 360° horizontally.

The RiScan Pro Software package for terrestrial 3D Laser Scan data can be used for many tasks such as sensor configuration and data acquisition, visualization, manipulation and archiving (data include scans, digital images, GPS data, and coordinates of the control and tie points). The interpretations that were done by the RiScan package have represented picking polylines on the point cloud to define boundaries between the lithological units in the area under investigation and the faults that cut the area (Figure 6.10a).

After the initial interpretation in RiScan, GoCAD was used to link the polyline segments into continuous stratigraphic unit boundaries (Figure 6.10b). The third software which was used for the structural modelling and analysis software package was the Move Software, (from Midland Valley Exploration Ltd). This was used to build geometrically valid geological interpretations, to improve models and to test and understand geological concepts. This software includes 2D/3D model building

and editing on surface or sub-surface models, and it has in-built tools or advanced structural modules such as Fracture, Geo-mechanical and Kinematic Modelling (2DMove, 3Dmove). The version used here was 2010.1 & 2012.1. (Figure 6.10c, shows examples).

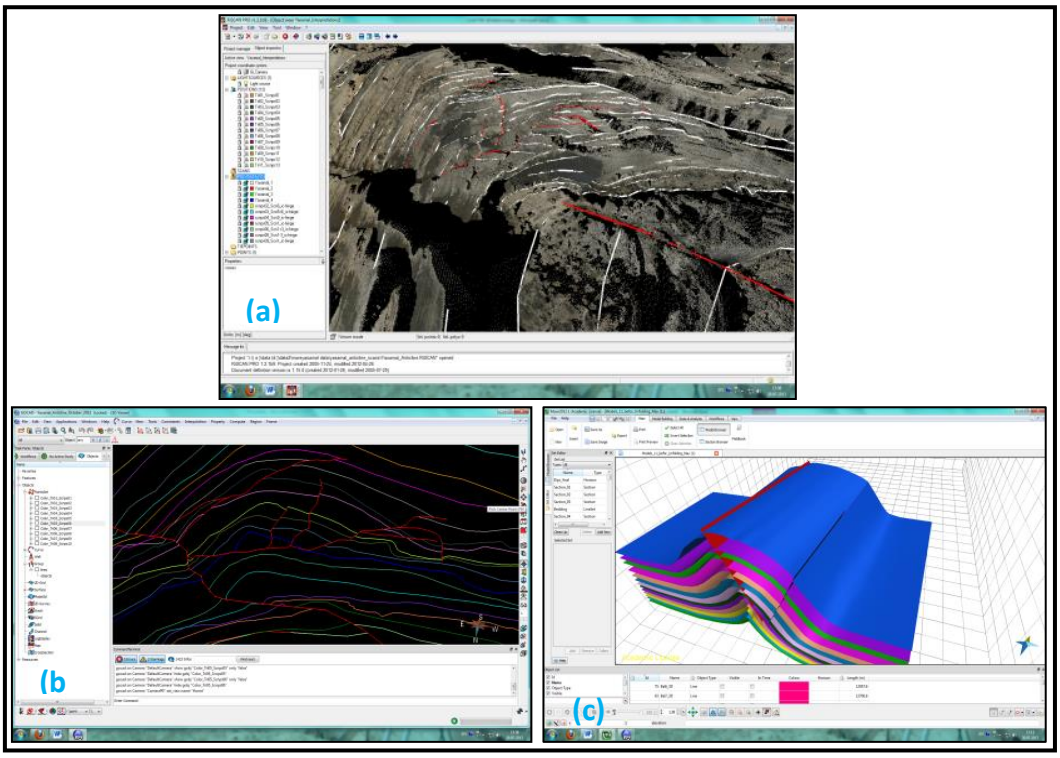

Figure 6.10. Examples of the data, their interpretations and results using a variety of software; (a) shows TLS data for Yasamal Anticline and their interpretation in RiScan-PRO, (b) is the same interpretation but after enhancement in GoCAD, and (c) shows a 3D models of the Yasamal Anticline in 3D-Move software.

6.3.4.1. Acquisition, Registration and Geo-referencing

The TLS dataset comprises data collected at twelve scan positions, covering an area of about five square kilometres of the Yasamal valley (Figure 6.11). With a good overlap between the different point clouds acquired from each position the data coverage is estimated at more than 50% of the entire scanned area. So, in order to reduce the data gaps (represented by the shadows, vegetation or buildings), a larger number of survey positions were used in a smaller area. The scan positions and their covered areas are illustrated in (Figure 6.11). All data have been geo-referenced in RiScan, within the WGS84 datum UTM coordinate system.

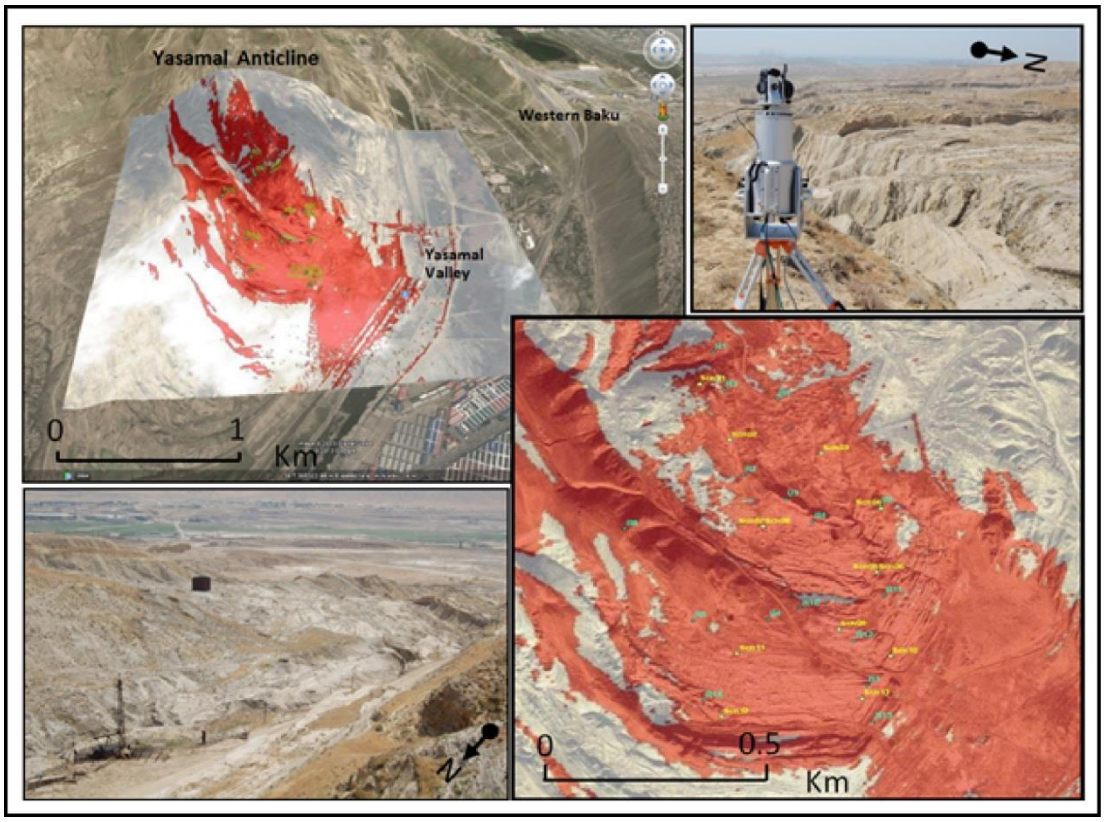

Figure 6.11. An overview of the area (on the Yasamal anticline) which was been covered by the Terrestrial Laser Scanning data (ground-based LiDAR). Yellow points refer to scan stations and light blue points refer to GPS survey points.

6.4. Detailed stratigraphy of Yasamal valley

At Yasamal Valley, strata of the Productive Series are well exposed along the south and southeast of the Yasamal anticlinal axis where the outcrops have an east-west orientation (Figure 6.12). The west flank of the fold includes good exposures of the ninth part of the Productive Series (Surakhany Suite). The suite term used here is a Soviet-era stratigraphic term and is equivalent to the "Formation" of the international usage.

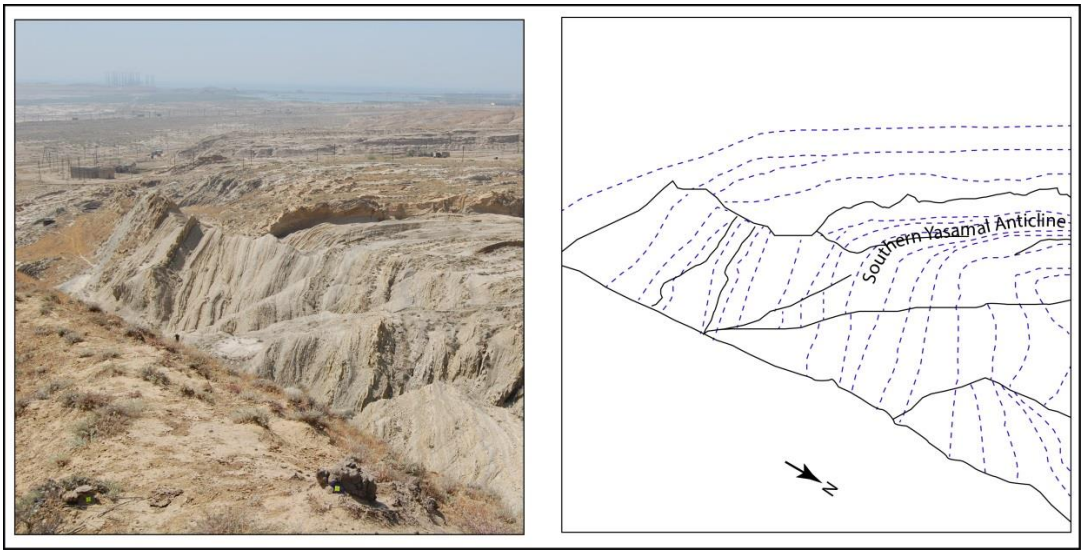

Figure 6.12. A photograph of the southern part of the anticline shows the east west orientation of the anticline's outcrops and the fold hinge plunging to the South.

6.4.1. The Productive Series at Yasamal

The thickness of the Productive Series in the Apsheron Peninsula is about 1500m which is thinner than that in the basin interior (Jones & Simmons, 1996) and based on the characteristics of the Productive Series lithologies, it is sub-divided into nine suites (Figure 6.13).

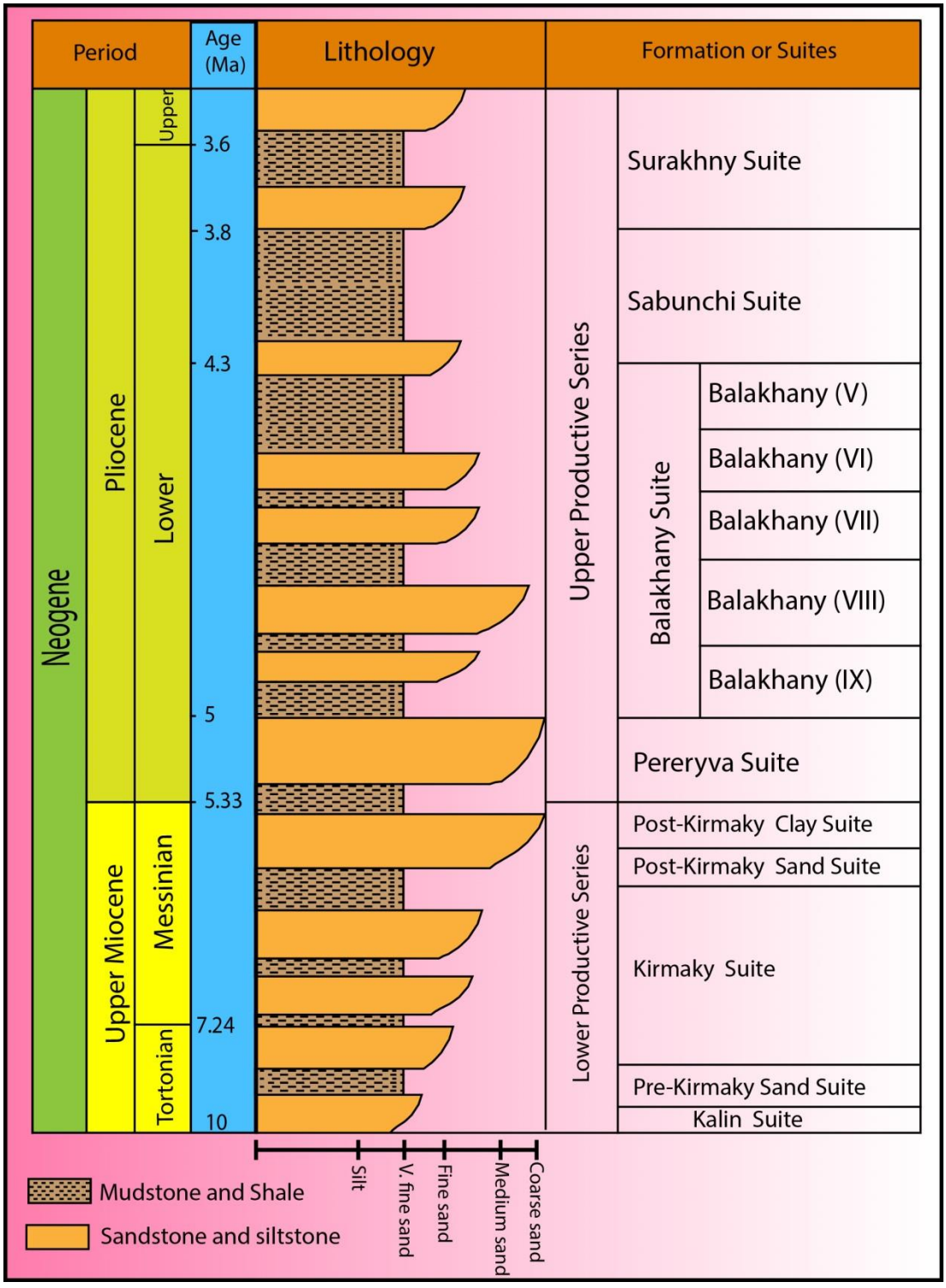

Figure 6.13. Stratigraphic column of the Productive Series at Yasamal Valley summarising the vertical changes in lithology through the series, modified after Devlin et al. (1999).

6.4.1.1. Lower Productive Series

1. Kalin Suite (KAS)

The first or the lower suite of the Lower Productive Series is called the Kalin Suite (KAS), and is widespread in almost the entire basin, without exposure at the surface. It is identified by previous subsurface studies as containing about 300m of a coarse-grained succession (Reynolds et al., 1998).

2. Pre-Kirmaky Sand Suite (PK)

The second suite of the lower Productive Series in the Apsheron Peninsula is exposed in a small area in the core of the Yasamal Anticline hinge, and covered by mud volcano flows in Lokbatan area to the south west of the Yasamal Valley.

3. Kirmaky Suite (KS)

The Kirmaky Suite represents the lowermost unit of the productive series that is obviously exposed in the Yasamal valley; it is about 270m thick, and can be divided into two parts: lower sand prone and upper argillaceous units. It is exposed in the southern part along the axis of the anticline.

4. Post-Kirmaky Suite

Approximately 140m thickness is exposed of the Post-Kirmaky Suite, and it is divided into two parts, the Sand and Clay Post Kirmaky Suites (NKP). The Post Kirmaky Sand Suite is dominated by sandstone especially in the lower part of the suite but changes towards the top to mudstones and siltstones. The Post Kirmaky Clay Suite (NKG) mainly contains mudstone and siltstone, and also some thin beds of sandstone, which are in an upward coarsening sequence (Figure 6.13) (Reynolds et al., 1998).

6.4.1.2. Upper Productive Series

The Upper Productive Series is exposed in the Yasamal anticline and comprises the Pereriva suite, Balakhany suite, Sabunchi suite, and Surakhany suite.

1. Pereriva Suite

The Pereriva Suite is an important producing suite in the offshore basin. Sandstone represents the predominant rock type exceeding 100m thick; the lower part is characterized by friable fine gravel, conglomeratic sandstones. Cross-bedding is present although the grain-size decreases upward to fine-grained sandstone. This sudden change to large grain size in the lower part of the suite has been interpreted to reflect a rapid drop in base level (Figure 6.14) (Reynolds et al., 1998). Hinds et al. (2004) interpreted that the alternation of the basal parts of channel fills, channel lags, and sandstones, may reflect either differences in the rates of subsidence or the fluctuation of the climate in sediment supply and discharge.

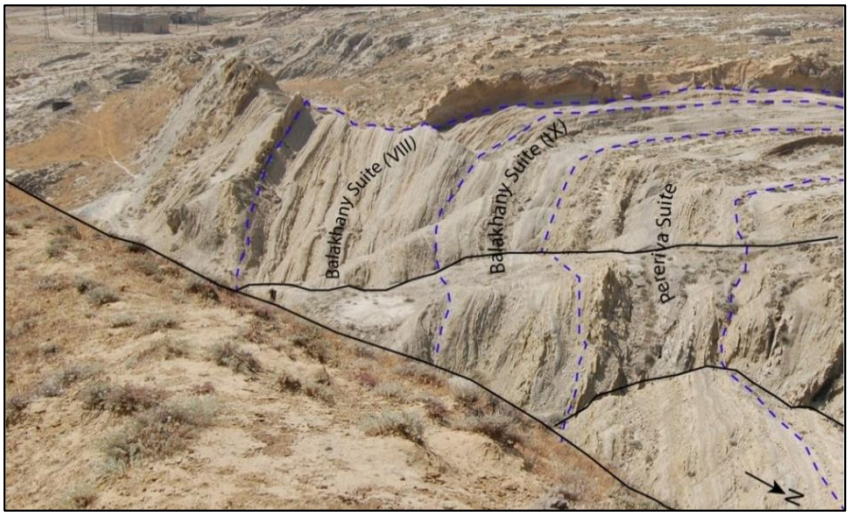

Figure 6.14. Photograph of the southern part of the Yasamal Anticline along the hinge, illustrating the contact of Balakhany Suite (IX) with the sand-prone Balakhany Suite (VIII) and the Pereriva Suite.

2. Balakhany Suite

The Balakhany Suite represents the most important hydrocarbon producing suite in the South Caspian Basin, and the main reservoirs in the Apsheron Peninsula. It comprises mostly fine grained sandstone intervals and intervening minor layers of siltstone. The suite has been subdivided into six units named (X, IX, VIII, VII, VI and V) from lower to upper, representing the second suite of Upper Productive Series and comprises 850m of the Lower Pliocene succession (Figure 6.13). The complete Balakhany Suite succession is not exposed in the Yasamal Valley, however five of the units are believed to be visible on the surface in Yasamal Valley (from IX to V).

a) Balakhany IX.

Most likely the lowermost deposit of the Balakhany Suite exposed at Yasamal Valley is the Balakhany IX which is about 60m thick. The unit can be subdivided into two based on the components of the mudstone and sandstone, the upper part is coarser grained (Figure 6.14). The upper unit consists of complex layers of ripple-coated fine to silty-sandstone (Reynolds et al., 1998). The mixture of mudstone and sandstone that comprising the unit led to division into a lower coarser grained part and an upper part finer grained.

b) Balakhany VIII.

It is not simple to discriminate the Balakhany VIII subunit from others in the Yasamal Valley as its contact is gradual. Sandstones are the main component of this subunit and their percentage decrease gradually upward with increasing mudstones alternations (Figure 6.14). The thickness of this subunit reaches about 100m. Hinds et al. (2004) have interpreted that there are few intervals of mudstones between the sheets of sandstone, comprising beds with decimetre thick climbing ripples.

c) Balakhany VII.

The base of the Balakhany VII is defined at the top of sandstone sheets of VIII (about 8 m), and its top represents the bottom of sandstone sheets of VI (about 5 m). The VII unit comprises sandstone and mudstone layers with thickness of about 5m, which differ in colour from grey to reddish brown, its whole thickness reach about 55m.

d) Balakhany VI.

This sand-prone subunit comprises mudstones, sandstone and medium to fine-grained sandstones that vary in colour from grey to yellowish brown, reaching a thickness of about 40m.

e) Balakhany V.

Likewise Balakhany VIII, the Balakhany V subunit is not easy to discriminate or define owing to the gradual variations in lithology however it is thought to have a thickness of about 55m. As a result, the base and top of the subunit are defined by the boundaries of the units above and below which are the Balakhany subunit VI and Sabunchi Suite respectively (Reynolds et al., 1998).

3. Sabunchi Suite

The Sabunchi Suite is about 200 m thick; its base is dominated by grey mudstone whereas its top is the base of a thick sandstone sheet. It is comprised of silty-sandstone which coarsens upward. The sandstones have colours of grey and yellow distributed randomly; the suite is exposed in the area under investigation along the anticline (Figure 6.15).

4. Surakhany Suite

The Surakhany Suite is about 500 m thick and represents the uppermost suite of the Productive Series. It is an argillaceous succession of clay-stone and siltstone, with small amounts of sandstone (Figure 6.15). Many traces of roots and small holes are almost vertically distributed in siltstone layers. Mudstone sheets are composed of finely laminated clay and silt, with differ in colour from dark grey to reddish brown. Intermittently the siltstones are inter-bedded with gypsum layers, and sedimentary structures are present in the form of ripple and convolute laminations, and cross-bedding. Good exposures exist at the southern and eastern part of the Yasamal Anticline.

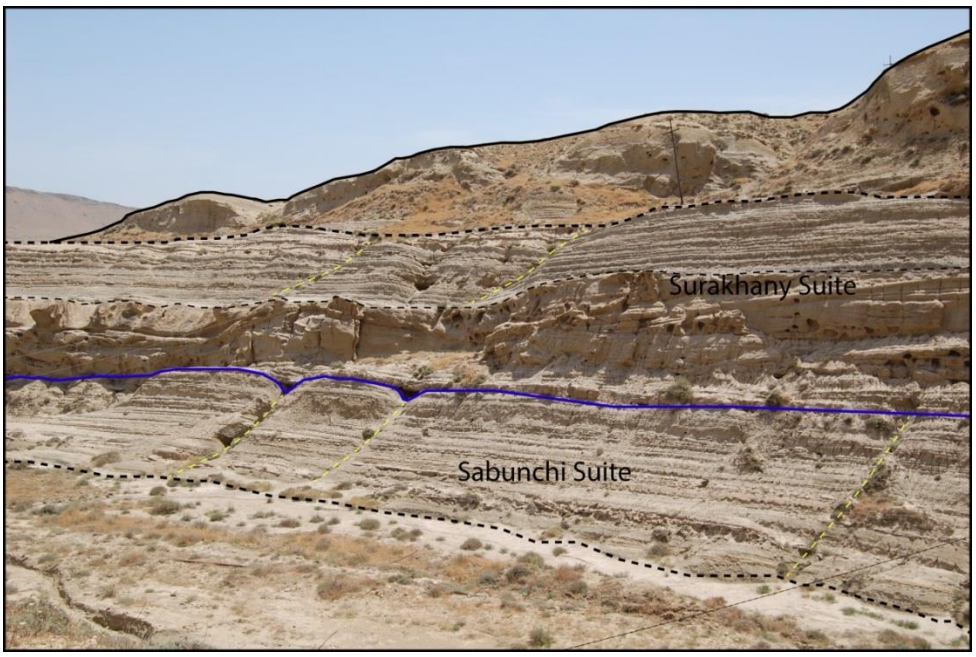

Figure 6.15. View of the south western side of the Yasamal Anticline, showing the uppermost suites of the Productive Series.

6.5. Structural Analysis of the Yasamal Anticline

With the objective of understanding the structural evolution of the Yasamal anticline in detail and to compare with previous studies, thirteen cross-sections of the anticline have been constructed using 2D Move (Figure 6.16). A 2D balanced restoration has been done for one of the sections chosen almost perpendicular to the N-S trending anticline hinge (cross section number (7) Figure 6.16), and the restoration results are shown in Figure 6.19.

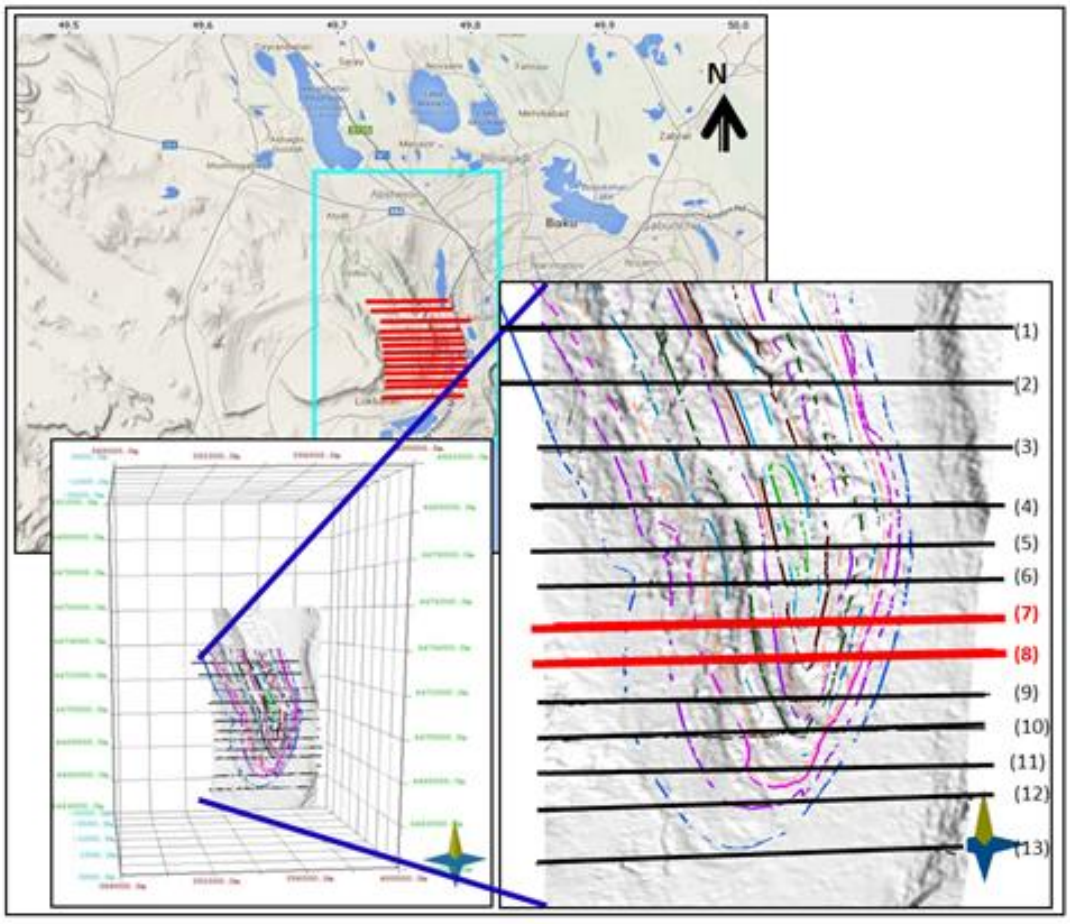

Figure 6.16. The places of thirteen E-W cross sections through the Yasamal Anticline, the red line illustrate the location of the section number (7) that has been used as a key of the restoration, whereas the other twelve sections are constructed in order to build the 3D model of the Anticline, and section number (8) with red colour illustrating the location of Figure 6.17a, b.

6.5.1. Geologic map and cross section construction

Once the initial interpretations of the Terrestrial laser scan data have been done, a geologic map of the area under investigation was produced illustrates the stratigraphic unit boundaries and the main faults that distributed in the Yasamal anticline (Figure 6.17a, b). Then 2D cross sections were constructed directly from the map in order to estimate the total shortening and calculate the longitudinal strain. Digital 3D field (TLS) and dip data collected at Yasamal have been used to create cross sections that were compared to those created from the published geological maps of the anticline, as well as a geologic map of Yasamal area with scale of 1:50,000, to interpret bedding and stratigraphic surfaces that define the major anticlinal structure, minor faults and other strain accommodation structures that have been observed.

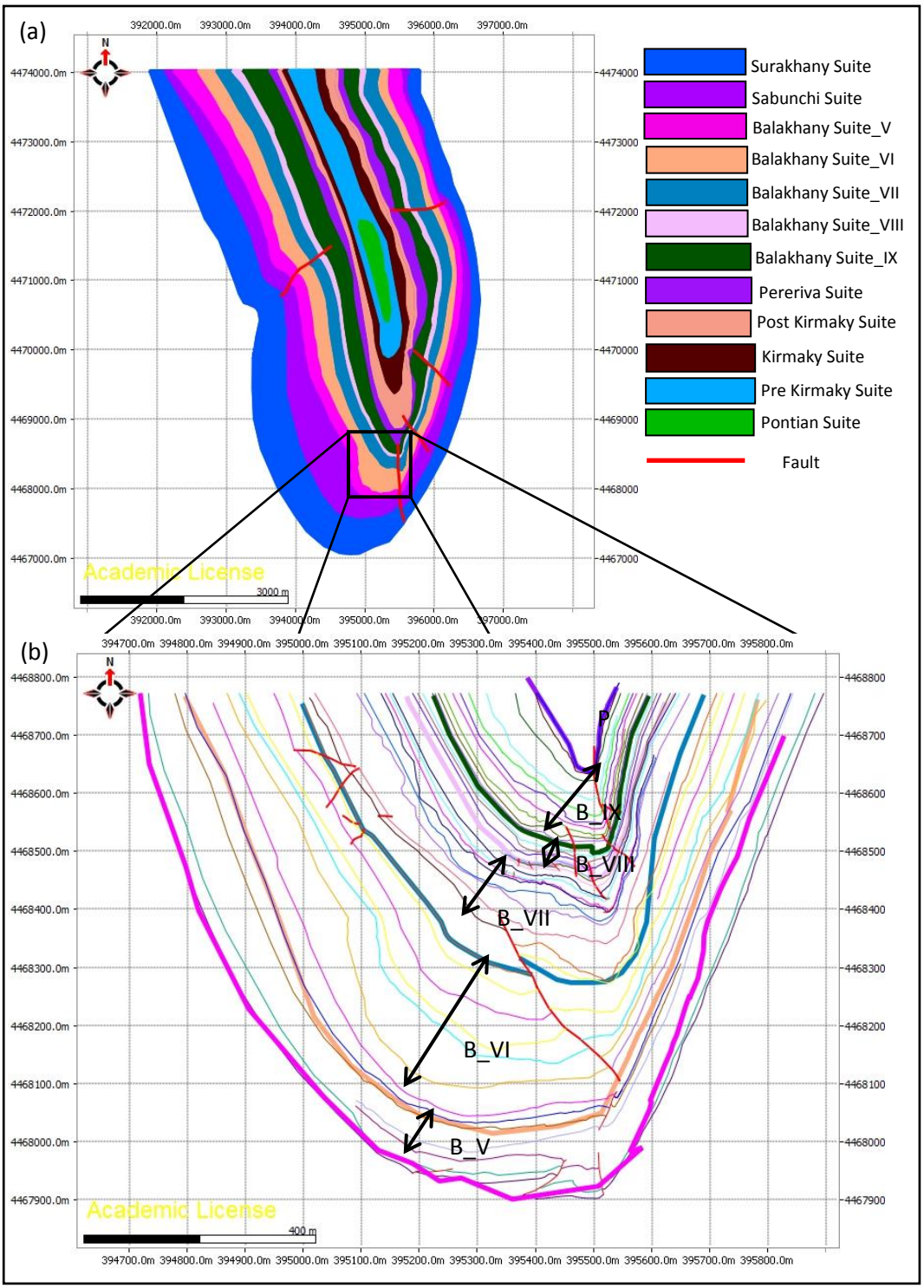

Figure 6.17. (a) Simplified geologic map of the Yasamal anticline drawn with using the laser scan interpretations digital data and published geologic maps of the area, and (b) is illustrating part of the laser scan interpretation of the southern part of the Yasamal anticline.

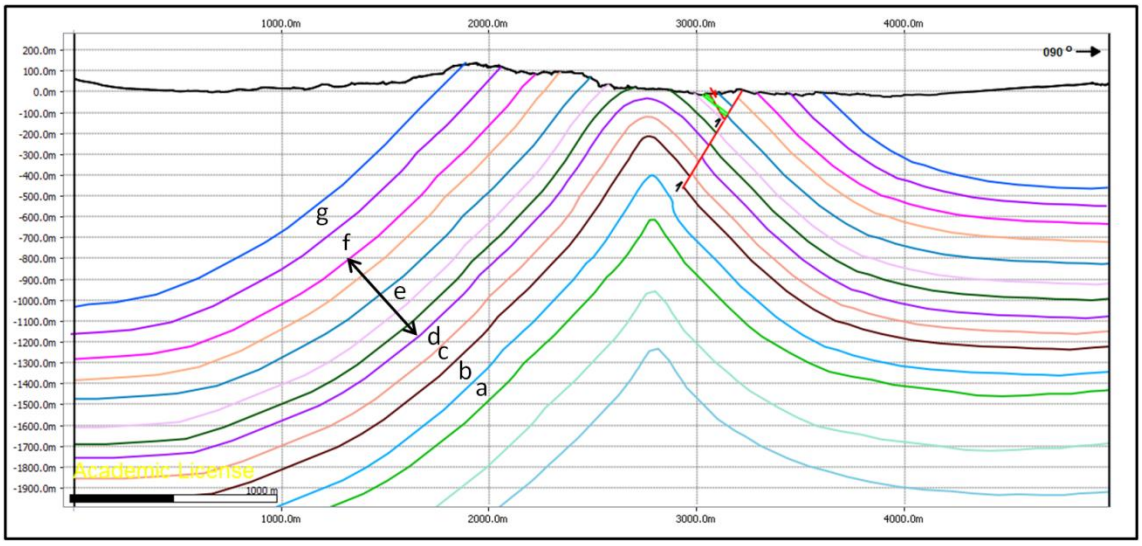

Figure 6.18.c An interpreted cross section along the Yasamal anticline shows the Pliocene Productive Series (Pre-Kirmaky, Kirmaky, Post-Kirmaky, Pereriva, Balakhany, Sabunchi and Surakhany suites from (a-g) respectively). The dip angles on the cross section constrained by the dip data from the field. (Section location is shown in Figure 6.16 (line no. 8)).

6.5.2. 2D Restoration

The main folding mechanisms that are widely recognized and used in cross sections restoration are the flexural slip for compressional domains and simple shear for extensional domains (Rouby et al., 2000; White et al., 1986). In the case of the flexural slip, the main rock discontinuities are the lithological bed boundaries (Suppe, 1983), and in the simple shear mode, the material acts as a granular medium (White et al., 1986). The restoration of the Yasamal anticline has been achieved by using the built-in algorithms in 2DMove. In particular, 'Fault Parallel Flow' in 'Move on fault' was used to restore the fault displacement, This algorithm is used for forward modelling and structural restorations of thrust and fault propagation folds (Midland_Valley, 2012), and 'Flexural Slip' to unfold the beds and return the horizons to their original position before the deformation. All horizons were unfolded from their present state to the Upper Miocene (Tortonian) (7.2 Ma),

which corresponds to the Kirmaky Suite of the Lower Productive Series. Where faults are present cutting the horizons, the kinematic Modelling Module 'Move on Fault' is used before applying the unfolding processes, restoring the hanging-wall horizons to match with the footwall horizons (their original position before the displacement) (Figure 6.19g).

And the steps that were followed to achieve the restoration of the cross section in Figure 6.19are in summary:

- As the horizons was faulted, the initial step was to restore the hanging-wall of the horizons back to their original positions to match the footwall using 'Move on Fault' function (f) to (e);
- From (e) to (d) the Surakhany Suite horizon was unfolded to horizontal.
- In the steps from (d) to (a) (the last step); the remaining horizons including the Kirmaky suite of Lower Productive Series were unfolded.

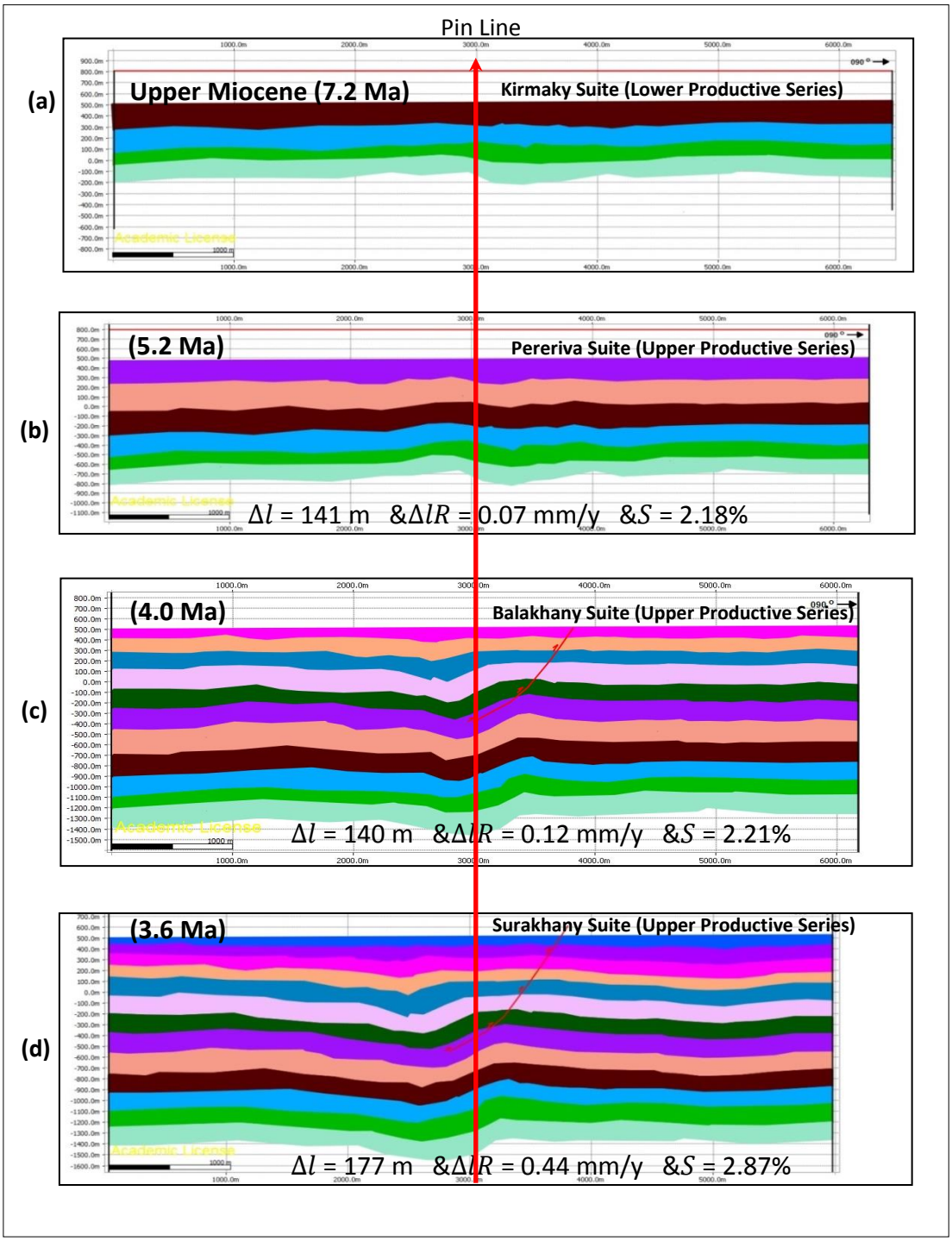
Pin Line
(a)
Upper Miocene (7.2 Ma)
Kirmaky Suite (Lower Productive Series)
(b)
(5.2 Ma)
Pereriva Suite (Upper Productive Series)
Δl = 141 m &ΔlR = 0.07 mm/y &S = 2.18%
(c)
(4.0 Ma)
Balakhany Suite (Upper Productive Series)
Δl = 140 m &ΔlR = 0.12 mm/y &S = 2.21%
(d)
(3.6 Ma)
Surakhany Suite (Upper Productive Series)
Δl = 177 m &ΔlR = 0.44 mm/y &S = 2.87%

Continued

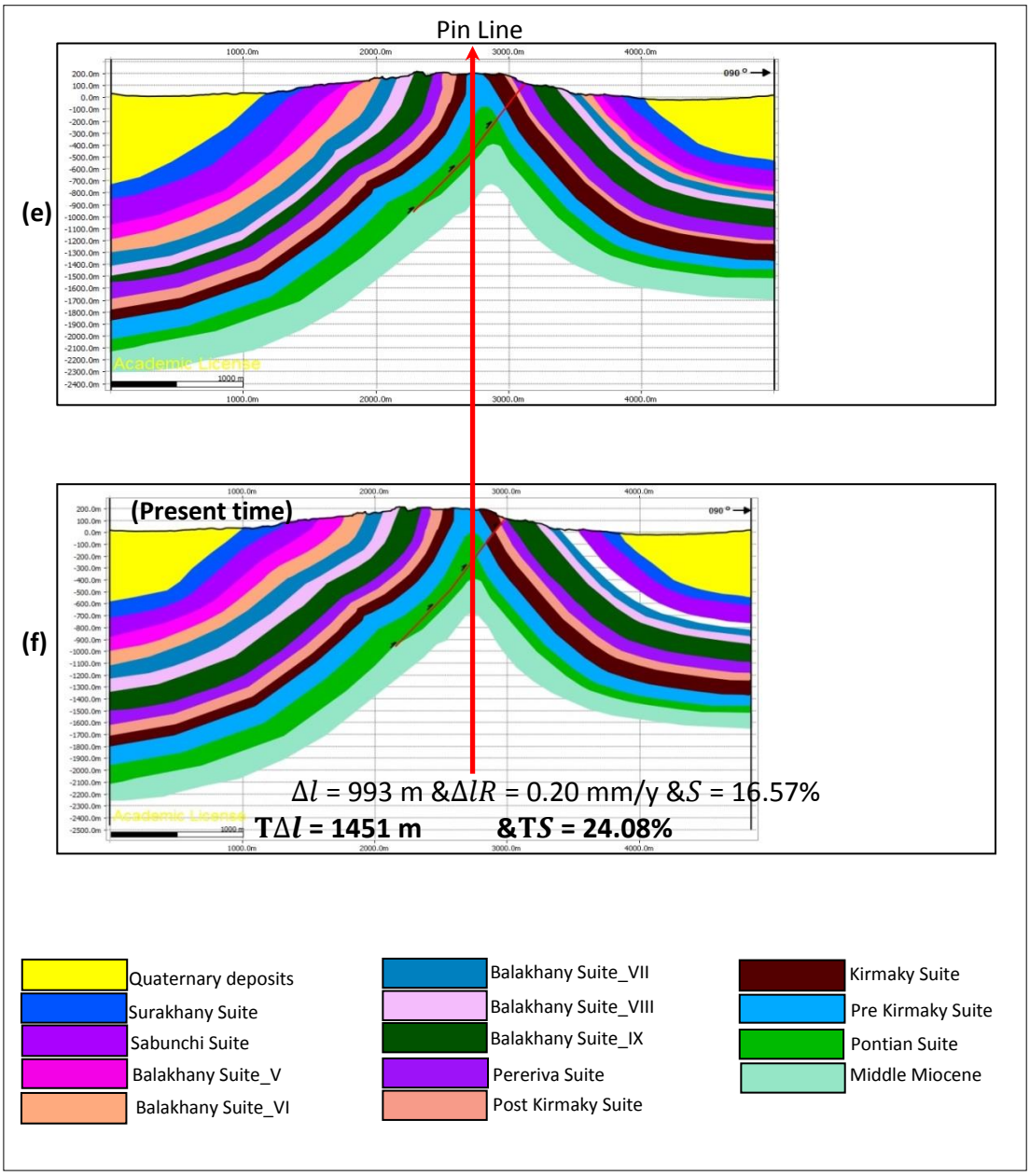

Figure 6.19. The balancing restoration of E-W cross section across the Yasamal Anticline in 2D MOVE, from Midland Valley, (location is shown in Figure 6.16. line no. (7)). the horizons are labelled and the individual amount of shortening accommodated on each stage is indicated. And the total amount of shortening that accommodated for the anticline since before deformation until the present time has shown under the stage (f). The vertical exaggeration of the cross section is (1). The shortening estimation calculated from stage (d) to (f) including stage (e) an there is no shortening estimation on (e) because of there is no evidence of the faulting time, just we know that it is after Pereriva Suite deposition.

6.5.3. Total-Shortening Estimates and longitudinal strain

The new mapping of the Yasamal anticline that was conducted from the laser scans data interpretation constrained by the digital datasets, and the balanced cross-sections that have been constructed and their restorations, allow determining the average shortening rate for the anticline.

Once the horizons have been restored and unfolded, the measurement of the length was calculated to assess the longitudinal strain. The shortening amounts and rates across the section through the fold evolution are calculated for intervals in the stratigraphic framework as shown in Figure 6.13and the results are given in Table 6.1. These shortening calculations results have been plotted in Figure 6.20to illustrate the statistical shortening of the section.

The shortening or the longitudinal strain (e) is defined as:

$$e = (l - lo)/lo \qquad \text{or} \qquad e = \Delta l/lo$$

Where:

(e): is the longitudinal strain.

(l): is the bed length after deformation (final length).

(lo): is the bed length before deformation (original length).

(Δl): is change in bed length.

The negative values of (e) reflect shortening (van der Pluijm and Marshak, 2004).

Table 6.1. The shortening estimates for the Yasamal Anticline with the line length calculating algorithm: L.d.p is the length of the deformation period, T-L.d.p is the total length of the deformation period, calculation of the horizons lengths(l), change of the horizon lengths (Δl), total change of the length (TΔl), the average of the length changes (A – ΔlR) and its percentage (P – TΔl) and shortening and total shortening percentage (S), (TS).

Stage (Fig 6.18)	Age (Ma)	L.d.p M	T-L.d.p M	l (m)	Δl (m)	$T\Delta l$ (m)	ΔlR (mm/y)	$A-\Delta lR$ (mm/y)	$P-T\Delta l$ (%)	S (%)	TS (%)
a	7.20	0.00	0.00	6451	0.00	0.00	0.000	0.000	0.00	0.00	0.00
b	5.20	2.00	2.00	6310	141	141	0.070	0.070	9.71	2.18	2.18
c	4.00	1.20	3.20	6170	140	281	0.116	0.087	19.3	2.21	4.39
d	3.60	0.40	3.60	5993	177	458	0.442	0.127	31.5	2.87	7.26
f	0.00	3.60	7.20	5000	993	1451	0.381	0.201	100	16.57	23.83

The total change in length for the Yasamal anticline horizons (from late Miocene to present time) was calculated at about 1450m and the total shortening or longitudinal strain reaches about 0.24 which is about 24 %, produced by a total shortening rate of approximately 0.2 mm/y (Table 6.1).

Since the Kirmaky suite (Lower Productive series) was deposited in the Upper Miocene, the average shortening rate has been 0.10 - 0.20mm/y, (Table 6.1and Figure 6.20) and was almost equal in all deformation stages, however the shortening rate accelerates in the stages (c) to (d) and (d) to (e) where the calculated average shortening rate reached to 0.44 and 0.39 respectively. And approximately 75% of the total shortening happened during these two stages over period of about three million years (Figure 6.19d,e). This suggests that there was accelerated shortening in the period after the completion of the Productive Series deposition. Also the results indicate that the anticline is still experiencing an E-W compression, however the rate curve is going down indicating deceleration of the shortening rate (Figure 6.20).

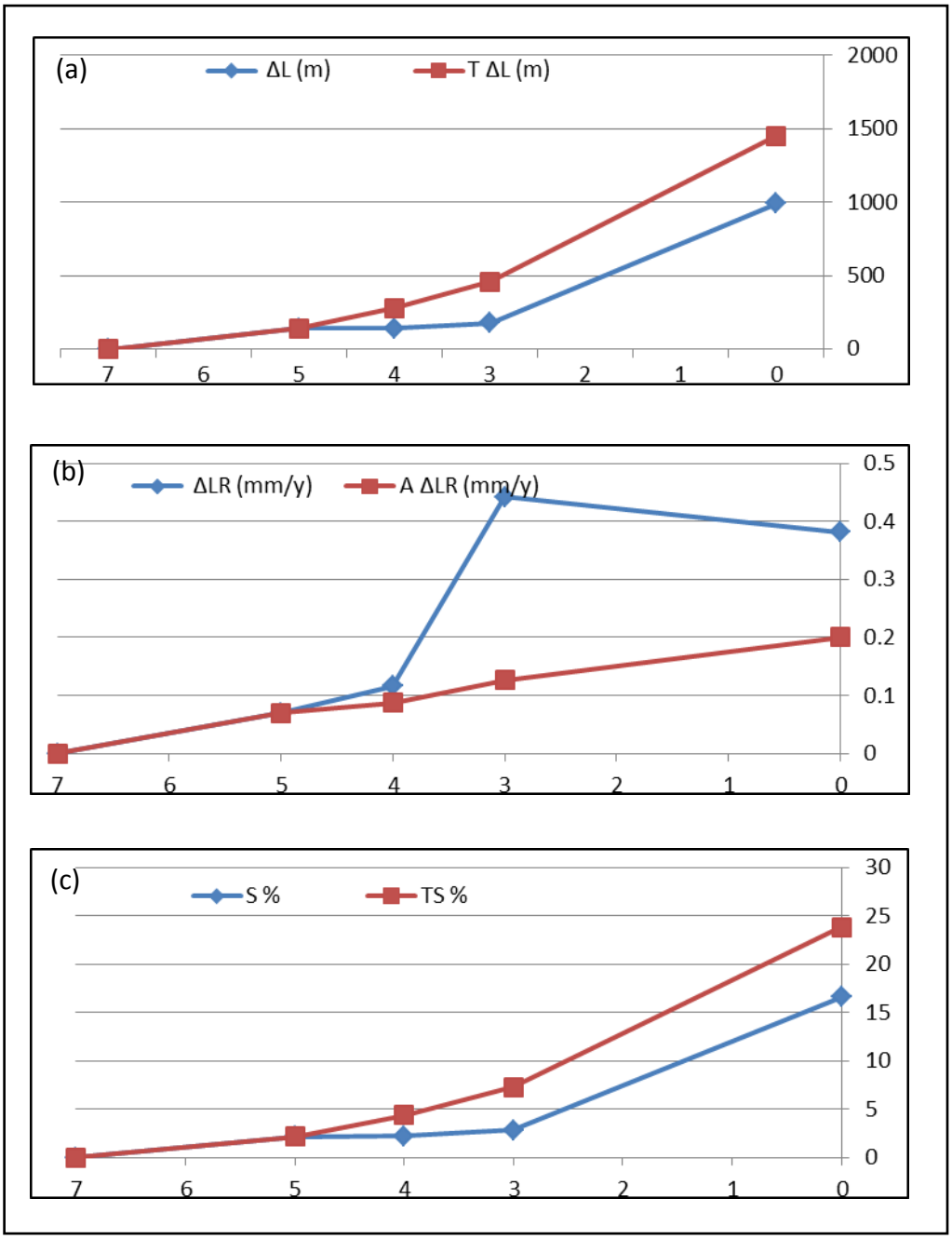

Figure 6.20. The plot diagrams of the deformation and shortening rates. (a) is showing the length changes of each stage with the stage before (Δl) and the length changes of each stage and all stages before, (b) is for the length change rate ΔlR and its average $A - \Delta lR$, and (c) is showing the percentage of the shortening accommodated of each stage (S) and the total shortening (TS).

6.5.4. Fault Throw Measurement

By using the thirteen sub-parallel cross sections that have been constructed (Figure 6.21a) based on the laser scan data and dip data, a 3D model of the Yasamal anticline was built (Figure 6.21b). This was achieved by joining the horizons from both sides of the anticline based on the assumption of the stratigraphic thickness constancy along the anticline to minimise errors in the surface reconstruction.

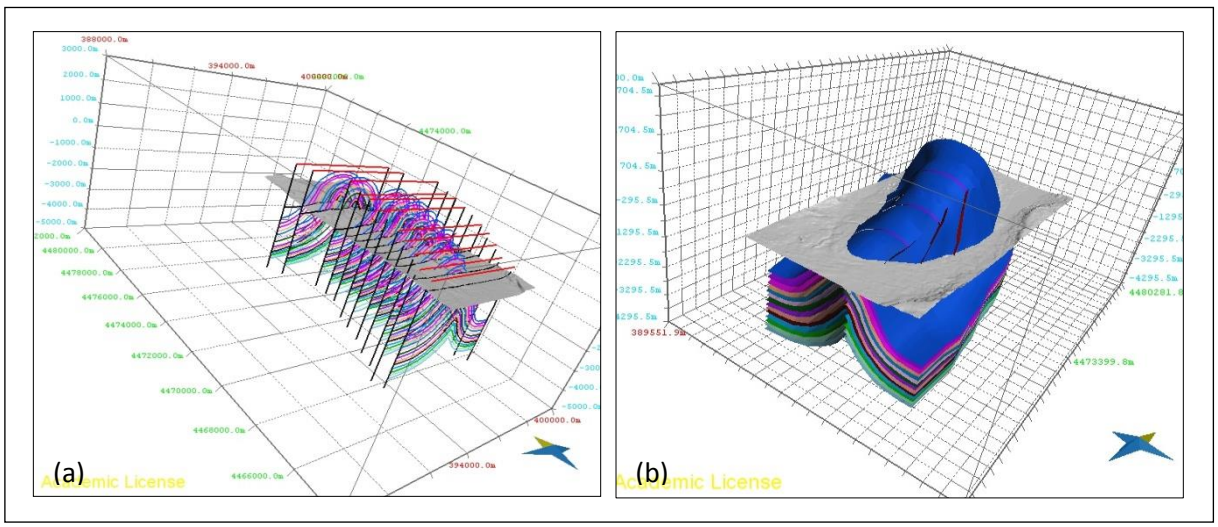

Figure 6.21. (a) View E-W cross sections that have been constructed along the Yasamal Anticline and; (b) is the 3D model of the anticline shows the faults that cut the structure. It also shows the fold plunging to the south and how the surface intersects the topography.

During the process of constructing the 3D model, the main reverse faults (F1, F2, F3 and F4) surfaces have been built. The horizons of (Balakhany Suite X, Balakhany Suite IX and Balakhany Suite VIII) were used to delineate the fault throws and displacement. A throw-distance chart has been plotted with the horizontal axis directed from the south end of each fault.

From the chart (Figure 6.22), it can be noted that the fault throws are reduced towards their southern end indicating that the faults die out towards the anticline crest in the region where it plunges southwards.

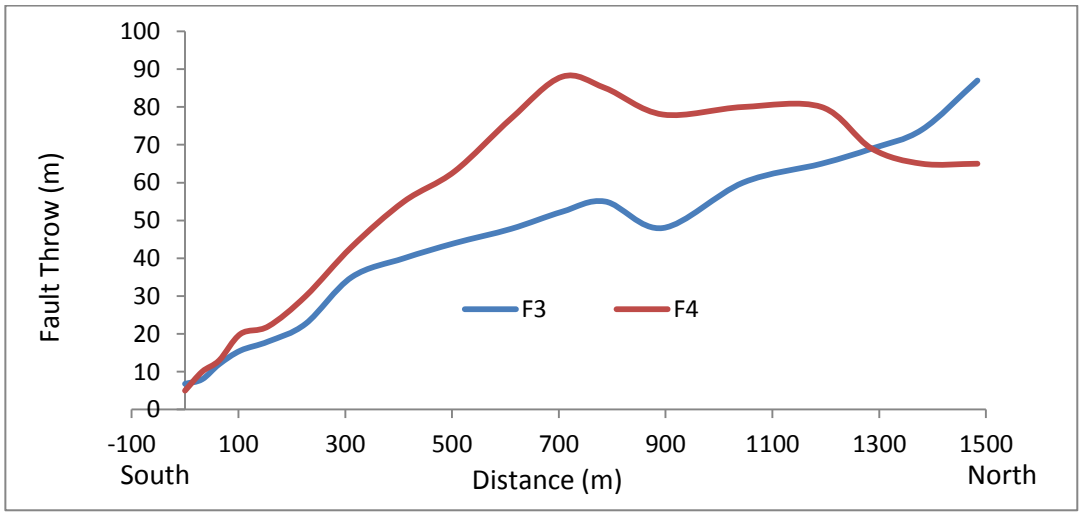

Figure 6.22. Illustration of the (Throw-Distance) chart of the faults (F3 and F4) to the south of the Yasamal anticline.

6.5.5. Anticline 3D model and its restoration

Once the horizon surfaces have been constructed in 3D to define the anticline (Figure 6.23), a kinematic restoration of the anticline was performed, to elucidate the dynamic evolution, using the 'Move on Fault' and the 'Unfold' functions in 3D Move. The kinematic models of the natural material is approximated by flexural slip and simple shear (Moretti et al., 2006), which can be incorporated in forward and backward modelling approaches.

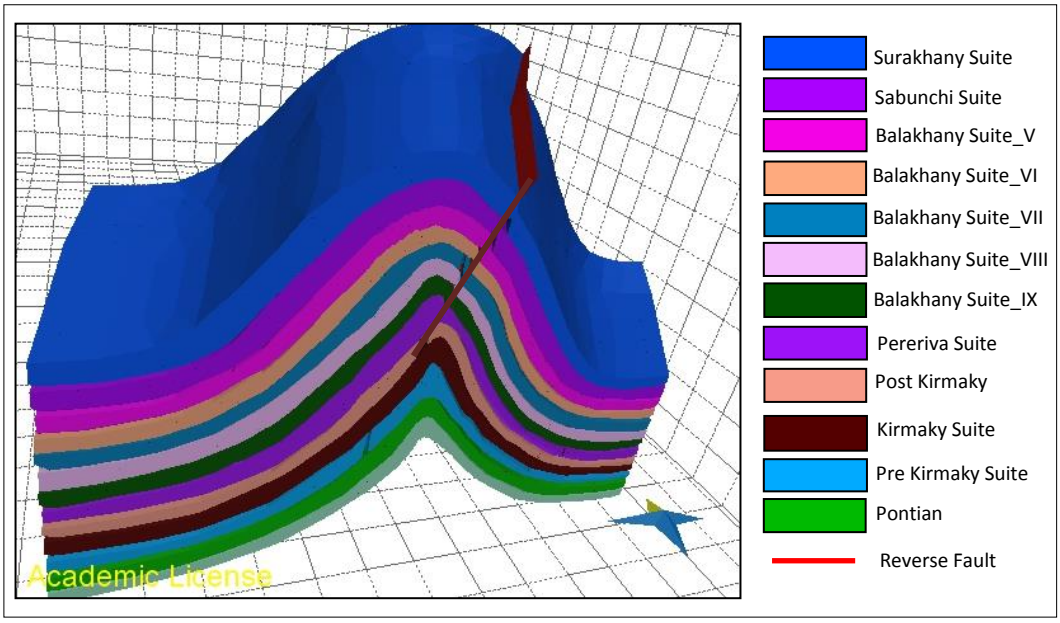

Figure 6.23. Block model of the southern part of the Yasamal anticline, as an example of the volume of each fault block.

6.5.5.1. 3D Restoration

The algorithms that have been used for 3D restoration in this study is the 'Fault Parallel Flow' function which is part of the 'Move on Fault' restoration technique and 'flexural-slip' which is part of the 'Unfold' toolset. The steps followed to attain the 3D restoration of the anticline are: 1) Move on Fault on all four major faults that cut the anticline (Figure 6.24a, b) and then; 2) unfold the folded horizons as they appear in Figure 6.24c).

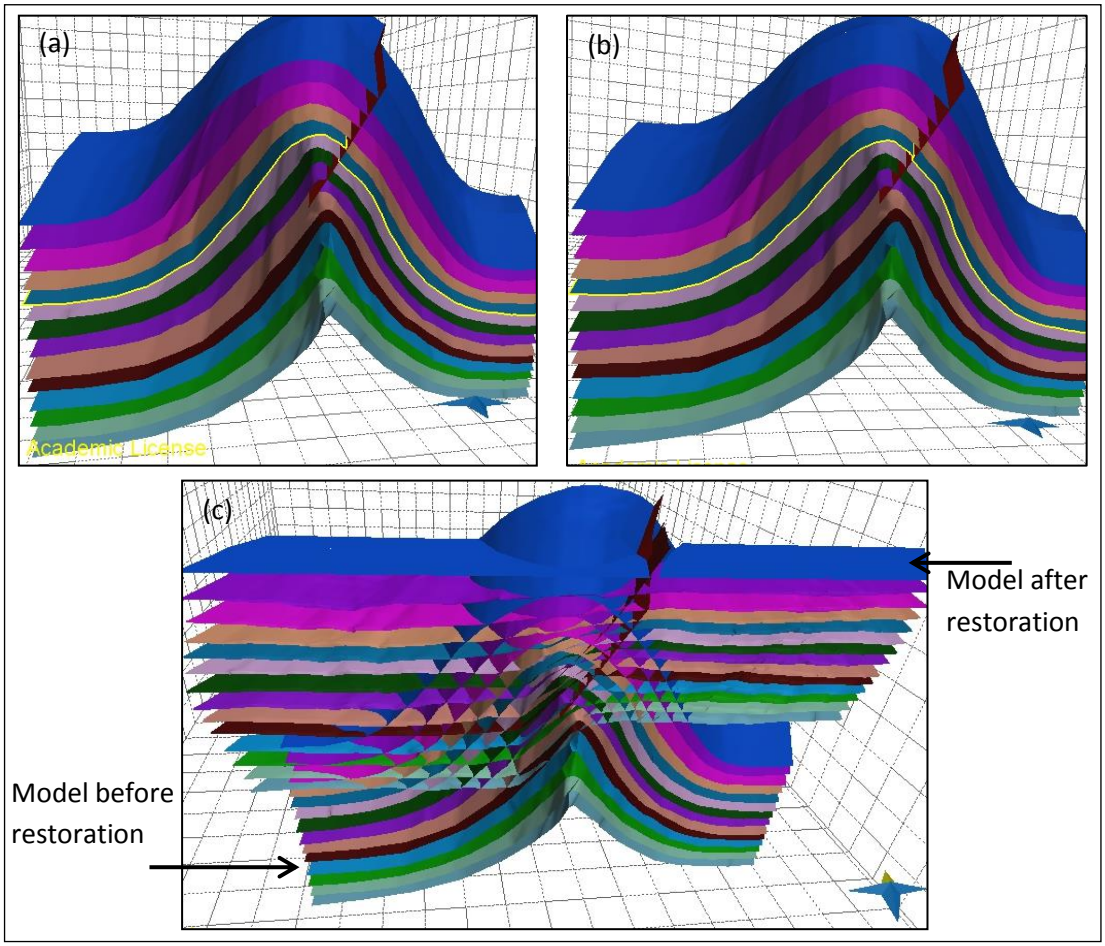

Figure 6.24. Example of the 3D restoration process (the southern Yasamal Anticline block as an example); (a) shows the model before 'Move on Fault' restoration, (b) is the block after 'Move on Fault' restoration, and (c) shows the block before and after 3D 'Unfold' restoration (see Figure 6.22 for the legend).

As these restoration procedures are reversible, the dynamic evolution of Yasamal anticline is revealed, and the suggestion of the geological history of the Yasamal structures could be drawn as below:

- Firstly, sedimentation of the Productive Series strata in the Upper Miocene and Lower Pliocene took place until the end of the Early Pliocene (about 3.4 Ma) (Figure 6.24.a).
- Secondly the Yasamal anticline was formed in reaction to ENE-WSW compression in the area.
- Then the upward-steepening reverse faults (F1, F2, F3 and F4) were developed with variable orientations (Figure 6.25b) to accommodate the stress required to initiate the folding.
- After that, some small faults were formed accommodating the strain including small normal faults).
- And finally the Yasamal anticline area is raised or uplifted and eroded as it appears in the present time (Figure 6.25c).

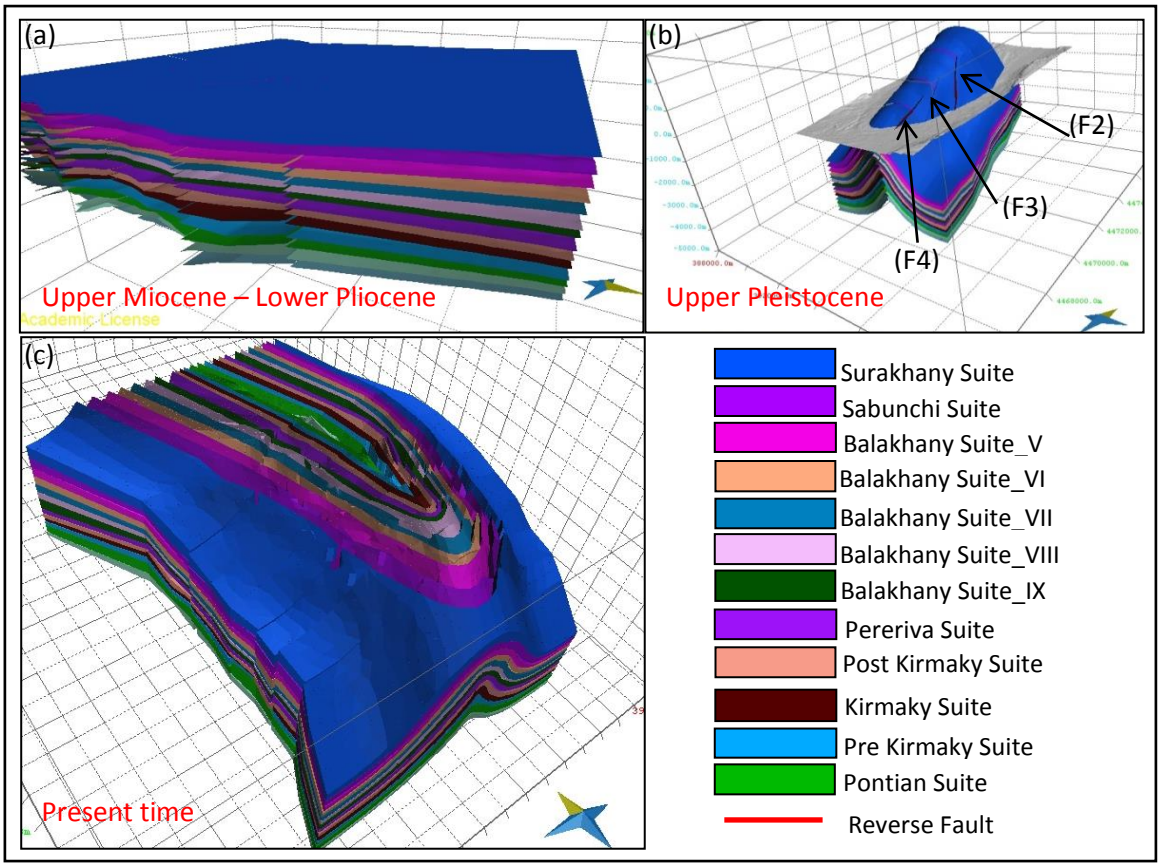

Figure 6.25.Illustration of the events of the Yasamal anticline; (a) views the area of the Yasamal Just before the deformation, (b) after deformation in Upper Pleistocene, and (c) shows the anticline in the present time after raising and eroding.

6.5.5.2. Strain Analysis to Predict Minor Structures

During the restoration process, strain was calculated and captured among the restoration steps using 3DMove. The main faults were developed to accommodate the overall strain of the anticline. There are many small scale features that can be observed from the laser scan data, however, they are removed from the model as these features are very small and do not affect the horizons that have been built where they just occur in one bed.

Once the model was simplified, it was restored to its original status and simultaneously the strains of the surface during the deformation are captured and mapped. Figure 6.26 is given as an example, and is a coloured surface showing the total movement of

the anticline horizons from the original status before deformation to the deformed surface in the present time.

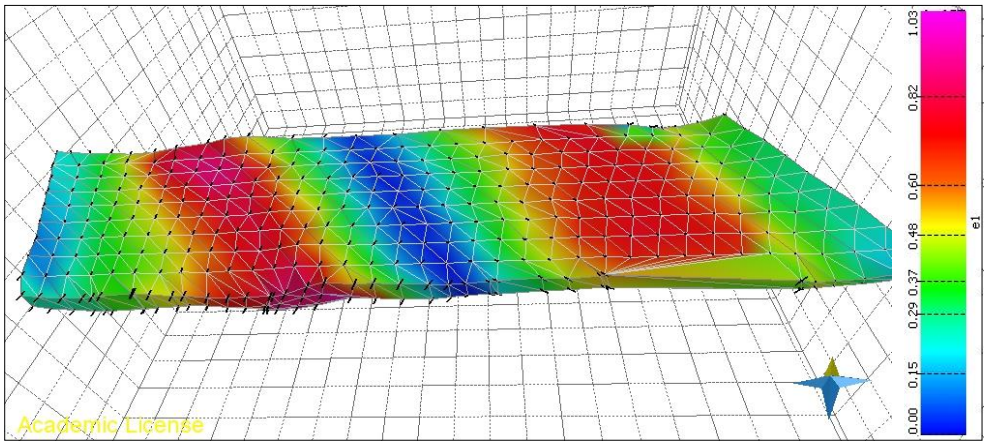

Figure 6.26. An example of the total extensional strain analysis **(e1)** of the southern block of the Yasamal anticline during the deformation (the surface is for the Surakhany Suite of the southern block of the anticline model).

In the four fault blocks of the anticline model the foot-walls show high compressional strains (e3), and the hanging-walls show low compressional strains (e3) and high extensional strain (e1) especially in the area of the anticline core. And the strains of the footwalls are almost uniform whereas of the hanging wall are not (Figure 6.27).

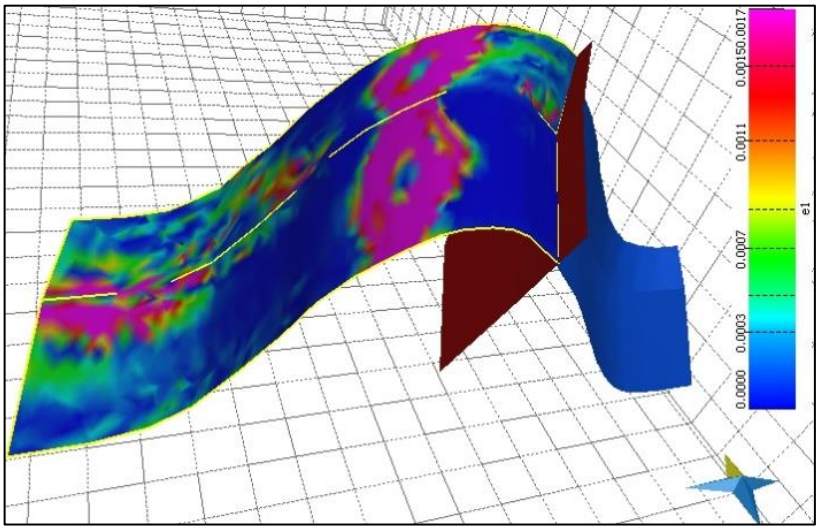

Figure 6.27. The southern Fault block of the anticline showing the extensional strain (e1) from the 'Move on Fault' restoration for fault (F4) which shows low extensional strain in the footwall whereas it is somewhat high in the hanging-wall especially in the core of the anticline. (In the colour; the extensional strain is increasing towards the pink colour and decreasing towards the blue).

The compressional strain (e3) and the extensional strain (e1) for the whole deformation that happened on the horizons have been analysed and presented in (Figure 6.28), where from the maps of the strains it can obviously be noted that the total compressional strain dominates the hinge line of the anticline, whereas extensional strain is dominating the anticline limbs.

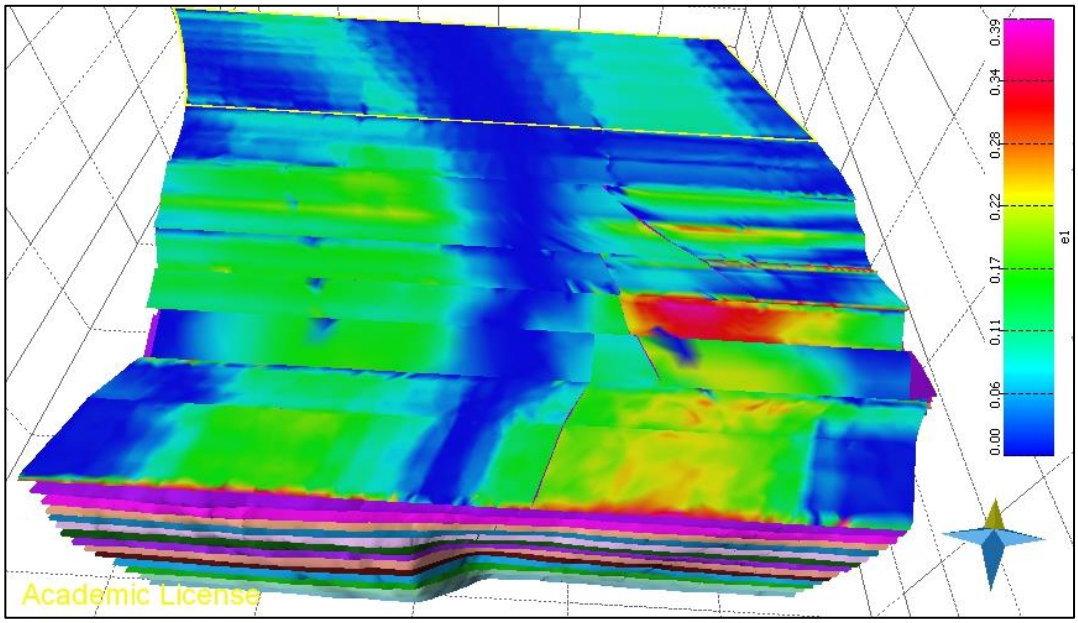

Figure 6.28. Model shows the Yasamal anticline area after restoration illustrating the total strain that accommodated to deform the area as it appears in the present time.

6.6. Discussion and Conclusions

In the oil industry, 2D and 3D seismic surveys and well-log data are the main input datasets for geological modelling interpretation in exploration and production. However in this part of the project I have demonstrated how 3D restorations of Yasamal anticline in the Apsheron Peninsula could be achieved using surface data represented by laser scan data and digital field data to test sub-surface fracture prediction. Where the investigation of the folding mechanisms are important to expect the evolution, geometry, distribution of deformation, and derived rock properties in this anticline and other detachment folds.

To incrementally restore the Yasamal anticline, the "Move package" was used in restoring the displacement on faults, unfold the geologic sections and calculate the accommodated strain. This can be applied to determine valid structural evolutions in other areas, such as elsewhere in the South Caspian Basin especially in the western part of the basin, as almost all individual folds in this part have the same properties that the Yasamal anticline has, where they have curved hinges such as Malyi Kharami anticline and Kirmaky anticline. The Yasamal anticline was appropriate for 3D reconstructions as it has excellent exposures, where the outcrops of the area reflect the geometry of the anticline and dip and stratigraphic projection of the anticline outcrops constrain the unit reconstruction.

The 3D model reconstruction of the layers below and above the Earth's surface gives an easy way to incrementally restoring the anticlines, as well as it gives a new insight into the structural evolution of the basin, where the model helps to envision the geometry of the growth strata. Yasamal anticline is a plunging anticline, where the model shows that the anticline hinge has an approximately 30° south-directed plunge. The area was characterized by a low rate of sedimentation and high rate of the uplift in

the Upper Pliocene, which was showed by the model restoration where the layers still accommodate a deformation amount after restoring the upper part of these layers.

The small or minor structures (accommodating the overall strain in the anticline) are developed throughout the entire anticline, although the hanging wall which represents the western part of the anticline shows the normal faults development. Compressional strain is present at the anticline hinge line, whereas extensional strain dominates the anticline limbs especially in the eastern flank of the anticline which represent the footwall. These suggest potential extensional structures development in the anticline flanks, which correspond with the field observations in the Yasamal valley confirming that the small normal faults are concentrated within the anticline flanks.

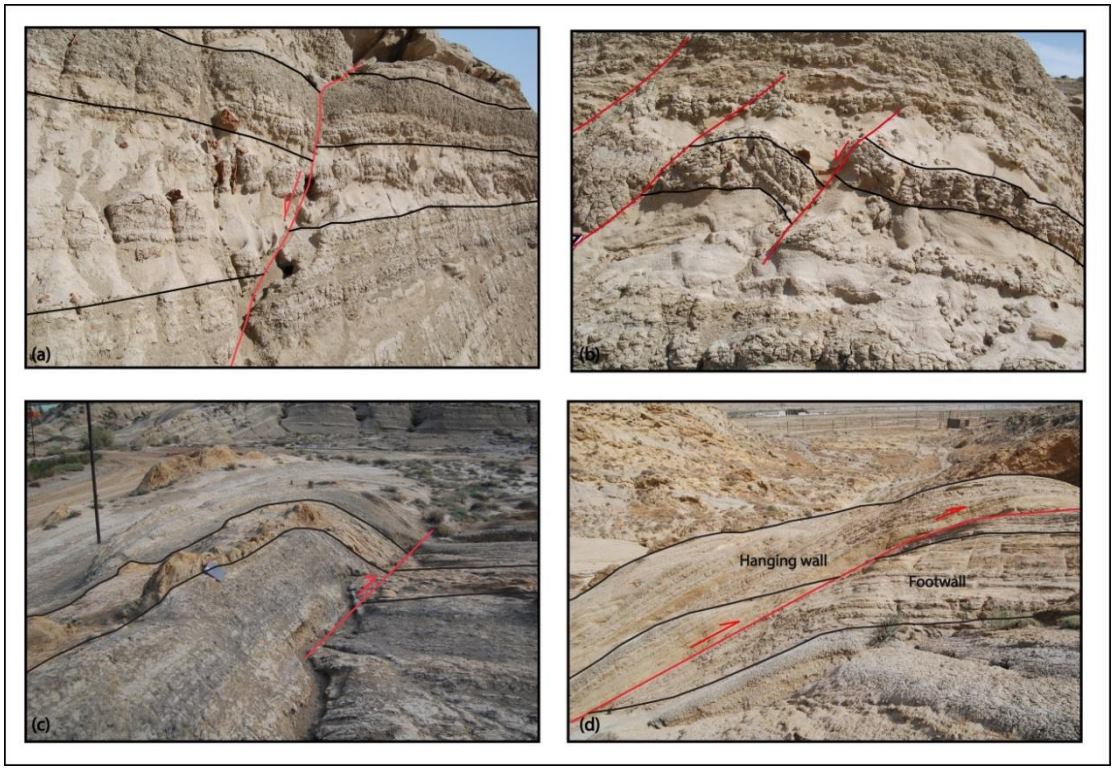

Figure 6.29. An example of the extensional structures (small normal faults) affecting the Yasamal anticline flanks (a) and (b), and the compressional structures (reverse faults) that affect the Yasamal anticline hinge area.

The strain analyses suggest that there is a potential development of the extensional structures in the anticline flanks especially in the southern part of the anticline. Also

these results correspond with the previous field observations in the Yasamal Valley which show that the small normal faults are existed within the anticline flanks (Figure 6.29 a, b). As well as the previous field observations in this area show that there are contractional deformation bands along the hinge area of the anticline, which also support the strain analyses results of the anticline (Figure 6.29 c, d).

Chapter VII

Conclusions and future works

7. Conclusions and future works

7.1. Introduction

The aim for this study was to understand the development of the structures and tectonic evolution of the Greater Caucasus and western onshore part of the South Caspian Basin. The overall objective is to describe the active structural styles in the fold and thrust belts of the Greater Caucasus and Apsheron Peninsula. The methodology included compilation and analysis of existing topographical, geological and structural databases. Topographic variations were investigated to understand the interplay between tectonics and geomorphic processes and climate of the Greater Caucasus range. Surface lineaments and structures were mapped, and their relationship with subsurface structures established by constructing geological cross-sections along the Greater Caucasus focusing on the eastern side of the mountain belt.

The main objectives of this project were; (i) Understanding the relationship between tectonics and geomorphic processes in the Caucasus Mountains, (ii) Construct regional geologic cross-sections showing major stratigraphic sequences and structures along Greater Caucasus Mountains by using the focal mechanisms of the earthquakes events, (iii) Evaluate the evolution and development of the Yasamal fold and produce a detailed map and cross sections of the anticline using structural data including laser scans, and (iv) Investigate strain accommodation mechanisms using 3D Move to unfold the Yasamal structure.

7.2. Concluding remarks

There are a number of conclusions that can be drawn from this work

- Earthquakes frequently occur in the eastern part of the Caucasus belt especially in itsnorth, whereas the western part of the belt is somewhat quiet.
- The elevations are decreasing gradually towards the west in the western part of the Caucasus but in the eastern part, they reduce sharply eastwards, and there is a high correlation between elevation changes and Moho depths underneath the Caucasus region.
- The local relief of the belt is extremely high, witha close relationship between main thrusts and the high relief along the belt, where almost all of large thrusts in the region are spatially distributed within the areas of high relief. However, the eastern part relief is apparently somewhat low comparing with the western part, even though the eastern is more active than the western part. Although the high areas in the belt have a much higher probability to be high relief areas than of the low elevation regions, the relief is low in some places that have high elevation, and vice versa.
- There is a correlation between elevation changes and climate between the east and west ends of the belt, where the gradual reduction of the mean altitude which characterises the western area of the belt, has a close relationship with a wetter climate in this part, and the sharp altitude decrease characterises the eastern part with a drier climate. On the other hand, the elevation changes on the north-western side of the belt are gradual, whereas on the south-western side they are sharp and steep. This is despite a climate in the south-western area of the belt that is wetter than the north-western part, thus the elevation change/climate

relationship across the Caucasus opposes the east-west along the mountain range. This dissimilarity in results might be because of the tectonic processes that have happened and are happening in the belt. Forthe eastern sideof thebelt, the elevation changes in the eastern part were gradualnorthwardwhereassomewhat steepsouthwarddespitethe climate is similarinthe both directions, with slightly drier to the north.

- In the Pyrenees Mountains, the elevation changes gradually to the west and steeply to the east, in a similar way to the GC topographic changes, the climate pattern is quite similar to that in the GC being wetter to the west than to the east. In the Northern Tibetan Plateau rim, the elevation chart shows that the elevations decreases sharply in both sides east and west of the plateau and the central region is inclined to the east. Correlating the elevation changes of the northern rim of the plateau with its climate, the precipitation rates of this rim of the plateau are roughly equal on both sides with a very small increase in the east side causing the steep elevation changes in both sides. In Himalayas, the elevations in the western part change sharply, whereas they decline gradually in the eastern part of the belt.
- The study area is highly faulted, with a complex geological pattern; the faulting style in the region is revers faulting, with a general NW-SE trend. According to previous GPS surveys, it appears that the belt is accommodating a minimum 5mm/year N-S shortening rate, and maximum rate of about 13mm/year, and although the eastern part has lower relief than in the western part of the belt, the convergence across the range increases towards the east.
- Seismicity of the eastern Greater Caucasus has greater intensity than the western part, and it has been recorded on both the north and south sides of the range,

whereas in the western side the earthquakes occur just in the southern side. Most events in the region occur in depths between 6km and 20 km, which indicate to the absence of sub-crustal earthquakes.

- It can be confirmed that the reverse focal mechanisms represent the main type in the Greater Caucasus, which are linked with the thrusting and NE-SW compression. There is a relationship between high magnitudes and the MCT with a significant displacement is accommodated, and the low magnitudes are associated with the minor faults that distributed along the belt.
- The frequency and spatial distribution of the folds are varied along the belt, and have different topographic aspects. Folding is more intense in the west than in the east of the belt, and is linear and parallel to each other in the west, whereas they are mostly curved and cut by mud volcanoes in the east of the belt. Most folds have the regional WNW-ESE trend of the main Greater Caucasus belt, but a few folds have a more east-west orientation. Fold axial traces are generally sub-parallel to each other, however, they do show differences in how they arranged. The traces are offset from each other in en echelon patterns that are either; random or systematically stepped offset associated with the strike-slip faults, however the random pattern represent the important pattern that distributed in the eastern side of the belt. The Greater Caucasus folds vary in length from a few meters to kilometres, and their plan shapes are different. Some of them have linear plan shapes distributed towards the central and western parts of the belt, and others have oval plan shapes, in addition a number of them have more curved or arcuate shapes.

- The most important and predominant faults that are distributed in the belt are reverse faults that mostly trend NW-SE parallel to the belt, such as the (MCT) dipping north and cutting almost the entire sedimentary cover. On the other hand the normal faults are rare in the belt and mostly seen in association with relatively small-scale collapse structures in the anticlinal flanks, and they are more distributed in the eastern part of the belt.
- For achieving the incrementally restore Yasamal anticline, “Move package” was used that restores displacement on faults and unfold the geologic sections with calculating the accommodated strain, which can be applied to determine valid structural evolutions in other areas, such as elsewhere in the South Caspian Basin or Greater Caucasus.
- Yasamal anticline appears appropriate to 3D reconstructions as it has excellent exposures, where the topographic outcrops of the area picture the shape of the anticline as the dip and stratigraphic projection of the anticline outcrops constrain the unit reconstruction.
- The 3D models reconstruction of the layers below and above the earth surface gives an easy way to incrementally restoring the anticline, as well as it gives a new insight into the structural evolution of the basin, where the model helps to envision the geometry of the growth strata. Yasamal anticline is a plunging thrust related anticline, where the model shows that the anticline has approximately 30° southern plunge. The area was characterized by low rate of sedimentation and high rate of the uplift in the Upper Pliocene, which showed by the model restoration where the layers still accommodate a deformation amount after restoring the upper part of these layers.

- The total compressional strain is dominating the anticline hinge line, whereas extensional strain is dominating the anticline wings especially in the eastern flank of the anticline which represent the footwall. These suggest potential extensional structures development in the anticline flanks, which correspond with the field observations in the Yasamal valley confirming that the small normal faults are concentrated within the anticline flanks.

7.3. Future works

- Determining the relationship between the Azerbaijani mud volcanoes with the faulting, folding (specially the curved hinge lines of the anticline) and regional structures.
- Determining the relationship between the elevations and exhumation level with the fast GPS vectors in the Greater Caucasus.
- Make an analogue for the offshore anticlines in the south Caspian Basin.

8. References

Abellan, A., Oppikofer, T., Jaboyedoff, M., Rosser, N. J., Lim, M., and Lato, M. J., 2014, Terrestrial laser scanning of rock slope instabilities: Earth Surface Processes and Landforms, v. 39, no. 1, p. 80-97.

Abrams, M. A., and Narimanov, A. A., 1997, Geochemical evaluation of hydrocarbons and their potential sources in the western South Caspian depression, Republic of Azerbaijan: Marine and Petroleum Geology, v. 14, no. 4, p. 451-468.

Adamia, S., Victor, A., Aleksandre, C., Zurab, K., and Nino, S., 2011a, Great Caucasus (Cavcasioni): A Long-lived North-Tethyan Back-Arc Basin: Turkish Journal of Earth Sciences, v. 20, p. 611-628.

Adamia, S., Zakariadze G , Tamar C, Nino S, Nino T, Aleksandre C, and G., A., 2011b, Geology of the Caucasus: A Review: Turkish Journal of Earth Sciences, v. 20, p. 489-544.

Adamia, S. A., Chkhotua, T., Kekelia, M., Lordkipanidze, M., Shavishvili, I., and Zakariadze, G., 1981, Tectonics of the Caucasus and adjoining regions: implications for the evolution of the Tethys ocean: Journal of Structural Geology, v. 3, no. 4, p. 437-447.

Adamia, S. A., Lordkipanidze, M. B., and Zakariadze, G. S., 1977, Evolution of an active continental margin as exemplified by the Alpine history of the Caucasus: Tectonophysics, v. 40, no. 3-4, p. 183-199.

Ahnert, F., 1970, Functional Relationships between Denudation, Relief, and Uplift in Large Mid-Latitude Drainage Basins: American Journal of Science, v. 268, no. 3, p. 243-&.

Alasset, P.-J., and Meghraoui, M., 2005, Active faulting in the western Pyrénées (France): Paleoseismic evidence for late Holocene ruptures: Tectonophysics, v. 409, no. 1-4, p. 39-54.

Allen, M., Jackson, J., and Walker, R., 2004, Late Cenozoic reorganization of the Arabia-Eurasia collision and the comparison of short-term and long-term deformation rates: Tectonics, v. 23, no. 2, p. TC2008.

Allen, M. B., Ghassemi, M. R., Shahrabi, M., and Qorashi, M., 2002a, Accommodation of late Cenozoic oblique shortening in the Alborz range, northern Iran: Journal of Structural Geology, v. 25, no. 5, p. 659-672.

Allen, M. B., Jones, S., Ismail-Zadeh, A., Simmons, M., and Anderson, L., 2002b, Onset of subduction as the cause of rapid Pliocene-Quaternary subsidence in the South Caspian basin: Geology, v. 30, no. 9, p. 775-778.

Allen, M. B., Morton, A. C., Fanning, C. M., Ismail-Zadeh, A. J., and Kroonenberg, S. B., 2006, Zircon age constraints on sediment provenance in the Caspian region: Journal Of The Geological Society, v. 163, p. 647-655.

Allen, M. B., Vincent, S. J., Alsop, G. I., Ismail-Zadeh, A., and Flecker, R., 2003, Late Cenozoic deformation in the South Caspian region: effects of a rigid basement block within a collision zone.: Tectonophysics, v. 366, no. 3-4, p. 223-239.

Alsop, G. I., and Holdsworth, R. E., 2002, The geometry and kinematics of flow perturbation folds: Tectonophysics, v. 350, no. 2, p. 99-125.

Artyushkov, E. V., 2007, Formation of the superdeep South Caspian basin: subsidence driven by phase change in continental crust: Russian Geology and Geophysics, v. 48, no. 12, p. 1002-1014.

Avdeev, B., and Niemi, N. A., 2011, Rapid Pliocene exhumation of the central Greater Caucasus constrained by low-temperature thermochronometry: Tectonics, v. 30.

Babault, J., Van den Driessche, J., Bonnet, S., Castelltort, S., and Crave, A., 2005, Origin of the highly elevated Pyrenean peneplain: Tectonics, v. 24, no. 2.

Bagirov, E., and Lerche, I., 1998, Potential oil-field discoveries for Azerbaijan: Marine and Petroleum Geology, v. 15, no. 1, p. 11-19.

Banks, C. J., Robinson, A. G., and Williams, M. P., 1997, Structure and Regional Tectonics of the Achara-Trialet Fold Belt and the Adjacent Rioni and Kartli Foreland Basins, Republic of Georgia: AAPG Memoir 68:Regional and Petroleum Geology of the Black Sea and Surrounding Region, Edited by A.G. Robinson, p. 331-346.

Bedford, D. P., and Barry, R. G., 1994, Glacier Trends in the Caucasus, 1960s to 1980s: Physical Geography, v. 15, no. 5, p. 414-424.

Berberian, M., 1983a, The southern Caspian: A compressional depression floored by a trapped, modified oceanic crust: Canadian Journal of Earth Sciences, v. 20, p. 163-183.

Berberian, M., 1983b, The southern Caspian: A compressional depression floored by a trapped, modified oceanic crust": Canadian Journal of Earth Sciences, v. 20, no. 2, p. 163-183.

Bishop, M. P., Shroder, J. F., Bonk, R., and Olsenholler, J., 2002, Geomorphic change in high mountains: a western Himalayan perspective: Global and Planetary Change, v. 32, no. 4, p. 311-329.

Bochud, M., 2011, Tectonics of the Eastern Greater Caucasus in Azerbaijan: PhD Thesis, v. 30, p. 207.

Brodu, N., and Lague, D., 2012, 3D terrestrial lidar data classification of complex natural scenes using a multi-scale dimensionality criterion: Applications in geomorphology: ISPRS Journal of Photogrammetry and Remote Sensing, v. 68, no. 0, p. 121-134.

Brunet, M.-F., Korotaev, M. V., Ershov, A. V., and Nikishin, A. M., 2003, The South Caspian Basin: a review of its evolution from subsidence modelling: Sedimentary Geology, v. 156, no. 1-4, p. 119-148.

Buryakovsky, L. A., Chilingar, G. V., and Aminzadeh, F., 2001, Petroleum Geology of the South Caspian Basin.

Caspers, H., 1957, Chapter 25: Black Sea and Sea of Azov: Geological Society of America Memoirs, v. 67V1, p. 801-890.

Clark, M. K., 2012, Continental collision slowing due to viscous mantle lithosphere rather than topography: Nature, v. 483, no. 7387, p. 74-U1502.

Clark, M. K., Royden, L. H., Whipple, K. X., Burchfiel, B. C., Zhang, X., and Tang, W., 2006, Use of a regional, relict landscape to measure vertical deformation of the eastern Tibetan Plateau: Journal of Geophysical Research-Earth Surface, v. 111, no. F3.

Dahlen, F. A., 1984, Noncohesive critical Coulomb wedges: An exact solution: Journal of Geophysical Research: Solid Earth, v. 89, no. B12, p. 10125-10133.

Dahlen, F. A., and Suppe, J., 1988, Mechanics, growth, and erosion of mountain belts: Geological Society of America Special Papers, v. 218, p. 161-178.

Davies, G. H., and Reynolds, S., J. R., 1996, Structural Geology of Rocks and Regions: book, p. 864.

Devlin, W. J., Cogswell, J. M., G. M. Gaskins, G. H. Isaksen, D. M. Pitcher, D. P. Puls, and K. O. Stanley, G. R. T. W., 1999, South Caspian Basin: Young, Cool, and Full of Promise: GSA TODAY, v. 9, no. 7, p. 1-32.

Dileka, Y., Imamverdiyevb, N., and Altunkaynak, S., 2010, Geochemistry and tectonics of Cenozoic volcanism in the Lesser Caucasus (Azerbaijan) and the peri-Arabian region: collision-induced mantle dynamics and its magmatic fingerprint.: International Geology Review, v. 52, p. 536-578.

Djevanshir, R. D., and Mansoori, G. A., 2000, Introduction to South Caspian Basin special issue: Journal of Petroleum Science and Engineering, v. 28, no. 4, p. 153-155.

Dotduyev, S. I., 1987, Nappe Structure of the Greater Caucasus Range: Geotectonics, v. 20, no. 5, p. 420-430.

Egan, S. S., Jon Mosar, Brunet, M.-F., and Kangarli, T., 2009, Subsidence and uplift mechanisms within the South Caspian Basin: insights from the onshore and offshore Azerbaijan region: Geological Society, London, Special Publications, v. 312 p. 219 - 240.

Ershov, A. V., Brunet, M.-F., Korotaev, M. V., Nikishin, A. M., and N. Bolotov, S., 1999, Late Cenozoic burial history and dynamics of the Northern Caucasus molasse basin: implications for foreland basin modelling: Tectonophysics, v. 313, no. 1-2, p. 219-241.

Ershov, A. V., Brunet, M.-F., Nikishin, A. M., Bolotov, S. N., Nazarevich, B. P., and Korotaev, M. V., 2003, Northern Caucasus basin: thermal history and synthesis of subsidence models: Sedimentary Geology, v. 156, no. 1-4, p. 95-118.

Eyer, J., Psuey, W., Hedberg, J., Rhine, J., Engekhart, D., Kuliev, K., Feyzullayev, A., and Mamedova, D., 1995, South Caspian Basin Project Year 1-Stratigraphy and sedimentation: University of South Carolina, Earth Sciences and Resources Institute, ESRI Technical Report 95-02-448, v. 3, p. 27.

Fielding, E., Isacks, B., Barazangi, M., and Duncan, C., 1994, HOW FLAT IS TIBET: Geology, v. 22, no. 2, p. 163-167.

Fielding, E. J., 1996, Tibet uplift and erosion: Tectonophysics, v. 260, no. 1–3, p. 55-84.

Finlayson, D. P., Montgomery, D. R., and Hallet, B., 2002, Spatial coincidence of rapid inferred erosion with young metamorphic massifs in the Himalayas: Geology, v. 30, no. 3, p. 219-222.

Firoozfar, A., Bromhead, E. N., Dykes, A. P., and Neshaei, M. A. L., 2012, Southern Caspian Sea Coasts, Morphology, Sediment Characteristics, and Sea Level Change: Proceedings of the Annual International Conference on Soils, Sediments, Water and Energy, v. 17.

Forte, A. M., Cowgill, E., Bernardin, T., Kreylos, O., and Hamann, B., 2010, Late Cenozoic deformation of the Kura fold-thrust belt, southern Greater Caucasus: Geological Society of America Bulletin, v. 122, no. 3-4, p. 465-486.

Frauenfeld, O. W., Zhang, T., and Serreze, M. C., 2005, Climate change and variability using European Centre for Medium-Range Weather Forecasts reanalysis (ERA-40) temperatures on the Tibetan Plateau: Journal of Geophysical Research: Atmospheres, v. 110, no. D2, p. D02101.

Frederic, G., O., C., G., J., and P., E., 2008, Regionalisation Des Precipitations Sur les Massifs Montagneux Francais A L'AIDE de Regressions locales et par types de temps: Climatologie, v. 5.

Froehlich, K., Rozanski, K., Povinec, P., Oregioni, B., and Gastaud, J., 1999, Isotope studies in the Caspian Sea: Science of the Total Environment, v. 238, p. 419-427.

Frydl, P. M., Sawlan, J. J., Rastegar, I., Sealy, B. E., Smith-Rouch, L.S., W., C.C.,, Kuramshina, N. S., Narimanov, A. A., Ibragimov, G. S., Javadova, A. S., Kerimov, A. K., and Mustafayev, Y. G., 1995, Geological and geochemical modeling of the northern part of the Baku Archipelago: Joint SOCAR Mobil Study., p. 125.

Gamkrelidze, I. P., 1986, Geodynamic evolution of the Caucasus and adjacent areas in Alpine time: Tectonophysics, v. 127, no. 3-4, p. 261-277.

Gilchrist, A. R., Summerfield, M. A., and Cockburn, H. A. P., 1994, Landscape Dissection, Isostatic Uplift, and the Morphologic Development of Orogens: Geology, v. 22, no. 11, p. 963-966.

Golonka, J., 2004, Plate tectonic evolution of the southern margin of Eurasia in the Mesozoic and Cenozoic: Tectonophysics, v. 381, no. 1-4, p. 235-273.

Gourley, J. J., and Vieux, B. E., 2005, A method for evaluating the accuracy of quantitative precipitation estimates from a hydrologic modeling perspective: Journal of Hydrometeorology, v. 6, no. 2, p. 115-133.

Granath, J. W., Baganz, O.W., 1996, A review of Neogene subsidence mechanisms for the south Caspian basin. 3rd Annual Meeting and Fieldtrip of IGCP Project nj369 ‘‘Comparative evolution of Peri-Tethyan rift basins’’. , p. 24- 25.

Green, T., Nazim Abdullayev, Jake Hossack, Riley, G., and Roberts, A. M., 2009, Sedimentation and subsidence in the South Caspian Basin, Azerbaijan: Geological Society, London, Special Publications, v. 312 p. 241 - 260.

Groshong, R. H., 2006, 3-D Structural Geology (A Practical Guide to Quantitative Surface and Subsurface Map Interpretation), Book.

Guliyev, I. S., Mamedov, P. Z., Feyzullayev, A. A., Huseynov, D. A., Kadirov, F. A., Aliyeva, E. H.-M., and M.F., T., 2003, Hydrocarbon Systems of the South Caspian Basin.: Nafta-Press, p. 206.

Gurbanov, A. G., Gazeev, V. M., Bogatikov, O. A., Naumov, V. B., Dokuchaev, A. Y., and Shevchenko, A. V., 2004, Elbrus active Volcano and its geological history, v. 6, p. 257-277.

Gurevich, A., E., and Chilingar, G., V., 1995, Abnormal pressures in Azerbaijan: A brief critical review and recommendations: Journal of Petroleum Science and Engineering, v. 13, no. 2, p. 125-135.

Hafkenscheid, E., Wortel, M. J. R., and Spakman, W., 2006, Subduction history of the Tethyan region derived from seismic tomography and tectonic reconstructions: Journal of Geophysical Research: Solid Earth, v. 111, no. B8, p. B08401.

Hatzfeld, D., and Molnar, P., 2010, Comparisons of the kinematics and deep structures of the Zagros and Himalaya and of the Iranian and Tibetan plateaus and geodynamic implications: Reviews of Geophysics, v. 48, no. 2, p. RG2005.

Hinds, D. J., Aliyeva, E., Allen, M. B., Davies, C. E., Kroonenberg, S. B., Simmons, M. D., and Vincent, S. J., 2004, Sedimentation in a discharge dominated fluvial-lacustrine system: the Neogene Productive Series of the South Caspian Basin, Azerbaijan: Marine and Petroleum Geology, v. 21, no. 5, p. 613-638.

Hollingsworth, J., Jackson, J., Walker, R., and Nazari, H., 2009, Extrusion tectonics and subduction in the eastern South Caspian region since 10 Ma: REPLY: Geological Society of America, v. 37, p. 199-200.

Hoogendoorn, R. M., Boels, J. F., Kroonenberg, S. B., Simmons, M. D., Aliyeva, E., Babazadeh, A. D., and Huseynov, D., 2005, Development of the Kura delta, Azerbaijan; a record of Holocene Caspian sea-level changes: Marine Geology, v. 222–223, no. 0, p. 359-380.

Hudson, S. M., Johnson, C. L., Efendiyeva, M. A., Rowe, H. D., Feyzullayev, A. A., and Aliyev, C. S., 2008, Stratigraphy and geochemical characterization of the Oligocene–Miocene Maikop series: Implications for the paleogeography of Eastern Azerbaijan: Tectonophysics, v. 451, no. 1–4, p. 40-55.

Immerzeel, W. W., van Beek, L. P. H., and Bierkens, M. F. P., 2010, Climate Change Will Affect the Asian Water Towers: Science, v. 328, no. 5984, p. 1382-1385.

Inan, S., Namik Yalçin, M., Guliev, I. S., Kuliev, K., and Akper Feizullayev, A., 1997, Deep petroleum occurrences in the Lower Kura Depression, South Caspian Basin, Azerbaijan: an organic geochemical and basin modeling study: Marine and Petroleum Geology, v. 14, no. 7-8, p. 731-762.

Jackson, J., 1992, Partitioning of Strike-Slip and Convergent Motion Between Eurasia and Arabia in Eastern Turkey and the Caucasus: J. Geophys. Res., v. 97, no. B9, p. 12471-12479.

Jackson, J., and Mckenzie, D., 1984, Active Tectonics of the Alpine Himalayan Belt between Western Turkey and Pakistan: Geophysical Journal of the Royal Astronomical Society, v. 77, no. 1, p. 185-+.

Jackson, J., Priestley, K., Allen, M. B., and Berberian, M., 2002, Active tectonics of the South Caspian Basin: Geophysical Journal International, v. 148, no. 2, p. 214-245.

Jarvis, A., H.I. Reuter, A. Nelson, and E. Guevara, 2008, Hole-filled SRTM for the globe Version 4, available from the CGIAR-CSI SRTM 90m Database (http://srtm.csi.cgiar.org). Additional Information: http://www.cgiar-csi.org/data/elevation/item/45-srtm-90m-digital-elevation-database-v41.

Joannin, S., Cornee, J. J., Munch, P., Fornari, M., Vasiliev, I., Krijgsman, W., Nahapetyan, S., Gabrielyan, I., Ollivier, V., Roiron, P., and Chataigner, C., 2010, Early Pleistocene climate cycles in continental deposits of the Lesser Caucasus of Armenia inferred from palynology, magnetostratigraphy, and Ar-40/Ar-39 dating: Earth and Planetary Science Letters, v. 291, no. 1-4, p. 149-158.

Jones, R. R., McCaffrey, K. J. W., Imber, J., Wightman, R., Smith, S. A. F., Holdsworth, R. E., Clegg, P., De Paola, N., Healy, D., and Wilson, R. W., 2008, Calibration and validation of reservoir models: the importance of high resolution, quantitative outcrop analogues: Future of Geological Modelling in Hydrocarbon Development, v. 309, p. 87-98.

Jones, R. W., and Simmons, M. D., 1996, A review of the stratigraphy of Eastern Paratethys (Oligocene-Holocene): Bulletin of the Natural History Museum London (Geology), v. 52, p. 25-49.

-, 1997, A review of the stratigraphy of Eastern Paratethys (Oligocene-Holocene), with particular emphasis on the Black Sea: Regional and Petroleum Geology of the Black Sea and Surrounding Region, v. 68, p. 39-51.

Kasperski. J., Delacourt. C., Allemand, P., Potherat. P., Jaud. M., and E., V., 2010, Application of a Terrestrial Laser Scanner (TLS) to the Study of the Sé chilienne Landslide (Isè re, France): Remote Sensing.

Katz, B., Richards, D., Long, D., and Lawrence, W., 2000, A new look at the components of the petroleum system of the South Caspian Basin: Journal Of Petroleum Science And Engineering, v. 28, no. 4, p. 161-182.

Kazmin, V. G., Sbortshikov, I. M., Ricou, L. E., Zonenshain, L. P., Boulin, J., and Knipper, A. L., 1986, Volcanic Belts as Markers of the Mesozoic-Cenozoic Active Margin of Eurasia: Tectonophysics, v. 123, no. 1-4, p. 123-152.

Kekelia, S. A., Kekelia, M. A., Kuloshvili, S. I., Sadradze, N. G., Gagnidze, N. E., Yaroshevich, V. Z., Asatiani, G. G., Doebrich, J. L., Goldfarb, R. J., and Marsh, E. E., 2008, Gold deposits and occurrences of the Greater Caucasus, Georgia Republic: Their genesis and prospecting criteria: Ore Geology Reviews, v. 34, no. 3, p. 369-386.

Khain, V. E., 1975, structure and main stages in the tectono magmatic development of the Caucasus: An attempt at Geodynamic interpretation.: American Journal of Science, v. 275-A, p. 131-156.

Khain, V. E., 1994, Geology of the Northern Eurasia (ex-USSR). Second Part of the Geology of the USSR. Phanerozoic Fold Belts and Young Platforms. : Gebru¨der Borntraeger, Berlin., p. 390 pp.

Khain, V. E., Sokolov, B. A., Kleshchev, K. A., and Shein, V. S., 1991, Tectonic and Geodynamic Setting of Oil and Gas Basins of the Soviet-Union: Aapg Bulletin-American Association of Petroleum Geologists, v. 75, no. 2, p. 313-325.

Klett, T. R., ., Ahlbrandt T. S. , Schmoker J. W. , and L., D. G., 1997, Ranking Of the World's Oil and Gas Provinces by Known Petroleum Volumes.: USGS C entral Region Energy Resources Team U. S. Department of the Interior Geological Survey.

Knapp, C. C., Knapp, J. H., and Connor, J. A., 2004, Crustal-scale structure of the South Caspian Basin revealed by deep seismic reflection profiling: Marine and Petroleum Geology, v. 21, no. 8, p. 1073-1081.

Knapp, J. H., Diaconescu, C.C., Connor, J.A., McBride, J.H., Simmons, M.D., , 2000, Deep seismic exploration of the South Caspian Basin: lithospheric-scale imaging of the world's deepest basin: AAPG's Inaugural Regional International Conference,, v. Abstract volume, p. 35- 37.

Koçyigit, A., Yilmaz, A., Adamia, S., and Kuloshvili, S., 2000, Neotectonics of East Anatolian Plateau (Turkey) and Lesser Caucasus: implication for transition from thrusting to strike-slip faulting: Geodinamica Acta, v. 14, no. 1-3, p. 177-195.

Kotliakov, V. M., and Krenkea, N., 1981, Glaciation actuelle et climat du Caucase. : Revue de Géographie Alpine, v. 64, p. 241-264.

Kotlyakov, V. M., and Krenke, A. N., 1980, Sovremennoe oledenenie i klimat. In: Gerasimov, I. P. (ed.), Alpy–Kavkaz: sovremennye problemy konstruktivnoi geografii gornykh stran. Nauchnye itogi franko-sovetskikh simpoziumov, p. 155-177.

Kroonenberg, S. B., Badyukova, E. N., Storms, J. E. A., Ignatov, E. I., and Kasimov, N. S., 2000, A full sea-level cycle in 65 years: barrier dynamics along Caspian shores: Sedimentary Geology, v. 134, no. 3-4, p. 257-274.

Kurtubadze, M., 2008, Climate zones of the Caucasus ecoregion: Caucasus ecoregion - environment and human development issues.

Labourdette, R., and Jones, R. R., 2007, Characterization of fluvial architectural elements using a three-dimensional outcrop data set: Escanilla braided system, South-Central Pyrenees, Spain: Geosphere, v. 3, no. 6, p. 422-434.

Lebedev, L. I., Aleksina, L. A., and Kulakova, L. S., 1987, Kaspiyskoe More-Geologiya I Neftegazonosnost: Moscow, Nedra,, p. 295.

Liu-Zeng, J., Tapponnier, P., Gaudemer, Y., and Ding, L., 2008, Quantifying landscape differences across the Tibetan plateau: Implications for topographic relief evolution: Journal Of Geophysical Research-Earth Surface, v. 113, no. F4.

Liu Xiaodong, ChengZhigang, and ZhangRan, 2009, The A1B Scenario Projection for Climate Change over the Tibetan Plateau in the Next 30-50 Years: Plateau Meteorology,, v. 28, no. (3), p. 475—484.

Mangino, S., and Priestley, K., 1998, The crustal structure of the South Caspian region: Geophysics Journal International, v. 133, p. 630-648.

Martin-Gonzalez, F., and Heredia, N., 2011, Complex tectonic and tectonostratigraphic evolution of an Alpine foreland basin: The western Duero Basin and the related Tertiary depressions of the NW Iberian Peninsula: Tectonophysics, v. 502, no. 1-2, p. 75-89.

Masson, F., Djamour, Y., Van Gorp, S., Chery, J., Tatar, M., Tavakoli, F., Nankali, H., and Vernant, P., 2006, Extension in NW Iran driven by the motion of the south Caspian basin: Earth and Planetary Science Letters, v. 252, no. 1-2, p. 180-188.

Mayringer, F., Treloar, P. J., Gerdes, A., Finger, F., and Shengelia, D., 2011, New Age Data from the Dzirula Massif, Georgia: Implications for the Evolution of the Caucasian Variscides: American Journal of Science, v. 311, no. 5, p. 404-441.

McCaffrey, K. J., W. and Jones, R. R., Holdsworth, R. E., Wilson, R. W., Clegg, P. a. I., J., Holliman, N., and Trinks, I., 2005, Unlocking the spatial dimension : digital technologies and the future of geoscience fieldwork.: Journal of the Geological Society, v. 162, p. 927-938.

Mekhtiyev, S. F., and Bagir-Zadeh, F. M., 1984, The map of oil and gas fields and prospective structures of Azerbaijan Republic, Baku: Academy of Sciences of Azerbaijan.

Melik-Pashaev, V. S., Khalilov, E. M., and Seregina, V. N., 1983, Abnormally-High Formation Pressures, p. 181.

Mellors, R. J., Jackson, J., Myers, S., Gok, R., Priestley, K., Yetirmishli, G., Turkelli, N., and Godoladze, T., 2012, Deep Earthquakes beneath the Northern Caucasus: Evidence of Active or Recent Subduction in Western Asia: Bulletin of the Seismological Society of America, v. 102, no. 2, p. 862-866.

Midland_Valley, 2012, Move on Fault Restoration Tutorial.

Ministry of Geology and Mineral Resources USSR, 1960, 1:200,000 Geology map K-39-(19, 25, 26, 31, 32, 33).

-, 1963, 1:50,000 Geology map K-39-124.

Mitchell, J., and Westaway, R., 1999, Chronology of Neogene and Quaternary uplift and magmatism in the Caucasus: constraints from K-Ar dating of volcanism in Armenia: Tectonophysics, v. 304, no. 3, p. 157-186.

Montgomery, D. R., 1994, Valley Incision and the Uplift of Mountain Peaks: Journal of Geophysical Research-Solid Earth, v. 99, no. B7, p. 13913-13921.

Montgomery, D. R., and Brandon, M. T., 2002, Topographic controls on erosion rates in tectonically active mountain ranges: Earth and Planetary Science Letters, v. 201, no. 3-4, p. 481-489.

Moretti, I., Lepage, F., and Guiton, M., 2006, KINE3D: a new 3D restoration method based on a mixed approach linking geometry and geomechanics: Oil & Gas Science and Technology-Revue D Ifp Energies Nouvelles, v. 61, no. 2, p. 277-289.

Mosar, J., Kangarli, T., Bochud, M., Glasmacher, U. A., RAST, A., BRUNET, M. F., and SOSSON, M., 2010, Cenozoic–Recent tectonics and uplift in the Greater Caucasus: a perspective from Azerbaijan: Geological Society, London, v. 340, p. 261-280.

Nadirov, R. S., Bagirov, E., Tagiyev, M., and Lerche, I., 1997, Flexural plate subsidence, sedimentation rates, and structural development of the super-deep South Caspian Basin: Marine and Petroleum Geology, v. 14, no. 4, p. 383-400.

Narimanov, A. A. a. P., I., 1995, Oil history, potential converge in Azerbaijan: Oil and Gas Journal, v. 93, no. 21, p. 32-39.

Peeters, F., Kipfer, R., Achermann, D., Hofer, M., Aeschbach-Hertig, W., Beyerle, U., Imboden, D. M., Rozanski, K., and Fröhlich, K., 2000, Analysis of deep-water exchange in the Caspian Sea based on environmental tracers: Deep Sea Research Part I: Oceanographic Research Papers, v. 47, no. 4, p. 621-654.

Philip, H., Cisternas, A., Gvishiani, A., and Gorshkov, A., 1989, The Caucasus: an actual example of the initial stages of continental collision: Tectonophysics, v. 161, no. 1–2, p. 1-21.

Price, N. J., and Cosgrove, J. W., 1990, Analysis of Geological Structures.: Cambridge University Press. Cambridge.

Priestley, K., Baker, C., and Jackson, J., 1994, Implications of Earthquake Focal Mechanism Data for the Active Tectonics of the South Caspian Basin and Surrounding Regions: Geophysical Journal International, v. 118, no. 1, p. 111-141.

Priestley, K., Baker, C., Jackson, J, 1994, Implications of earthquake focal mechanism data for the active tectonics of the South Caspian Basin and surrounding regions: Geophysical Journal International v. 118, p. 111 - 141.

Ramsay., J. G., 1967, Folding and Fracturing of Rocks: book, p. 568.

Reilinger, R., McClusky, S., Vernant, P., Lawrence, S., Ergintav, S., Cakmak, R., Ozener, H., Kadirov, F., Guliev, I., Stepanyan, R., Nadariya, M., Hahubia, G., Mahmoud, S., Sakr, K., ArRajehi, A., Paradissis, D., Al-Aydrus, A., Prilepin, M., Guseva, T., Evren, E., Dmitrotsa, A., Filikov, S. V., Gomez, F., Al-Ghazzi, R., and Karam, G., 2006, GPS constraints on continental deformation in the Africa-Arabia-Eurasia continental collision zone and implications for the dynamics of plate interactions: Journal of Geophysical Research-Solid Earth, v. 111, no. B5.

Reilinger, R. E., McClusky, S. C., Souter, B. J., Hamburger, M. W., Prilepin, M. T., Mishin, A., Guseva, T., and Balassanian, S., 1997, Preliminary estimates of plate convergence in the Caucasus collision zone from global positioning system measurements: Geophysical Research Letters, v. 24, p. 1815 -1818.

Reynolds, A. D., Simmons, M. D., Bowman, M. B. J., Henton, J., Brayshaw, A. C., 4, Ali-Zade, A. A., Guliyev, I. S., Suleymanova, S. F., Ateava, E. Z., Mamedova, D. N.,

and Koshkarly, R. O., 1998, Implication of outcrop geology for reservoirs in the Neogene, Apsheron Peninsula, Azerbaijan AAPG Bulletin v. 82, p. 25-49.

Rezanov, I. A., and Chamo, S. S., 1969, Reasons for absence of a 'granitic' layer in basins of the South Caspian and Black Sea type: Canadian Journal of Earth Sciences, v. 6, no. 4, p. 671-678.

Ritz, J. F., Nazari, H., Ghassemi, A., Salamati, R., Shafei, A., Solaymani, S., and Vernant, P., 2006, Active transtension inside central Alborz: A new insight into northern Iran-southern Caspian geodynamics: Geology, v. 34, no. 6, p. 477-480.

Robinson, A. G., Banks, C. J., Rutherford, M. M., and Hirst, J. P. P., 1995, Stratigraphic and Structural Development of the Eastern Pontides, Turkey: Journal of the Geological Society, v. 152, p. 861-872.

Robinson, A. G., E.T. Griffith, A.R. Gardiner, and Home., A. K., 1997, Petroleum geology of the Georgian fold and thrust belts and foreland basins: Regional and petroleum geology of the Black Sea and surrounding region: AAPG, v. 68, p. 347-367.

Rodriguez, E., Morris, C. S., Belz, J. E., Chapin, E. C., Martin, J. M., Daffer, W., and Hensley, S., 2005, An assessment of the SRTM topographic products, Jet Propulsion Laboratory, Pasadena, California. : Technical Report p. 1-143.

Rosser, N. J., Petley, D. N., Lim, M., Dunning, S. A., and J., A. R., 2005, Terrestrial laser scanning for monitoring the process of hard rock coastal cliff erosion.: Quarterly Journal of Engineering Geology and Hydrogeology, v. 38, p. 363-375.

Rouby, D., Xiao, H., and Suppe, J., 2000, 3D Restoration of Complexly Folded and Faulted Surfaces Using Multiple Unfolding Mechanisms: American Association of Petroleum Geologists Bulletin, v. 84, p. 805-829.

Royden, L. H., Burchfiel, B. C., and van der Hilst, R. D., 2008, The Geological Evolution of the Tibetan Plateau: Science, v. 321, no. 5892, p. 1054-1058.

Ruban, D. A., Henrique Zerfass, and Yang, W., 2007, A new hypothesis on the position of the Greater Caucasus Terrane in the Late Palaeozoic-Early Mesozoic based on palaeontologic and lithologic data: Trabajos de Geologia, Univ. de Oviedo, v. 27, p. 19-27.

Saintot, A., and Angelier, J., 2002, Tectonic paleostress fields and structural evolution of the NW-Caucasus fold-and-thrust belt from Late Cretaceous to Quaternary: Tectonophysics, v. 357, no. 1-4, p. 1-31.

Saintot, A., Brunet, M. F., Yakovlev, F., Sebrier, M., Stephenson, R., Ershov, A., Chalot-Prat, F., and Mccann, T., 2006a, The Mesozoic-Cenozoic tectonic evolution of the Greater Caucasus: European Lithosphere Dynamics, v. 32, p. 277-289.

Saintot, A., Marie, F., Oise, B., Fedor, Y., Michel Se, B., Randell, S., Andrei, E., Franc¸ O, C., and Tommy, M., 2006b, The Mesozoic–Cenozoic tectonic evolution of the Greater Caucasus, p. 177-189.

Shengalaya, G. S., 1978, Trekhmemaya gravitatsionnaya model glubinovo stroeniya zemnoi kori Kabkaza: Sov. Geol, v. 12, p. 102-107.

Shevchenko, V. I., 1972, The rootless Dar'yalskiy and Gviletskiy granite plutons of the central Caucasus: Russian original: Dokl. Akad. Nauk SSSR 204, p. 95-97.

Shikalibeily, E. S., and Grigoriants, B. V., 1980, Principal features of the crustal structure of the south-caspian basin and the conditions of its formation: Tectonophysics, v. 69, no. 1–2, p. 113-121.

Shroder, J. F., Bishop, M. P., Copland, L., and Sloan, V. F., 2000, Debris-covered Glaciers and Rock Glaciers in the Nanga Parbat Himalaya, Pakistan: Geografiska Annaler: Series A, Physical Geography, v. 82, no. 1, p. 17-31.

Smith-Rouch, L. S., 2006, Oligocene–Miocene Maykop/Diatom Total Petroleum System of the South Caspian Basin Province, Azerbaijan, Iran, and Turkmenistan: U.S. Geological Survey Bulletin 2201, p. 1-27.

Sobel, E. R., Hilley, G. E., and Strecker, M. R., 2003, Formation of internally drained contractional basins by aridity-limited bedrock incision: Journal of Geophysical Research-Solid Earth, v. 108, no. B7.

Sosson, M., Rolland, Y., Müller, C., Danelian, T., Melkonyan, R., Kekelia, S., Adamia, S., Babazadeh, V., Kangarli, T., Avagyan, A., Galoyan, G., and Mosar, J., 2010b, Subductions, obduction and collision in the Lesser Caucasus (Armenia, Azerbaijan, Georgia), new insights: Geological Society, London, Special Publications, v. 340, no. 1, p. 329-352.

Souque, C., Fisher, Q. J., Casey, M., and Bentham, P., 2010, Structural controls on mechanical compaction within sandstones: An example from the Apsheron Peninsula, Azerbaijan: Marine and Petroleum Geology, v. 27, no. 8, p. 1713-1724.

Stampfli, G., Marcoux, J., and Baud, A., 1991, Tethyan margins in space and time: Palaeogeography, Palaeoclimatology, Palaeoecology, v. 87, no. 1-4, p. 373-409.

Stephan J. D, Gregory W. R, Nazim R. A, and G, T. J., 2008, Petroleum Systems Dynamics of the South Caspian Basin: Houston Geological Society Bulletin, , v. Volume 50, p. Page 15

Stocklin, J., 1974, Northern Iran: Alborz mountains. In: Spencer, A. (Ed.), Mesozoic-Cenozoic orogenic belts: data for orogenic studies: Geological Society Special Publication, v. 4, p. 213-234.

Stokes, C. R., Gurney, S. D., Shahgedanova, M., and Popovnin, V., 2006, Late-20th-century changes in glacier extent in the Caucasus Mountains, Russia/Georgia: Journal of Glaciology, v. 52, no. 176, p. 99-109.

Suppe, J., 1983, Geometry and Kinematics of Fault-Bend Folding: American Journal of Science, v. 283, no. 7, p. 684-721.

Tan, O., and Taymaz, T., 2006, Active tectonics of the Caucasus: Earthquake source mechanisms and rupture histories obtained from inversion of teleseismic body waveforms: Postcollisional Tectonics and Magmatism in the Mediterranean Region and Asia, v. 409, p. 531-578.

Tawadros E. D, Dmitry Ruban, and Efendiyeva, M., 2006, Evolution of NE Africa and the Greater Caucasus: Common Patterns and Petroleum Potential: The Canadian Society of Petroleum Geologists, the Canadian Society of Exploration Geophysicists, the Canadian Well Logging Society Joint Convention., p. 531-538.

Thomas, J. C., Cobbold, P. R., Shein, V. S., and Le Douaran, S., 1999, Sedimentary record of late Paleozoic to Recent tectonism in central Asia -- analysis of subsurface data from the Turan and south Kazak domains: Tectonophysics, v. 313, no. 3, p. 243-263.

Tong, K., Su, F., Yang, D., Zhang, L., and Hao, Z., 2013, Tibetan Plateau precipitation as depicted by gauge observations, reanalyses and satellite retrievals: International Journal of Climatology, p. n/a-n/a.

Triep, E. G., Abers, G. A., Lernerlam, A. L., Mishatkin, V., Zakharchenko, N., and Starovoit, O., 1995, Active thrust front of the Greater Caucasus - the April 29, 1991, Racha earthquake sequence and its tectonic implications: Journal of Geophysical Research-Solid Earth, v. 100, no. B3, p. 4011-4033.

Twiss, R. J., ., and Moores, E. M., 1992, Structural geology: University of Calfornia at Davis, p. 532.

van der Pluijm, B. A., and Marshak, S., 2004, Earth Structure an introduction to structural geology and tectonics.

Webster, P. J., Magaña, V. O., Palmer, T. N., Shukla, J., Tomas, R. A., Yanai, M., and Yasunari, T., 1998, Monsoons: Processes, predictability, and the prospects for prediction: Journal of Geophysical Research: Oceans, v. 103, no. C7, p. 14451-14510.

Wessel, P., and Smith, W. H. F., 1998, New, improved version of the Generic Mapping Tools released: : Eos (Transactions, American Geophysical Union), v. 79, p. 579.

White, N. J., Jackson, J. A., and Mckenzie, D. P., 1986, The Relationship between the Geometry of Normal Faults and That of the Sedimentary Layers in Their Hanging Walls: Journal of Structural Geology, v. 8, no. 8, p. 897-909.

Yakubov, A. A., Alizade, A.A, 1971, Mud Volcanoes of the Azerbaijan SSR. Publishing House of the Academy of Sciences of the Azerbaijan SSR, Baku, p. 258.

Yanai, M. H., Li, C. F., and Song, Z. S., 1992, Seasonal Heating of the Tibetan Plateau and Its Effects on the Evolution of the Asian Summer Monsoon: Journal of the Meteorological Society of Japan, v. 70, no. 1B, p. 319-351.

Yilmaz, A., Adamia, S., Chabukiani, A., Chkhotua, T., ErdoGan, K., Tuzcu, S., and KarabiyikoGlu, M., 2000, Structural Correlation of the Southern Transcaucasus (Georgia)-Eastern Pontides (Turkey): Geological Society, London, Special Publications, v. 173, no. 1, p. 171-182.

Yusifov, M., and Rabinowitz, P. D., 2004, Classification of mud volcanoes in the South Caspian Basin, offshore Azerbaijan: Marine and Petroleum Geology, v. 21, no. 8, p. 965-975.

Zeitler, P. K., Meltzer, A. S., Koons, P. O., Craw, D., Hallet, B., Chamberlain, C. P., Kidd, W. S. F., Park, S. K., Seeber, L., Bishop, M., and Shroder, J., 2001, Erosion, Himalayan geodynamics, and the geomorphology of metamorphism: GSA Today, v. 11, p. 4-9.

Zonenshain, L. P., and Pichon, X., 1986, Deep basins of the Black Sea and Caspian Sea as remnants of Mesozoic back-arc basins: Tectonophysics, v. 123, no. 1-4, p. 181-211.